NASA Contractor Report 158965

(NASA-CR-158965) THE TOTAL IN-FLIGHT SIMULATOR (TIFS) AERODYNAMICS AND SYSTEMS: DESCRIPTION AND ANALYSIS Final Report (Calspan Corp., Buffalo, N. Y.) 283 p HC A13/MF A01 CSCL 14B G3/09
N79-14113
Unclas
41010

Calspan

THE TOTAL IN-FLIGHT SIMULATOR (TIFS) AERODYNAMICS AND SYSTEMS - DESCRIPTION AND ANALYSIS

D. Andrisani II, H. Daughaday, J. Dittenhauser, E. Rynaski

Calspan Report No. AK-5280-F-10 (Revision 1)

Prepared For:

National Aeronautics and Space Administration
Langley Research Center
Hampton, VA 23665

and

Air Force Flight Dynamics Laboratory
Air Force Systems Command
Wright Patterson Air Force Base,
Ohio 45433

Contract No. F33615-73-C-3051

Calspan Corporation
Buffalo, New York 14221

FOREWORD

The TIFS aircraft mathematical model development program described in this report was sponsored by the Langley Research Center of the National Aeronautics and Space Administration. It was conducted by the Flight Research Department of the Calspan Corporation, Buffalo, New York as Task 15 of the Air Force Flight Dynamics Laboratory Contract F33615-73-C-3051. The Calspan Project Engineer was Edmund G. Rynaski and the NASA Program Director was Mr. D. B. Middleton.

The authors would like to express their gratitude to the NASA personnel in the ACT program office for their helpful suggestions and stimulating discussion. Particular thanks are due to L. W. Taylor, R. V. Hood, D. B. Middleton, and I. Abel. The authors wish to acknowledge and give special appreciation for the assistance provided by the Air Force Flight Dynamics Laboratory, Control Criteria Branch. The FLEXSTAB results presented in this report could not have been possible without the generous assistance of R. Schwanz and C. Stockdale in teaching Calspan personnel to use the FLEXSTAB system.

TABLE OF CONTENTS

TABLE OF CONTENTS, CONT'D

LIST OF FIGURES

LIST OF FIGURES, CONT'D

LIST OF FIGURES, CONT'D

LIST OF FIGURES, CONT'D

LIST OF TABLES

LIST OF TABLES, CONT'D

LIST OF SYMBOLS

b	wing span
$\bar{c}$	reference chord
f	frequency (Hz)
g	gravity constant 9.8 m/sec^2 (32.2 ft/sec^2)
h_p	pressure altitude
n_x, n_y, n_z	body axis components of accelerometer signals in g units
p, q, r	body axis components of angular velocity
p_s	static pressure
$\bar{q}, \bar{q}_c$	dynamic pressure
s	Laplace operator
t_c, t_k	temperature in ^{o}C and ^{o}K respectively
u, v, w	body axis components of linear velocity
u	control vector
x	state vector
x_1	vector of rigid body response variables
x_2	vector of structural mode response variables
x_n, y_n, z_n	horizontal or vertical tail coordinate axes
$x_{L_{M_1}}, x_{L_{M_2}}$	distance of lumped masses M_1 and M_2 from elastic axis
C_l, C_m, C_n	body axis components of moment coefficients
$-C_D, C_Y, -C_L$	wind axis components of aerodynamic force coefficient excluding thrust
C_H	hinge moment coefficient
E	modulus of elasticity in tension
F	matrix of stability derivatives
G	matrix of control derivatives
G	modulus of elasticity in shear
H	altitude
I	identity matrix
I_{xx}, I_{yy}, I_{zz}	area moments of inertia about local x-x, y-y, and z - z axes
J	torsional stiffness factor
K	spring constant
M	Mach number

LIST OF SYMBOLS, CONT'D

M_1, M_2	lumped masses used in structural model
S	wing area
S_a, S_e, S_z	areas of aileron, elevator and DLF, respectively
V	true airspeed
W	airplane weight, fuel weight
X, Y, Z	Reference Axis System (X-Fus. Sta. = 137.5 in. = 3.493 m)
X_N, Y_N, Z_N	thin body aerodynamic coordinate system (used in FLEXSTAB)
α, α_{FRL}	angle of attack with respect to true airspeed
α_I	inertial angle of attack, referenced to inertial velocity vector
α_g	gust angle of attack
β	angle of sideslip with respect to true airspeed
β_I	inertial angle of sideslip, referenced to inertial velocity vector
β_g	gust sideslip angle
γ	flight path angle
$\delta_e, \delta_a, \delta_r, \delta_x$ $\delta_y, \delta_z, \delta_F, \delta_T$	control deflection of the TIFS elevator, aileron, rudder, throttle, side force surface, direct lift flap, Fowler flap, and the model throttle, respectively
δ_{sa}	symmetric aileron deflection
δ_{tt}	trim tab deflection
ζ	damping ratio
η_w	fraction of wing span
η_i	generalized coordinate for i^{th} structural mode
θ	pitch attitude
ρ	air density
Φ	power spectral density
ϕ	bank angle
$(\ )_p$	value at pilot station
$(\ )_a$	pertaining to aileron
$(\ )_e$	pertaining to elevator
$(\ )_z$	pertaining to DLF
$(\ )_{FRL}$	referred to fuselage reference line

$(\ )_g$	gust component of ( )
$(\ )_I$	inertial component of ( )

ABBREVIATIONS AND ACRONYMS

ACT	Active Control Technology
AIC	Aerodynamic Influence Coefficient Program
AT/TIFS	Air Transport TIFS
BL	Body line
C.G.	Center of gravity
DLF	Direct Lift Flap
FLEXSTAB	Name of aeroelastic computing system derived from the words FLEXible and STABility
F.S.	Fuselage station
FRL	Fuselage Reference Line
GD	Geometry Definition program
IAS	Indicated Air Speed
ISIC	Internal Structural Influence Coefficient Program
LSA	Linear System Analysis program
NM	Normal Modes program
PSD	Power spectral density
SD+SS	Static Derivative and Static Stability program
SFS	Side Force Surface
TIFS	Total In-Flight Simulator
W.L.	Waterline

Section 1

INTRODUCTION

The National Aeronautics and Space Administration has undertaken a significant program of active control technology research and development. The feasibility of the use of this technology has been demonstrated in a number of military research programs and by NASA (References 1, 2). These and other programs of research and study (References 3, 4) indicate that the proper application of Active Control Technology (ACT) can reduce the structural weight and drag and therefore bringing about substantial weight savings. In addition, active control technology can be expected to have direct benefits in terms of fatigue life of the vehicle, thereby making the technology additionally cost effective. The potential benefits to transport aircraft are obvious in terms of fuel saving and extended vehicle service life.

Under the sponsorship of NASA Langley, the Calspan Corporation has undertaken a program of vehicle definition or mathematical modeling of the Total In-Flight Simulator (TIFS) aircraft in preparation for control system development and design of an ACT system for the TIFS. In addition, a major part of the effort also involves design changes to the control system that would allow the ailerons to be operated collectively as well as differentially to enhance the ability of the vehicle to perform the dual function of maneuver load control and gust alleviation.

Ref. 1. NASA Symposium on Advanced Control Technology and Its Potential for Future Transport Aircraft. NASA TM X-3409, August 1976.

2. Hood, R. V.: "A Summary of the Application of Active Controls Technology on the ATT System Studies." NASA Symposium on Advanced Control Technology and Its Potential for Future Transport Aircraft. NASA TM X-3409, August 1976.

3. Rynaski, E. G. and Weingarten, N. C.: "Flight Control Principles for Control Configured Vehicles." Air Force Flight Dynamics Laboratory Report AFFDL-TR-71-154, January 1972.

4. Stockdale, C. K. and Poyncer, R. D.: "Control Configured Vehicle Ride Control System (CCV RCS)." Air Force Flight Dynamics Laboratory Report AFFDL-TR-73-83, July 1973.

The major emphasis of this study, however, was to mathematically predict the rigid body and flexible equations of longitudinal motion using the FLEXSTAB program.

This report is organized in three main sections. Section 2 describes the elastic and aerodynamic analysis of the TIFS airplane using the FLEXSTAB program. Included in this analysis is a definition of the vehicle geometry, the mass and stiffness distribution, the calculated mode frequencies and mode shapes and the resulting aerodynamic equations of motion of the flexible vehicle. Comparisons with data taken during the ground vibration and flight tests of the vehicle are made. Section 3 describes the control and instrumentation system that presently exists on TIFS, including performance and flight test data on the control and instrumentation system. Section 3 also contains an analysis of the existing elevator servo system and proposed modifications to the system to improve its performance.

Conclusions and recommendations are included at the ends of Sections 2 and 3. Large parts of these sections are devoted to an evaluation of the accuracy and usefulness of existing data and recommendations for the accumulation of additional flight and ground data.

Section 2

ELASTIC AND AERODYNAMIC ANALYSIS

2.0 THE TIFS AIRPLANE

The USAF/Calspan Total In-Flight Simulator (TIFS) airplane, as shown in Figure 1 is probably the most complete and versatile control configured and variable stability aircraft ever constructed. TIFS has been designed to have independent control of all six degrees of rotational and translations of freedom of rigid body motion. The aircraft is equipped with large servo-driven direct lift flaps for independent control of lift forces. Side forces are independently controlled through large vertical surfaces built into the wings. The propellers are used for longitudinal force control and the conventional ailerons, elevator and rudder are used for roll, pitch and yaw control. All of these control surfaces are driven by full authority electrohydraulic servos. Aside from the side force control surfaces, TIFS' most distinctive feature is the addition of a complete and removable second cockpit on the nose of the airplane. The capability of either masking the presently installed simulation cockpit, or easily removing it and adding a completely new one is unique. The instrument displays are readily changed. The airplane has been flown with a wheel controller, a side stick controller and with a center stick. The wheel controller, center stick and rudder pedals are equipped with variable feel systems including nonlinear functions. A more detailed description of this aircraft as well as its capability is given in Reference 5.

A number of research projects and simulations of specific airplanes have been performed using the Air Force TIFS airplane. These include simulations of the space shuttle, the B-1 bomber and the Concorde supersonic transport; a flight research program to explore use of side force control in both automatic and manual modes, to counter crosswinds during crosswind landings; and flight demonstrations of multiplex techniques for flight control.

Ref. 5. Reynolds, P. A., Wasserman, R., Fabian, G. J. and Motyka, P. R.: "Capability of the Total In-Flight Simulator (TIFS)." Air Force Flight Dynamics Laboratory, AFFDC TR-72-39, July 1972.

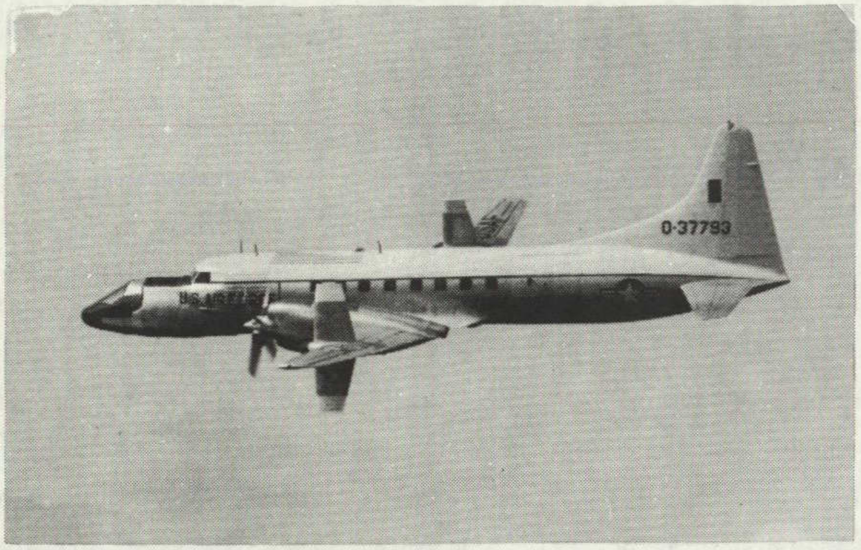

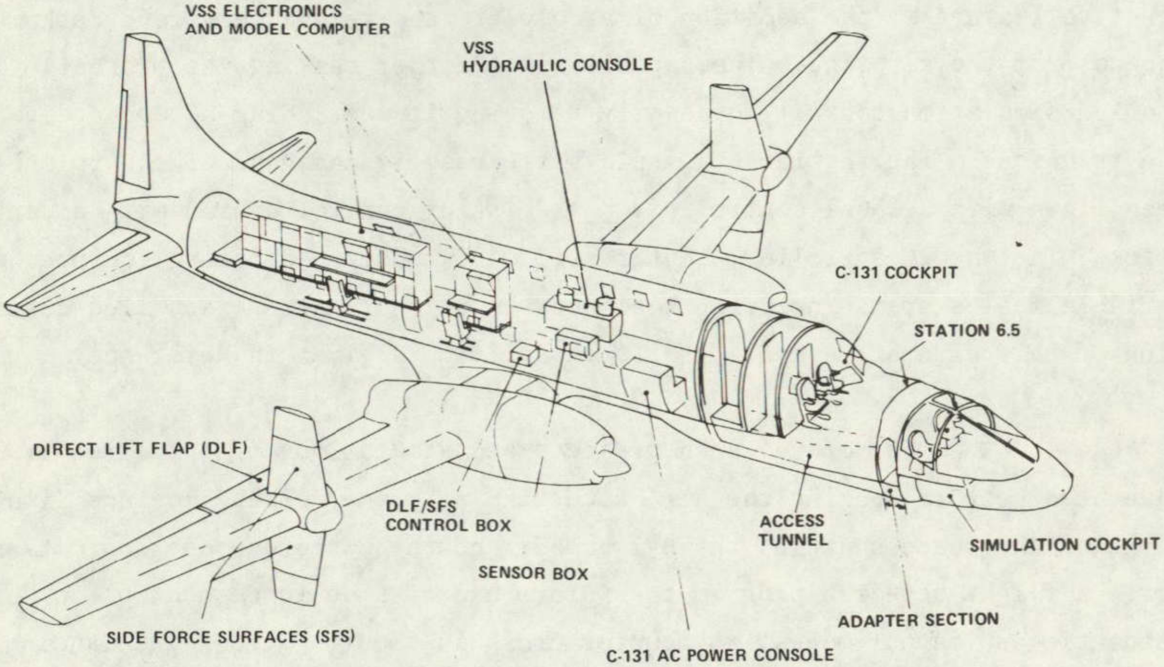

Figure 1 USAF FLIGHT DYNAMICS LABORATORY TOTAL IN-FLIGHT SIMULATOR

craft into linear equations of motion and to investigate control system-airframe interactions and b) the computer program was immediately available to Calspan through the Air Force Flight Dynamics Laboratory.

FLEXSTAB provided the following combined computational capability that made its application suitable for this program.

1) Capability to accurately analyze a very large number of structural modes.

2) Capability to retain the static deflection of all modes deleted in the analysis (Residual Elastic Formulation of the Equations of Motion).

3) A first order unsteady aerodynamic effect.

4) Capability to improve the completeness of the geometric model and therefore improve the aerodynamic model (e.g., engine nacelles and side force surfaces).

5) Ability to very accurately compute symmetric, antisymmetric and combined dynamic properties of an airframe.

In the discussions to follow concerning the finite element structural and aerodynamic models of the TIFS prepared for input to Flexstab, the detailed description of analytical procedures employed in FLEXSTAB will be omitted. Detailed documentation of the program is provided by Reference 7.

A simplified block diagram showing the sequence of computations in the FLEXSTAB system,as used for this ACT TIFS study, is shown in Figure 2.

Ref. 7. "A Method for Predicting the Stability Characteristics of Control Configured Vehicles". Air Force Flight Dynamics Laboratory Report AFFDL-TR-74-91, November 1974.

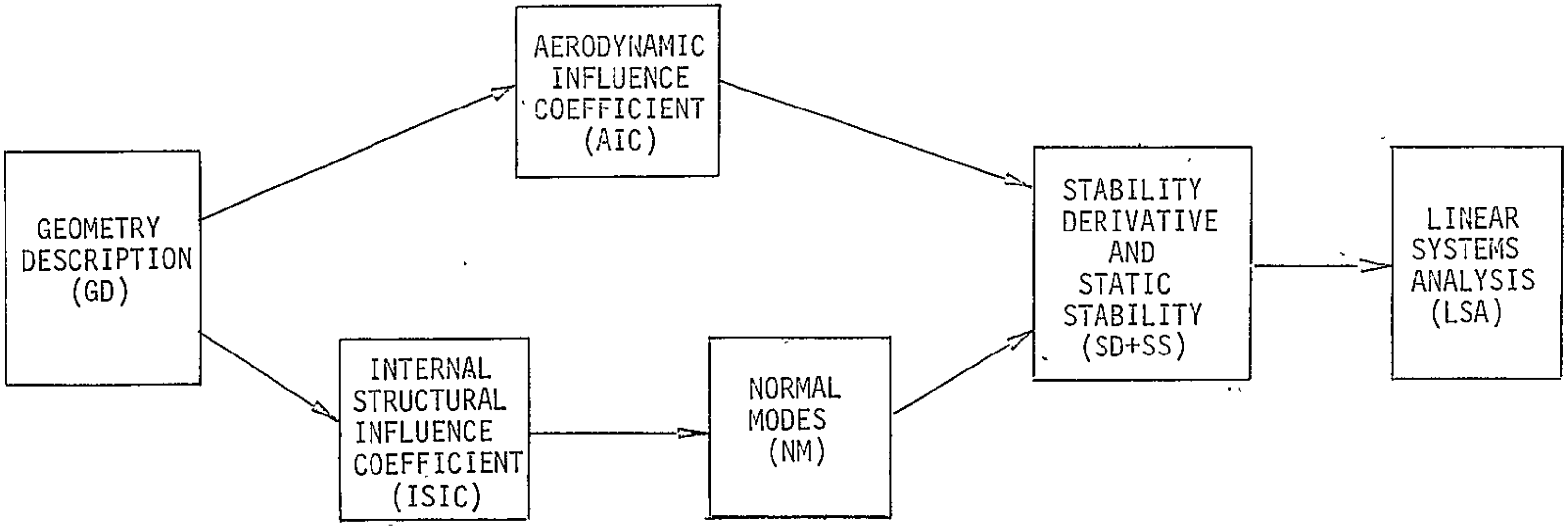

Figure 2 FLEXSTAB SYSTEM COMPUTATIONAL SEQUENCE

Each block is a separate program or module and is run separately. The starting point is the Geometry Definition (GD) program which defines the geometry of the vehicle. Structural properties of the vehicle are input in terms of mass and inertia distributions into the Internal Structural Influence Coefficient (ISIC) program. This program uses thin beam theory to compute structural influence coefficients for the vehicle. Computation of the normal vibration modes is performed in the Normal Modes (NM) program using the ISIC program outputs. The steady and unsteady aerodynamic properties of the vehicle are computed in terms of aerodynamic influence coefficients in the Aerodynamic Influence Coefficient (AIC) program. The aerodynamic theory employed is a linear first order approximation to unsteady, inviscid, unseparated subsonic or supersonic flow equations. Computation of stability and control derivatives, analysis of vehicle static and dynamic stability and formation of the vehicle equations of motion are performed in the Stability Derivative and Static Stability (SD+SS) program. The final program employed in the TIFS analysis was the Linear Systems Analysis (LSA) program. The classical techniques of open or closed loop analysis are performed in this program, i.e. Bode plots, Nyquist plots, and root locus.

2.2 TIFS GEOMETRY DEFINITION

The baseline TIFS configuration consisted of the General Purpose canopy with side-force surfaces installed and gear up, i.e. the standard TIFS configuration. The resulting geometric representation used in FLEXSTAB is shown in Figure 3.

The following geometric approximations were found to be either necessary or desirable in formulating the aircraft model:

1) The point at which the wing dihedral changes from 4.83°(inner wing) to 6.5° (outer wing) was moved from Convair Station 8 (a distance of 4.2909 meters or 168.933 inches perpendicular to the aircraft plane of symmetry) to the engine nacelle centerline (3.81 meters or 150 inches from the plane of symmetry).

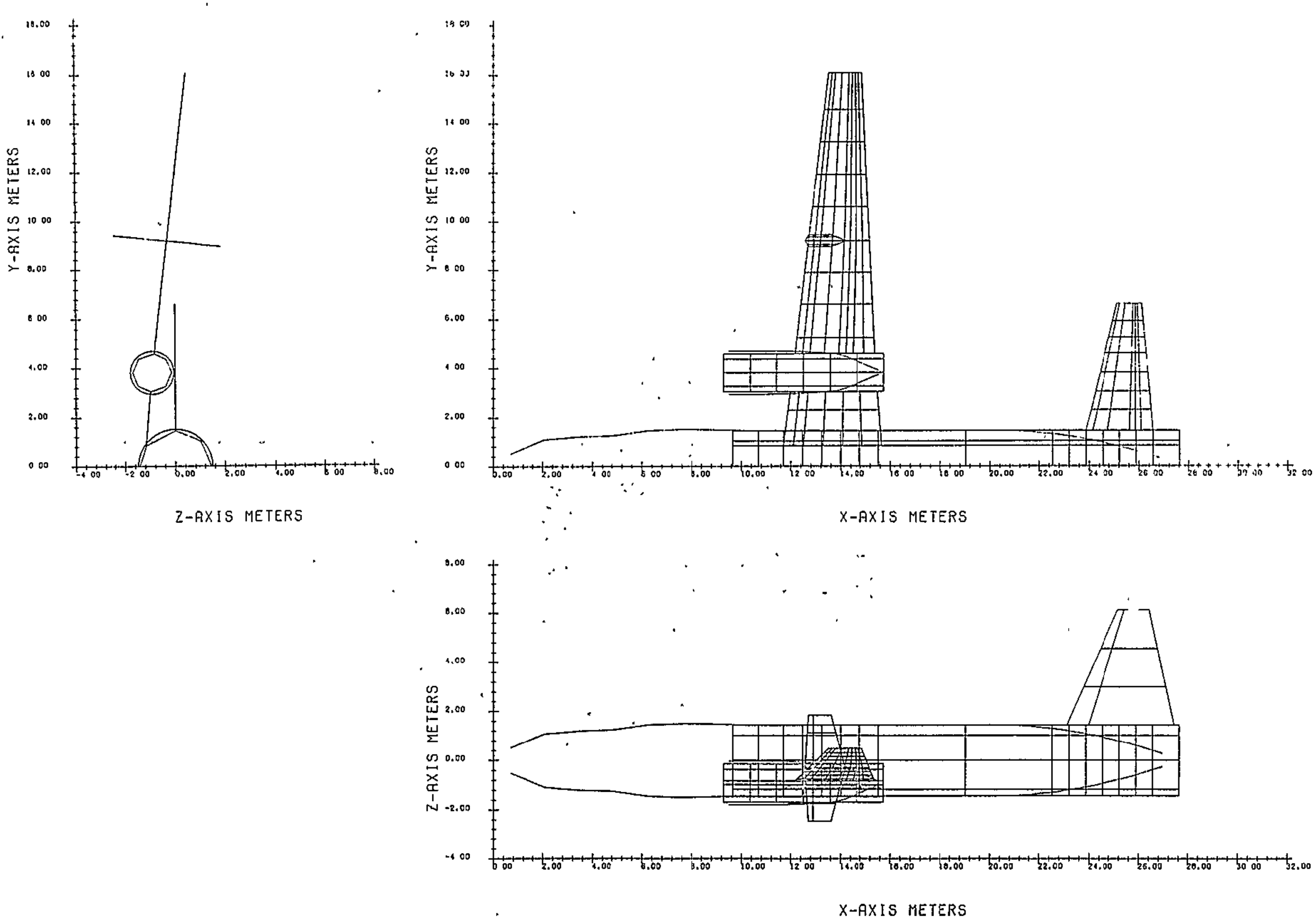

Figure 3 TIFS FLEXSTAB GEOMETRIC REPRESENTATION

This was desirable to simplify the FLEXSTAB model but had the effect of raising the wing panels outboard of Convair Station 8 by a vertical distance of .0142 meters or .558 inches.

2) In FLEXSTAB the geometry of the inner wing panel is described with respect to a local axis system (X_N, Y_N, Z_N) whose X_N axis is parallel to the X axis shown on Figure 3 and whose X_NY_N plane coincides with a mean surface for this thin body. Plane X_NY_N is oriented with respect to the Reference Axis System by a rotation about the X_N axis of magnitude equal to the dihedral angle. The manufacturer's inner panel chord plane of the TIFS airplane does not lie in the X_NY_N plane because of a 4° angle of incidence. Consequently, the geometry for the FLEXSTAB model of TIFS was developed with the incidence removed by assuming the actual wing rotated by 4° about a line perpendicular to the plane of symmetry and located at the intersection of the elastic axis of the wing with the plane of symmetry. Because the wing has dihedral, this rotation also had the effect of moving the wing tip .115 meters or 4.528 inches forward.

3) The side-force surface fairing was ignored.

4) The engine nacelle was taken to be a closed body, i.e. no flow through the nacelle was assumed. The TIFS engine is a turboprop engine which derives only approximately 10% of its total thrust from flow through the engine.

5) The fuselage and engine nacelle were represented with circular cross sections with the correct cross sectional area and correct area centroid location in the Z direction.

6) The only planar lifting surface with a thickness distribution was the wing.

7) The interference body cross section which is used in FLEXSTAB to determine the interference effects between the horizontal stabilizer, vertical tail and fuselage is required to be identical to one used for the wing/fuselage intersection. The interference body used in the TIFS model had a larger radius than the actual fuselage in the region of the horizontal tail and thus enclosed a portion of the horizontal tail. Consequently, the geometric positions of the horizontal and vertical tails were changed in accordance with the recommendations in the FLEXSTAB User's Manual. The thin bodies used to represent the horizontal and vertical tails were moved outboard and upward respectively enough to expose the same surface areas as obtained with the actual fuselage. Correct sweep angles of leading and trailing edges and correct tip chords were maintained in this process.

8) Exposed areas used in FLEXSTAB are listed in the table below:

Area	m^2	ft^2
Horizontal Tail per side (with elevator)	9.46	101.815
Vertical Tail (with rudder, without dorsal fin)	13.0	139.84
Elevator per side (with tabs)	3.34	35.87
Direct Lift Flap per side (aft of hinge line)	4.19	45.0
Aileron per side (aft of hinge line)	2.09	22.6

9) The TIFS was assumed to have a vertical plane of symmetry. Actual TIFS modifications of the forward fuselage are not symmetric due to the crew access tunnel to the evaluation cockpit.

It is recognized that the horizontal tail aspect ratio is effectively increased when the thin bodies representing the left hand and right hand sides of the tail are moved outboard as discussed above in Item 7. This geometric change would have some effect on rolling moments developed by the horizontal tail but is believed to be of secondary importance in considering longitudinal stability and control. Of the geometric approximations made, the shape of the fuselage cross section and the treatment of the engines and nacelles are likely to most seriously affect the accuracy of the analytical results. The forward fuselage of the TIFS is roughly the shape of a rounded triangle. As a result, the lifting effectiveness and therefore the destabilizing effect on longitudinal static stability may be greater than predicted by FLEXSTAB. To correctly model the engines both the propeller and direct thrust slipstreams and their corresponding effects on wing, fuselage and tail would have to be incorporated in some way into the FLEXSTAB model. A study of techniques to accomplish this task was beyond the scope of this contract and therefore not attempted.

2.3 DESCRIPTION OF MASS AND STIFFNESS PROPERTIES OF USAF/TIFS

In this section a description is given of the mass and stiffness properties of TIFS. The basic TIFS airplane is the Convair 580 which is the version of the Convair powered by two Allison 501-D13 turboprop engines. Mass and stiffness distributions for TIFS were derived by review and analysis of data for the reciprocating engine Convair 340 airplane, data describing the Allison prop-jet engine conversion, and data concerning structural modifications made in the development of TIFS.

Mass and stiffness parameters given in this section were the basis for inputs prepared for the Structural Influence Coefficient Program (ISIC) of FLEXSTAB which was used in computing structural vibration modes. A printout of the computer inputs to the ISIC program is reproduced in Appendix A. In general, the basic parameters which are presented are limited to those which could be utilized within the modeling constraints of the ISIC program. However, the fore and aft bending stiffness of the wing and some engine inertia and stiffness parameters which cannot be handled directly by ISIC are also included.

2.3.1 Wing Parameters

The TIFS airplane was received by Calspan prior to modification as a reciprocating-engine C-131B aircraft. TIFS direct-lift wing flaps and side-force surface actuators were installed on this airplane before powerplant conversion. Inertia parameters for making a wing flutter analysis of this interim configuration were derived by correcting data for the Convair 340 given in Reference 8. Inertia parameters for making a wing flutter analysis of this interim configuration were derived by correcting data for the Convair 340 given in Reference 8. Intertia data for 30 sections of the TIFS modification. Contributions due to the TIFS direct-lift flaps and side-force surface modifications were distributed to the same stations and combined with the distributions for the 340 wing.

Subsequently, these data were updated for the completely modified TIFS wing including the engine change and were used in the wing flutter analysis for the Air Transport TIFS (AT/TIFS). These distributions of wing mass, mass unbalance about the elastic axis, and moment of inertia about the elastic axis are also applicable for USAF/TIFS and are used in this report. Table 1 lists the distributions for the zero fuel condition. The table also shows the weight distribution for a fuel load of 1451.5 Kg/side (3200 lbs/side) obtained by interpolation of data for other fuel conditions. The parameters given are in English units as obtained from the original data. They are converted to metric units in Table 2 which were used in the FLEXSTAB solution.

Ref. 8. Johnson, N. S., and Krueger, N. A.: "Wing Stress Analysis – Model 340." Report ZS-340-006, Part I, Consolidated Vultee Aircraft Corp., 31 October 1951, NASA CR-158891.

The wing elastic axis is assumed to be at 36.5% of the wing chord which is the position used in the Convair 340 flutter analysis (Reference 9). This elastic axis is midway between the front and rear spars. The c.g. of the fuel in the tanks between the spars is assumed to be on the wing elastic axis. The effective moment inertia of the fuel was assumed to be 2/5 of the values computed treating the fuel as a rigid body. Table 2 presents the total inertia distributions for the wing including both structural and fuel weights. An equivalent dumbbell mass representation is also given for the distributed weight at each listed station except Sta. 3.825 m (Sta. 150.53 in.). The equivalent properties are converted to metric units which were used in the FLEXSTAB representation of TIFS.

The treatment of the engine sprung weight and nacelle weight which are assumed to act at Sta. 3.825 m (150.53 in.) are taken up in a later section. The properties of the side-force surface vanes are not included in Table 1 and are also discussed separately in a later section. However, the side-force surface actuators, fairing, etc. which are integral parts of the wing are included with the wing weight.

Ref. 9 Pancu, C. D., and Hiroshige, K.: "Model 340 Main Fixed and Movable Control Surface Flutter Analysis." Report ZU-340-003, Consolidated Vultee Aircraft Corp., 28 August 1951. NASA CR-158893.

TABLE 1

DISTRIBUTIONS OF WING WEIGHT, STATIC MOMENT ABOUT ELASTIC AXIS AND MOMENTS OF INERTIA ABOUT ELASTIC AXIS

NOTES: 1) Elastic axis at 36.5% chord.
2) Values of parameters are per side and are in English units as obtained from original data. These parameters are converted to metric units in Table 2.

Sta.-in. (Chord plane)	Weight (lbs)		Static Moment (in. lbs)		Moment of Inertia (lbs. in^2)	
	Zero Fuel* Cond.	Fuel	Zero Fuel* Cond.	Fuel	Zero Fuel* Cond.	Fuel
28.38	502		5,036		480,243	
48.38	566		5,941		534,359	
150.53	3,319	270	-146,977	0	10,600,042	23,316 (Engine sprung weight)
150.53	3,122		-400,552		58,663,798	
205.75	501	1,358	7,831	0	422,119	110,382
259.53	337	1,009	4,431	0	271,366	68,028
308.53	372	454	6,596	0	249,886	24,950
363.53	516	109	– 591	0	332,523	5,165
	26		– 734		20,935	
401.25	129		1,470		76,908	
436.00	99		490		35,353	
478.07	131		874		42,796	
531.16	94		776		35,074	
594.37	91		754		25,311	
Total	9,805	3,200				

* Values as determined for AT/TIFS less effect of wing tip booms not on USAF/TIFS.

TABLE 2

REPRESENTATION OF WING INERTIA PROPERTIES WITH DUMBBELL MASSES [Fuel Mass = 1451.5 Kg/Side (Fuel Weight = 3200 lbs/Side)]

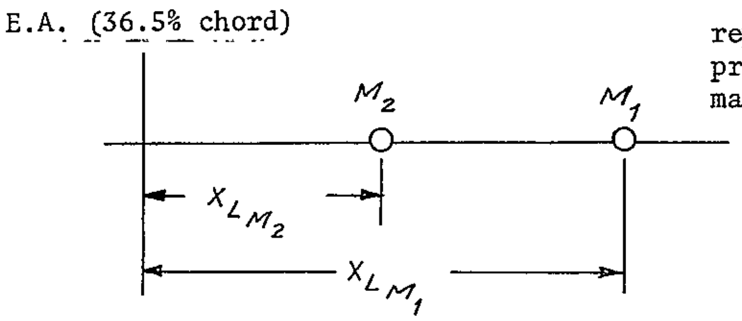

representation of inertia properties by equivalent masses

Parameters from Table 1 in English Units					Equivalent Properties-Metric Units		
Sta. (in)	Sta. (m)	Weight (lbs)	Unbalance about EA (in.lbs)	Moment of Inertia about EA (lbs in^2)	X_{LM_2} (m)	X_{LM_1} (m)	$M_1 = M_2 = \frac{\Delta m}{2}$ (Kg)
0.0	0.0						
28.38	0.721	502	5,036	480,243	-.488	.998	113.8
88.38	2,245	566	5,941	534,359	-.467	1.000	128.4
150.53	3.823	6,711	-547,529	69,287,156			
205.75	5.226	1,859	7,831	532,501	-.309	.523	421.6
259.53	6.592	1,346	4,431	339,394	-.316	.478	305.3
308.53	7.837	826	6,596	274,836	-.214	.619	187.3
363.53	9.234	651*	-1,325	358,623	-.646	.542	197.6
401.25	10.192	129	1,470	76,908	-.259	.838	29.3
436.00	11.074	99	490	35,353	-.338	.589	22.5
478.07	12.143	131	874	42,796	-.257	.596	29.7
531.16	13,491	94	776	35,074	-.234	.653	21.3
594.37	15.097	91	754	25,311	-.157	.578	20.6
Total		13,005					1,427.4

*Does not include SFS vanes.

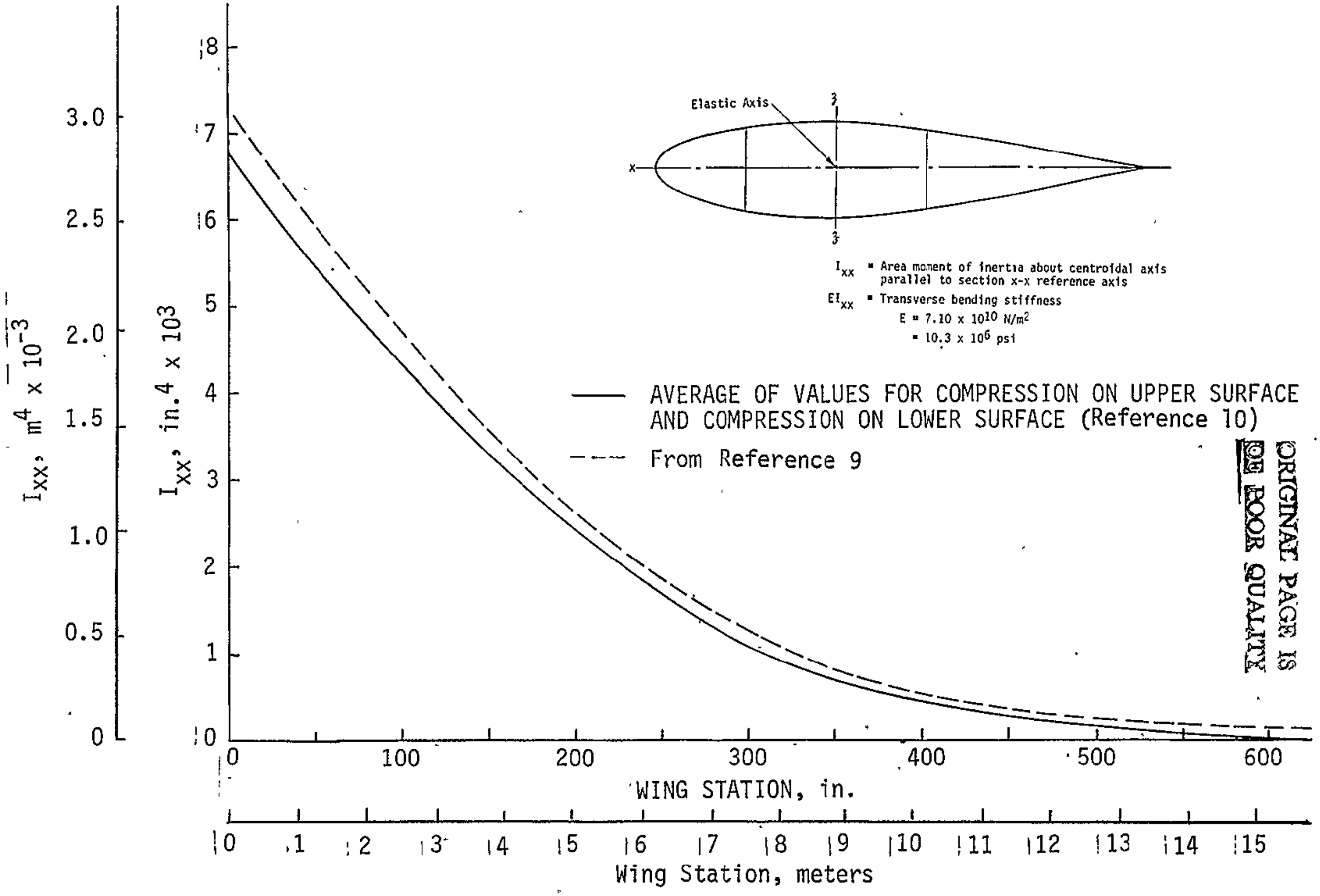

Figure 4 AREA MOMENT OF INERTIA I_{xx} VS. SPANWISE POSITION ON WING

Comparatively few modifications were made to the basic wing structure in the development of TIFS and the wing stiffness of TIFS was assumed to be the same as for the reciprocating-engine version of the Convair. Figure 4 compares structural moments of inertia used in the Convair 340 flutter analysis (Reference 9) to the average section properties computed with compression on the upper or lower surfaces as given in Reference 10. The out of plane bending stiffness used in the TIFS analysis is based on the I_{xx} curve from Reference 9. Figure 5 provides the I_{33} moment of inertia from Reference 10 which is the basis for the assumed fore and aft bending stiffness used for ACT TIFS. Figure 6 presents a plot of the torsional stiffness factor J from Reference 9 which was used to obtain the torsional stiffness of TIFS.

In analyzing TIFS, the stiffness curves or Figures 4, 5 and 6 were approximated by step curves which were constant between concentrated mass stations. Table 3 lists the constant values used between stations in this approximation.

The wing vertical shears on the TIFS airplane are primarily carried into the fuselage by wing fittings located approximately at body line (1.397 m). Figure 7 taken from the Convair 440 maintenance manual presents sketches of the wing to fuselage attachment fittings. In developing a model for the wing to fuselage attachment, the fuselage vertical deflection was assumed equal to the wing vertical deflection at the attachment fittings rather than at the centerline of the airplane. However, the wing cannot be assumed to be cantilevered from the fuselage at the attachment fittings because there is a change of wing slope at the fittings due to bending deflections in the wing carry-through structure.

Figure 8 indicates how the effect of wing bending inboard of the fuselage attachment fittings was simulated in the structural model. As shown

---

Ref. 10. Krueger, J. A., and Johnson, N. S.: "Wing Stress Analysis – Model 340." Report ZS-340-006, Part II, Consolidated Vultee Aircraft Corp., 18 February 1952. NASA CR-158892.

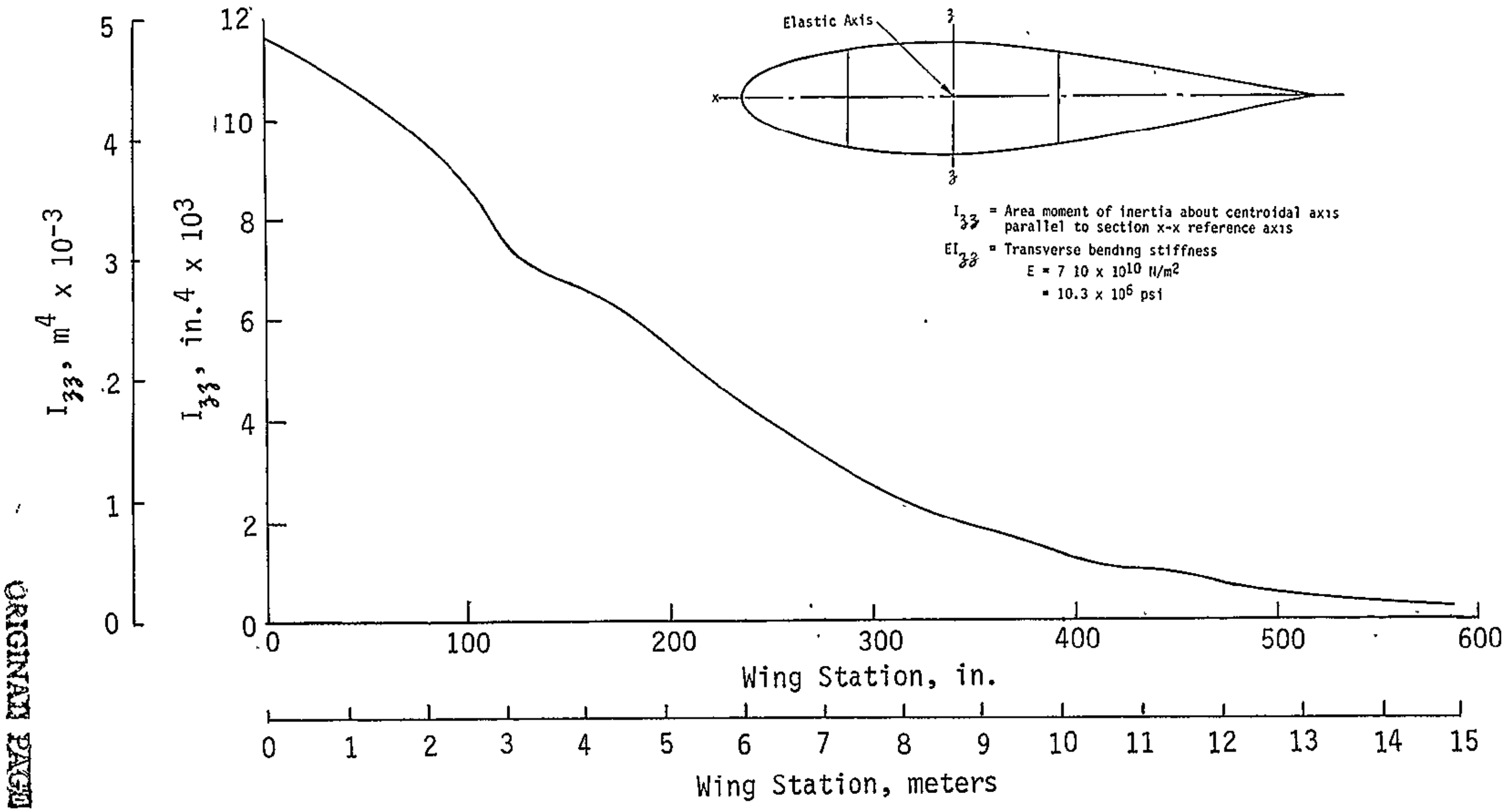

Figure 5 STRUCTURAL MOMENT OF INERTIA I_{zz} VS. SPANWISE POSITION (UPPER SURFACE COMPRESSION) (Reference 10)

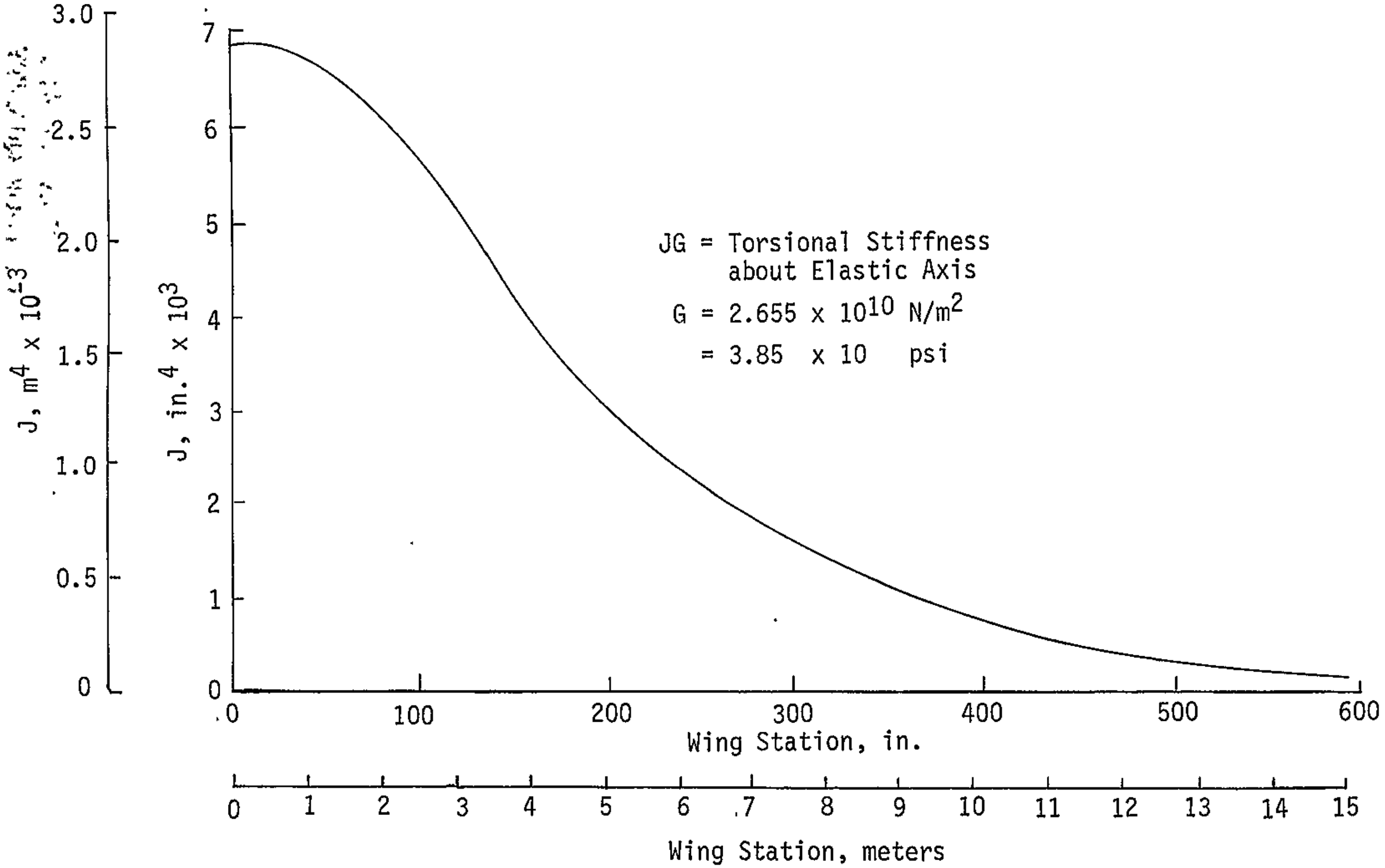

Figure 6 TORSIONAL STIFFNESS FACTOR J VS. SPANWISE POSITION ON WING (Reference 9)

TABLE 3

WING STIFFNESS

Station		EI_{xx}, Beam Bending		EI_{zz}, Fore & Aft Bend.		JG, Torsional Stiffness	
in.	m	10^{10} lbs in^2	10^8 N m^2	10^{10} lbs in^2	10^8 N m^2	10^{10} lbs in^2	10^7 N m^2
0.0	0.0						
		6.747*	1.936*				
28.38	0.721						
		6.747*	1.936*				
55.00	1.397						
		5.614	1.611	10.043	2.882	2.420	6.945
88.38	2.245						
		4.429	1.271	7.952	2.282	2.002	5.745
150.53	3.823						
		3.142	.902	6.386	1.833	1.348	3.869
205.75	5.226						
		2.189	.628	4.491	1.289	.9548	2.740
259.53	6.592						
		1.494	.429	3.203	.919	.6853	1.967
308.53	7.837						
		.9476	.272	2.112	.606	.4810	1.380
363.53	9.234						
		.6386	.1833	1.494	.429	.3385	.9714
401.25	10.192						
		.4841	.1389	1.082	.311	.2503	.7183
436.00	11.074						
		.3502	.1005	.876	.251	.1887	.5415
478.07	12.143						
		.2575	.0739	.464	.133	.1309	.3757
531.16	13.491						
		.1802	.0517	.278	.0798	.0770	.2210
594.37	15.097						
		.144	.041	.206	.0591	.0470	.0135
635.64	16.145						

*Represented by an equivalent section in computer model.

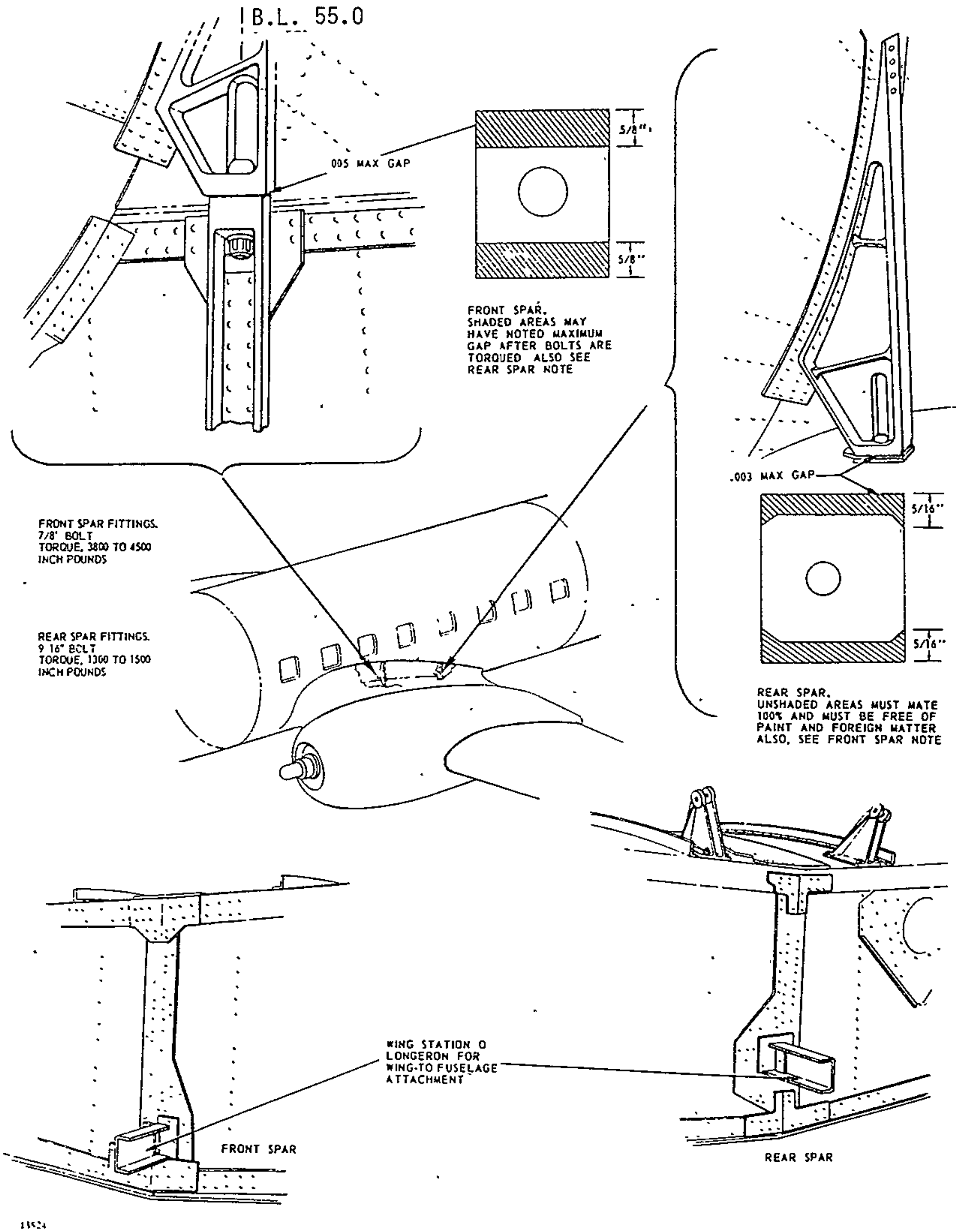

Figure 7 WING TO FUSELAGE ATTACHMENT

(a) SYMMETRIC BENDING OF TIFS WING

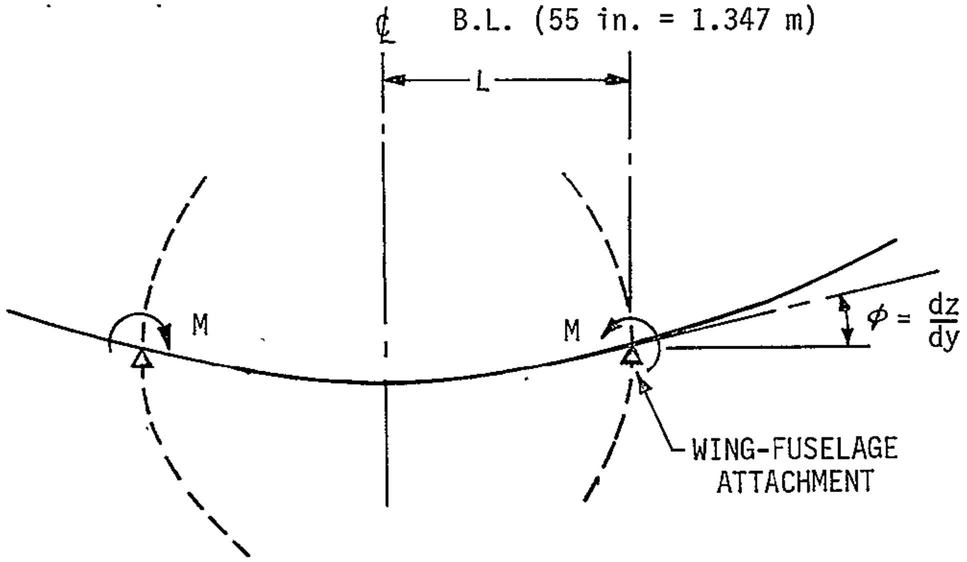

$$\phi_{TIFS} = \frac{LM}{(EI)_{TIFS}} = \text{SLOPE DUE TO BENDING}$$

$(EI)_{TIFS}$ = BENDING STIFFNESS OF CARRY-THROUGH STRUCTURE

(b) WING MODEL IN ATTACHMENT REGION

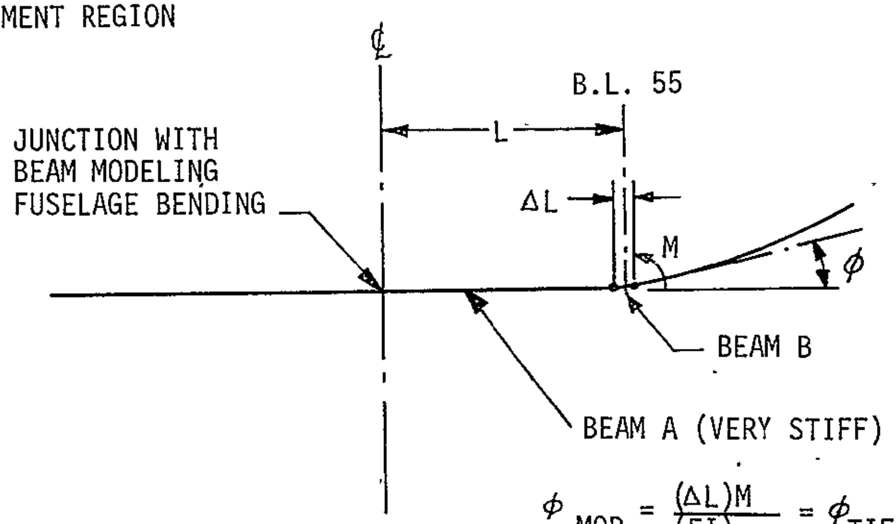

$$\phi_{MOD} = \frac{(\Delta L)M}{(EI)_{MOD}} = \phi_{TIFS}$$

$$\frac{(EI)_{MOD}}{(EI)_{TIFS}} = \frac{\Delta L}{L}$$

Figure 8 SIMULATION OF WING TO FUSELAGE ATTACHMENT on diagram (a), symmetric bending of TIFS was analyzed assuming that all wing shear is taken into the fuselage at the attachment (BL 55 in = 1.397 m). However, it is assumed that no wing bending moments are taken out at these fittings and that the bending moments for the left and right wings balance each other at the centerline.

The beam model representing the fuselage is at the centerline in diagram (b) of Figure 8. The inbound portion of the wing is simulated by two beams designated A and B. Beam A which extends from the centerline almost to B.L. (1.397 m) is assumed very stiff so that its deflections are negligible. A low bending stiffness is selected for beam B in order that the change in slope of the wing model due to bending will be the same as that for the actual TIFS wing at the spanwise location of the attachment fittings. However, beam B is so short that its deflection does not result in appreciable difference between the fuselage vertical deflection and the vertical deflection of the wing at the attachment.

2.3.2 Engine Sprung Weight, Engine Mounts Installation and Nacelle

The FLEXSTAB structural model developed for TIFS included modeling of motion of the engine sprung mass due to vibration isolator deflections. Results of vibration mode computation given in this report are limited to the case where the nacelle and engine isolators were assumed rigid. This was accomplished by assuming beams used to represent vibration isolators to be very stiff. Consequently, some of the parameters given below were not required but have been included to indicate how engine motions could be simulated in future computations with FLEXSTAB.

Figure 9 is a drawing of the engine mounts installation taken from the Allison/Convair maintenance manual. It shows the engine sprung weight system consisting of the propeller, transmission and engine which are supported by three Lord vibration isolators, two forward and one aft. Pertinent parameters are given below for the inertia properties, mount geometry, and isolator stiffnesses of this system.

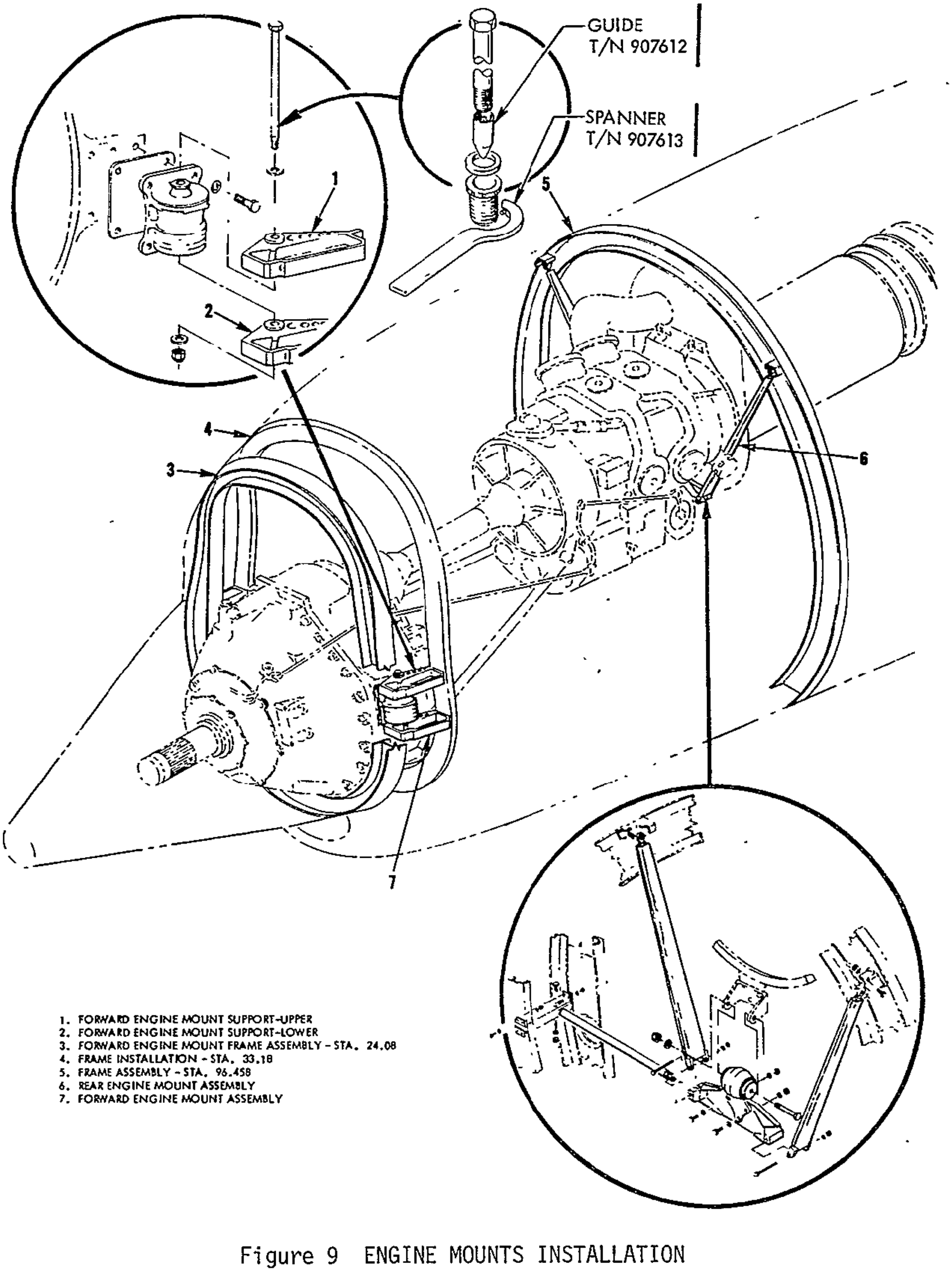

1. FORWARD ENGINE MOUNT SUPPORT-UPPER
2. FORWARD ENGINE MOUNT SUPPORT-LOWER
3. FORWARD ENGINE MOUNT FRAME ASSEMBLY - STA. 24.08
4. FRAME INSTALLATION - STA. 33.18
5. FRAME ASSEMBLY - STA. 96.458
6. REAR ENGINE MOUNT ASSEMBLY
7. FORWARD ENGINE MOUNT ASSEMBLY

Figure 9 ENGINE MOUNTS INSTALLATION

Inertia Properties of Sprung Weight

M = 1416.1 Kg (W = 3122 lbs)
I_{pitch} = 2128 Kg m^2
I_{yaw} = 2127 Kg m^2
I_{roll} = 295.9 Kg m^2
Ref. c.g. = (0.483 m) aft of reduction gear mount pad ℄
= (0.178 m) above power section centerline

Mount Geometry

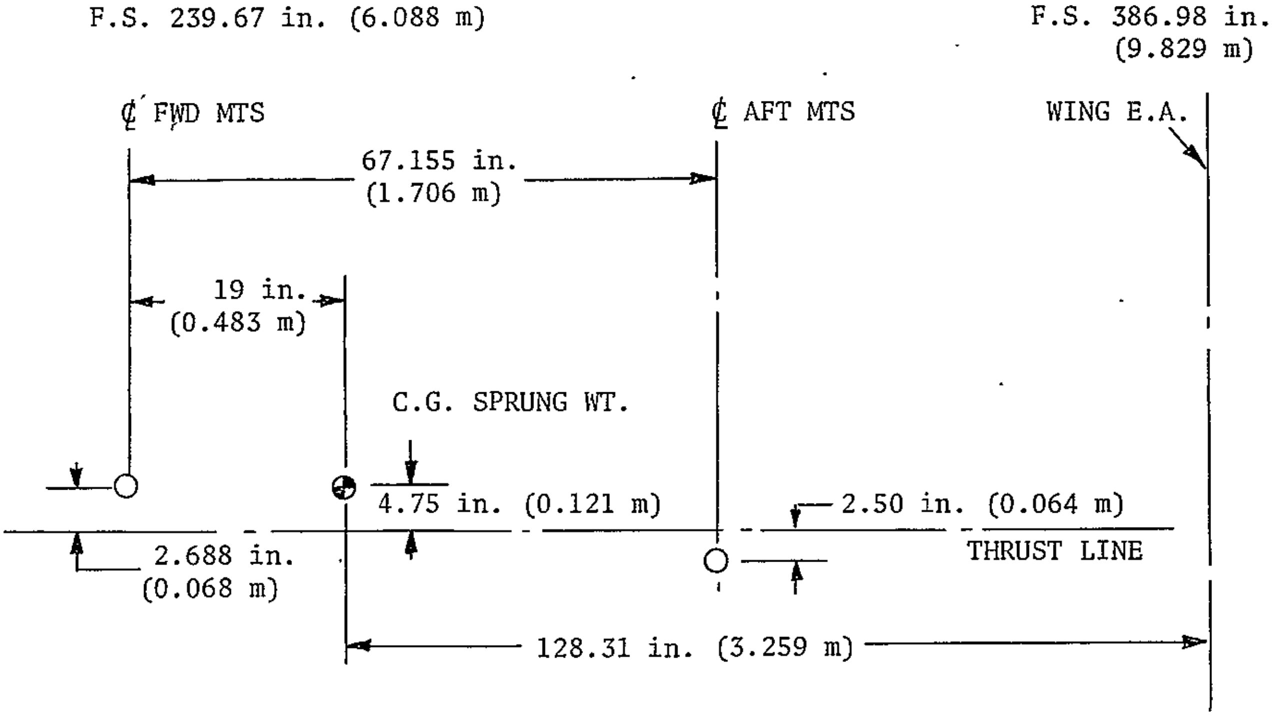

Vibration Mount Stiffnesses

Right front mt. (15.375 in. = 0.391m right of thrust line):

K_{vert} (static) = 13,000 lbs/in. = 2.28 x 10^6 N/m
K_{vert} (dynamic) = 17,000 lbs/in. = 2.98 x 10^6
$K_{fore\ \&\ aft}$ (static) = $K_{lateral}$ = 16,000 lbs/in. = 2.80 x 10^6
$K_{fore\ \&\ aft}$ (dynamic) = $K_{lateral}$ = 21,000 lbs/in. = 3.68 x 10^6

Left front mt. (15.375 in. = 0.391m left of thrust line):

Same as for right front mount.

Aft mt. (On thrust line):

K_{vert} (static) = 10,000 lbs/in. = 1.75 x 10^6 N/m
K_{vert} (dynamic) = 13,000 lbs/in. = 2.28 x 10^6
$K_{lateral}$ (static) = 12,000 lbs/in. = 2.10 x 10^6
$K_{lateral}$ (dynamic) = 15,000 lbs/in. = 2.63 x 10^6

Since only simple beam finite elements are used in the ISIC program of FLEXSTAB, it was not possible to model all six rigid body degrees of freedom of the sprung weight as restrained by the vibration isolators. However, the vertical and side translation degrees of freedom could be represented by the model indicated on the sketch below where the sprung weight system is treated as a concentrated mass.

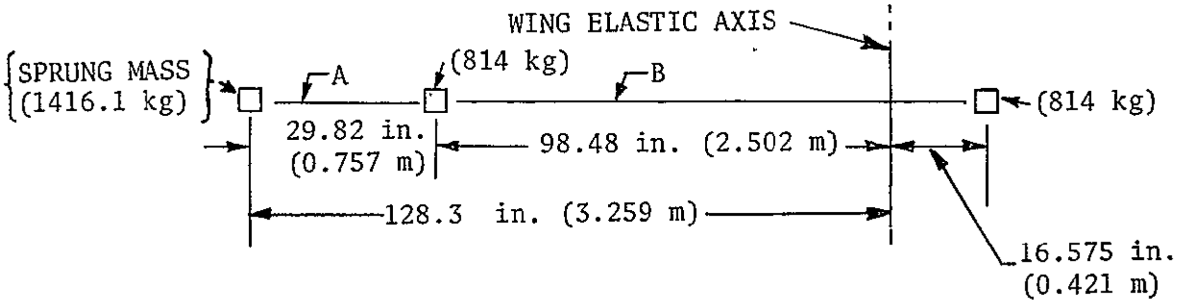

A — Beam representing vertical and lateral stiffness of vibration isolators

B — Rigid beam connecting dumbbell masses

The effect of the concentrated sprung mass of 1416.1 Kg (W = 3122 lbs) was subtracted from the total inertia properties distributed to wing Sta. 150.53 in. (3.823m) as follows and the remaining properties were represented by the dumbbell masses indicated in the sketch.

	Weight [Mass]	Unbalance About EA	Moment of Inertia About EA
Total at Sta. 150.53 (from Table 2)	6711 (lbs) [3044 (Kg)]	-547529 (in.lbs) [- 6308 (m Kg)]	69287156 (lbs in^2) [20276 (Kg m^2)]
Effect of concentrated engine mass	3122 (lbs) [1416.1 (Kg)]	-400553 (in.lbs) [- 4615 (m Kg)]	51390898 (lbs in^2) [15039 (Kg m^2)]
Remaining properties which were represented by dumbbell masses	3589 (lbs) [1627.9 (Kg)]	-146976 (in.lbs) [- 1693 (m Kg)]	17896257 (lbs in^2) [5237 (Kg m^2)]

The required vertical bending stiffness of beam "A" in the sketch to represent the dynamic properties of the vibration isolators is as follows:

$$K_{vert}(\text{Total}) = (2 \times 17{,}000) + 13{,}000 = 47{,}000 \text{ lbs/in.}$$

$$(EI_{yy}) = \text{vertical bending stiffness of beam "A"}$$

$$= \ell^3 K/3 = (47{,}000)(29.82)^3/3 = 4.15 \times 10^8 \text{ lbs. in}^2$$

$$= 1.194 \times 10^6 \text{ N m}^2$$

The uncoupled vertical vibration frequency of the sprung weight on beam A is then,

$$f_{vert} = \frac{1}{2\pi} \sqrt{\frac{(47000)(386)}{3122}} = 12.13 \text{ Hz.}$$

Similar computations for the lateral stiffness give,

$$K_{lat}(\text{Total}) = (2 \times 21000) + 15000 = 57000 \text{ lbs/in.}$$

(EI_{33}) = Required lateral bending stiffness of beam A
—— —— = 5.03×10^8 lbs in^2 (1.448×10^6 N m^2)
f_{lat} = 13.36 Hz = uncoupled lateral vibration frequency of sprung weight on vibration isolators .

2.3.3 Fuselage Parameters

The development of TIFS involved extensive structural modifications affecting both the stiffness and weight distributions of the fuselage. Installation of special electronic equipment made further changes in weight distribution.

Table 4 presents the fuselage mass distribution used in the present report in preparing inputs for FLEXSTAB. It was obtained by redistributing the panel point masses to fuselage stations located at 1.5 m intervals along the fuselage axis. As noted, the distribution does not include the weights of the horizontal and vertical tails. The last column gives the distributed masses for one side of the fuselage as required for the ISIC inputs.

The representation of the fuselage by concentrated masses along its axis is an approximation since there are mass moments of inertia for each fuselage section associated with each concentrated mass. However, these section moments of inertia are not given because they are neglected in the ISIC program.

Figure 10 shows plots of the effective structure moments of inerti used in computing fuselage vertical and lateral bending stiffnesses while Figure 11 gives a plot of the factor J used in computing fuselage torsional stiffness. These curves were approximated by a series of steps in treating

TABLE 4

FUSELAGE MASS DISTRIBUTION*

Sta. (in)	X‡ (in)	X‡ (m)	Weight (lbs) (Both Sides)	M(kg) (One Side)
-117.82	19.69	.5	432.1	98.0
- 78.44	59.06	1.5	604.1	137.0
- 19.38	118.12	3.0	1708.9	387.6
+ 39.68	177.18	4.5	1866.2	423.2
+ 98.74	236.24	6.0	2922.1	662.7
+157.80	295.30	7.5	1824.4	413.8
+216.86	354.36	9.0	1324	300.3
275.92	413.42	10.5	1116.9	253.3
334.98	472.48	12	1422.5	322.6
394.04	531.54	13.5	1278.5	290.0
453.10	590.60	15	2022.2	458.6
512.16	649.66	16.5	1197.5	271.6
571.22	708.72	18	1744.6	395.7
630.28	767.78	19.5	1826.3	414.2
689.34	826.84	21	1619.9	367.4
748.40	885.96	22.5	1469.7	333.3
807.46	944.96	24	1136.4	257.7
866.52	1004.02	25.5	994.2	225.5
949.11	1086.61	27.6	155.8	35.3
			26666.0	6047.8

*Does not include horizontal or vertical tail

‡X - Fus. Sta. = 137.5 in. = 3.493 m

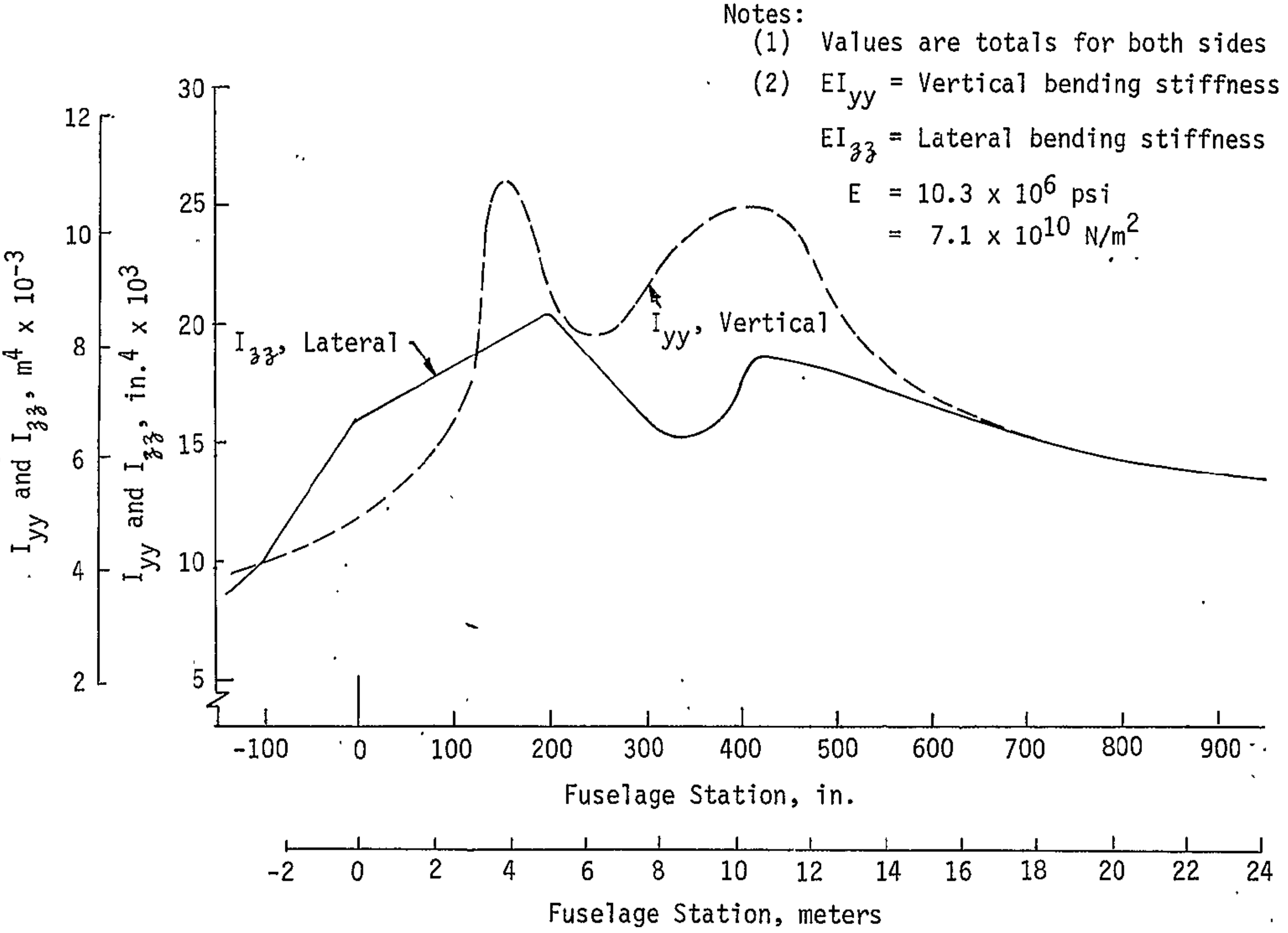

Notes:
(1) Values are totals for both sides
(2) EI_{yy} = Vertical bending stiffness
EI_{zz} = Lateral bending stiffness
$E = 10.3 \times 10^6$ psi
$= 7.1 \times 10^{10}$ N/m^2

Figure 10 TIFS EFFECTIVE AREA MOMENTS OF INERTIA USED IN COMPUTING FUSELAGE VERTICAL AND LATERAL BENDING STIFFNESSES

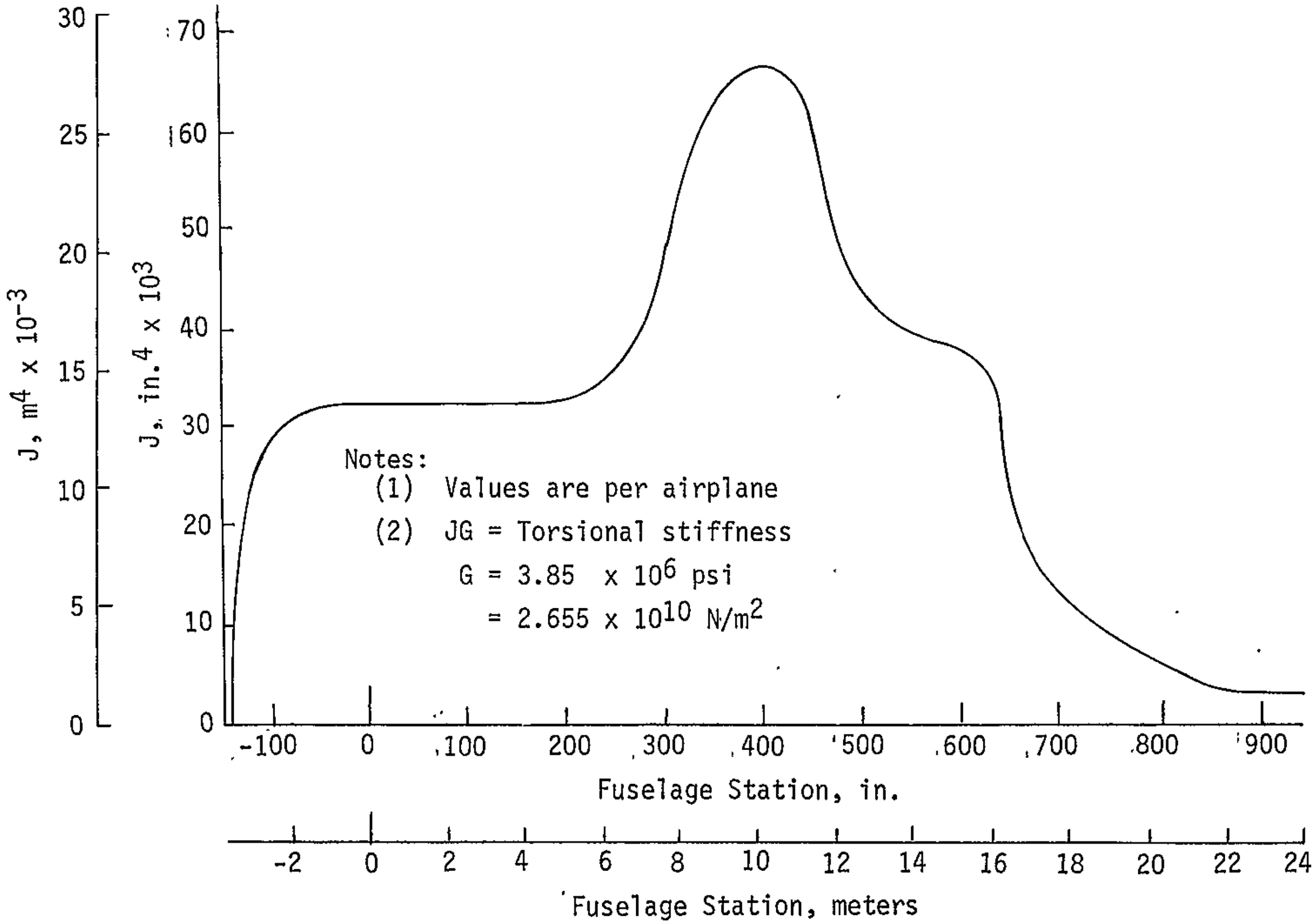

Notes:
(1) Values are per airplane
(2) JG = Torsional stiffness
$G = 3.85 \times 10^6$ psi
$= 2.655 \times 10^{10}$ N/m^2

Figure 11 TIFS FUSELAGE TORSIONAL STIFFNESS FACTOR, J (Reference 11) the fuselage as a series of finite element beams each one having constant stiffness. Table 5 indicates the stiffnesses used in this approximation.

It will be noted that the vertical, lateral, and torsional stiffnesses given in the last three columns of Table 5 are for both sides of the fuselage. The ISIC program requires fuselage stiffnesses for both sides as inputs while the mass inputs are for only one side.

2.3.4 Parameters for Side Force Surfaces (SFS)

Table 6 presents SFS inertia distributions which were used for both the upper and lower SFS vanes. Both the unbalance and moments of inertia are given about the SFS pivot or hinge line which was taken to be the SFS elastic axis. A dumbbell representation of this data is also presented for use in FLEXSTAB.

The structural model for the SFS's used finite elements which permitted torsion about their elastic axes and transverse bending. However, the following stiffness data are only given for future reference and were not used for the structural mode computations discussed in this report. The computations were carried out assuming the side force surfaces to be effectively rigid and substituting very high stiffnesses for the finite elements.

Bending and torsional stiffnesses of the SFS's were approximated by a series of steps giving constant stiffness parameters between the stations to which the inertia parameters were distributed. These results are given in Table 7.

The computed cantilever bending frequency for the SFS was 52.68 Hz while vibration test results (Reference 12) gave a SFS bending or rocking

---

Ref. 12. Balcerack, J. C. and White, Jr., R. P.: "Ground Vibration Tests, AF/TIFS Convair 580 Airplane", RASA Report 71-06, May 1971. NASA CR-158895.

TABLE 5 - FUSELAGE STIFFNESSES (TOTALS FOR BOTH SIDES)

X* (m)	Vertical Bending $EI_{yy} \times 10^{-8}$ (Nm^2)	Lateral Bending $EI_{zz} \times 10^{-8}$ (Nm^2)	Torsion $JG \times 10^{-8}$ (Nm^2)
0.0			
	2.953	2.923	2.798
1.5			
	3.254	3.978	3.626
3.0			
	3.616	4.882	3.637
4.5			
	4.309	5.273	3.637
6.0			
	6.268	5.665	3.660
7.5			
	7.051	6.027	3.716
9.			
	5.966	5.544	4.052
10.5			
	6.509	4.821	5.451
12			
	7.352	4.761	7.163
13.5			
	7.443	5.484	7.275
15			
	6.629	5.454	5.540
16.5			
	5.635	5.743	4.533
18.			
	5.123	5.002	4.205
19.5			
	4.821	4.761	2.451
21.			
	4.550	4.520	1.242
22.5			
	4.369	4.369	.8394
24			
	4.249	4.249	.5260
25.5			
	4.188	4.188	.3917
27.623			

*X - Fus. Sta. (m) = 3.493 m

TABLE 6

SFS MASS DISTRIBUTION (Upper or Lower Vane)

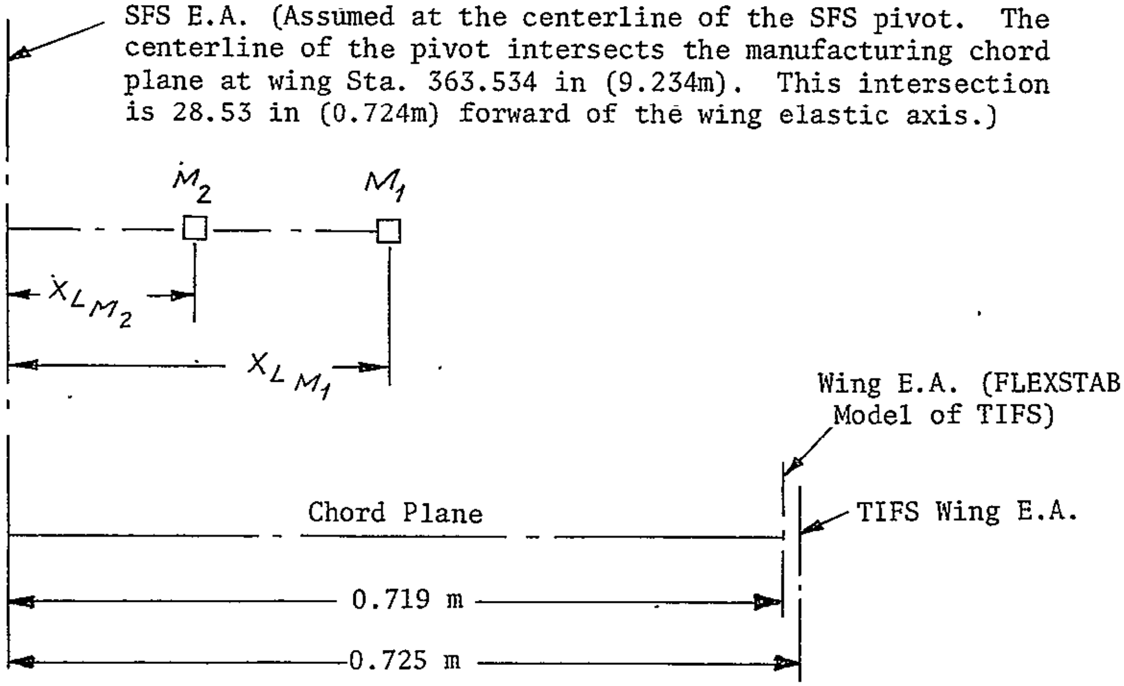
SFS E.A. (Assumed at the centerline of the SFS pivot. The centerline of the pivot intersects the manufacturing chord plane at wing Sta. 363.534 in (9.234m). This intersection is 28.53 in (0.724m) forward of the wing elastic axis.)

SFS STA.		Weight	Mom. About H.L. (Tail Heavy)	Mom. of Inertia About H.L.	FLEXSTAB PARAMETERS		
(in)	(M)	(lbs)	(in. lbs.)	(lbs. in^2)	X_{LM_2} (m)	X_{LM_1} (m)	$M_1 = M_2$ Kg
7.75	0.197	26.41	63.9	3157	-0.209	0.332	5.989
15.00	0.381	15.73	138.7	3883	-0.106	0.554	3.568
25.00	0.635	34.56	291.1	3490	0.075	0.353	7.838
42.50	1.080	0.77	81.5	1800	-0.074	0.458	2.443
55.00	1.397	11.79	82.0	1500	-0.049	0.402	2.674
70.00	1.778	6.26	39.5	1020	-0.122	0.442	1.420
82.50	2.096	1.12	6.3	180	-0.146	0.431	0.259
							24.186

TABLE 7

SFS STIFFNESS PROPERTIES

(UPPER OR LOWER VANES)

SFS	Sta	EI, Bending Stiffness		GJ, Torsional Stiffness	
(in.)	(m)	(lbs in^2)	(N m^2)	(lbs in^2)	(N m^2)
0					
		$.294 \times 10^{8}$ ‡	8.43×10^{4} ‡	4.7×10^{8}	1.35×10^{6}
7.75	0.197				
		5.4×10^{8}	1.55×10^{6}	4.05×10^{8}	1.16×10^{6}
15.00	0.331				
		4.7×10^{8}	1.35×10^{6}	3.30×10^{8}	9.47×10^{5}
25.0	0.635				
		3.8×10^{8}	1.09×10^{6}	2.30×10^{8}	6.6×10^{5}
42.5	1.080				
		2.0×10^{8}	5.7×10^{5}	1.0×10^{8}	2.9×10^{5}
55.0	1.397				
		1.2×10^{8}	3.4×10^{5}	$.45 \times 10^{8}$	1.29×10^{5}
70.0	1.778				
		$.05 \times 10^{8}$	1.4×10^{4}	$.08 \times 10^{8}$	2.3×10^{4}
82.5	2.096				
		$.04 \times 10^{8}$	1.1×10^{4}	$.07 \times 10^{8}$	2.0×10^{4}
85.0	2.159				

‡ Effective value accounting for flexibility of bearing housing attachment.

frequency of only 16.7 Hz. It is believed that this discrepancy was caused by flexibility in the attachment of the SFS bearing housing to the wing and was accounted for by reducing the effective stiffness of the inboard section of the SFS model.

No correction was made to the computed SFS torsional stiffness because the measured torsional frequency of 52.68 Hz is above the frequency range of interest in the current program.

2.3.5 Horizontal and Vertical Tail Parameters

Horizontal and vertical tail parameters are based on data given in Reference 11. Inertia parameters from this report were represented by dumbbells for convenience in preparing ISIC inputs to the FLEXSTAB program.

The elastic axis of the horizontal tail is modeled by two segments as shown in the sketch on Table 8. A rigid segment perpendicular to the plane of symmetry extends out to the stabilizer-fuselage attachment where it joins a second segment at Fuselage Sta. 836.532 in. (21.248 m) and Body line 38.938 in. (0.989 m). The second segment is inclined aft at an angle of 7.07° and is at approximately 49% of the portion of the chord forward of the elevator hinge line.

Table 8 indicates the positions and properties of the dumbbells used to represent the inertia parameters of the horizontal tail. The most inboard dumbbell is located 3.5 in (.089 m) inboard of the connection between the elastic axis segments. The remaining dumbbells are all on the outer segment.

Figure 12 presents plots of the structural moments of inertia, I, and torsional stiffness factor, J, used in computing the out-of-plane bending stiffness (EI) and torsional stiffness (GJ) of the horizontal tail. The

---

Ref. 11. Rodriguez, M. B.: "Commercial Total In-Flight Simulator Empennage Flutter Analysis," General Dynamics Convair Division Report GDE-DDE-69-001, 13 March 1969. NASA CR-158894.

TABLE 8

HORIZONTAL TAIL INERTIA PROPERTIES*

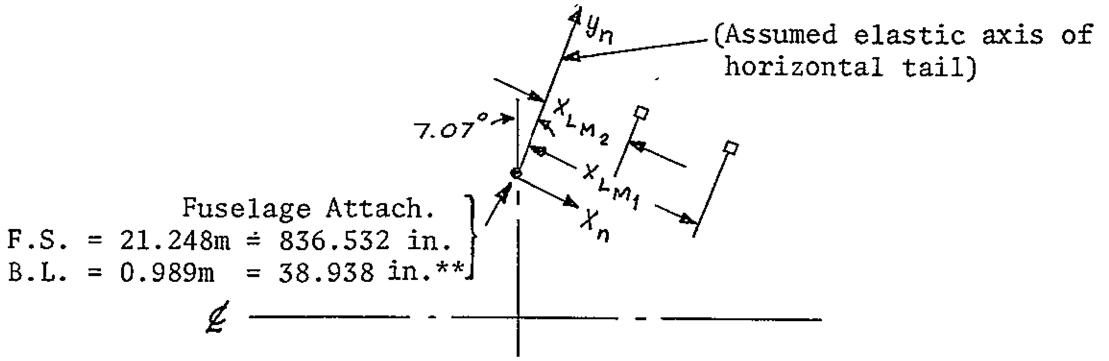

y_n		x_{LM_1}		x_{LM_2}		$M_1 = M_2$	
(in)	(m)	(in)	(m)	(in)	(m)	(lb m)	(Kg)
†		27.60	.701	-17.81	-.452	22.7	10.30
11.22	0.285	38.13	.968	- 1.82	-.0462	40.1	18.18
39.75	1.010	35.49	.901	- .61	-.0155	41.75	18.94
68.22	1.733	30.28	.769	- 2.66	-.0676	32.25	14.62
96.70	2.456	27.07	.688	- 1.47	-.0373	27.0	12.24
125.19	3.180	22.54	.573	- 2.39	-.0607	19.7	8.93
153.62	3.902	19.06	.484	- 3.54	-.0899	13.9	6.30
182.14	4.626	15.64	.410	- 3.36	-.098	6.2	7.82
192.87	4.899	17.60	.447	- 2.95	-.0749	2.16	.98
							93.31

* Based on data from Ref. 11.

† Assumed to act as dumbbell parallel to ℄ and rigidly attached to fuselage 3.5 in (.089m) inboard of indicated fuselage attachment.

** In FLEXSTAB model of TIFS attachment point moved outboard to body line 64.605 in (1.641m).

(Reference 11)

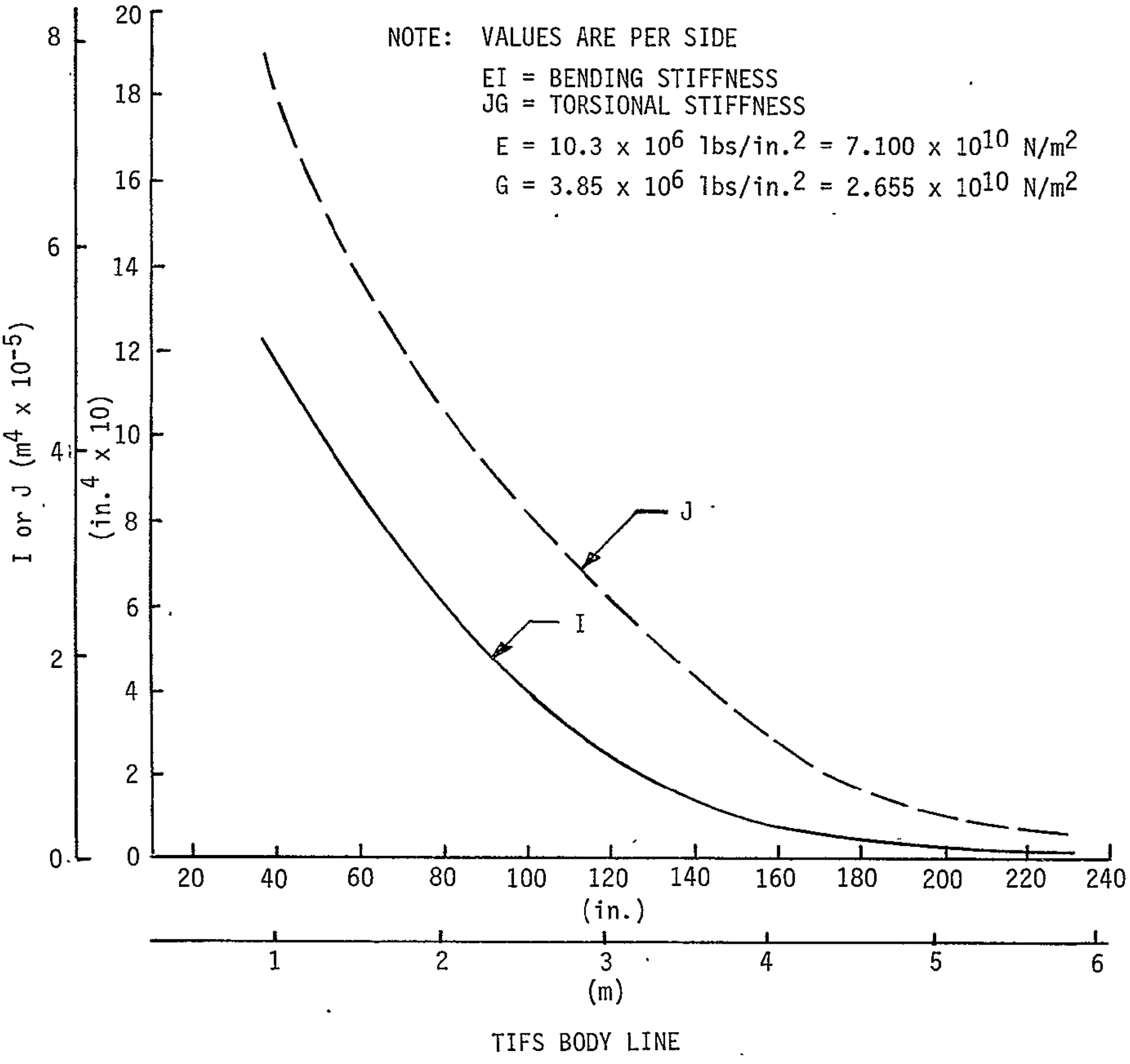

Figure 12 ACT TIFS HORIZONTAL TAIL STIFFNESS

abcissa on this figure is the body line or distance outboard of the plane of symmetry as measured on the actual TIFS airplane. In the FLEXSTAB model of TIFS, the root of the horizontal tail is moved outboard for aerodynamic reasons by extending the rigid segment of the elastic axis by 25.667 in. (0.652 m). This extension acts as a portion of the fuselage and has no effect on the computed symmetric vibration modes.

The elastic axis for the vertical tail is represented by two segments as shown in the sketch on Table 9. The inboard rigid segment runs up perpendicular to the fuselage axis to the vertical tail-fuselage attachment. It joins the second segment at Fuselage Sta. 827.4 in. (21.016 m) and waterline 94.788 in. (2.408 m). The second segment which is inclined aft at 12.57° is at approximately 48% of the portion of the chord forward of the rudder hinge line. Table 9 gives the positions and properties of the dumbbells used to represent inertia parameters of the vertical tail. The structural moments of inertia, I, for out-of-plane bending and the torsion constant, J, for the vertical tail are plotted on Figure 13 as a function of the waterline. The bending stiffness (EI) and torsional stiffness (GJ) of the vertical tail were computed using these factors.

Mass Summary

A summary of the component masses for the TIFS airplane which were given previously is listed below:

1/2 Wing (excluding engine and nacelle) = 2 x 1427.4 = 2854.8 Kg
One engine and nacelle (one side) = 3044.1 Kg
1/2 Fuselage = 6047.8 Kg
Upper SFS (one side) = 2 x 24.186 = 48.4 Kg
Lower SFS (one side) = 2 x 24.186 = 48.4 Kg
Horizontal Tail (one side) = 2 x 93.31 = 186.6 Kg
Vertical Tail (one side) = 2 x 59.93 = 119.9 Kg
Total (one side) = 12,350.0 Kg
=(27,227.1 lbs)

TABLE 9

VERTICAL TAIL INERTIA PROPERTIES*

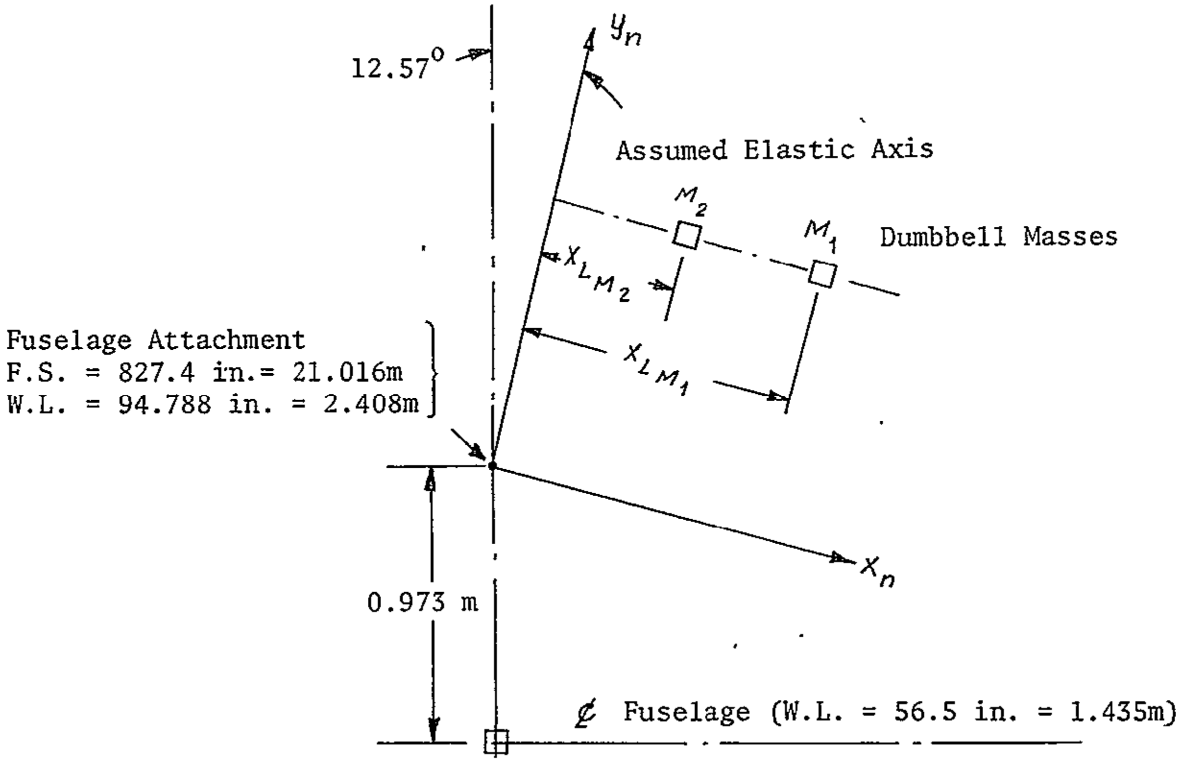

y_n		X_{LM_1}		X_{LM_2}		$M_1 = M_2$	
(in)	(m)	(in)	(m)	(in)	(m)	(lb m)	(Kg)
9.630	.245	52.24	1.327	-30.30	- .770	30	13.61
32.911	.836	56.56	1.429	-22.47	-0.571	24.4	11.07
57.757	1.467	46.15	1.172	-19.86	-0.428	20.1	9.12
83.582	2.123	38.31	0.973	-14.73	-0.374	16.35	7.42
108.019	2.744	32.46	0.824	- 9.32	-0.237	13.75	6.24
136.014	3.455	24.77	0.629	- 1.42	-0.036	15.95	7.23
164.300	4.173	18.36	0.466	+ 1.40	+0.025	11.55	5.24
							59.93

*Based on data from Ref. 11 (Values are for one side).

In FLEXSTAB model of TIFS attachment point moved up to water line 124.703 in. = 3.167m to put vertical tail above fuselage interference body.

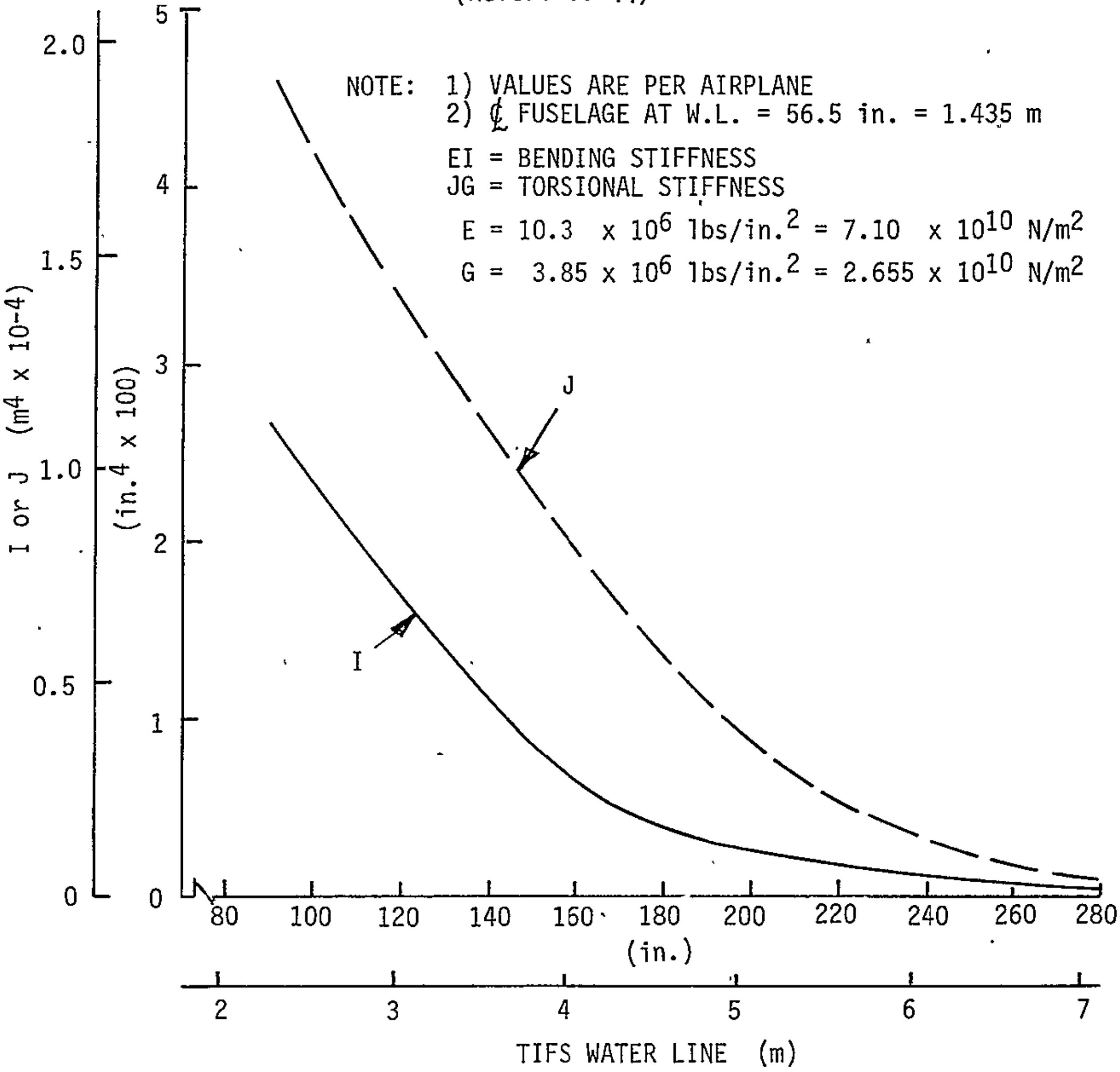
(Reference 11)

NOTE: 1) VALUES ARE PER AIRPLANE
2) ℄ FUSELAGE AT W.L. = 56.5 in. = 1.435 m

EI = BENDING STIFFNESS
JG = TORSIONAL STIFFNESS
$E = 10.3 \times 10^6$ lbs/in.^{2} = 7.10×10^{10} N/m^2
$G = 3.85 \times 10^6$ lbs/in.^{2} = 2.655×10^{10} N/m^2

Figure 13 ACT TIFS VERTICAL TAIL STIFFNESS

2.3.6 Results of Frequency and Mode Shape Computation Performed With the FLEXSTAB Program

Table 10 summarizes natural frequencies for the first seven symmetric vibration modes of the TIFS airplane which were computed with the FLEXSTAB program assuming high rigidity for the nacelles and SFS's. These modes are believed sufficient to represent dynamic responses in the frequency range where control by collective ailerons, DLF's and/or elevators is feasible. The effect of deflections in higher frequency modes was treated quasi-statically by utilizing the Residual-Elastic option of FLEXSTAB.

The computed modes are "free-free" modes for the entire airplane and involve motions of all structural components. Nevertheless, it is sometimes helpful to characterize the motions in the various modes although admittedly a somewhat arbitrary procedure. This has been done on the table which indicates characteristic and auxiliary motions.

Figures 13 to 19 present isometric sketches of the various modes which were drawn from modal deflections found in the FLEXSTAB computations. Some intuition concerning the relative effectiveness of the various control surfaces for controlling these seven modes can be obtained from an examination of the drawings. In general, the vibration amplitudes of the TIFS airplane are comparatively small and can be treated adequately with linear analyses. However, the vibration amplitudes on the sketches have been greatly exaggerated in order to indicate small motions which would otherwise not be visible. Motions of the SFS's and vertical tail have been omitted to simplify the drawings.

The output of the Normal Modes program of FLEXSTAB gives the modal displacements and rotations at each aerocentroid used in the aerodynamic model. The motion at a few of these aerocentroids are indicated with arrows on the figures.

TABLE 10

TIFS SYMMETRIC VIBRATION MODES COMPUTED WITH FLEXSTAB

SYM MODE NO.	FREQUENCY (Hz) RIGID NACELLE & SFS'S	CHARACTERISTIC MOTION	SECONDARY MOTION
1	3.02	1st Wing Bending	Fus. & H. T. Bending
2	4.65	1st Wing Torsion	Wing, Fus., & H. T. Bending
3	6.09	1st Fus. Bending in Phase With H. T. Bending	Wing Bending
4	6.90	H. T. Bending Out of Phase With 1st Fus. Bending	Wing Bending
5	9.01	2nd Wing Bending	Fus. & H. T. Bending
6	15.10	2nd Fus. & H. T. Bending	Wing Bending and Torsion
7	17.25	Outer Wing Panel Bending and Torsion	

f_1 = 3.02 Hz (Symmetric)

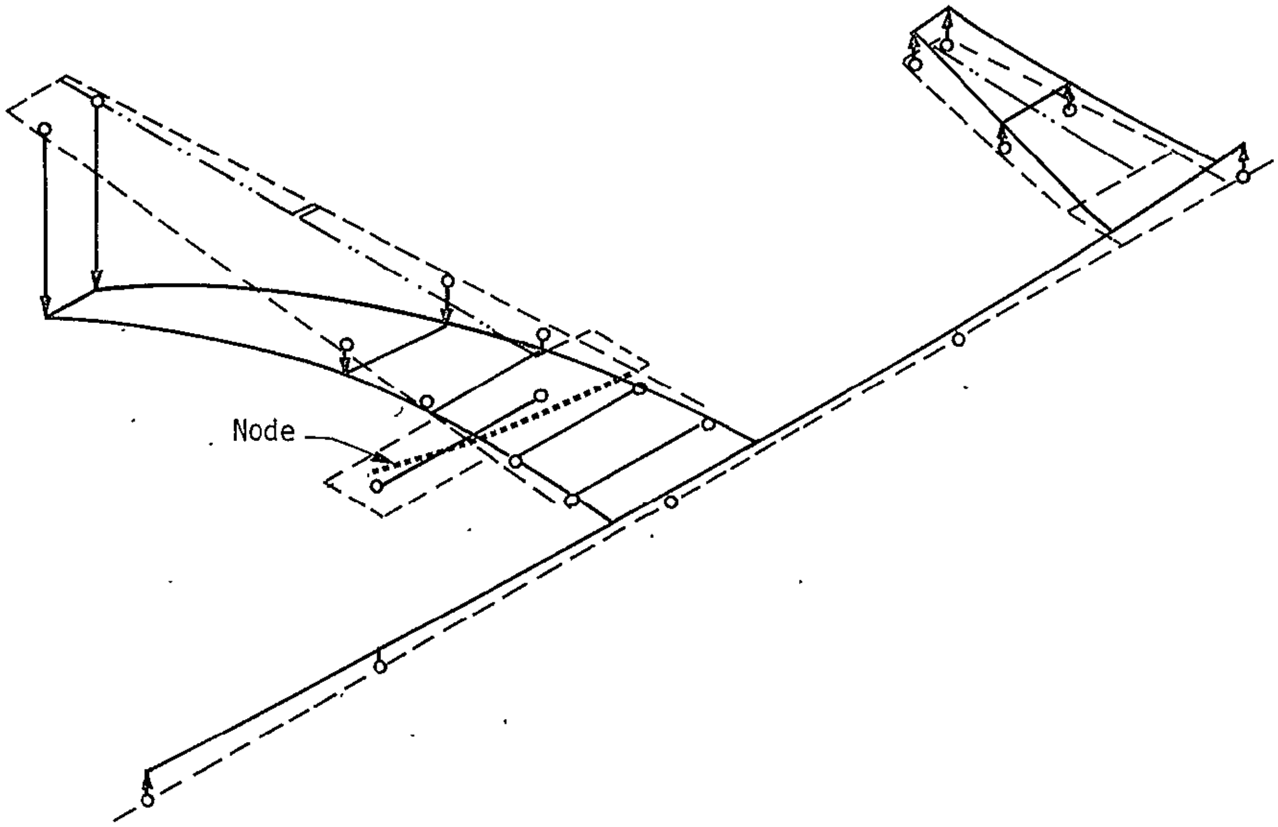

Figure 14 1st Wing Bending

$f_2 = 4.65$ Hz (Symmetric)

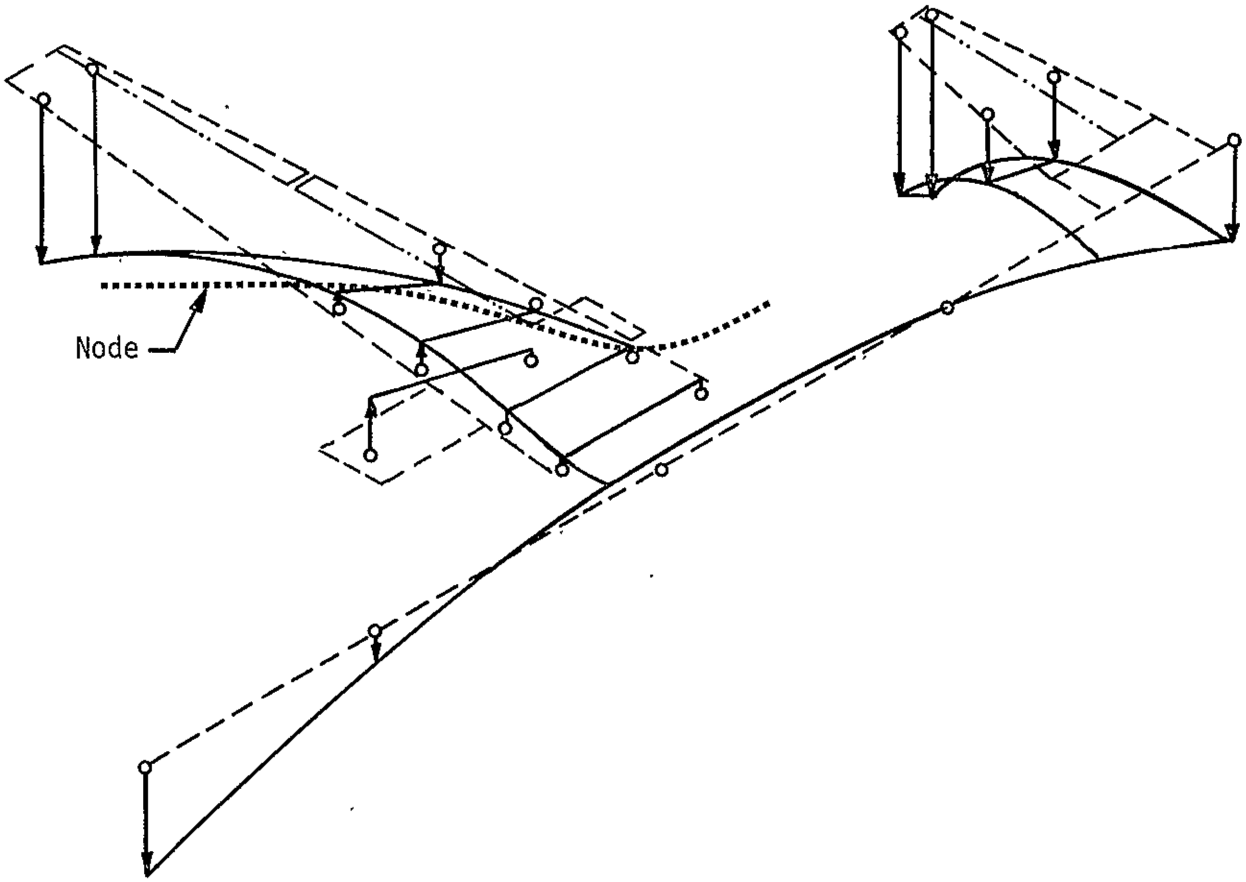

Figure 15 1st WING TORSION COUPLED WITH WING, FUSELAGE, AND HORIZONTAL TAIL BENDING

$f_3 = 6.09$ Hz (Symmetric)

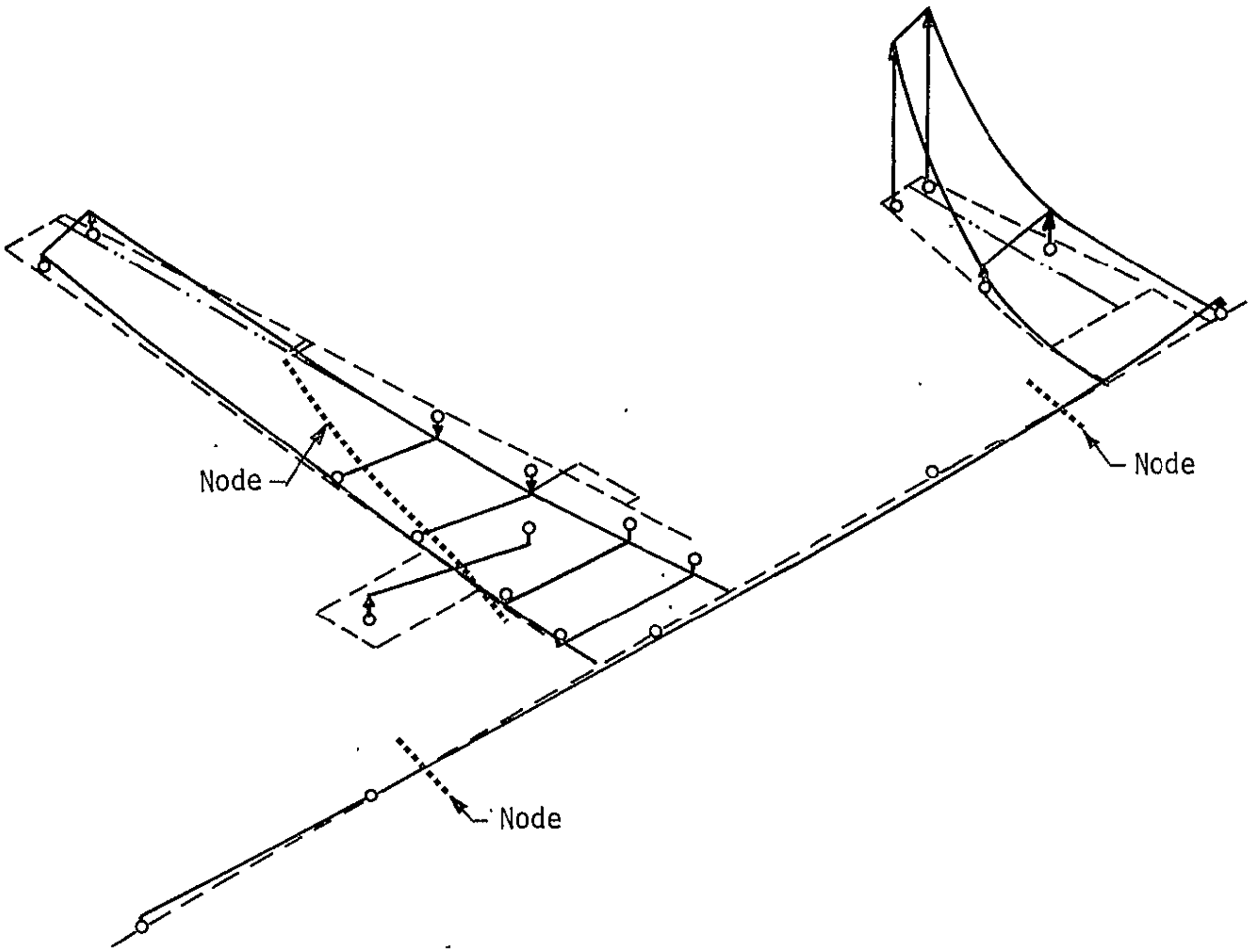

Figure 16 FIRST FUSELAGE BENDING IN PHASE WITH HORIZONTAL TAIL BENDING, WING BENDING

f_4 = 6.90 Hz (Symmetric)

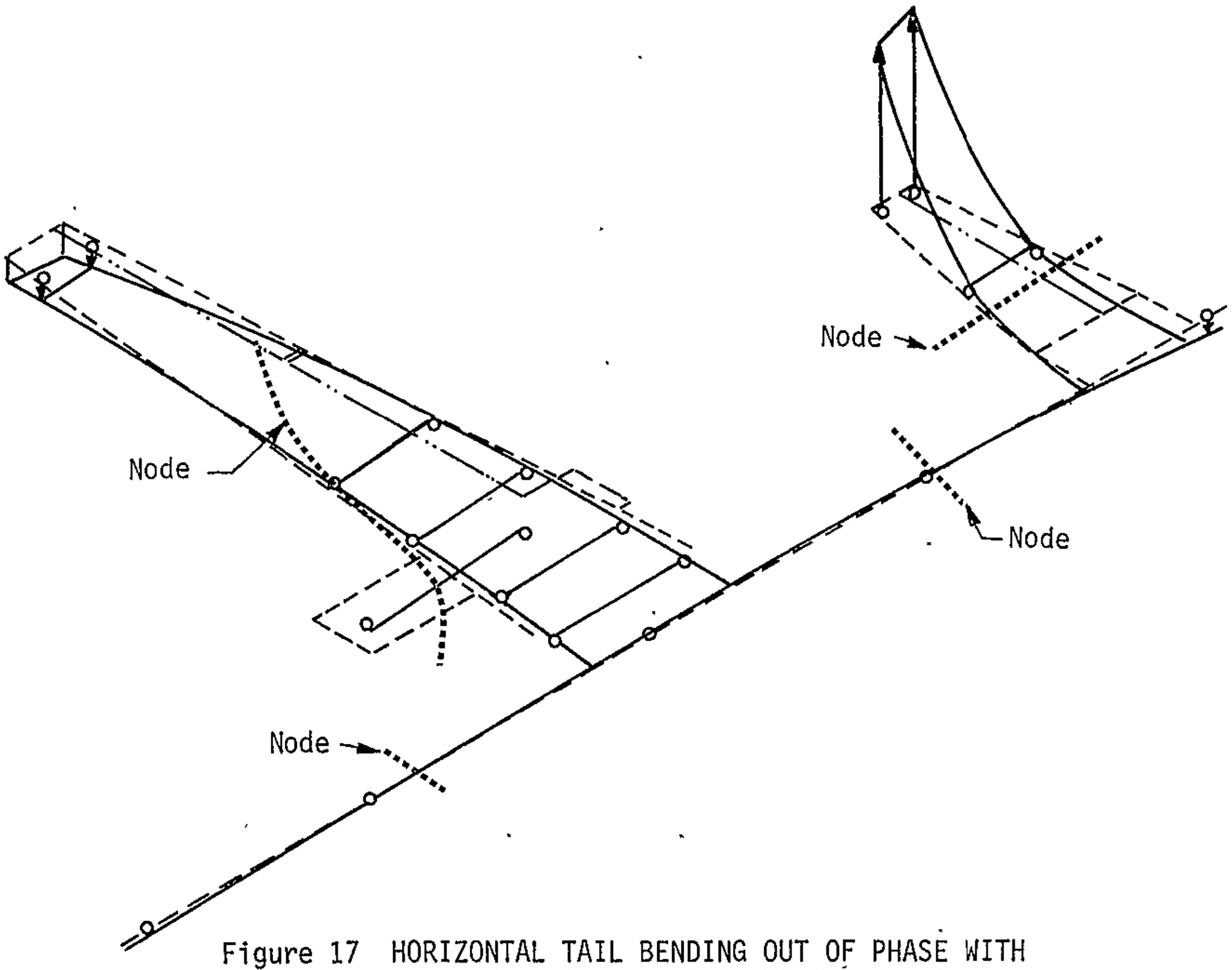

Figure 17 HORIZONTAL TAIL BENDING OUT OF PHASE WITH FIRST FUSELAGE BENDING, WING BENDING

f_5 = 9.01 Hz (Symmetric)

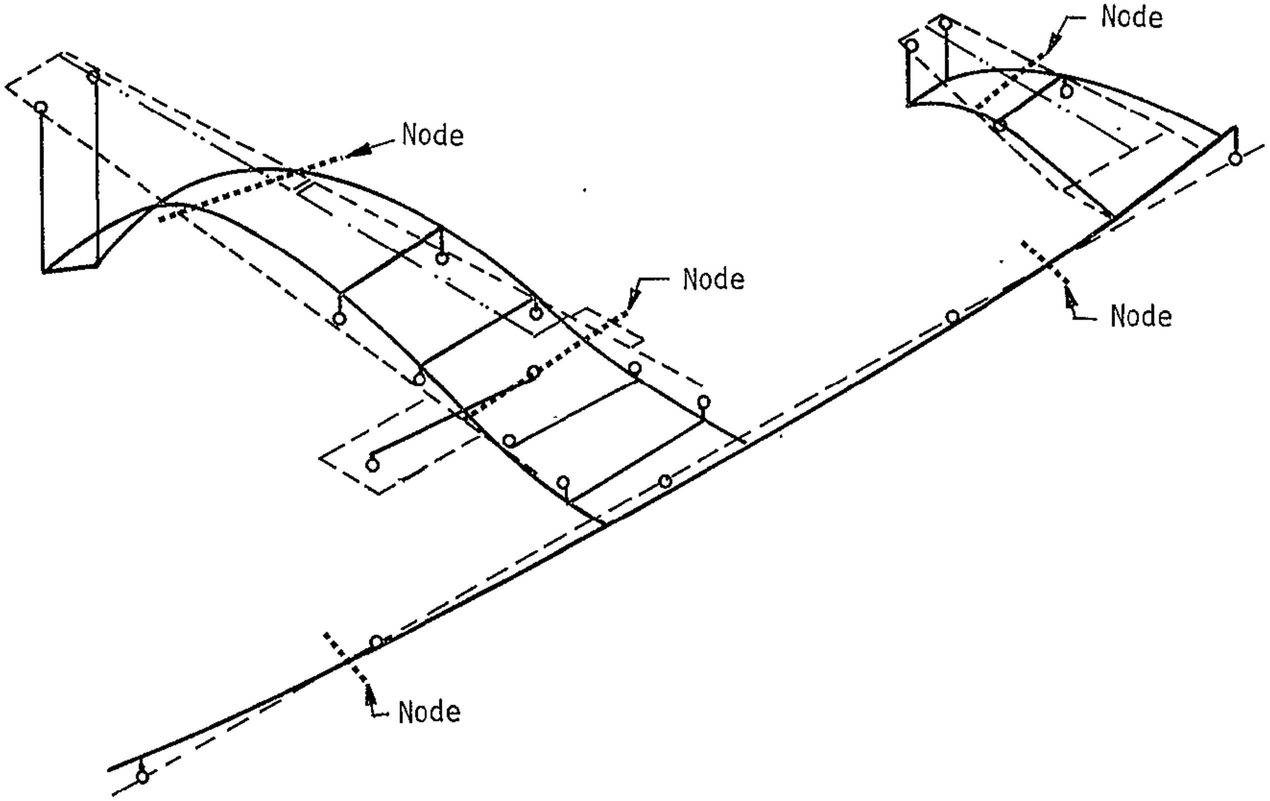

Figure 18 2nd WING BENDING COUPLED WITH FUSELAGE AND HORIZONTAL TAIL BENDING

$f_6 = 15.10$ Hz (Symmetric)

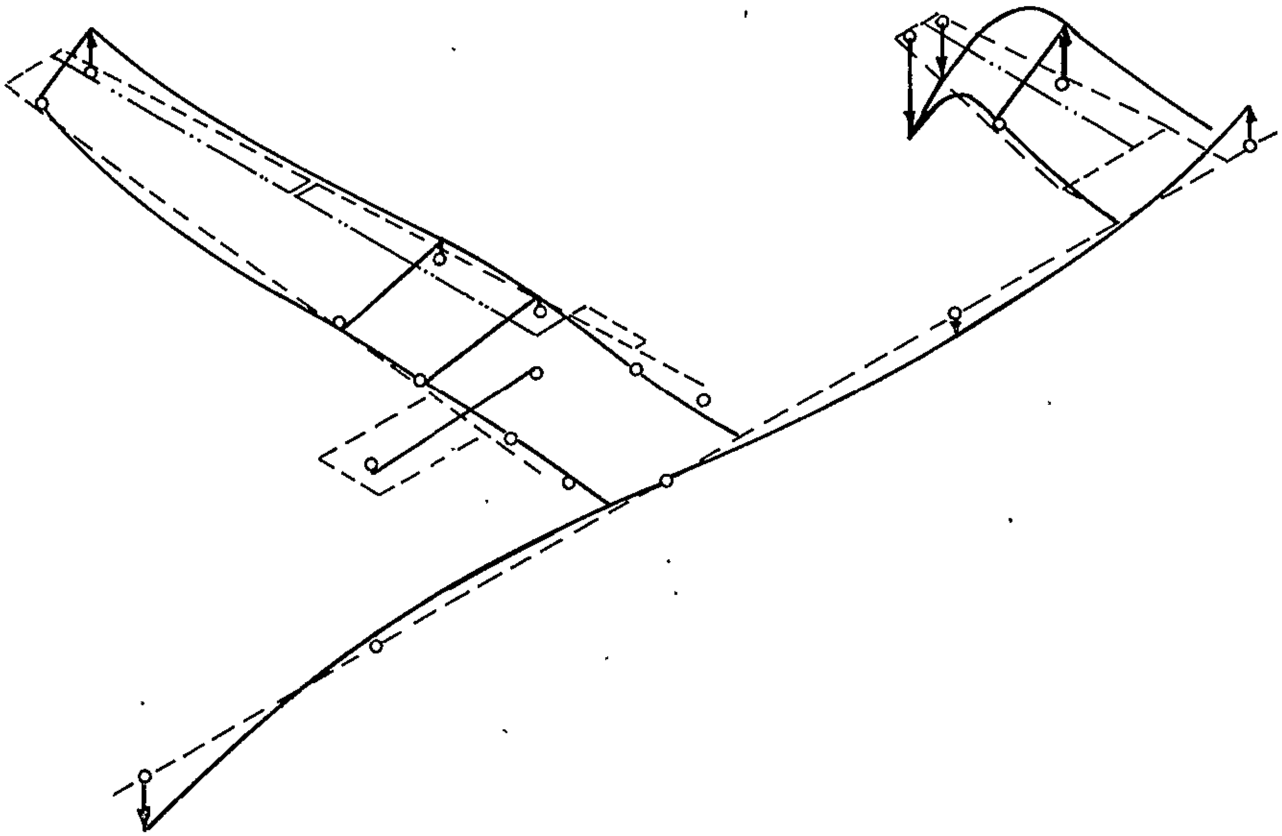

Figure 19 2nd FUSELAGE BENDING AND 2nd HORIZONTAL TAIL BENDING COUPLED WITH WING BENDING AND TORSION MOTION

f_7 = 17.25 Hz (Symmetric)

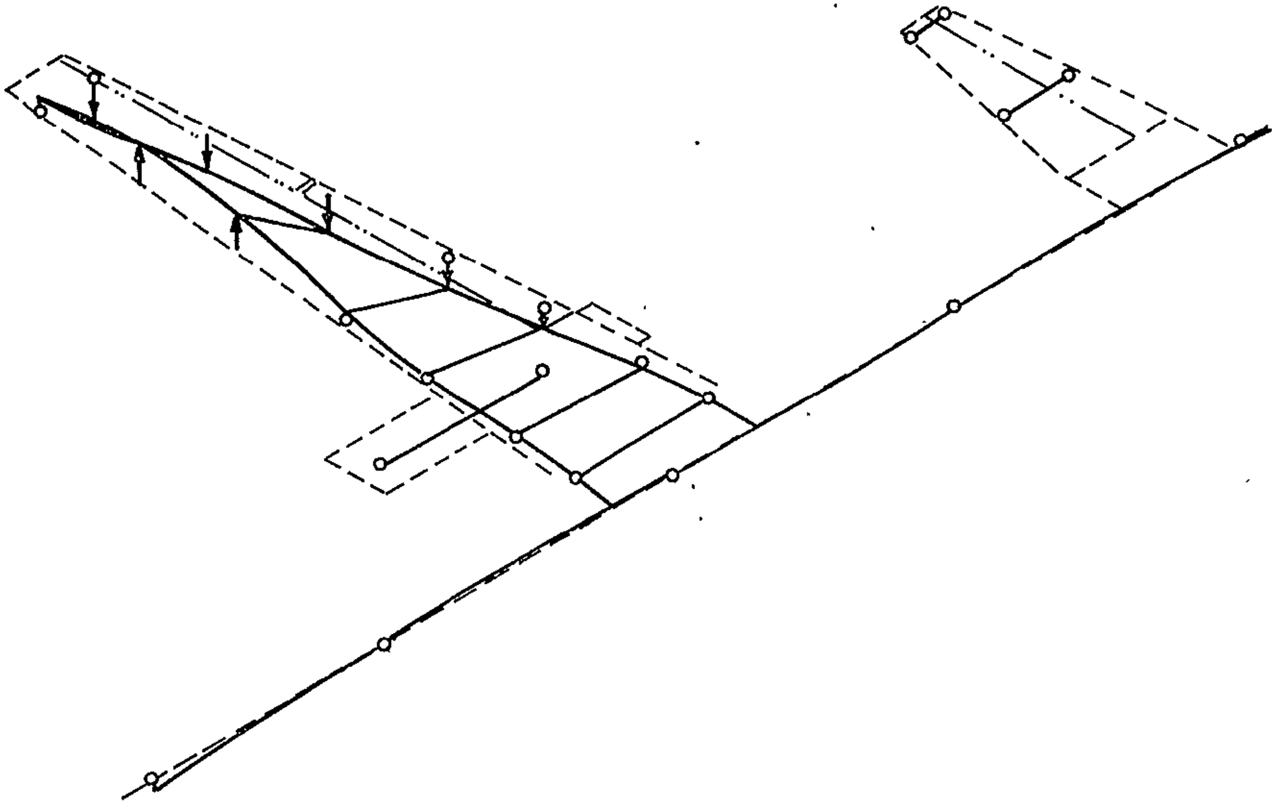

Figure 20 HIGHER MODE WING BENDING AND TORSION

The lowest frequency mode (f_1 = 3.02 Hz) which is shown on Figure 14 is a typical 1st wing bending mode with the wing tips moving out-of-phase with the forward and aft fuselage and horizontal tail motion. It would be expected that the collective ailerons and DLF's would be most effective in controlling this mode. Elevator control forces would also do appreciable work in a virtual deflection in this mode and might also be used for control.

The second symmetric mode (f_2 = 4.65 Hz) was characterized as being primarily first wing torsion because its frequency was close to the one computed for uncoupled torsion assuming no bending and the wing clamped at its root. However, it can be seen from Figure 15 that considerable wing, fuselage and horizontal tail bending movements are involved in the coupled motion. Again it appears that collective aileron, DLF, and elevator inputs could all affect the modal response.

Figure 16 shows the relative deflections for mode 3 (f_4 = 6.09 Hz). Fuselage bending in this mode is such that the deflections of the nose and aft ends of the fuselage are in phase with wing tip deflections whereas they were out-of-phase for the first mode. Also the relative amplitude of the horizontal tail bending is very large and is in phase with deflections of the aft end of the fuselage.

In contrast, Figure 17 shows the fourth mode (f_4 = 6.90 Hz). The tip bending of the horizontal tail is out-of-phase with aft fuselage deflection resulting in a nodal line running across the horizontal tail. However, this nodal line is quite far inboard and it would be expected that the elevator would be effective in controlling this mode as well as mode 3 shown on Figure 16.

Mode 5 (9.01 Hz) shown on Figure 18 is characterized as a typical wing second bending mode. Again appreciable fuselage and horizontal tail bending are present. It appears that the direct lift flaps would be the most effective surfaces for controlling second wing bending. Nodal lines cross both the aileron and elevator which would tend to decrease their effectiveness for controlling this mode.

The sixth mode (f_6 = 15.10 Hz) which is shown on Figure 19 is characterized by 2nd fuselage bending and 2nd horizontal tail bending although considerable wing bending and torsion are also present. The seventh mode (f_7 = 17.25 Hz) which is shown on Figure 20 is even more difficult to characterize. However, it is noted that although significant bending and torsional deflections are found on the outer wing panel, deflections are small on other parts of the airplane.

2.3.7 Comparison of TIFS Vibration Modes Computed Using FLEXSTAB with Previous Results

Table 11 presents a comparison of TIFS vibration frequencies computed by the FLEXSTAB program with previous results. The frequencies given for the preliminary ACT study were computed by coupling together modal results which had been determined for the wing, fuselage, and horizontal tail separately. In contrast the FLEXSTAB frequencies were obtained from a solution for the eigenvalues of a structural model for the entire airplane which was based on somewhat different fundamental parameters than used in the earlier study. In both solutions, the nacelles and SFS's were assumed to have high rigidity.

The listed ground vibration test modes correspond to the principal peaks found in a symmetric wing survey up to 11.5 Hz carried out with vertical excitation applied by shakers located at the wing tips. The wing fore and aft bending and engine vibration modes were not excited in these tests or included in the FLEXSTAB results in Table 11. Vibration modes associated with these degrees of freedom are believed to have a comparatively small influence on the response of the TIFS airplane to atmospheric turbulence.

TABLE 11

TIFS MEASURED AND COMPUTED STRUCTURAL FREQUENCIES

SYM MODE NO.	MODE CHARACTERIZATION	PRELIM. ACT STUDY ref. 6	FREQUENCY (Hz)		
			FLEXSTAB COMPUTATION	GROUND VIBRATION TEST ref. 12	FLIGHT TEST IN ATMOSPHERIC TURBULENCE*
1	1st Wing Bending	2.80	3.02	3.3	3.12
2	1st Wing Torsion	4.58	4.65	4.9	5.0
3	Fus. & H. T. Bending	5.56	6.09	6.6	7.13
4	Fus. & H. T. Bending	6.89	6.90	7.5	**
5	2nd Wing Bending	8.26	9.01	9.7	9.99
6	2nd Fus. & H. T. Bending	16.59	15.10	NA	17.13
7	Wing Outer Panel Mode		17.25	NA	NA

* Peaks in power spectrum of normal acceleration at pilot station (insufficient data to characterize modes)

** No peak observed

The last column in the table presents results obtained from flight tests in atmospheric turbulence. The frequencies listed are the frequencies corresponding to the power spectrum peaks of normal acceleration at the pilot's station. Insufficient data were present to characterize the vibration modes associated with the peaks in the spectrum, but they have been associated somewhat arbitrarily with the computed and ground vibration test modes. Furthermore, it should be pointed out that the frequencies of the spectrum peaks can be influenced by zeroes in the gust input/normal acceleration transfer function arising from unsteady aerodynamic effects at gust entry. Thus they would not be expected to agree exactly with frequencies obtained from the poles of the transfer function.

Figures 21 to 25 present a comparison of vibration nodal lines determined from the mode computation by FLEXSTAB to those measured in the ground vibration tests (Reference 12). Results for the first symmetric wing bending mode presented on Figure 21 show the measured and computed node lines to lie in the nacelle region and to be fairly close together.

Computed and measured nodal lines for the first symmetric torsion mode which are presented on Figure 22 are of the same general form, but are widely separated in the region inboard of the nacelle. Nodal lines which are located off the wing surface are determined as if narrow rigid wing sections perpendicular to the wing elastic axis extended both forward and aft of the actual planform.

The peculiar behavior of the nodal lines inboard of the nacelle can be explained by the spanwise variation of the pitching motion of the wing sections. This phenomenon will be discussed considering the situation depicted on Figure 5. Here there is a very small nose down pitch angle at the wing root, but torsional deformation of the wing structure causes nose-up sectional pitch angles a short distance outboard.

The small nose-down pitch angle at the wing root in conjunction with an upward vertical deflection results in a section node which is too far

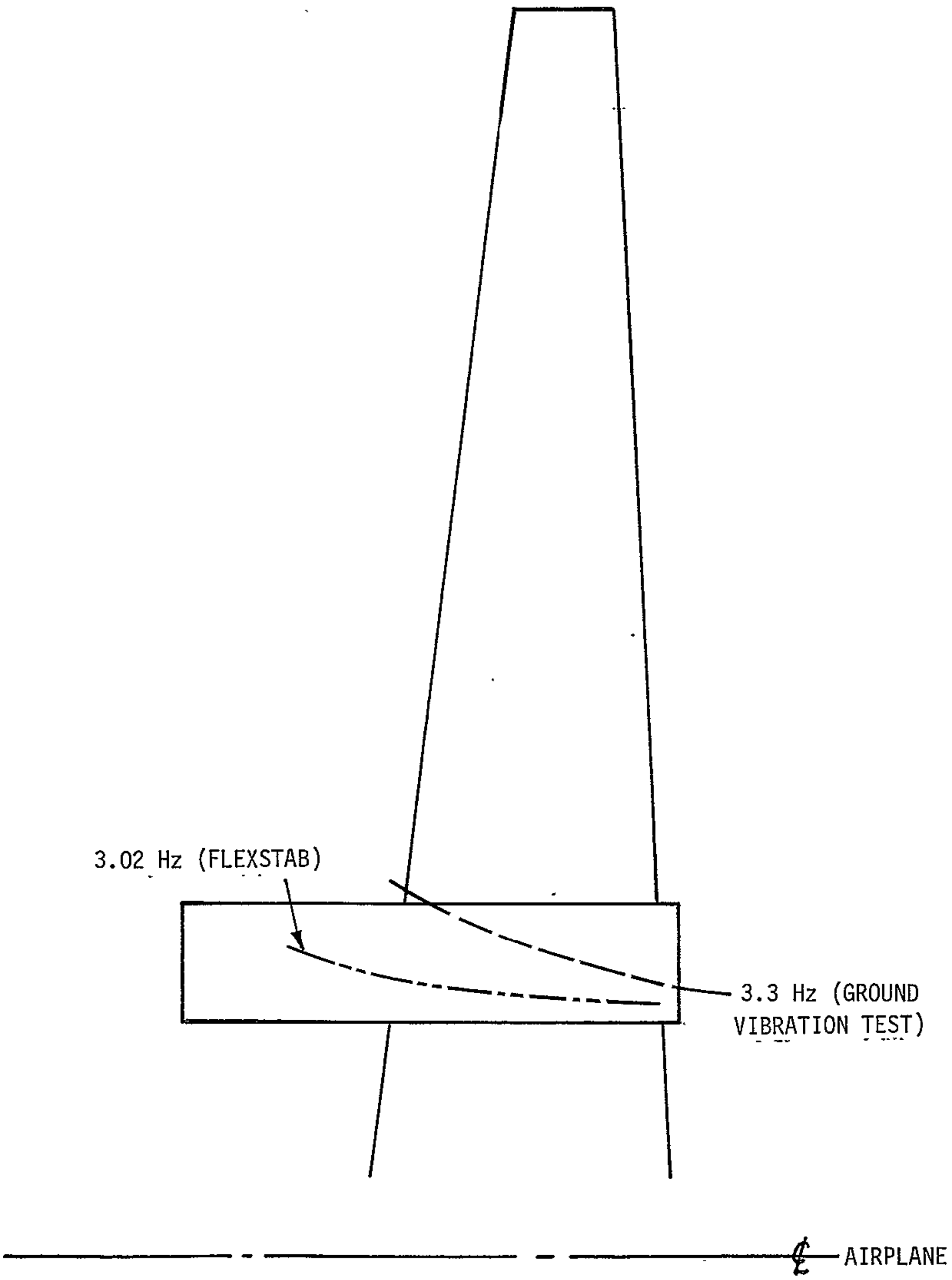

Figure 21 NODAL LINES FOR 1st SYMMETRIC WING BENDING

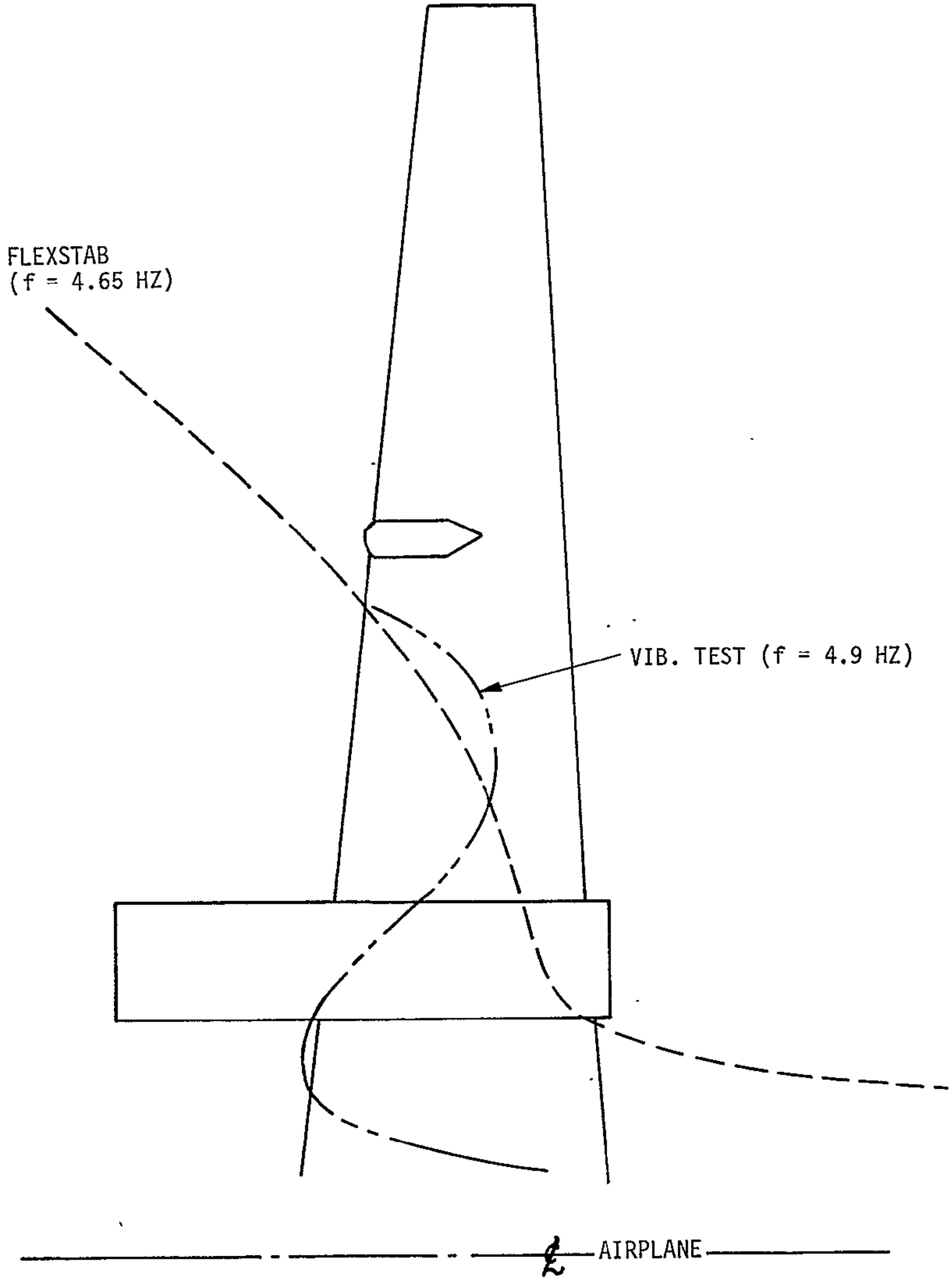

Figure 22 NODAL LINES FOR 1st SYMMETRIC TORSION MODE

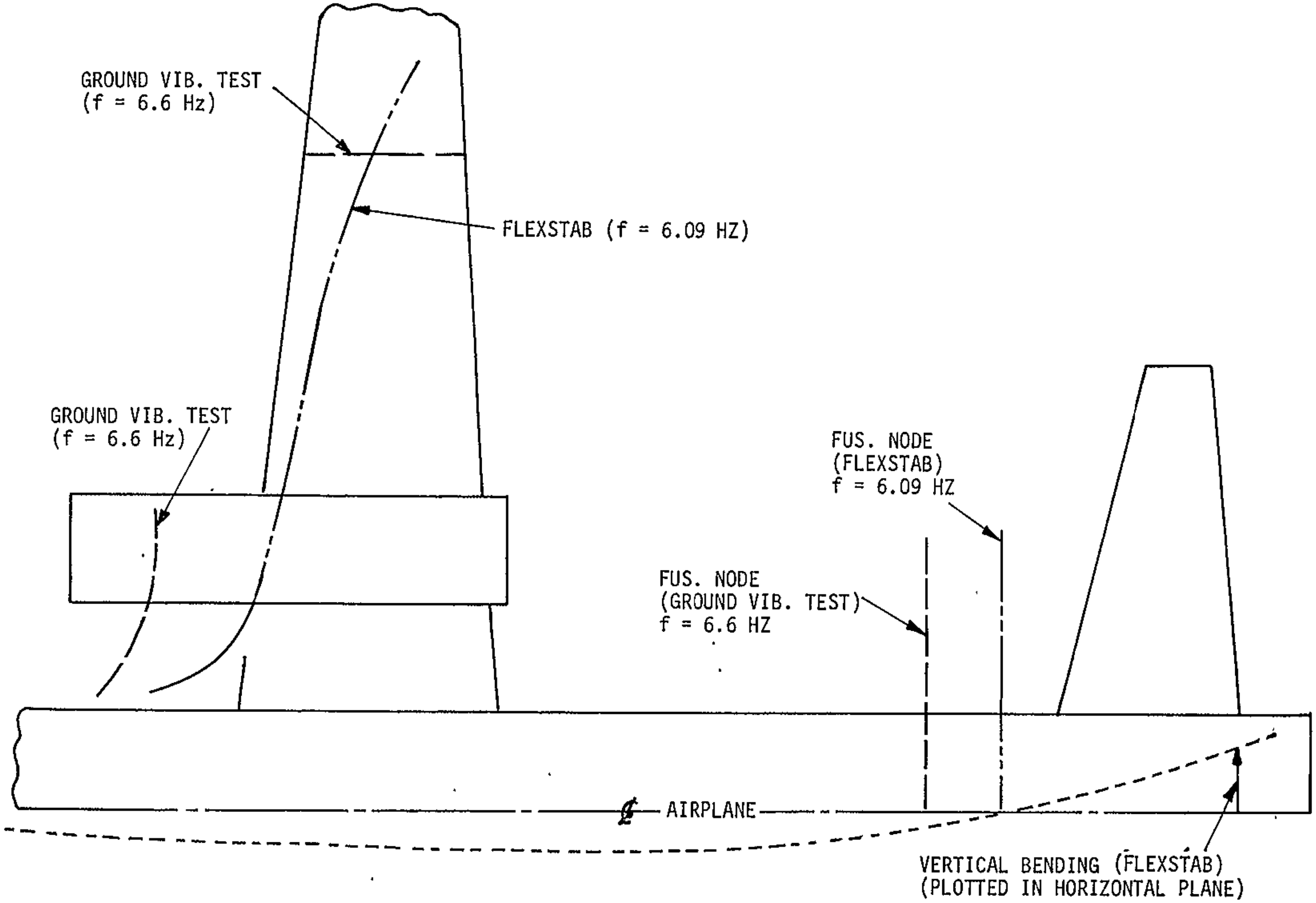

Figure 23 NODAL LINES FOR 1st SYMMETRIC FUSELAGE BENDING MODE

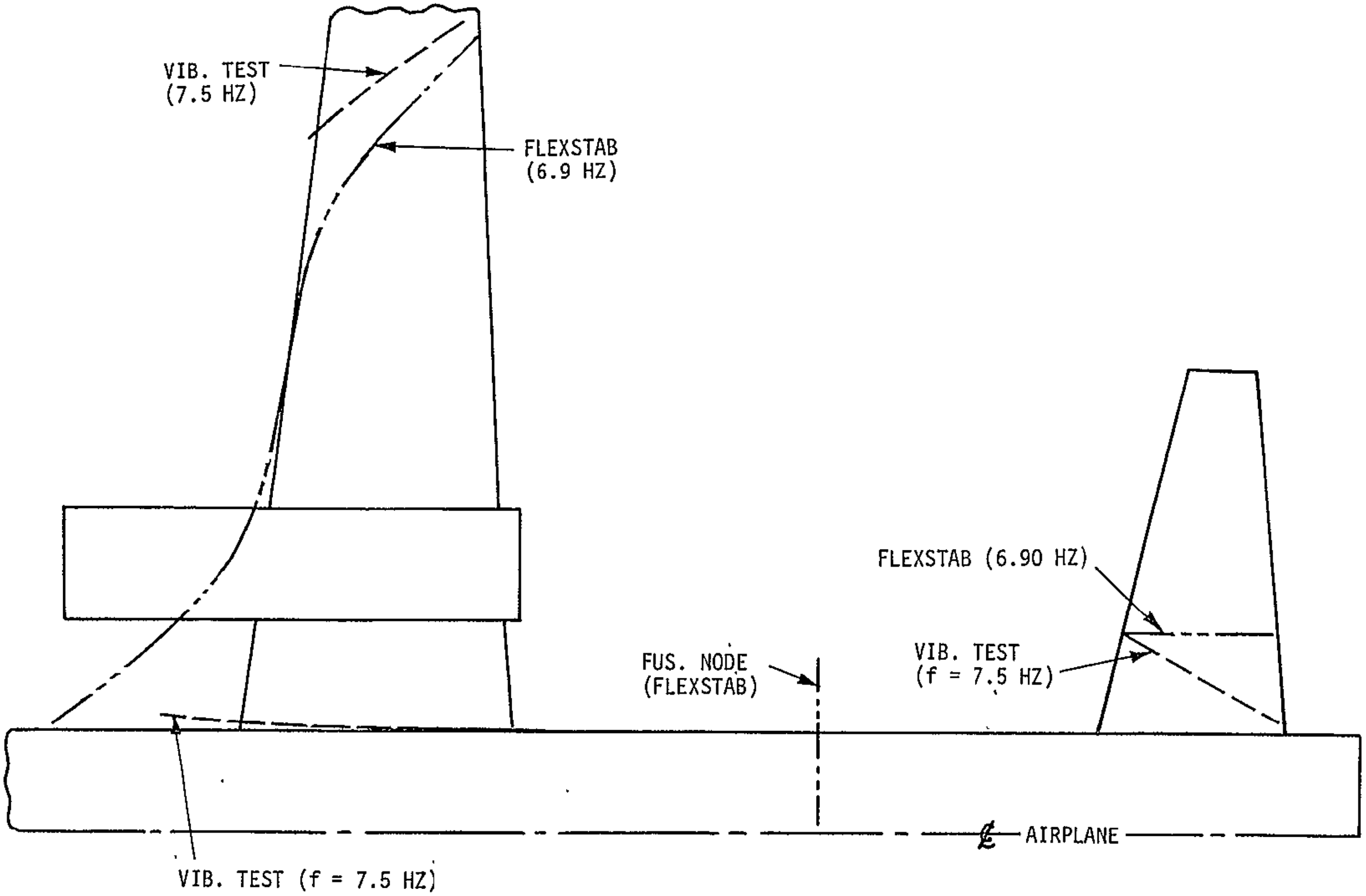

Figure 24 NODAL LINES FOR 1st SYMMETRIC HORIZONTAL TAIL BENDING MODE

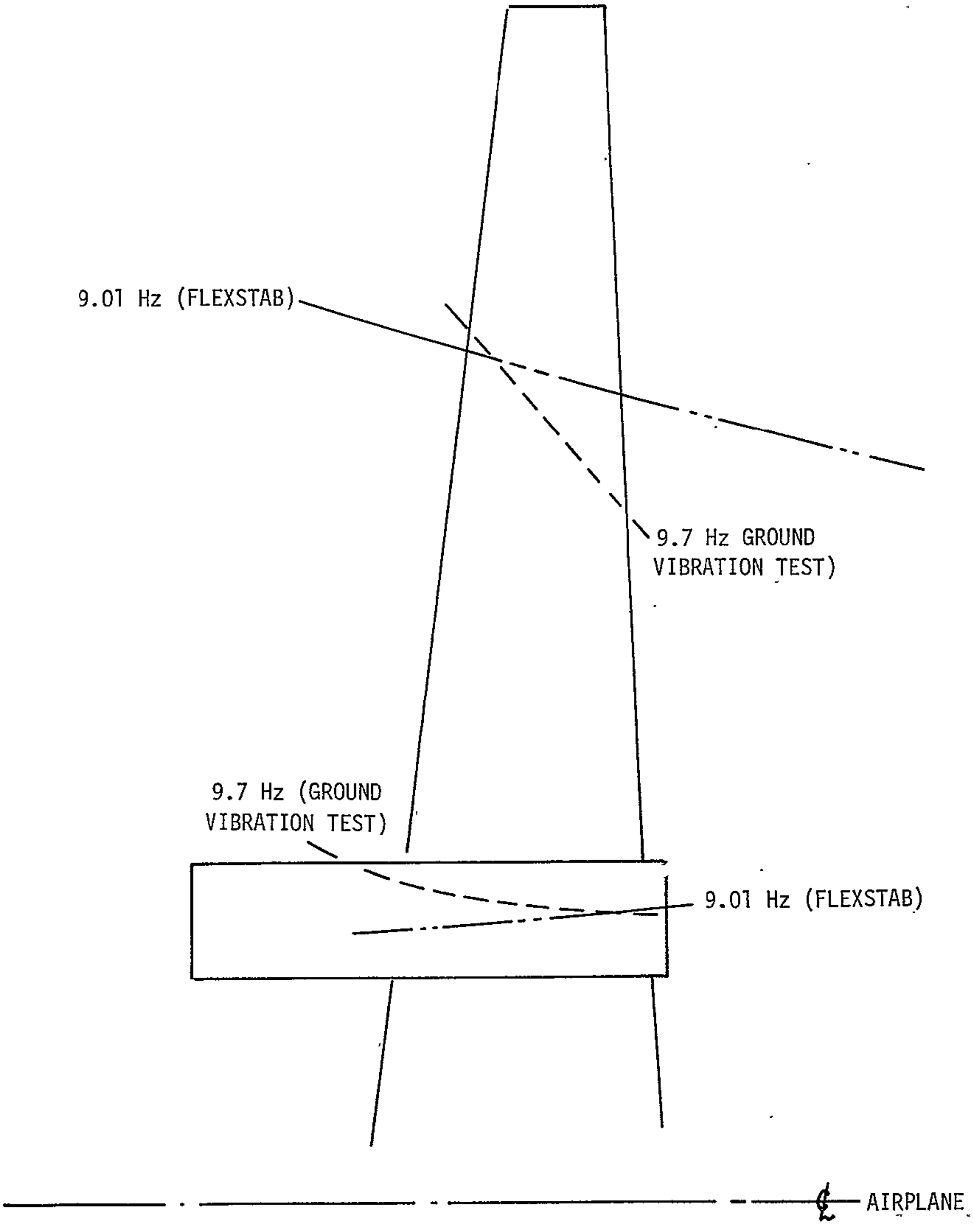

Figure 24 NODAL LINES FOR 2nd SYMMETRIC WING BENDING

forward to plot on Figure 22. Moving slightly outboard, the section node goes forward toward infinity as the nose-down pitch angle approaches zero. Still further outboard where a nose-up pitch angle develops and where there is still an upward vertical deflection at the elastic axis, the section node is aft of the wing. Thus as the nose-up section pitch angle increases from zero with spanwise position, the nodal line comes in from infinity aft of the wing towards the trailing edge as indicated on Figure 22. It is evident that in the region where the section pitch angles are small that small differences between the computed and measured pitch angles results in large differences between the computed and measured nodal lines.

Figure 23 shows nodal lines obtained for the mode characterized as first symmetric fuselage bending. The shape of the fuselage vertical bending curve as computed by FLEXSTAB is plotted in the horizontal plane in order to indicate how the fuselage node was determined. The measured fuselage node was somewhat forward of the one obtained from the FLEXSTAB solution, but it should be noted that both theory and ground vibration test results indicated vertical motion of the aft fuselage and horizontal tail to be in phase.

Theoretical and measured nodal lines on the wing are also compared on Figure 23 for the mode characterized as first symmetric fuselage bending. They are found to be in general agreement. The vibration test results as reported in Reference 12 did not define the position of the nodal line which is outside the planform of the outer wing panel, but it is believed to be approximately parallel to the one obtained from the FLEXSTAB results.

Nodal lines are shown on Figure 24 for the mode characterized by first symmetric horizontal tail bending. Both FLEXSTAB and vibration test results indicate nodal lines crossing the inboard portion of the horizontal tail. The line obtained in vibration tests is at a greater angle to chord line than the one predicted by the theoretical solution indicating greater horizontal tail torsion. This difference might be associated with the fact that the FLEXSTAB solution treated the stabilizer and elevator as an integral unit.

The FLEXSTAB solution for the first horizontal tail bending mode indicated a fuselage node approximately midway between the wing and horizontal tail. Presumably such a node was also present in the vibration tests, but its position was not recorded.

Measured and computed nodal lines are shown on Figure 24 which run diagonally across the outer wing panel and are in substantial agreement. However, again the vibration test results do not define the nodal line position off the wing planform.

Figure 24 indicates a nodal line observed at the wing root in the vibration test as reported in Reference 12. It is believed that the result is spurious, but insufficient original data were available to verify or disprove this conclusion.

Results for the 2nd symmetric wing bending mode which are presented on Figure 25 shows a good agreement between the computed inboard nodal line and the one found in the ground vibration tests. The measured and computed outboard nodal lines are found at approximately the same spanwise station. However, the nodal line obtained in the ground vibration tests crosses the wing at a greater angle relative to the centerline of the airplane indicating more torsion. Possibly this difference could be attributed to aileron or DLF deflections which were not considered in the FLEXSTAB analysis, but might have occurred during the vibration tests (although not recorded in Reference 21).

2.3.8 Discussion of Results of Vibration Analysis

In the preceding sections vibration mode computations have been discussed and compared with frequencies and mode shapes measured in ground vibration tests of the TIFS airplane. It is concluded that the analysis has provided a reasonable description of the principal structural vibration modes throughout the frequency range contemplated for active control of TIFS by collective aileron, direct lift flap and elevator inputs. All of the computed frequencies are within 8% of those measured in the ground vibration tests. The analytical results have been obtained using the original estimates for the mass and stiffness distributions for the airplane and these parameters have not been adjusted or "tweaked" to improve agreement between test and theory.

It is recognized that several possible sources of error existed in obtaining these results. As discussed earlier, some known limitations were placed on the analysis by the use of the Internal Structural Influence Coefficient Program (ISIC) of FLEXSTAB for the generation of coefficients used in the normal modes computations. ISIC places certain constraints on the representations of slender bodies (e.g. fuselages and nacelles) and on thin bodies (i.e. the wings, SFS's, tail surface). The effects of these limitations on the TIFS structural mode computations are summarized below.

1. It was necessary to model fuselage inertia properties with concentrated masses spaced along the fuselage axis. Fuselage panel effects of the mass distribution away from the fuselage axis could not be represented with concentrated moments of inertia in FLEXSTAB. (This approximation is not believed to have introduced appreciable errors.)

2. Representation of wing inertia properties was by dumbbell masses in the plane of the wing. The ISIC routine does not permit modeling the effects of the mass distribution transverse to the chord plane. (These approximations are not believed significant.)

3. The thin body representation of the wing did not permit fore and aft bending. On the other hand, the computed uncoupled fore and aft bending frequency of the TIFS wing is 4.83 Hz which is within the frequency range of interest for active control. It would be expected that a corresponding coupled mode of approximately the same frequency would be found by a more complete analysis including chordwise bending. However,

it is believed there should be little excitation in flight of the coupled mode primarily involving wing fore and aft bending so its neglect should not have a large influence on the computed responses of the TIFS airplane. Some fore and aft wing bending exists in all actual coupled modes of the TIFS airplane. The importance of this motion could be evaluated by comparison of results obtained using the ISIC program of FLEXSTAB in computing normal modes with those obtained with the NASTRAN program including fore and aft bending.

4. In the present FLEXSTAB solution, the engine and nacelle were treated as a slender body whose inertia properties could be represented by concentrated masses along its axis. The inertial forces due to the nacelles are not completely represented because the rotational inertias of the engine/nacelle are neglected. The addition of engine degrees of freedom would have some influence on the vibration modes discussed in this report as well as adding modes primarily involving engine motion. It will be possible to evaluate these effects by comparison with vibration modes for TIFS being computed with NASTRAN.

It is believed that further study will show that the limitations of the ISIC program which have been listed above are not serious in applying FLEXSTAB to ACT TIFS. However, the External Structural Influence Coefficient (ESIC) option of FLEXSTAB might be used if a more rigorous structural modeling were desired; this program makes it possible to incorporate results from NASTRAN into the FLEXSTAB analysis.

Uncertainties and shortcomings in the basic parameters provide another source of error in the vibration analysis results. Some of these are listed and discussed below:

1) Fineness of wing weight distribution

Twelve spanwise stations were used in the wing mass distribution on Table 1. It is believed that this distribution is fine enough for analyzing vibration modes in the frequency range treated in the present report. Additional panel points would be required to obtain a more accurate description of the third and fourth wing bending modes.

2) Wing elastic axis

The wing elastic axis assumed in describing TIFS was based on an early analysis of the Convair airplane. No experimental data is available to verify this assumption. The assumed elastic axis could easily be off by 5%.

3) Engine sprung weight and nacelle inertia properties

Only limited inertia data were available on the Allison Prop-Jet conversion of the Convair and the most recent data was obtained verbally. Consequently, the engine c.g. and moments of inertia are possible sources of error.

4) Fuselage stiffness

Estimates of fuselage stiffness properties could be in error for parts of the fuselage where there are cutouts and redundant structure.

5) Control surface degrees of freedom

The fact that control surface degrees of freedom are not included in the analysis may have resulted in some differences between measured and computed nodal lines. However, this is not strictly an error but the result of comparing modes which should not be identical.

2.3.9 Recommendations for Improving Structural Representation

Several procedures might be used to refine the structural representation of TIFS developed in this report. Perhaps the simplest, which was suggested by NASA personnel at the final oral report, would be to assume that the computed mode shapes are correct and merely substitute measured for computed natural frequencies.

A first step in a more extensive program to improve the structural representation would be an evaluation of the validity of the simplifications made in computing vibration modes as discussed previously. This would include an analytical evaluation of the effects of fore and aft bending of the wing and the engine degrees of freedom.

However, it is more likely that remaining differences between measured and computed frequencies and shapes of the principal structural vibration modes are due to errors in basic parameters used in the analysis. Improved fundamental parameters might be obtained by more refined analyses or by appropriate tests while improvement in modal parameters could also be obtained directly by parameter identification techniques.

A sophisticated modern finite element analysis might be made to improve structural parameters involving a detailed breakdown of the wing, tail, and side force surfaces. A structural model generated with an external program such as NASTRAN or Atlas could be incorporated into FLEXSTAB with the ESIC routine and used in subsequent computations of stability and control derivatives. This would be a costly procedure because of the difficulty of assembling the required data and determining required computer inputs. Such an approach is not believed justified because classical beam-type analyses should be adequate for the comparatively high aspect ratio TIFS configuration. However, some further analysis is believed worthwhile to check the validity of the assumed wing elastic axis.

As mentioned previously,there are uncertainties concerning the stiffness of the TIFS fuselage because of cutout and redundant structure. Critical areas of the fuselage could be reanalyzed to obtain new effective stiffness estimates. Alternatively vibration analyses could be carried out to determine the effect of using different fuselage effective stiffnesses within the range of their uncertainty for critical fuselage stations.

If engine degrees of freedom are found to influence the computed vibration modes, further verification should be made of engine sprung weight inertia properties. This might be accomplished by a detailed weight and balance analysis of the engine-transmission system or by experimental determination of the required properties. Furthermore, if it is established that engine degrees of freedom can make a significant contribution to the response of TIFS to turbulence, analyses should be carried out to determine the effect of gyroscopic moments on the responses.

A possible explanation which has been suggested for some of the discrepancies between measured and computed mode shapes is that the control surface degrees of freedom were not included in the analytical solution, but may have influenced the vibration test results. This question could be investigated by finding the effect of coupling control surface motions with some of the computed modes. However, it is believed that structural modes which are computed with locked control surfaces will be the most satisfactory for use as a basis for analyzing the flight responses of TIFS. Inertial forces due to control surface movement can then be treated as forcing functions exciting the structural modes.

Although the currently proposed flight tests of the TIFS airplane are concerned with longitudinal response, it is believed important to obtain a model for antisymmetrical structural vibrations of TIFS. Atmospheric turbulence will excite both longitudinal and lateral responses and a knowledge of the antisymmetric structural modes will help in separating these effects.

Finally, it should be pointed out that the current vibration test data for the TIFS airplane does not provide a complete description of the structural vibration modes to compare with the analytical solutions. A more refined vibration test would be required to obtain this information. An alternative procedure would be to compare modal response data measured in flight with analytical predictions. This procedure is recommended since the instrumentation required could also be used in parameter identification to determine the actual parameters desired for active control system design.

2.4 AERODYNAMICS CALCULATIONS AND RESULTS

2.4.1 Selection of Flight Conditions

In order to span an adequate flight range, three flight conditions were selected for analysis. These conditions roughly corresponded to landing, climb and cruise configurations for the TIFS airplane. The climb configuration was chosen because flight records of the TIFS flying in actual atmospheric turbulence were earlier obtained at this condition.

Trim conditions are summarized in Table 12. Also shown in the table are the trim α , δ_e and thrust required for trim as predicted by FLEXSTAB. A number of important properties of the TIFS used for all flight conditions are listed in Table 13.

The relationship between the three flight conditions and the TIFS flight envelope is shown in Figure 26. Also shown in Figure 26 is the direct lift flap capability in terms of lift coefficient and acceleration and the various structural and aerodynamic limitations to the flight envelope.

The aircraft weight of 2.42×10^5 N and the weight distribution was obtained based on the best information available for the TIFS as of May 1971, the date near which both ground vibration tests and flutter flight tests were conducted. Fuel load of 14,200 N/side corresponds to the fuel present during the ground vibration tests and is a typical full load for the TIFS.

TABLE 12

TRIM FLIGHT CONDITIONS ANALYZED

	"LANDING"	CLIMB	CRUISE	
M	.2	.246	.456	FLEXSTAB INPUTS
H (meters)	61.	1402.	3048	
q (Newtons/meter^2)	2819.68	3629.23	10155.37	
α degrees	7.0227	4.641	-.5188	FLEXSTAB OUTPUTS
θ degrees	7.0227	4.641	-.5188	
Thrust (Newtons)	34,283.	24,576.	5973	
Elevator angle (deg)	-2.517	-1.400	+1.477	
Lift Coefficient	1.005	.781	.279	

NOTES:

1) For all flight conditions
$\gamma = 0$, trim angular rates and bank angle are zero.

2) "Landing" is actually a landing approach condition selected for analysis. No flap deflections were used for this condition which explains the high thrust required to obtain trim.

TABLE 13

MISCELLANEOUS CONSTANTS

Wing Mean Aerodynamic Chord 2.90 m

Wing Area 85.47 m^2

Wing Span 32.11 m

Location of LE of Reference Chord (from nose) 12.405 m

Center of Gravity (Reference Axis System*)

$X = 13.2381$ m

$Y = 0$ m

$Z = -.3357$ m

C.G. Position 28.7% MAC

$I_{pitch} = 746{,}900$ Kg m^2 = Pitching moment of inertia of total airplane about C.G.

$M = 24700$ Kg = Total airplane mass

*The reference axis system is an orthogonal axis system with origin on the plane of symmetry at the nose of the TIFS. Positive X is aft, positive Y is out the right wing and positive Z is up.

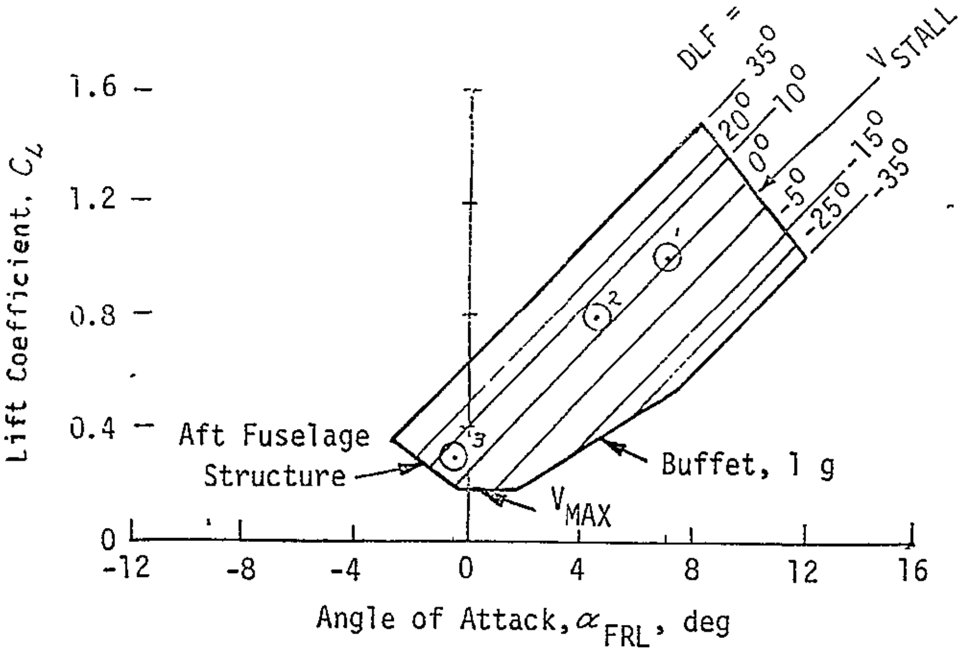

DIRECT LIFT FLAP CAPABILITY

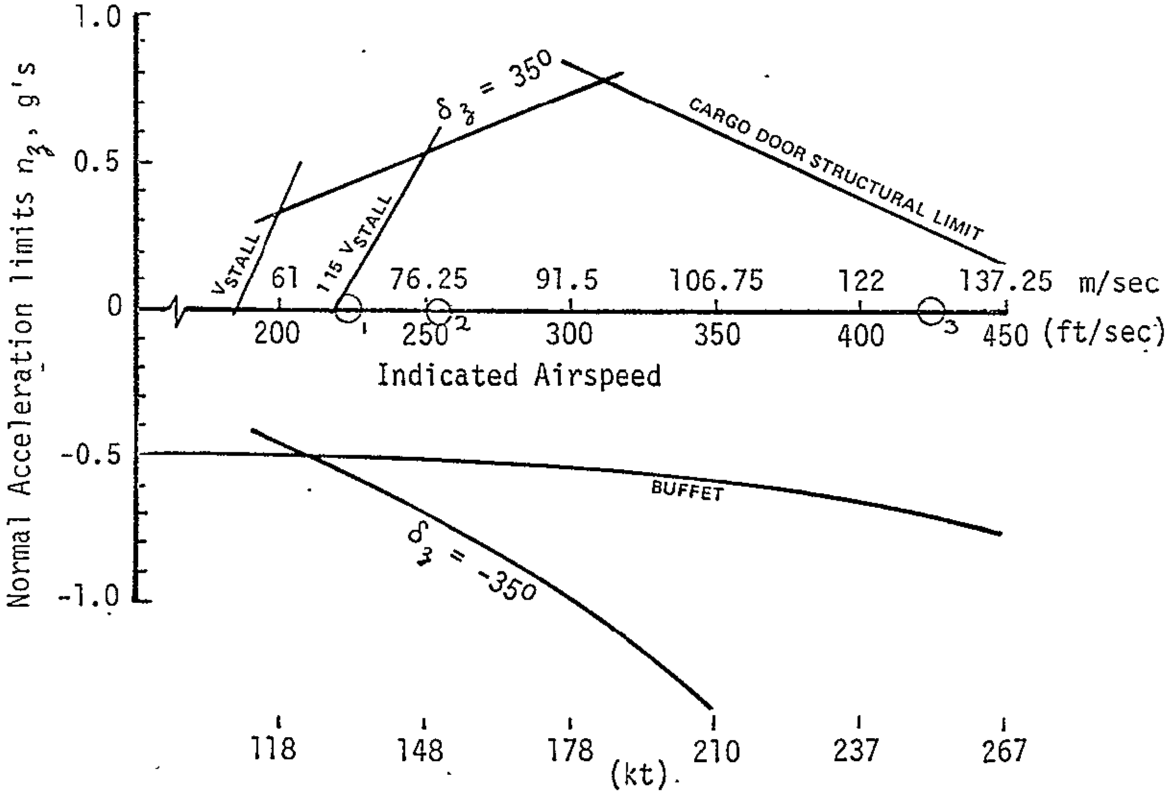

Figure 26 TIFS n_z CAPABILITY WITH DIRECT LIFT FLAPS ALONE TRIMMED AT: $\delta_F = \delta_e = 0$

All analysis in this report is for the TIFS in the clean configuration, i.e. all controls initially at zero deflection and gear up. Although the landing configuration would normally require some flap deflection; this was not included in the analytical model because parameter identification results were for essentially clean configurations and because of limitations in the possible trim inputs of the FLEXSTAB computer program. The effects of flap deflection on TIFS aerodynamics is included in Reference 5.

2.4.2 Rigid Body Stability and Control Parameters

Although the primary contribution of FLEXSTAB in aircraft analysis is in the formulation of the flexible equations of motion as opposed to computing rigid body stability and control derivatives, it is interesting to compare the FLEXSTAB rigid body or quasistatic results with results obtained using other techniques. Two sets of stability and control parameters are available. The first representing a combination of wind tunnel, analytical, and flight test derived results was published in Reference 5. This document contains the best description of the TIFS derivatives available at that time. The second source of stability and control parameters was obtained using the Calspan Beysian Maximum Liklihood Parameter Estimation program (BML). This technique determines parameters of a given dynamic mathematical model which minimizes the mean square errors between the responses of the model and responses of the aircraft measured in flight.

The results of the parameter estimation methods are subject to the following qualification. The elevator, rudder and aileron control surface measurements were not available directly. Instead, the output of each control surface servo piston was measured which may differ from the control surface response due to effects such as linkage flexibility. Surface position is not a direct feedback quantity. The net effect of this is that available measurement of elevator motion (i.e. the servo output) for the elevator inputs available may differ from the actual elevator motion. This may introduce errors in identification of the pitching moment derivatives and surface effectiveness. Flexibility in the aileron linkage is less significant.

The FLEXSTAB program yields stability derivatives computed in several ways. The first assumes that the aircraft is totally rigid. These parameters would be comparable to wind tunnel test results using a rigid wind tunnel model. Another useful form of parameter estimates assumes that the aircraft is flexible but that the structural modes (generally at high frequencies) deflect instantaneously. Using this assumption, each rigid body stability and control derivative will be modified by an aeroelastic correction term to account for elasticity.

The nature of these quasistatic corrections are described more precisely below. The system equations are given by:

$$\dot{x}_1 = F_{11}x_1 + F_{12}x_2 + G_1 u$$

$$\dot{x}_2 = F_{21}x_1 + F_{22}x_2 + G_2 u$$

where x_1 is a vector of rigid body response variables
x_2 is a vector of structural mode response variables
u is a vector of control inputs
F_{ij} are matrices of stability derivatives
G_1 are matrices of control effectiveness derivatives

The quasistatic assumption requires that $\dot{x}_2 = 0$. Therefore the following algebraic equation results:

$$0 = F_{21}x_1 + F_{22}x_2 + G_2 u$$

or

$$x_2 = -F_{22}^{-1}F_{21}x_1 - F_{22}^{-1}G_2 u$$

Substituting this result into the differential equation for x_1 yields

$$\dot{x}_1 = \left[F_{11} - F_{12}F_{22}^{-1}F_{21}\right]x_1 + \left[G_1 - F_{12}F_{22}^{-1}G_2\right]u$$

$$\dot{x}_1 = F_{qs}x_1 + G_{qs}u$$

where F_{qs} and G_{qs} are the quasistatic stability and control parameter matrices.

Note that the eigenvalues and eigenvectors of F_{11} are not the same as those for F_{qs}.

Comparison of the various parameter estimates are shown in Table 14 for the cruise condition. Lift and drag coefficients are the usual wind axis quantities and all derivatives are nondimensional. The column entitled "Best Estimates July 1972" is from Reference 5 and the "Parameter Identification" column is from the BML results. Both contain quasistatic derivatives and can be compared directly only to each other and to the column "FLEXSTAB Quasistatic". The "FLEXSTAB, Rigid" column is included to show the contribution of the quasistatic correction.

Drag parameters are difficult to predict using linear theories which ignore viscous and separated flow effects, are difficult to obtain from parameter identification methods using short record lengths, and relatively easy to obtain in wind tunnel models. As a result, the C_{D_α} and $C_{D_{\delta_z}}$ from the "Best Estimates July 1972" are recommended for ACT modeling of the TIFS. Other drag parameters are not considered significant at this time.

The estimates of lift curve slope between the "Best" and parameter identification results agree with each other to within three percent. As might be expected, the lift curve slope was overpredicted by FLEXSTAB. For the lift due to direct lift flap, $C_{L_{\delta_z}}$, agreement is apparent between "Best, 1972" and FLEXSTAB Quasistatic but not with the parameter identification results. Reference 5 has shown that the direct lift flap effectiveness is a nonlinear function of deflection whose most linear region is $\delta_z = -3.5 \pm 5^\circ$. The value shown in the "Best, 1972" column and for the FLEXSTAB result is linearized about $\delta_z = 0$, while the parameter identification results define the best linear fit over the flap input range $-8 < \delta_F < 4$. These results are not directly comparable. To resolve this inconsistency it is recommended that inputs be applied to the TIFS direct lift flap in flight

TABLE 14

COMPARISON OF PARAMETER ESTIMATES
CRUISE CONDITION C.G. = .266 $\bar{c}$

	BEST ESTIMATES JULY 1972 (QUASISTATIC)	BML PARAMETER IDENTIFICATION (QUASISTATIC)	FLEXSTAB ESTIMATES (QUASISTATIC)
C_{D_α} (1/rad)	.124	.09	.185
C_{D_q} (1/rad)	0	0	.0278
$C_{D_{\delta_e}}$ (1/rad)	.0142	~	-.00074
$C_{D_{\delta_z}}$ (1/rad)	.026	.004	~
$C_{D_{\delta_{sa}}}$ (1/rad)	~	~	~
C_{L_α} (1/rad)	6.02	5.85	6.38
C_{L_q} (1/rad)	0	0	15.7
$C_{L_{\delta_e}}$ (1/rad)	.63	~	.727
$C_{L_{\delta_z}}$ (1/rad)	1.32 (Note 1)	.96	1.28
$C_{L_{\delta_{sa}}}$ (1/rad)	.53 (Note 2)	.181 (Note 2)	.595
C_{m_α} (1/rad)	-.43	-.494	-2.15
C_{m_q} (1/rad)	- 45	-24.3	-39.6
$C_{m_{\delta_e}}$ (1/rad)	-2.18	-2.2	-2.71
$C_{m_{\delta_z}}$ (1/rad)	-.155	-.117	-.347
$C_{m_{\delta_{sa}}}$ (1/rad)	~	~	-.345
$C_{m_{\dot{\alpha}}}$ (1/rad)	-15.6	-8.4	~

Notes: 1) This is a linearization about δ_z = 0 of this nonlinear aerodynamic effectiveness.

2) Estimated from rolling moment due to asymmetric aileron deflection.

3) The notation ~ denotes information not available.

which limit flap motion to the linear range $\delta_z = -3.5 \pm 5^\circ$ and that the parameter estimate resulting from that input be utilized in the linear design of the ACT control systems.

In determining the lift due to symmetric aileron in the "Best" and parameter identification, it was assumed that the rolling moment due to asymmetric aileron deflection, $C_{\ell_{\delta_a}}$, could be converted directly from a moment to a force derivative by the appropriate nondimensional length. The computation is as follows:

Define the control deflections

$$\delta_a = \delta_a^R - \delta_a^L$$

$$\delta_{sa} = \frac{\delta_a^R - \delta_a^L}{2}$$

where δ_a^R and δ_a^L are the deflection of the right and left ailerons respectively, positive down.

The total rolling moment due to asymmetric aileron deflection is given by:

$$C_\ell(\delta_a) = C_{\ell_{\delta_a}} \delta_a = C_{\ell_{\delta_a}} \delta_a^R - C_{L_{\delta_a}} \delta_a^L .$$

The moment on each side of the aircraft is given by:

$$C_\ell^R = C_{\ell_{\delta_a}} \delta_a^R$$

$$C_\ell^L = -C_{\ell_{\delta_a}} \delta_a^L$$

If it can be assumed that the center of pressure of each aileron is a distance X_{CP} from the plane of symmetry, then the total lift force due to aileron deflection will be

$$C_{L_{TOTAL}} = C_{L_{\substack{RIGHT\\AILERON}}} + C_{L_{\substack{LEFT\\AILERON}}} = -\frac{b}{X_{CP}} C_{\ell_{\delta_a}} \delta_a^R - \frac{b}{X_{CP}} C_{\ell_{\delta_a}} \delta_a^L$$

$$= -\frac{b}{X_{CP}} C_{\ell_{\delta_a}} (\delta_a^R + \delta_a^L) = -\frac{2b}{X_{CP}} C_{\ell_{\delta_a}} \left(\frac{\delta_a^R + \delta_a^L}{2} \right) = -\frac{2b}{X_{CP}} C_{\ell_{\delta_a}} \delta_{sa}$$

If the ailerons are deflected asymmetrically, then $\delta_a^L = -\delta_a^R$ and $C_{L_{TOTAL}} = 0$ as expected. For the TIFS, the following properties apply:

$X_{CP} \cong$ 11.8 meters (38.7 ft) Reference 6

b = 32.2 meters (105.3 ft)

$C_{\ell_{\delta_a}} = \begin{cases} -.0975 \text{ "Best, 1972" and Convair, Reference 24} \\ -.0333 \text{ Parameter Identification} \\ \qquad \text{high speed } \alpha \cong 0^\circ \end{cases}$

Therefore,

$C_{L_{\delta_{sa}}} = \begin{cases} +.53 \text{ "Best 1972" and Convair} \\ +.181 \text{ Parameter Identification} \end{cases}$

In the parameter identification effort, the actual aileron surface deflection was not measured. This may explain the discrepancy in rolling and lifting effectiveness of the ailerons. However, the measured aileron servo output is not believed to be substantially different from the aileron surface position.

Additional experimental analysis performed in 1971 (Reference 11) using a combination of simple analytical techniques as well as analog matching indicate that $C_{\ell_{\delta_a}} = -.0418$ at $\alpha = 5^\circ$. This compares favorable with the parameter identification result, $C_{\ell_{\delta_a}} = -.039$ at $\alpha = 5^\circ$, but not with the "Best Estimate July 1972", $C_{\ell_{\delta_a}} = -.0975$ for all α.

Ref. 13. Riedler, A. D. et al: "Aerodynamic Data Flight Criteria and Unit Load Distribution for Structural Design of the Model 340 Airplane Turboprop Configuration," Consolidated Vultee Aircraft Corp. Report No. ZU-340-001, August 1951. NASA CR-158890.

This discrepancy in aileron lift effectiveness is considered to be perplexing in light of the fact that the TIFS ailerons are identical aerodynamically to the Convair 340 ailerons. It is recommended that the actual aileron lifting and rolling effectiveness be measured in flight again with and without side force surfaces before ACT control policies are implemented.

Few stability derivatives are more important than the pitching moment due to angle of attack, C_{m_α}. Table 14 shows that the "Best Estimate July 1972" agrees well with the parameter identification result. However, FLEXSTAB predicts a substantially more stable aircraft. The exact cause of this discrepancy is not known at this time.

The pitch damping derivatives, $C_{m_{\dot{\alpha}}}$ and C_{m_q} are in reasonable agreement between "Best" and FLEXSTAB. The parameter identification result indicates lower damping, but this is believed to be the result of phase errors in the measurements of the elevator due to flexibility in the actuating mechanism. It is recommended that these derivatives be verified by parameter identification using the elevator position sensor rather than the elevator servo output.

The pitching effectiveness of the elevator, $C_{m_{\delta_e}}$, was noted in the parameter identification effort to be a function of dynamic pressure. It is believed that this resulted due to aeroelastic effects on the elevator actuation mechanism. However, the extrapolation to zero dynamic pressure of the parameter identification results agreed reasonably well with the "Best Estimate 1972". FLEXSTAB overpredicted the control effectiveness by 23%. This overprediction is not unusual since flow over trailing edge devices is frequently partially separated, an effect for which the theory has not accounted.

It should be recalled that FLEXSTAB was not expected to produce as accurate rigid body stability and control derivatives as available from other sources. The proper use of the FLEXSTAB system would involve using the

AIC correction program to modify the lifting capability of panels whose effectiveness was not correctly modeled. An example might be decreasing the lifting capability of the tail panels in order to more closely match C_{m_α} and $C_{m_{\delta_e}}$. Certainly all control surfaces should be so corrected. In this way the generalized forcing terms on the structural mode equations would be more accurate as well.

Comparison of quasistatic derivatives at the landing and climb configuration are shown in Tables 15 and 16, respectively.

2.4.3 Flexible Aircraft Equations of Motion

The flexible equations of motion of the TIFS aircraft have been computed at two flight conditions, climb and cruise, for symmetric motion only. Time prohibited computation at the third flight condition.

The form of the equations of motion is as follows:

$$Ax + B\dot{x} + C\ddot{x} = 0$$

where $x^T = [u, w, \dot{q}, \theta, \eta_1, \eta_2, \eta_3, \eta_4, \eta_5, \eta_6, \eta_7]$

A, B, C are square matrices of dimension 11 x 11

u = component of inertial velocity in X direction, m/sec

w = component of inertial velocity in Z direction, m/sec

q = pitch rate, rad/sec

θ = pitch attitude, rad

η_i are structural mode deflections of the aircraft

The seven structural modes are those modes discussed earlier in Section 2.3 of this report in order of increasing vibration frequency. Sensor equations have not yet been formulated. The equations of motion were computed using the Residual Elastic formulation in which the differential equations are corrected for the static effects of higher order structural modes above the seventh mode. The coefficients (A, B, C) to the above equations are included in Appendix B.

TABLE 15

COMPARISON OF PARAMETER ESTIMATES
LANDING CONDITION, C.G. = .266 $\bar{c}$

	BEST ESTIMATE JULY 1972 QUASISTATIC	BML PARAMETER IDENTIFICATION (QUASISTATIC)	FLEXSTAB ESTIMATES (QUASISTATIC)
C_{D_α}	.447	.69	1.15
C_{D_q}	0	0	1.33
$C_{D_{\delta_e}}$	.0511	~	.0832
C_{L_α}	6.02	5.05	5.78
C_{L_q}	0	0	15.20
$C_{L_{\delta_e}}$	.63	~	.805
C_{m_α}	-1.33	-1.05	-1.97
C_{m_q}	-45.0	-24.3	-39.1
$C_{m_{\delta_e}}$	-2.18	-2.2*	-3.09
$C_{m_{\dot{\alpha}}}$	-15.6	-8.4	

* Extrapolated to $q = 0$.

TABLE 16

COMPARISON OF PARAMETER ESTIMATES
CLIMB CONDITION, C.G. = .266 $\bar{c}$

	BEST ESTIMATE JULY 1972 (QUASISTATIC)	BML PARAMETER IDENTIFICATION (QUASISTATIC) (NOTE 1)	FLEXSTAB ESTIMATES (QUASISTATIC)
C_{D_α}	.348	+.43	.854
C_{D_q}	0	0	.919
$C_{D_{\delta_e}}$	.0397	~	.0559
C_{L_α}	6.02	5.3	5.88
C_{L_q}	0	0	15.3
$C_{L_{\delta_e}}$	.63	~	.779
C_{m_α}	-.93	-.68	-1.98
C_{m_q}	-45.0	-24.3	-39.0
$C_{m_{\delta_e}}$	-2.18	-2.2 (Note 2)	-3.05
$C_{m_{\dot{\alpha}}}$	-15.6	-8.4	~

NOTES:

1) These results are interpolated from data at other flight conditions.
2) Extrapolated to q = 0.

The set of stability and control derivatives of the rigid body degrees of freedom corresponding to the above equations of motion are also shown in Appendix B. The column labeled "elastic increment" represents the static elastic correction for the structural modes not modeled dynamically in the equations of motion.

For the cruise condition, the following rigid body stability derivatives were chosen for subsequent calculations. It is felt that these values are the most accurate for the TIFS airplane.

$$C_{L_\alpha} = 5.92/\text{rad}$$
$$C_{m_\alpha} = -.26/\text{rad about c.g.} = .266\ \bar{c}$$

These changes are reflected in the cruise equations and stability derivatives in Appendix B.

An assessment of the accuracy of these equations must be postponed until sensor equations from FLEXSTAB can be computed. At that time comparisons of computed and observed responses of the TIFS in turbulence or responses to specific control inputs should be compared. These comparisons will be performed before control loops are closed around the TIFS aircraft.

The flexible equations of motion computed to date have included symmetric degrees of freedom only. An analysis of the importance of antisymmetric degrees of freedom on the overall objectives of this contract will be undertaken.

2.4.4 Aerodynamic Hinge Moments

Computation of hinge moments via theoretical means was not productive for the TIFS because of the presence of aerodynamic balance and tabs on the various control surfaces. The ailerons, for instance, are aerodynamically balanced using a Frise balance method. The resulting hinge moments are nonlinear functions of α and δ_a . Estimated aileron hinge moments obtained by Convair (Reference 13) are shown in Figure 27 and reveal that for small α the hinge moments are not dependent on α, for small δ_a the hinge moments vary linearly with δ_a and for large δ_a and α the functional dependence is nonlinear. Trim tabs on both ailerons are actuated by two sources. A trim knob in the cockpit allows the pilot to change the trim tab position by ± 7°. In addition, the trim tab is slaved to the aileron position for hinge moment control. The combined relationship between trim tab deflection δ_{tt} and aileron position is shown in Figure 28. Hinge moments about the aileron hinge axis can be computed as shown below.

$$HM = q\, S_a\, \bar{c}_a \left[C_{H_a}(\delta_a, \alpha) + C_{H_{a\delta_{tt}}}\, \delta_{tt} \right]$$

where S_a = area of one aileron aft of hinge line $(\not{H})$ = $\begin{cases} 21.91 \text{ ft}^2 \\ 2.035 \text{ m}^2 \end{cases}$

$\bar{c}_a$ = average aileron chord aft of $\not{H}$ = $\begin{cases} 1.26 \text{ ft} \\ .384 \text{ m} \end{cases}$

$C_{H_a}(\delta_a, \alpha)$ = C_{H_a} from Figure 4

q = dynamic pressure

$C_{H_{a\delta_{tt}}}$ = -.0028 per degree = trim tab effectiveness

δ_{tt} = trim tab deflection, is a function of δ_a and pilot's trim command, Figure 5

HM = hinge moment due to deflection of one aileron

Elevator aerodynamic hinge moments are shaped by two servo tabs, one on each tailplane. Deflections of each tab are determined by elevator deflection in a nonlinear relationship (tab deflection measured with respect to the elevator is down for both positive and negative elevator deflections). Gearing on the left hand tab, called the control tab, is not the same as on the right hand tab, called the trim tab. The trim tab has the additional function of trimming control wheel forces, an action which is initiated via a trim wheel in the cockpit. Total control column forces experienced by the pilot are a function not only of the aerodynamic hinge moments, but also the actions of a bungee spring (down spring) and a bobweight (control yoke balance weight).

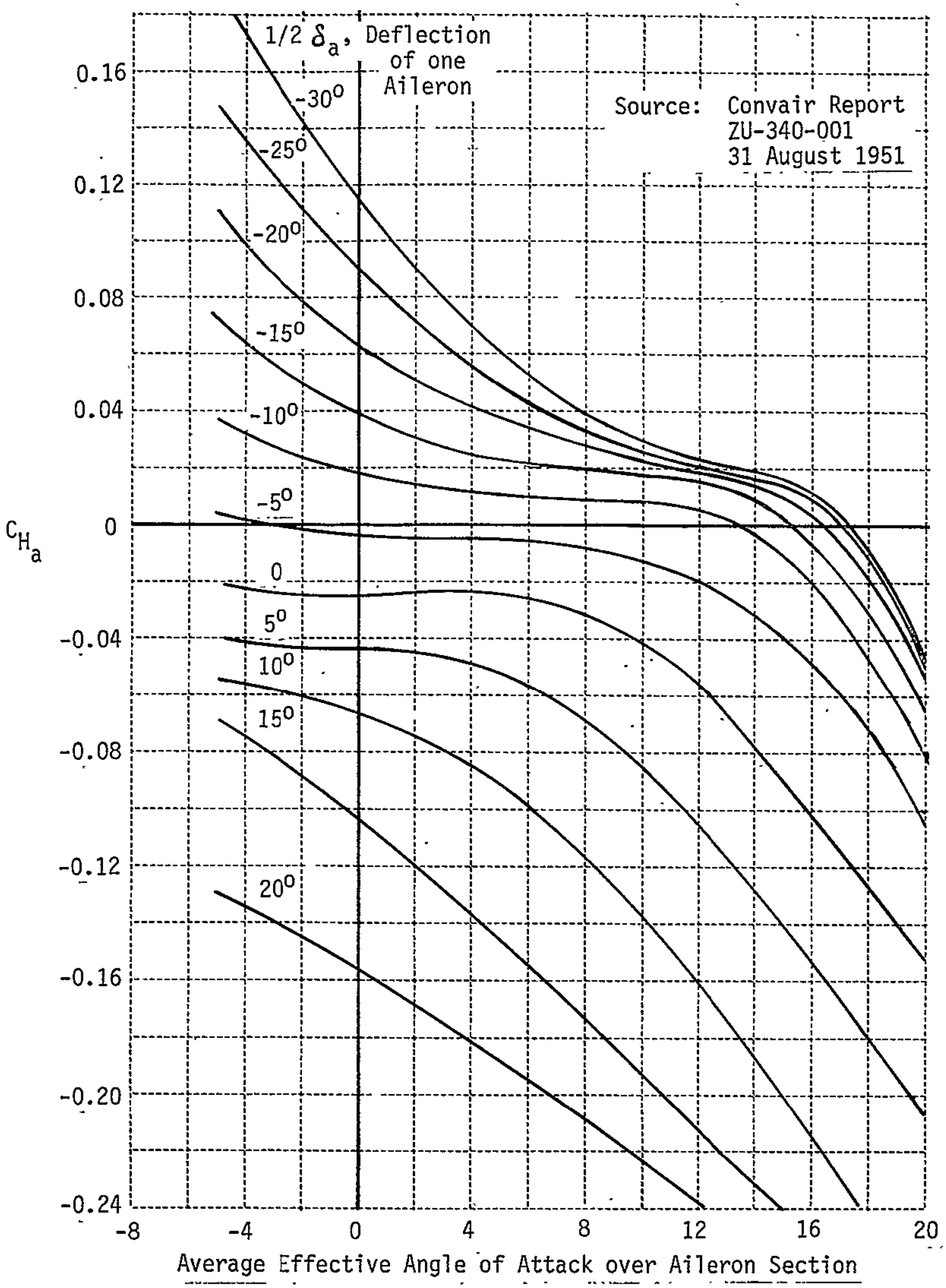

Figure 27 ESTIMATED AILERON HINGE MOMENTS

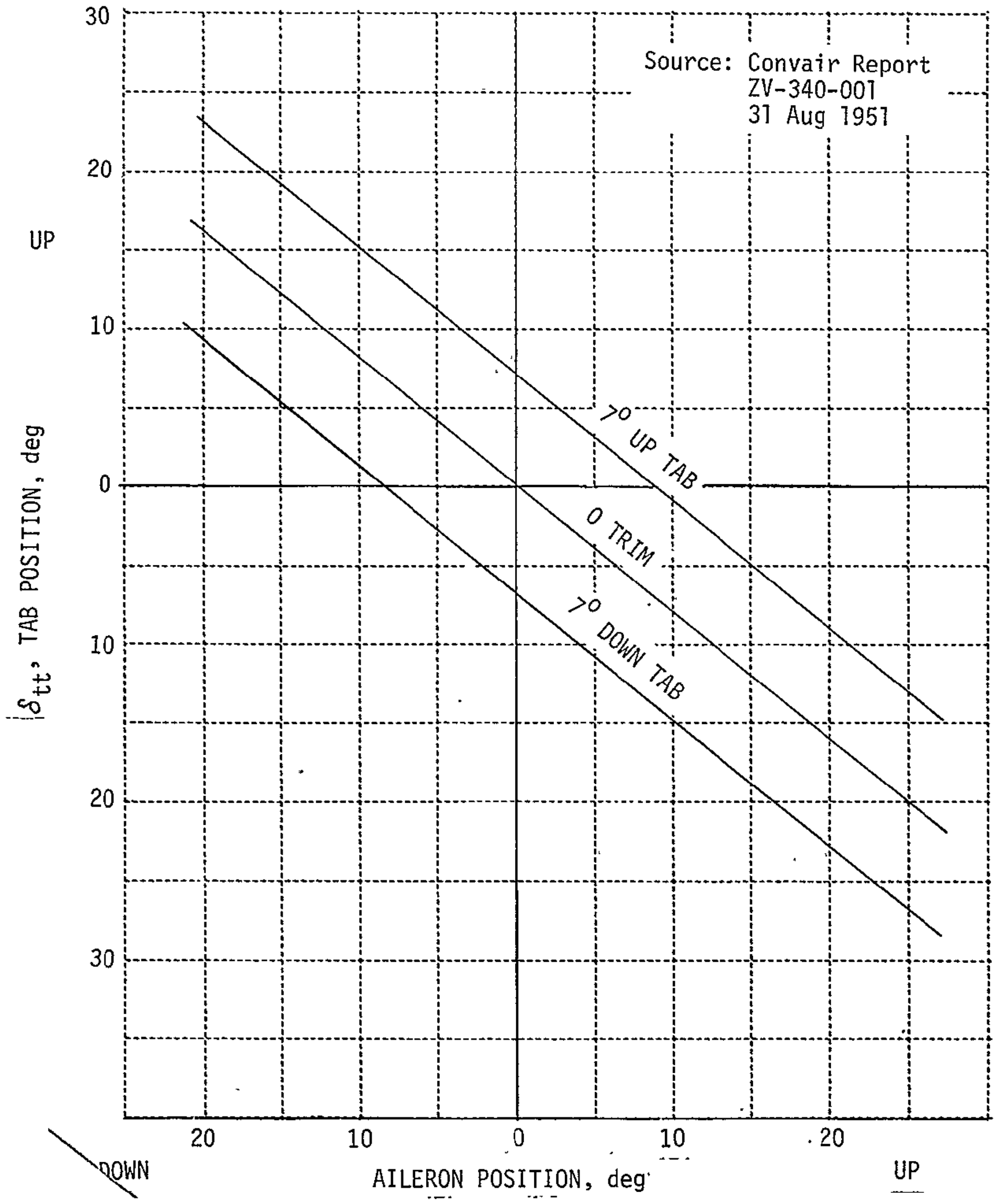

Source: Convair Report ZV-340-001 31 Aug 1951

Figure 28 AILERON TAB POSITIONS

C-2

The aerodynamic hinge moment about the elevator hinge line can be computed as follows:

$$HM = q S_e \bar{c}_e \left[C_{H_{e_\alpha}} \alpha + C_{H_{e_{\delta_e}}} \delta_e + C_{H_{e_{\delta_{tt}}}} \delta_{tt} + C_{H_{e_{\delta_{ct}}}} \delta_{ct} \right]$$

where S_e = elevator area aft of $H\!\!\!\!L$ = 71.32 ft^2
$\bar{c}_e$ = RMS chord of elevator aft of $H\!\!\!\!L$ = 2.28 ft
$C_{H_{e_\alpha}}$ = elevator hinge moment due to α = -.002/deg
$C_{H_{e_{\delta_e}}}$ = elevator hinge moment due to δ_e = -.0033/deg
$C_{H_{e_{\delta_{tt}}}}$ = trim tab effectiveness = -.0051/deg
$C_{H_{e_{\delta_{ct}}}}$ = control tab effectiveness = -.0037/deg
HM = hinge moment due to combined action of both left and right elevator surfaces

Trim tab and control tab positions are not currently measured on the TIFS. However, for each control surface the hinge moment can be computed from the differential pressure at the surface actuator.

Hinge moments for the direct lift flap which, like the aileron, has a nose seal, have been estimated from flight test measurements of differential pressure at the DLF actuator. Data was obtained for various flap deflections and angles of attack and was reported in Reference 14. A cross plot of hinge moment versus DLF deflection for constant angle of attack, shown in Figure 29, reveals that the hinge moment coefficient is nearly a linear function of DLF deflection. A linear approximation to this family of curves leads to the following representation of the DLF hinge moment.

$$HM = q S_z \bar{c}_z \left[C_{H_\alpha} \alpha + C_{H_{\delta_z}} \delta_z \right]$$

where q = dynamic pressure
S_z = area of one DLF, 4.161 m^2 (44.79 ft^2)

Ref. 14. Flight Research Staff: "Development, Design and Fabrication of the Total In-Flight Simulator (TIFS). Air Force Flight Dynamics Laboratory Report AFFDL-TR-71-77, August 1971.

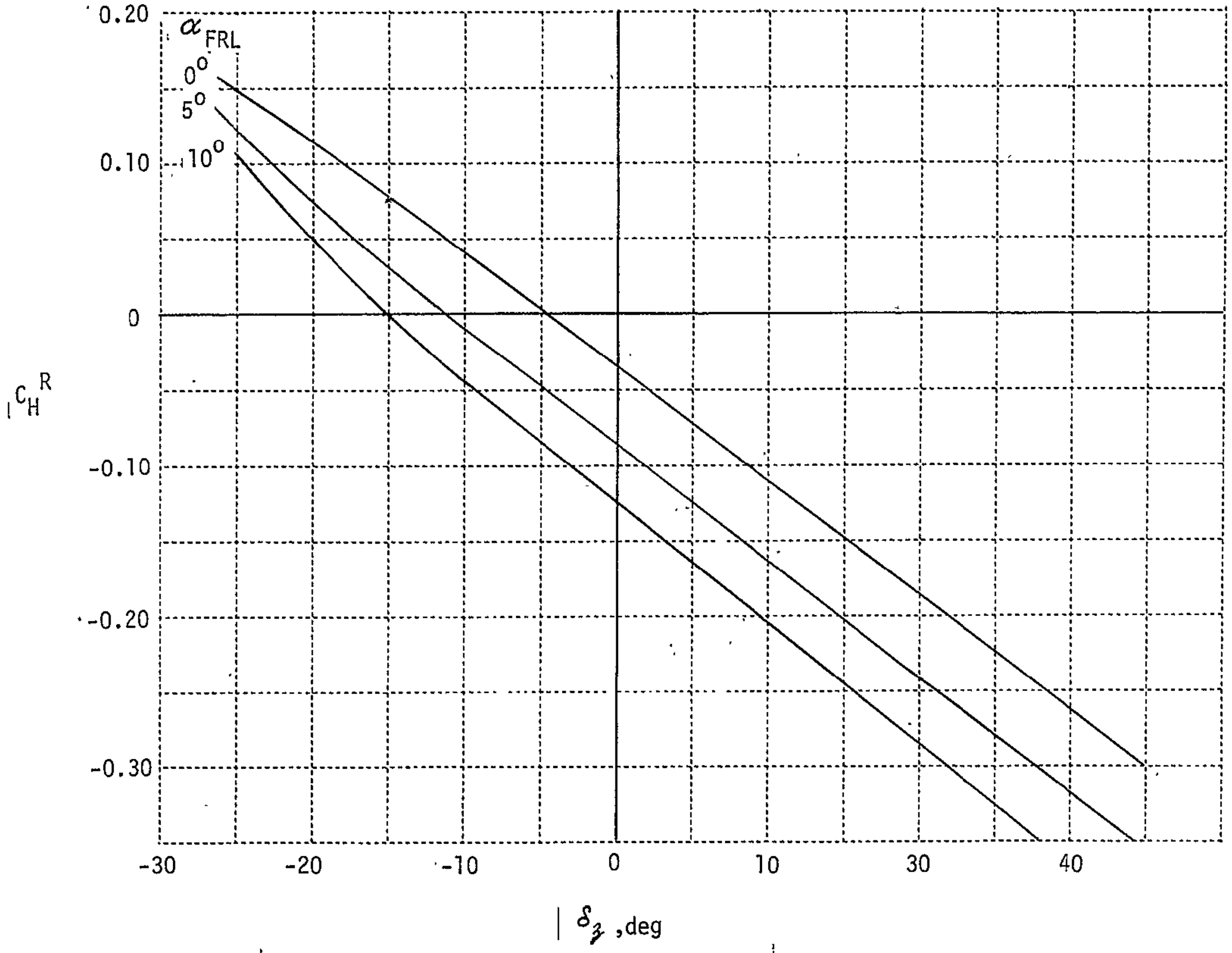

Figure 29 DLF HINGE MOMENT COEFFICIENT VS. DLF DEFLECTION

$\bar{c}_z$ = average chord of DLF, .677 m, (2.22 ft)
C_{H_α} = -.094/deg
$C_{H_{\delta_z}}$ = -.0075/deg
HM = hinge moment due to deflection of one flap

Aerodynamic hinge moment data for the aileron and elevator were obtained for the Convair 340 based on both wind tunnel testing and flight testing of the Convair 240. Because the 340 and TIFS are very similar aircraft, the hinge moment data so derived are considered to be representative of the actual TIFS hinge moment data. Direct assessment of accuracy is not possible without more thorough study of Convair's techniques. More accurate hinge moment data might be obtained by direct measurement in flight using differential pressure across the surface actuator.

Computations of the direct lift flap hinge moments were based on the following relationship:

$$C_H = \frac{\Delta P_z \, K_z(\delta_z)}{12 \, q \, S_z \, \bar{c}_z}$$

where ΔP_z is the actuator pressure
$K_z(\delta_z)$ product of actuator piston area and effective arm
S_z $\bar{c}_z$ and q are respectively flap area, flap mean chord and dynamic pressure.

The primary sources of error in this computation will be in measuring dynamic pressure and actuator pressure. Estimates of the accuracy of q and ΔP_z are ± 5% and ± 8% respectively. For the worst case, the resulting accuracy for C_H would be of the order of ± 14%. Better accuracy could be obtained by more accurate calibration of both sensors.

2.4.5 Pressure Distribution Data

Two sources of pressure or load distribution data are available. The first was utilized by Convair in the basic design of the Convair 340 series aircraft, Reference 13. Except for the effects of flaps and side force surfaces, this data is considered to be representative of the TIFS. The second source of data is FLEXSTAB which computes the pressure coefficient for numerous points on the aircraft for the trim configuration of the loaded, flexible aircraft. In producing the pressure distribution data, the pressures on the upper and lower lifting surfaces of the aircraft are differenced and nondimensionalized by the appropriate constant, i.e.

$$C_p = \frac{P_{lower} - P_{upper}}{\bar{q}}$$

If $C_{P_{ij}}$ and S_{ij} are the pressure coefficient and area of the aerodynamic panel in the ith spanwise row and jth chordwise row of the wing, then the lift load for the j chordwise row is given by

$$\frac{L_i}{q\,\Delta Y_i} = \frac{1}{\Delta Y_i} \sum_{i=1}^{NC} C_{P_{ij}} S_{ij}$$

where L_i is the lift on the ith chordwise row
q is dynamic pressure
ΔY_i is the width of the ith chordwise row.

The lift load distribution obtained above can be compared directly to the lift load distribution computed by Convair in the following manner.

$$\frac{dL'(y)}{q} = c(y)\; C_\ell(y) = c(y)\, C_{\ell_a}(y)\, C_L + c\, C_{\ell_b}$$

where $dL'(y)$ is the lift per unit span
$c(y)$ is the local wing chord
$C_\ell(y)$ is the local lift coefficient
$C_{\ell_a}(y)$ is the additional lift distribution

C_{ℓ_b} is the basic lift distribution, the lift distribution when $C_L = 0$

C_L is wing lift coefficient.

A comparison of lift load distribution computed by FLEXSTAB and Convair is shown in Figure 30. Very reasonable agreement is apparent except at the wing tip where an additional chordwise row in the FLEXSTAB model is needed. From this, it is reasonable to conclude that FLEXSTAB and Convair will also predict approximately equal wing root bending moments.

The FLEXSTAB pressure coefficient data corresponding to this condition is included in Appendix C. Convair data in the form of additional and basic lift load distributions are shown in Figures 31 and 32. The additional load distribution due to aileron deflection is not currently available from FLEXSTAB, however, the Convair estimate is shown in Figure 33.

The moment distribution corresponding to the above-mentioned pressure distributions are not yet available from FLEXSTAB though they can be computed from the data of Appendix C. The Convair estimated moment distribution about the wing elastic axis (36.5%) is shown in Figure 34..

Chordwise pressure distributions as computed by FLEXSTAB at three locations are shown in Figures 35 and 36. These figures represent pressure coefficient distributions at the trim configuration with flap and ailerons undeflected. Pressure distribution plots provided by Convair based upon wind tunnel tests of a Convair 240 model corrected to the 340 configuration, are shown in Figures 37 and 38. Pressure distributions for two aileron deflections are presented in Figures 39 and 40. The total pressure coefficient is computed from these figures from the following:

$$\left.\frac{\Delta P}{q}\right|_{C_\ell \neq 0} = \left.\frac{\Delta P}{q}\right|_{C_\ell \neq 0} + C_\ell \left(\frac{\Delta P}{q}\right)_{additional}$$

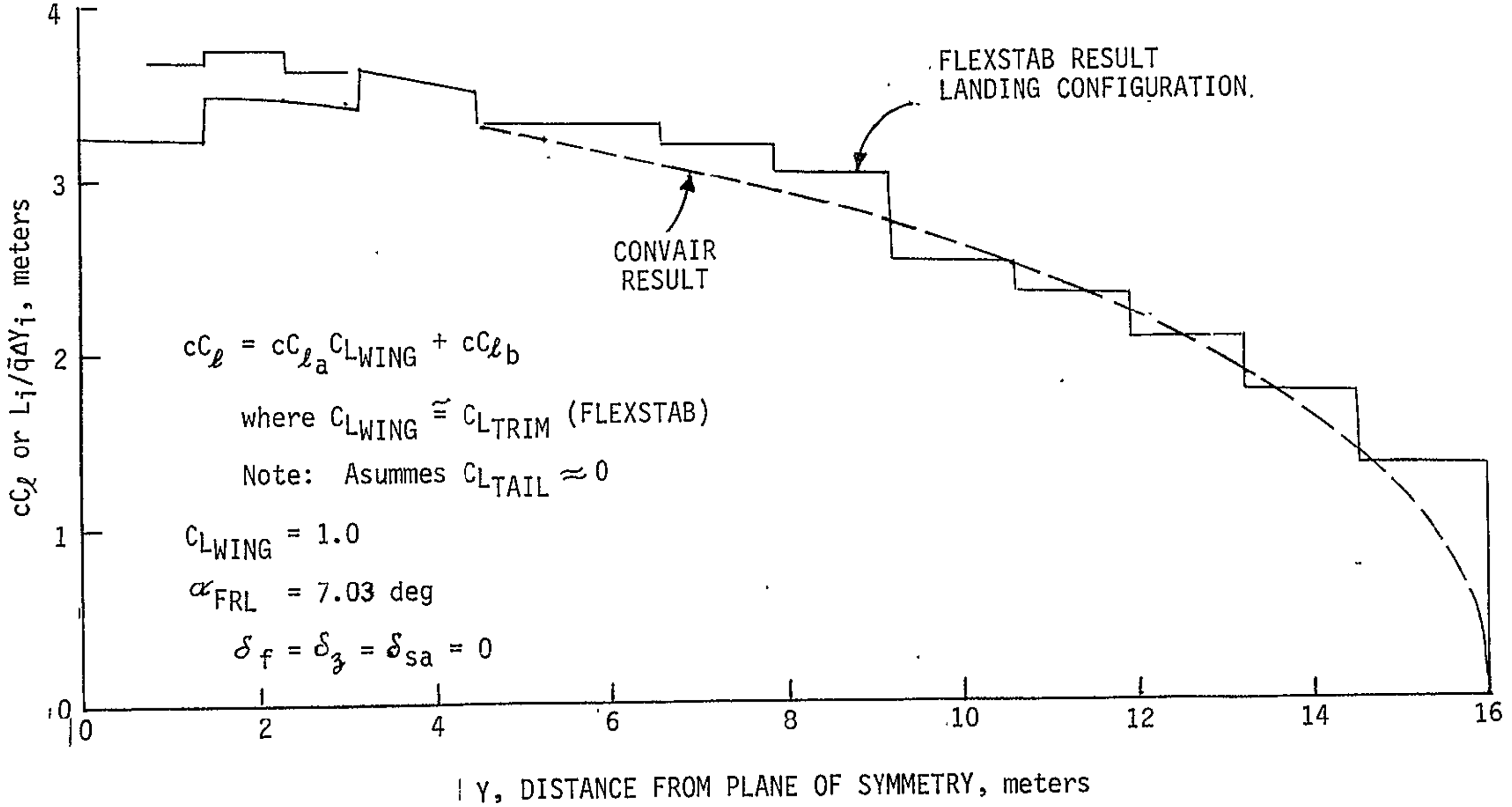

Figure 30 TOTAL WING LIFT LOAD DISTRIBUTION

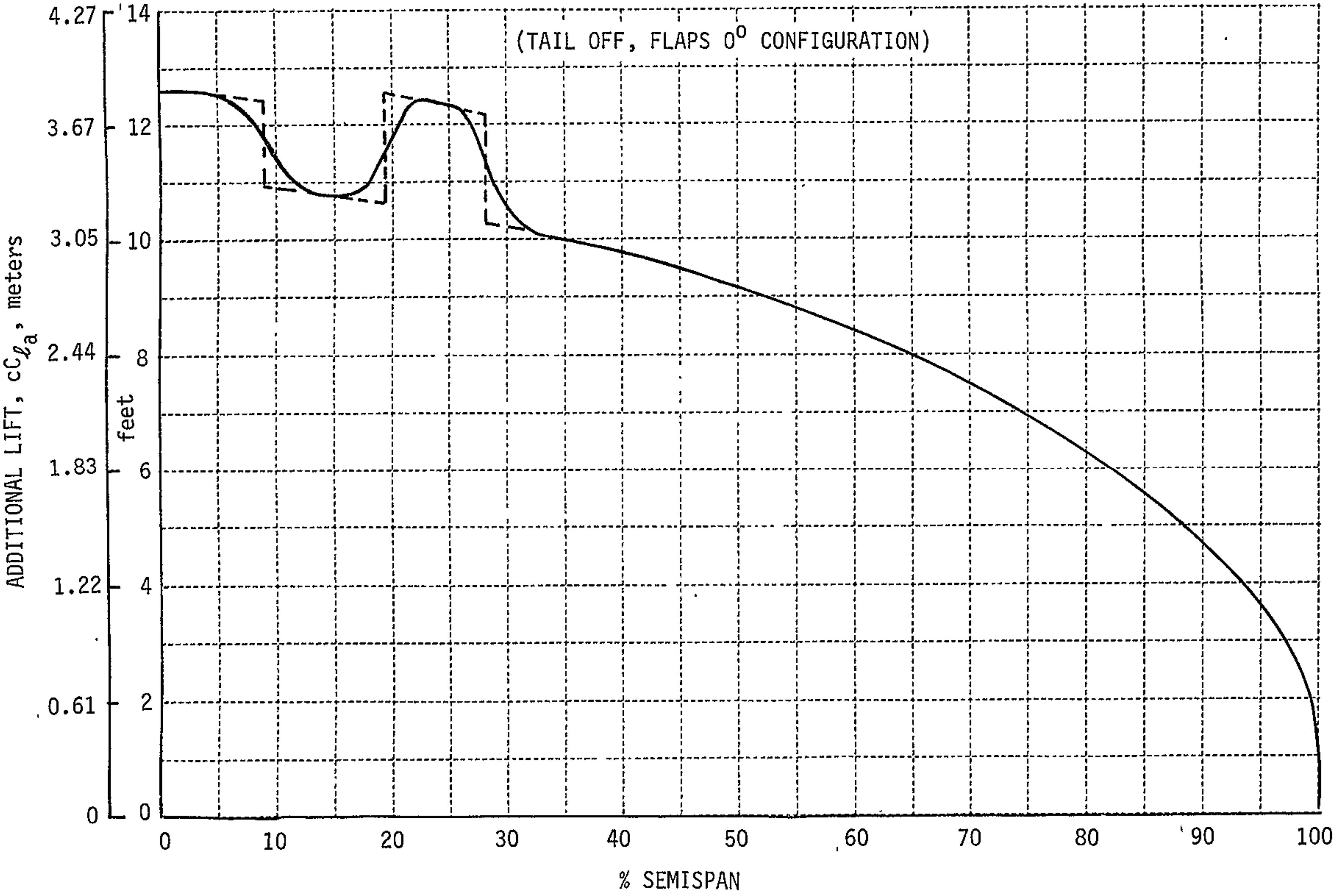

Figure 31 ADDITIONAL LIFT LOAD DISTRIBUTION

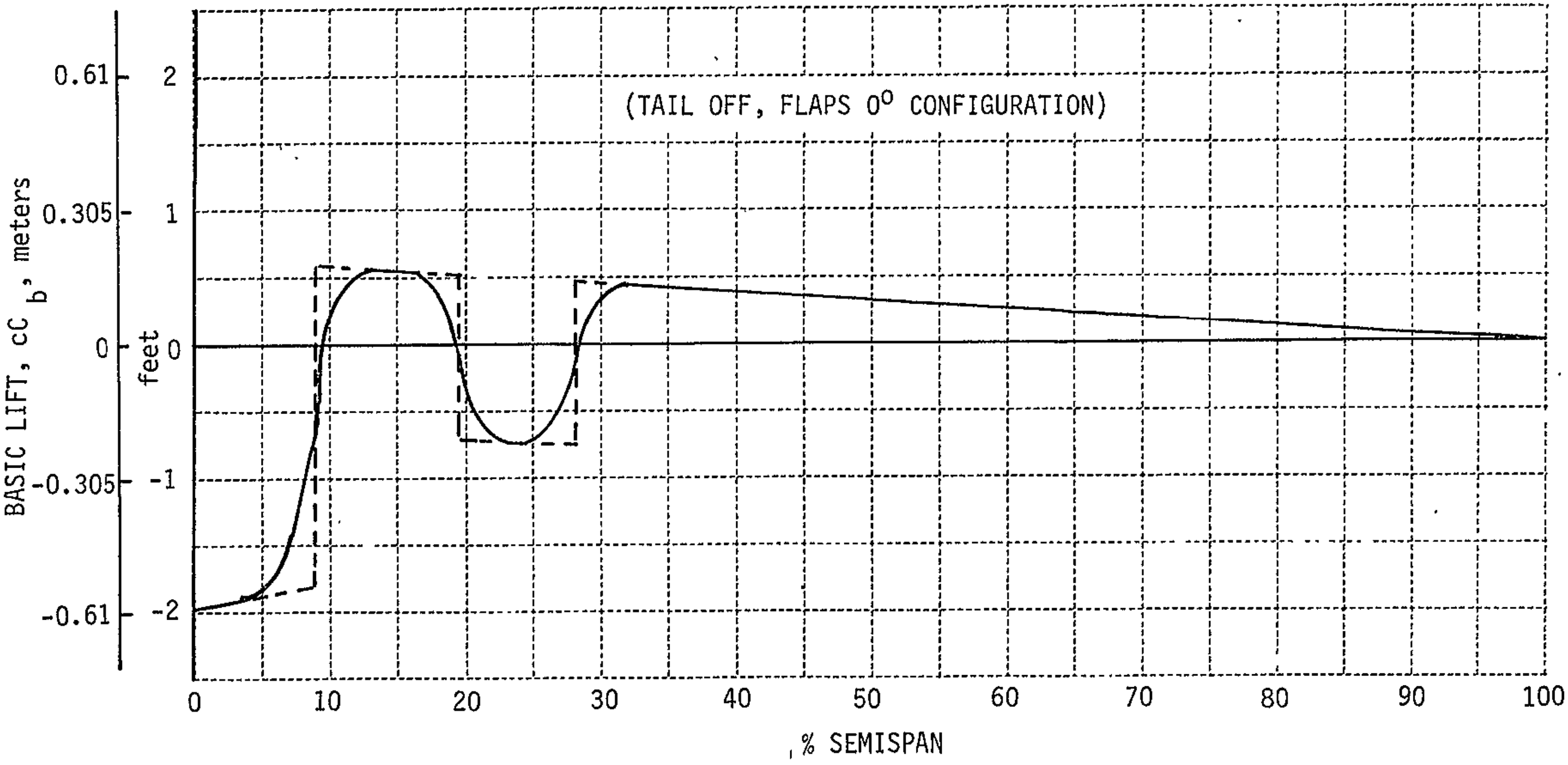

Figure 32 BASIC LIFT LOAD DISTRIBUTION

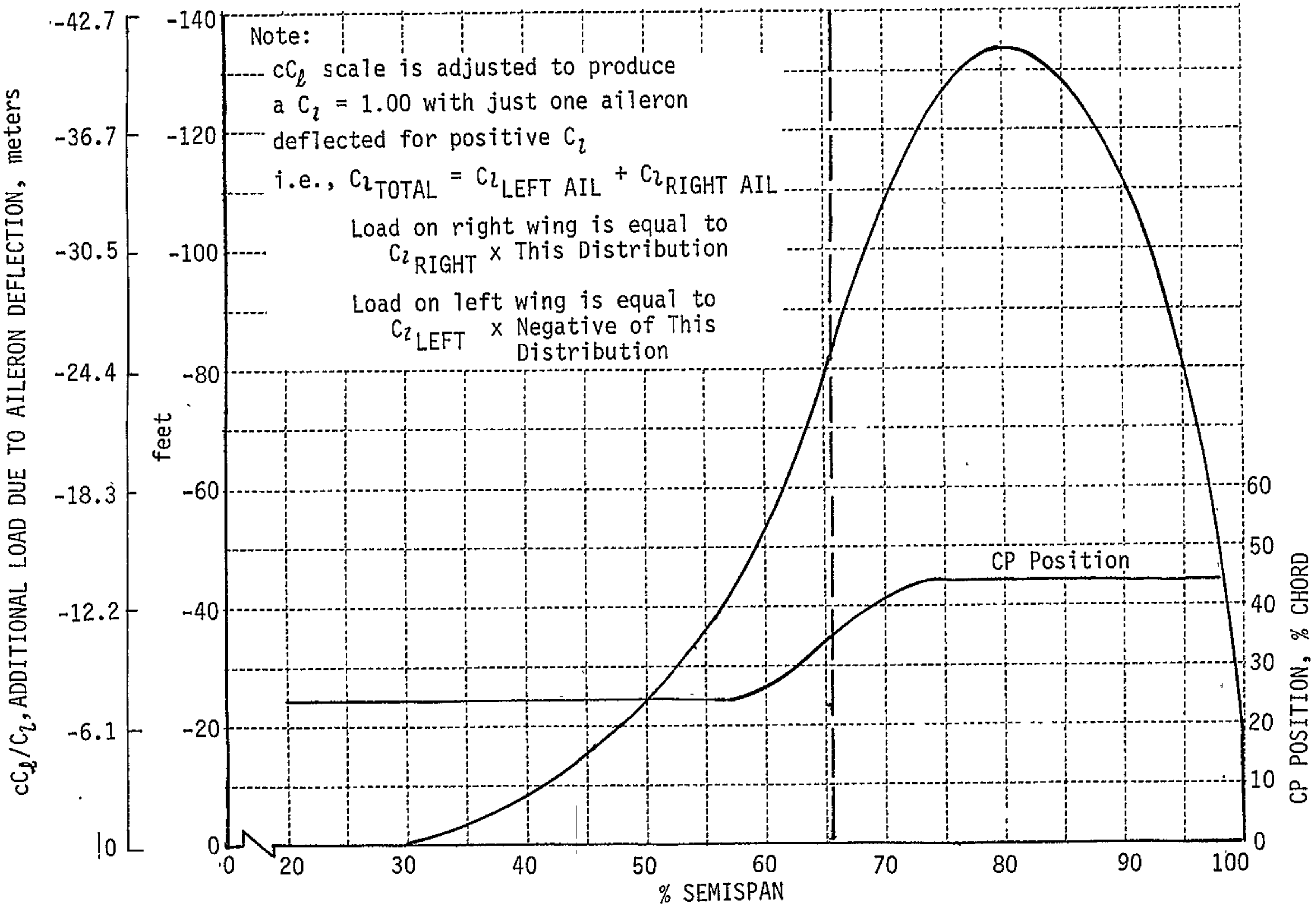

Figure 33 WING LOAD DISTRIBUTION DUE TO AILERON DEFLECTION

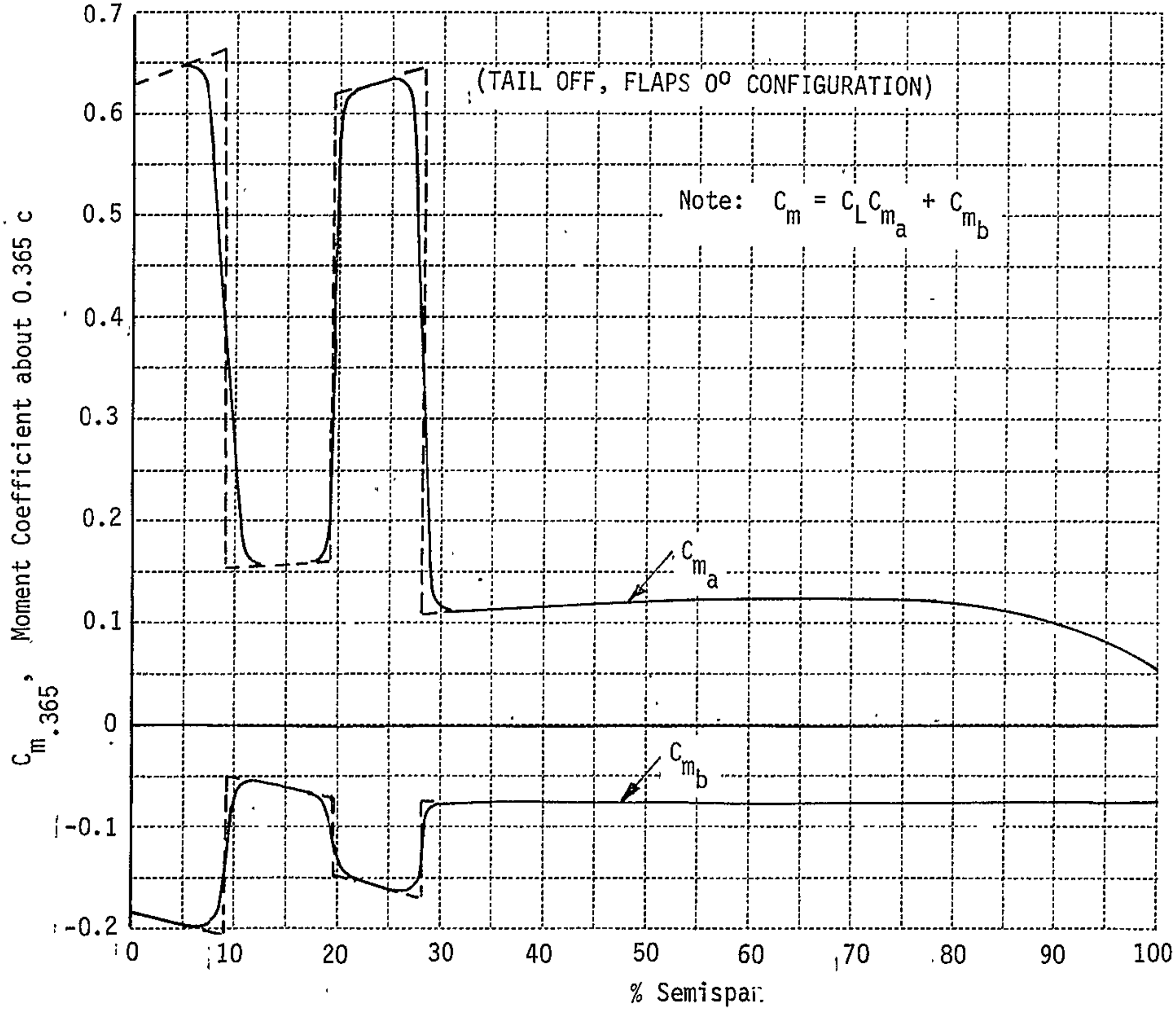

Figure 34 MOMENT DISTRIBUTION ABOUT THE 36.5% LOCAL CHORD LINE

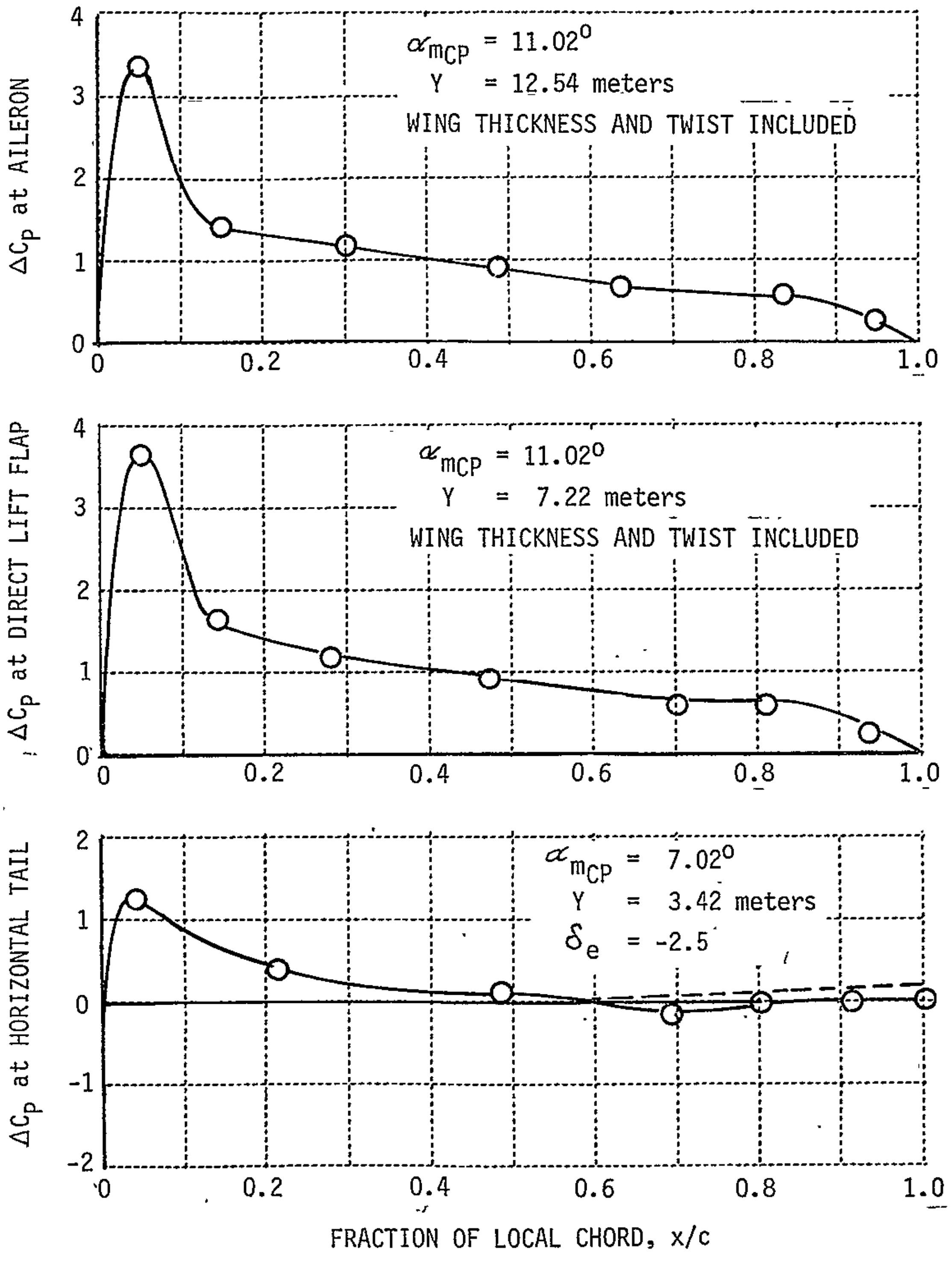

Figure 35 PRESSURE COEFFICIENT AT TRIM
α_{FRL} = 7.02°, LANDING, M = 0.2, H = 61 meters

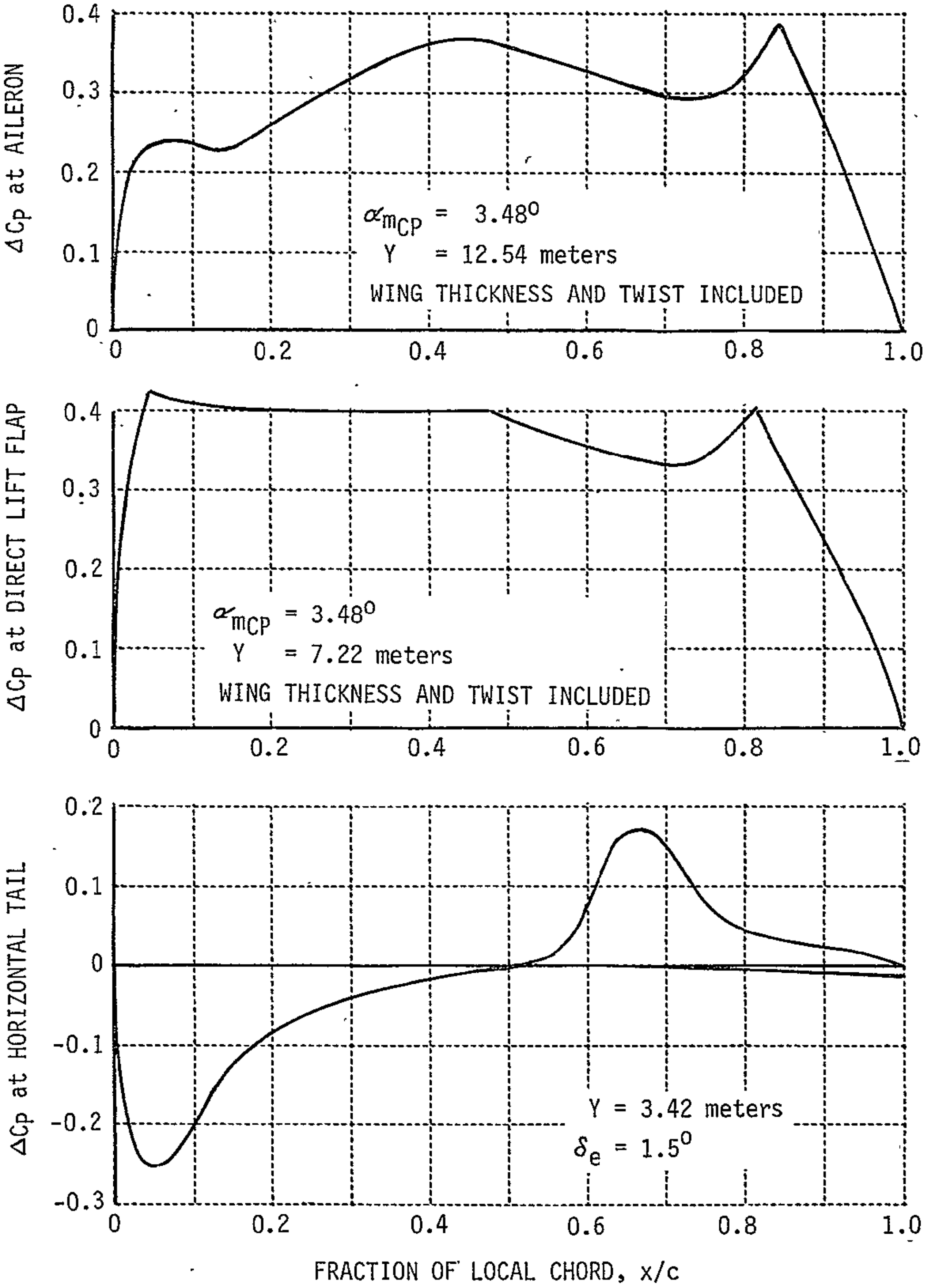

Figure 36 PRESSURE COEFFICIENT AT TRIM
α_{FRL} = -0.52°, CRUISE, M = 0.456, H = 3048 meters

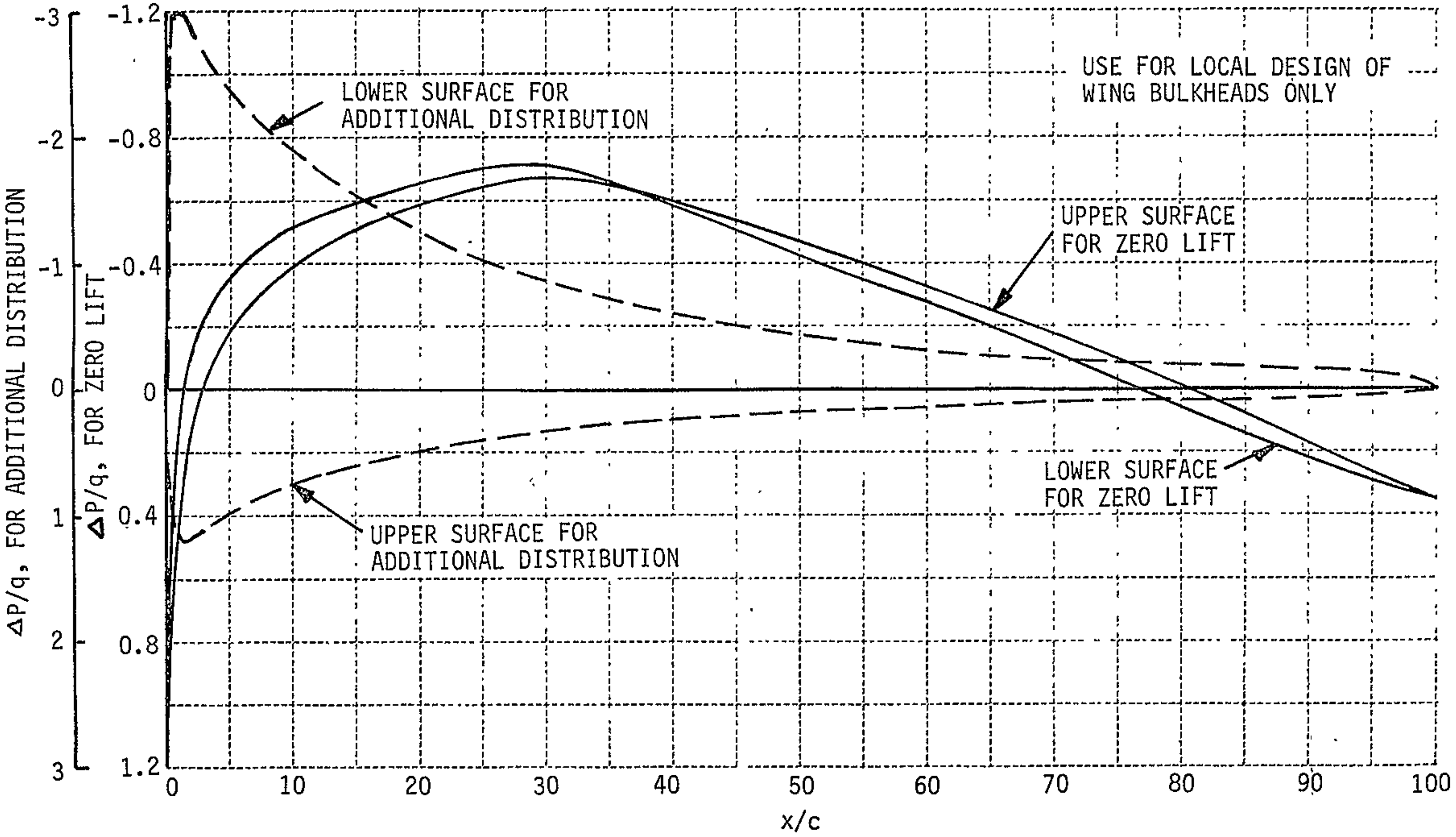

Figure 37 PRESSURE DISTRIBUTION ON ROOT SECTION

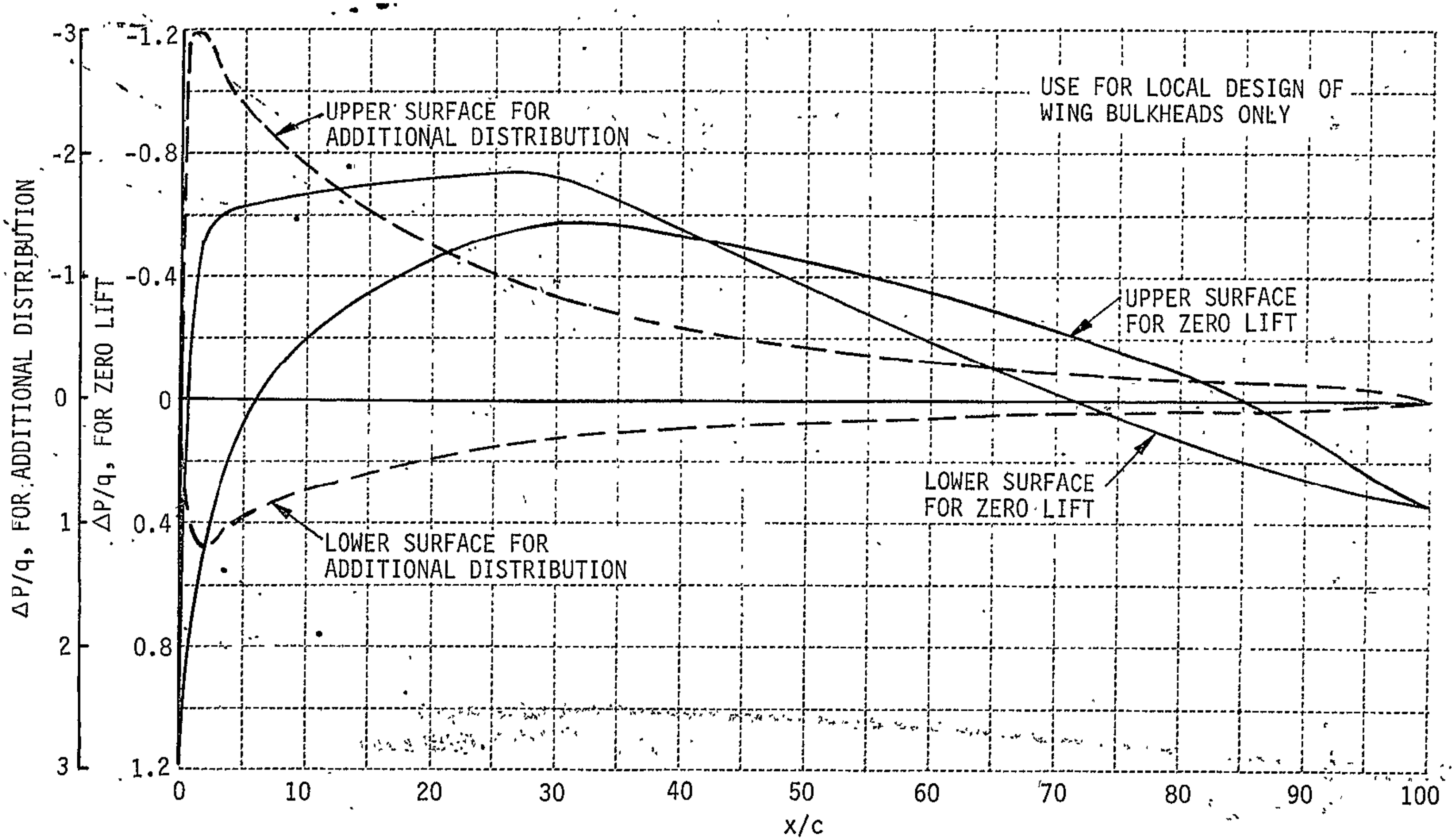

Figure 38 PRESSURE DISTRIBUTION OUTBOARD OF BREAK SECTION

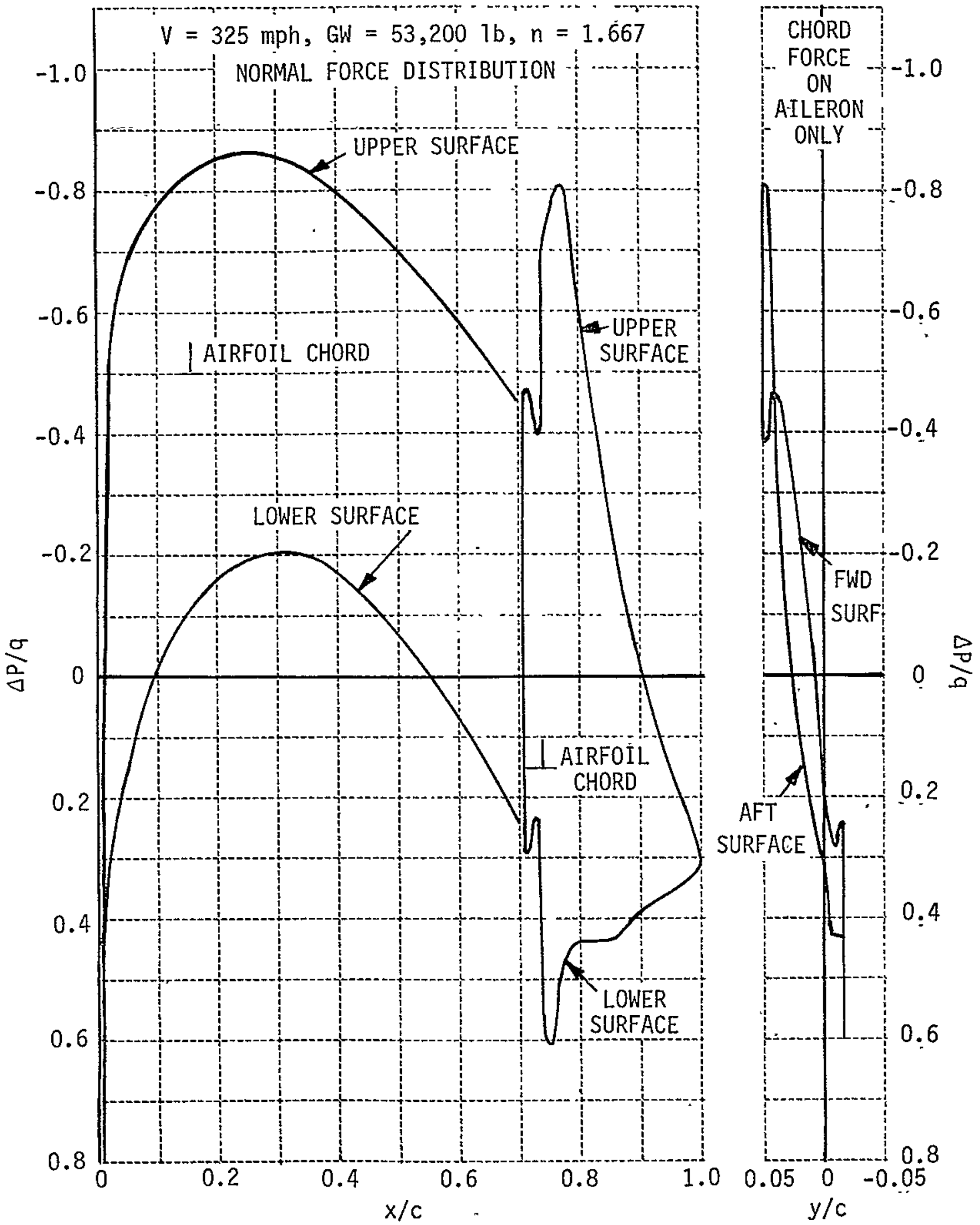

Figure 39 PRESSURE DISTRIBUTION AT $\eta_w = 0.80$, $\delta_a = 11.6^{\circ}$ DOWN

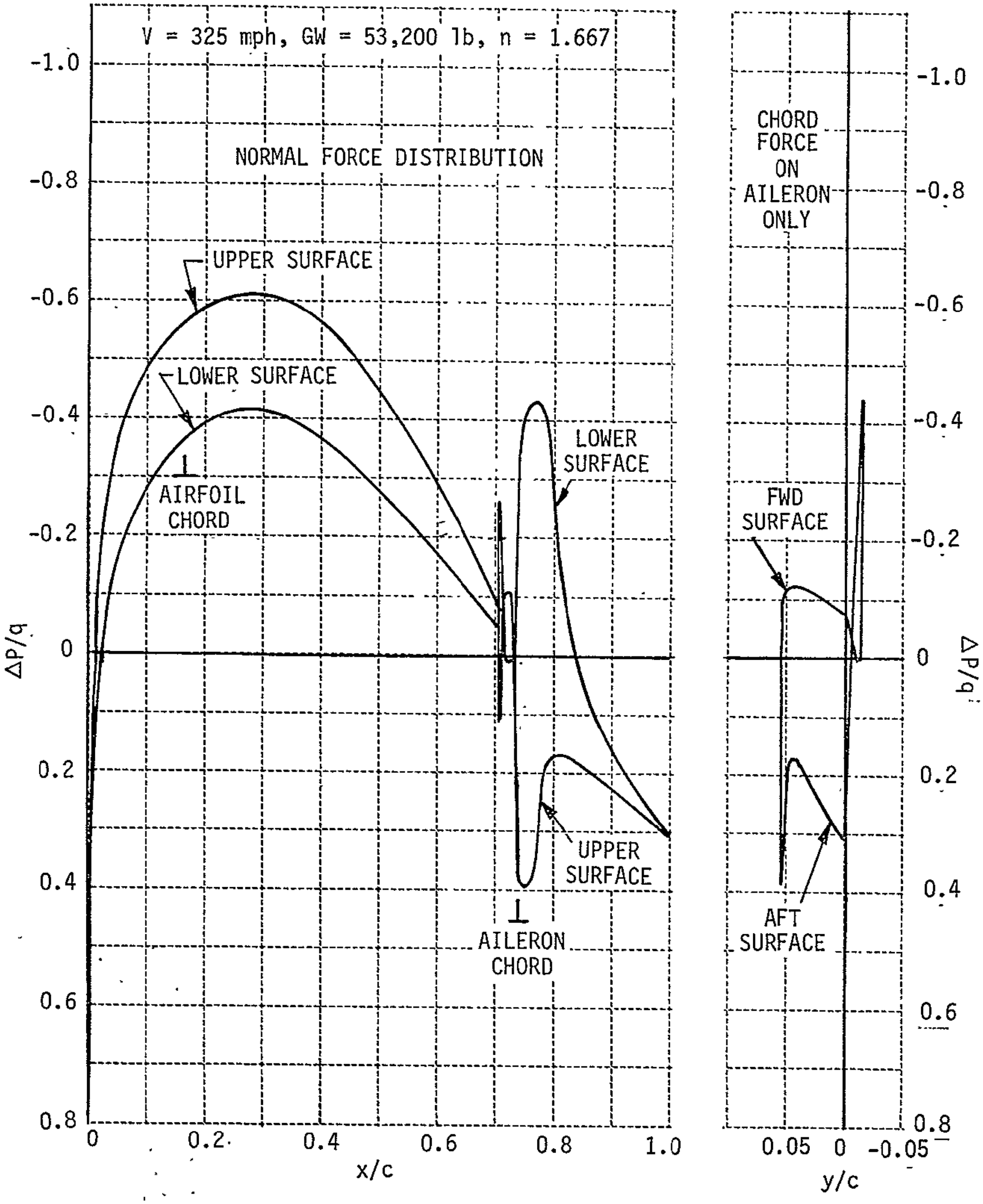

Figure 40 PRESSURE COEFFICIENT AT η_{ω} =0.80, δ_a = 15° UP

where C_ℓ = section lift coefficient
ΔP = local static pressure minus free stream static pressure
q = dynamic pressure

Direct comparison of FLEXSTAB and Convair pressure distributions have not as yet been completed.

The accuracy of the pressure-load data presented in this section is not known at this time. A study of the accuracy of the Convair techniques was not made. FLEXSTAB pressure distributions, on the other hand, are subject to the following qualifications. Comparison between wind tunnel pressure data and FLEXSTAB predictions for the B-52 aircraft, Reference 7, Vol. IV, has indicated that in the region of the leading edge ($x/c < .05$) FLEXSTAB substantially overpredicts the differential pressure. The excessive peak near the leading edge is caused by the leading-edge aerodynamic singularity inherent in the aerodynamic theory. In the TIFS model the leading edge panel was approximately 10% of the local chord, much larger than for the B-52 model. Since one pressure is computed for each panel the effect of the larger panel was one of averaging the theoretical pressure distribution over the width of the panel thereby reducing the effect of the leading edge singularity. In addition, FLEXSTAB will not account for separated flow phenomena which may exist at certain flight conditions (e.g., in landing where $\alpha_{FRL} = 7^\circ$, $\alpha_{WING\ ROOT} = 11^\circ$). In regions of separated flow FLEXSTAB will also overpredict the pressure coefficient. A quantitative assessment of the accuracy of pressure distribution data is not available at this time.

Section 3

SENSOR AND SERVO SYSTEM

3.1 INTRODUCTION

This section briefly describes the TIFS servo and sensor concepts, installation and general arrangement. Dynamic and static performance information for the servos and the instrumentation are described in more detail, because these are the characteristics of the system pertinent to an ACT control system configuration for the aircraft.

3.2 GENERAL INSTRUMENTATION AND SERVO SUBSYSTEM DESCRIPTION

The electronic system for TIFS is composed of the subsystems arranged in Figure 41 and listed as follows:

1. Sensors and Sensor Electronics — The sensors measure various angles, rates and accelerations of the TIFS aircraft. These sensor outputs are converted to properly scaled DC voltages representing parameters used in the control of the TIFS.

2. Feel System — A feel system for each evaluation pilot provides variable force versus position gradients for the elevator and aileron control wheel and the rudder pedals. This control system can simulate a linear spring feel or nonlinear feel characteristics composed of variable amounts of deadband, breakout force and hysteresis.

3. Surface and Throttle Servos — Electrohydraulic servos control the position of the elevator, aileron, rudder, flaps and side force surfaces. Magnetic powder clutch servos are used for the throttle position servos. Rate and acceleration stabilization techniques are provided to shape the dynamic responses of these servos.

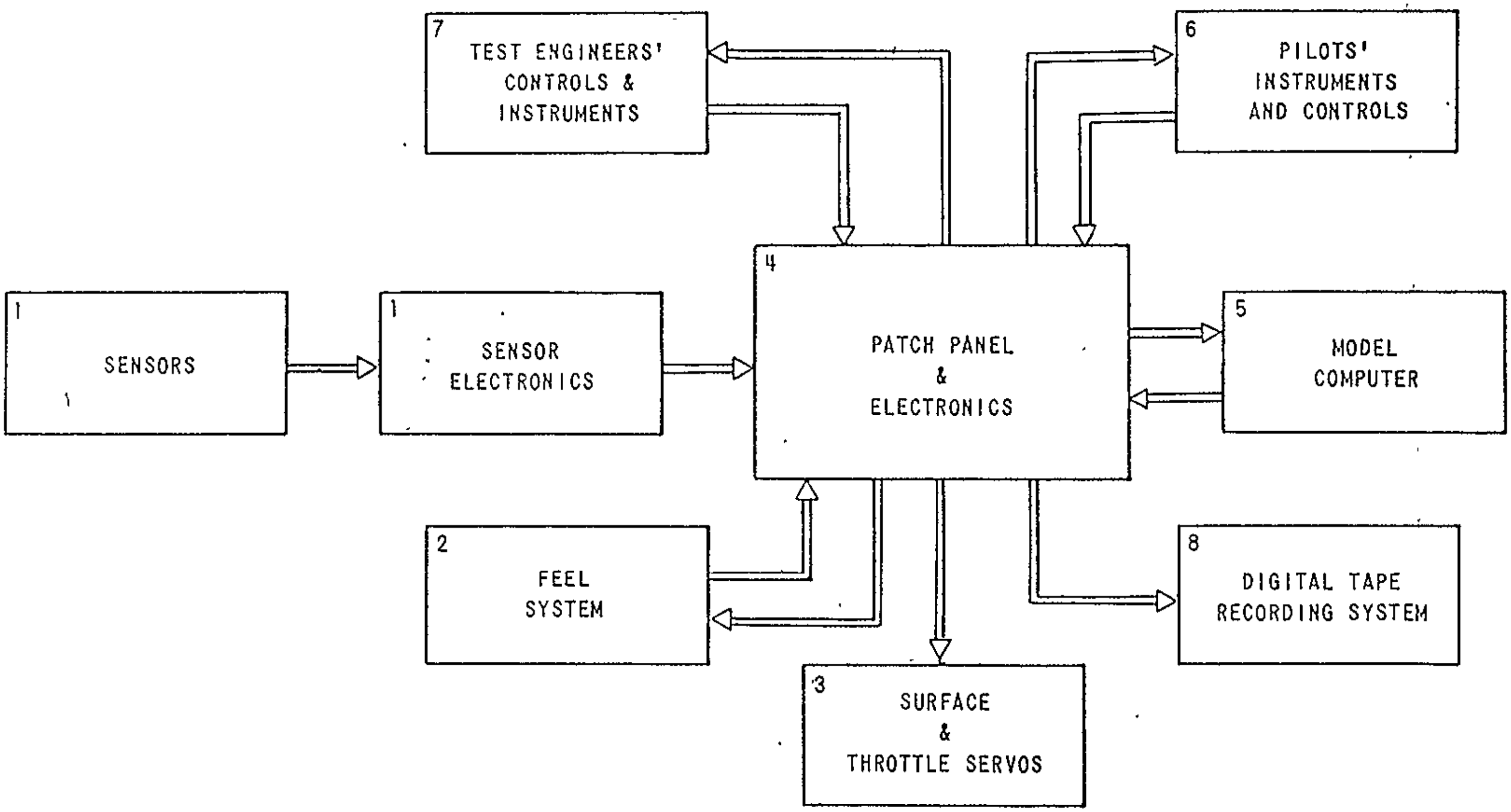

Figure 41 TIFS ELECTRONIC SYSTEM BLOCK DIAGRAM

4. Model-Following - Response-Feedback Patch Panel Electronics — The MF-RF patch panel ties together all of the other subsystems of the TIFS electronics. The most important function of the electronics is to process the signals between the TIFS input variables and airplane variables to provide the required surface and throttle position commands.

5. Model Computer — The model computer provides command augmentation between the pilot control stick input commands and the input signals to the control surface servos. This computer can be programmed for as simple as a first order lag to a multi-controller dynamic system representing the equations of motion of a complete aircraft for model-following operation.

6. Pilot Instruments and Controls — Servo driven flight and engine instruments are provided for each evaluation pilot. The inputs to each instrument can be patched on the MF-RF panel from the sensors or the model computer. Throttle, wing-sweep, flap, and speed-brake levers are mounted on the center control console. Each provides a proportional electrical signal for simulated control inputs.

7. Test Engineers' Control and Instrument Panels — Two test engineers control and monitor the operation and performance of the TIFS system on separate panels. One panel contains switches and status lights that control and indicate the engagement sequence of the various subsystems. The other panel contains instruments and a strip chart recorder to monitor the model-following performance.

8. Digital Tape Recording System — Fifty-eight channels of digital recording are provided with tape coding compatible with the IBM 360 computer system. A ground playback unit is provided which can play back any 8 channels simultaneously on an analog recorder.

3.3 SURFACE SERVOS

A simplified block diagram of a typical surface servo is presented in Figure 42. The surface position feedback signal is subtracted from the command signal, with the resultant error signal used to current drive the hydraulic flow control valve. High frequency position feedback for the system is obtained from the strut position while low frequency and DC feedback are obtained from the surface position. The surface rate and acceleration terms are available to shape the dynamic response of the servo.

An additional feature of the servo loop is the auto balance system which electronically nulls surface command signals before system engagement to avoid undesirable transients.

An electronic safety trip system is built into the patch panel electronics. If a predetermined maximum safe surface rate is exceeded or if a system failure causes an abrupt high level surface rate command, the system is automatically disconnected. Also available on the panel are the outputs of electrical differential pressure gages mounted across each actuator. Any combination of these signals may be monitored by the electronic safety trip system.

Pressure limiting check valves are coupled around each hydraulic actuator to prevent damage to the surfaces due to excessive surface hinge moments. In addition to these precautions, either safety pilot may disengage the system at any time by using a dump button if he feels that excessive control rates or vibrations are occurring.

To ensure that the flight control surfaces can be easily operated by the safety pilot when the TIFS system is "off", several safeguards are provided but are not discussed in this report.

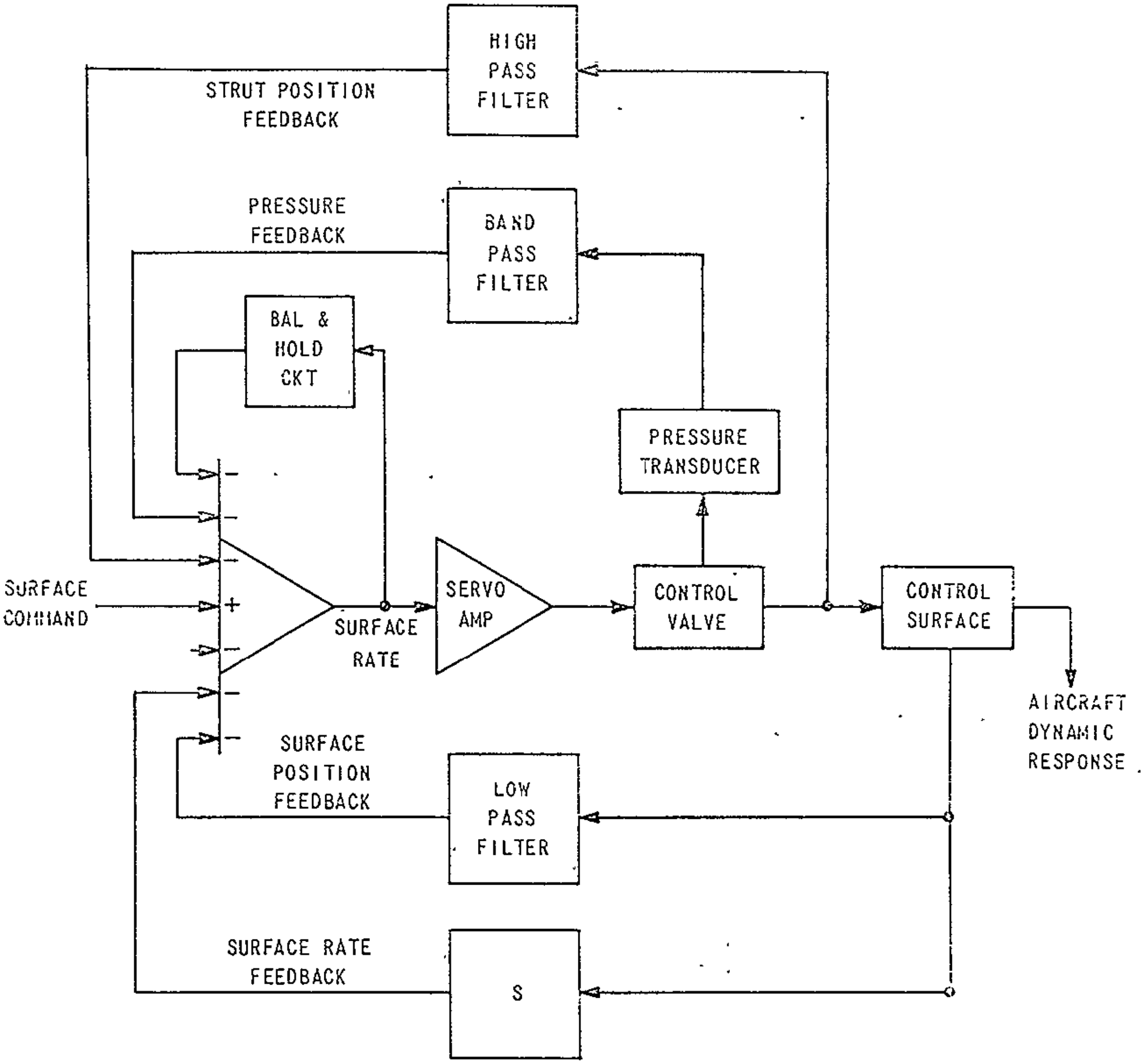

Figure 42 SIMPLIFIED DIAGRAM OF TYPICAL SURFACE POSITION SERVO

3.3.1 Surface Servo Performance

Intuitively, it can be reasoned that the best way to stabilize the highly resonant loads of the TIFS surface servos would be to use a notch or antiresonant network. At various times it has been proposed to insert passive networks inside a servo loop to accomplish this cancellation of system dynamics. The idea is fine on paper; however, in practice this approach presents problems. Once a configuration of passive circuit elements is tuned to give the required antiresonant characteristic, system operation relies on an unchanging load resonance and an unchanging compensation characteristic. Since both these effects are very powerful, any drift of load resonance or compensation circuitry will prevent cancellation of the resonance or compensation circuitry will prevent cancellation of the resonance and may possibly result in system instability.

However, it can be shown that pressure feedback in a resonant-loaded position servo is a form of antiresonant feedback which is continually slaved to the exact load resonance phenomena. For this reason, all of the surface servos incorporate pressure feedback. The block diagrams for the surface servos (Figure 42) show that the pressure signal is not connected directly to the servo summing junction but is first passed through a band-pass filter. Without this filter static position errors would be produced due to the force being generated by the actuator.

The primary position feedback signal for the surface servos is shown in the block diagrams to come from the actuator for the elevator, SFS and DLF servos, whereas the aileron and rudder servos use information near the surface being controlled. Surface position feedback was used in these servos to remove static position errors due to flexure in the links between the actuators and the surfaces. Linkage flexure is a more significant problem for the primary surfaces on the airplane because the actuators for these surfaces are connected to the original torque tubes and cables which are more flexible than the linkages in the side force surface and direct lift flap.

Surface position feedback was tried on the elevator servo as well as the aileron and rudder servos. However, the low natural frequency quency of the elevators produced significantly lower frequency response for this servo when surface position feedback was used. Consequently, it was decided to use strut position feedback for the elevator servo even though positional errors of 5 - 10% occur as a function of aerodynamic loads on the surface.

In addition to the primary feedback signals shown in Figure 42, the TIFS electronic system provides signals proportional to surface rate and surface acceleration which may be used to improve the response of the servo. Although rate feedback should theoretically provide damping, the amount of improvement which could be obtained when it was used in the TIFS servos was minimal.

The block diagrams also show that when surface position feedback is used, it is low-pass filtered and the high frequency information is obtained from the strut position transducer. This technique makes it possible to obtain wide-bandwidth servos with good surface positioning accuracy. If surface position were used alone with the low-pass filter removed, stability criteria would necessitate lower gains with poorer dynamic performance.

The frequency response of the TIFS surface servos is shown in Figures 43 through 50. The in-flight servo surface frequency response is shown in Figure 51 through 55. On some of the surface servos, particularly the elevator servo, the effect of aerodynamic loading can be seen to have the effect of introducing a first order lag that will be a function of flight condition. At maximum dynamic pressure, this lag will reduce the bandwidth of the elevator surface servo down to about 1.5 Hz. This effect has been verified by in-flight experimentation.

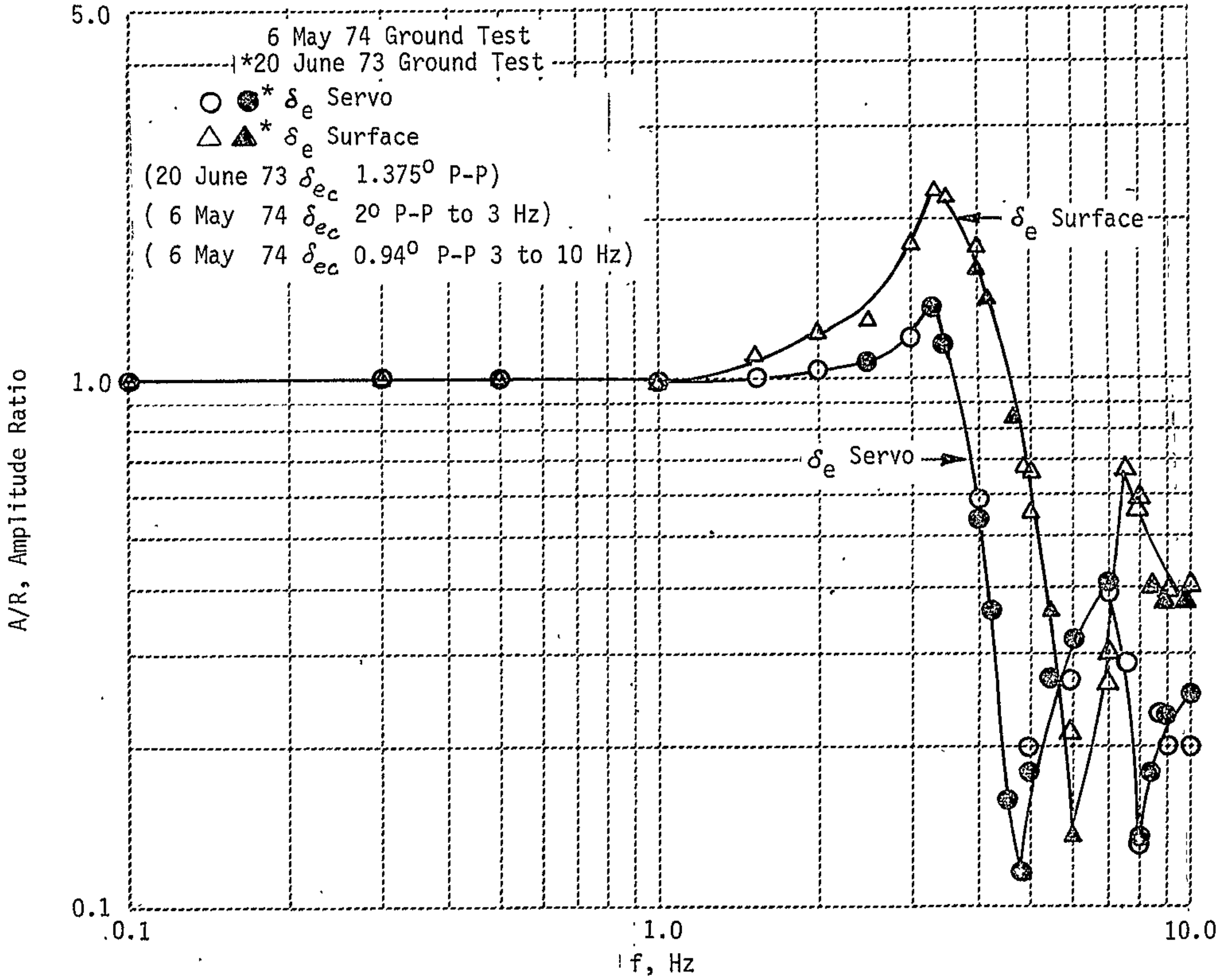

Figure 43 TIFS ELEVATOR FREQUENCY RESPONSE

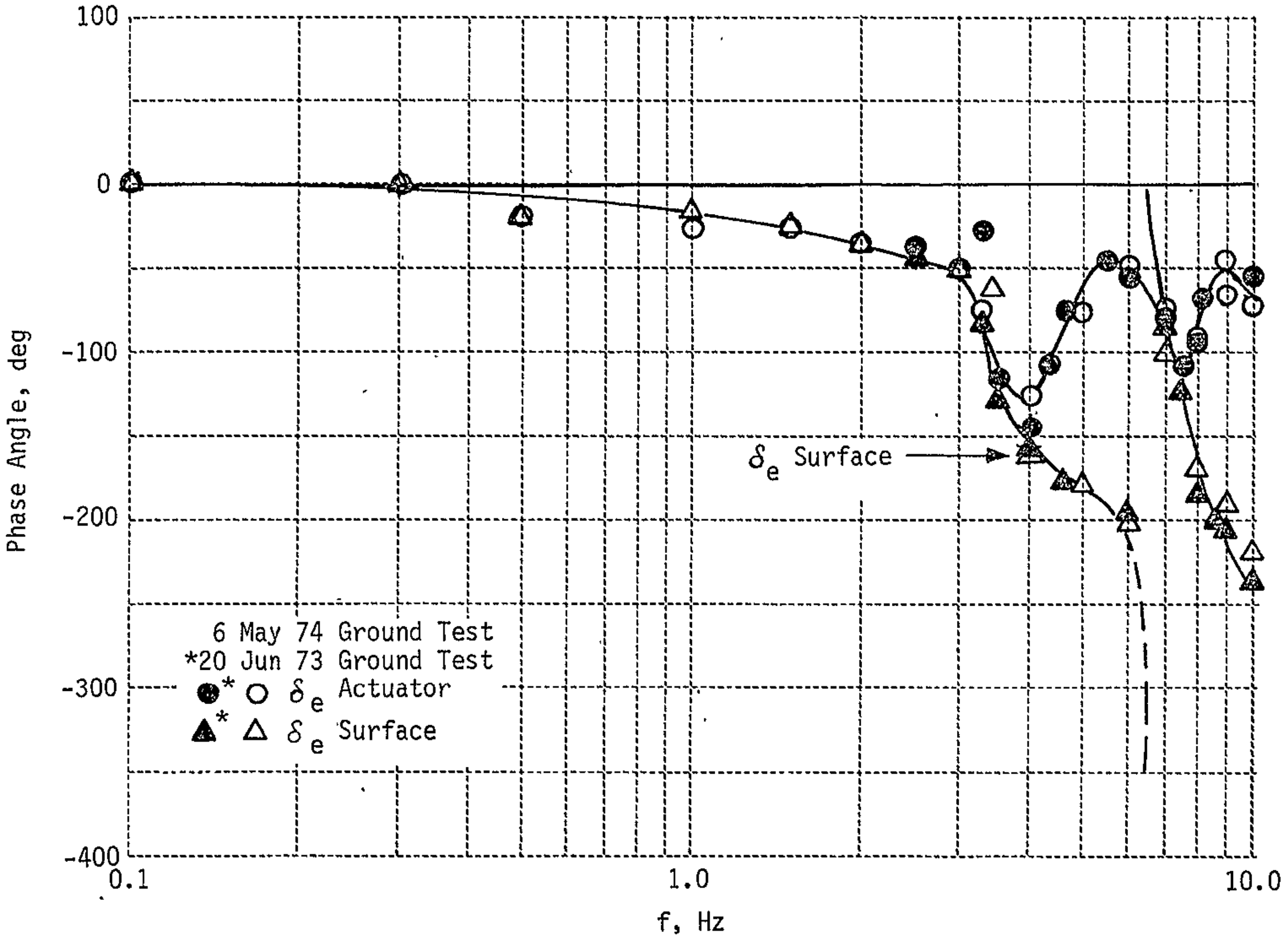

Figure 44 TIFS ELEVATOR FREQUENCY RESPONSE

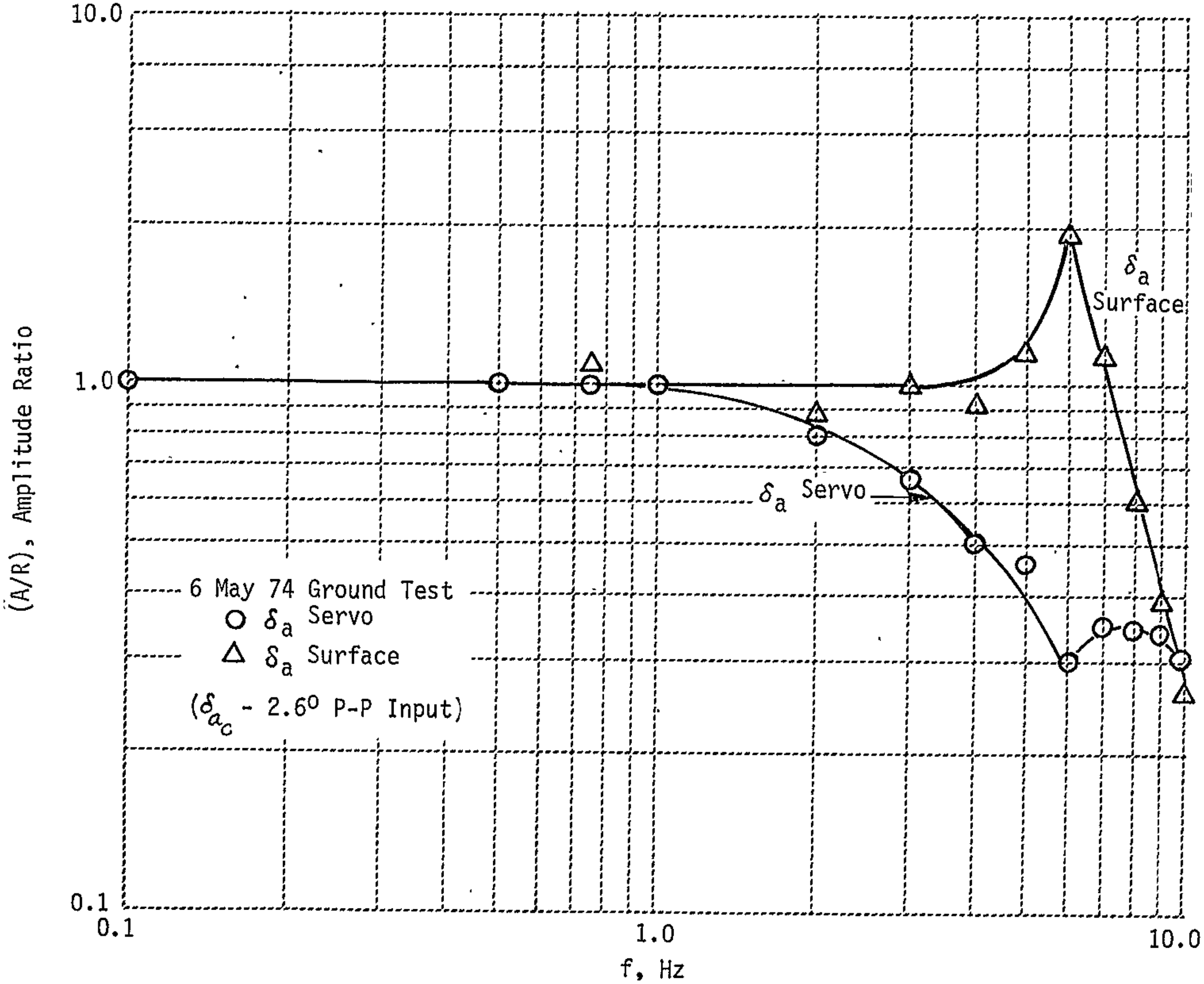

Figure 45 TIFS AILERON FREQUENCY RESPONSE

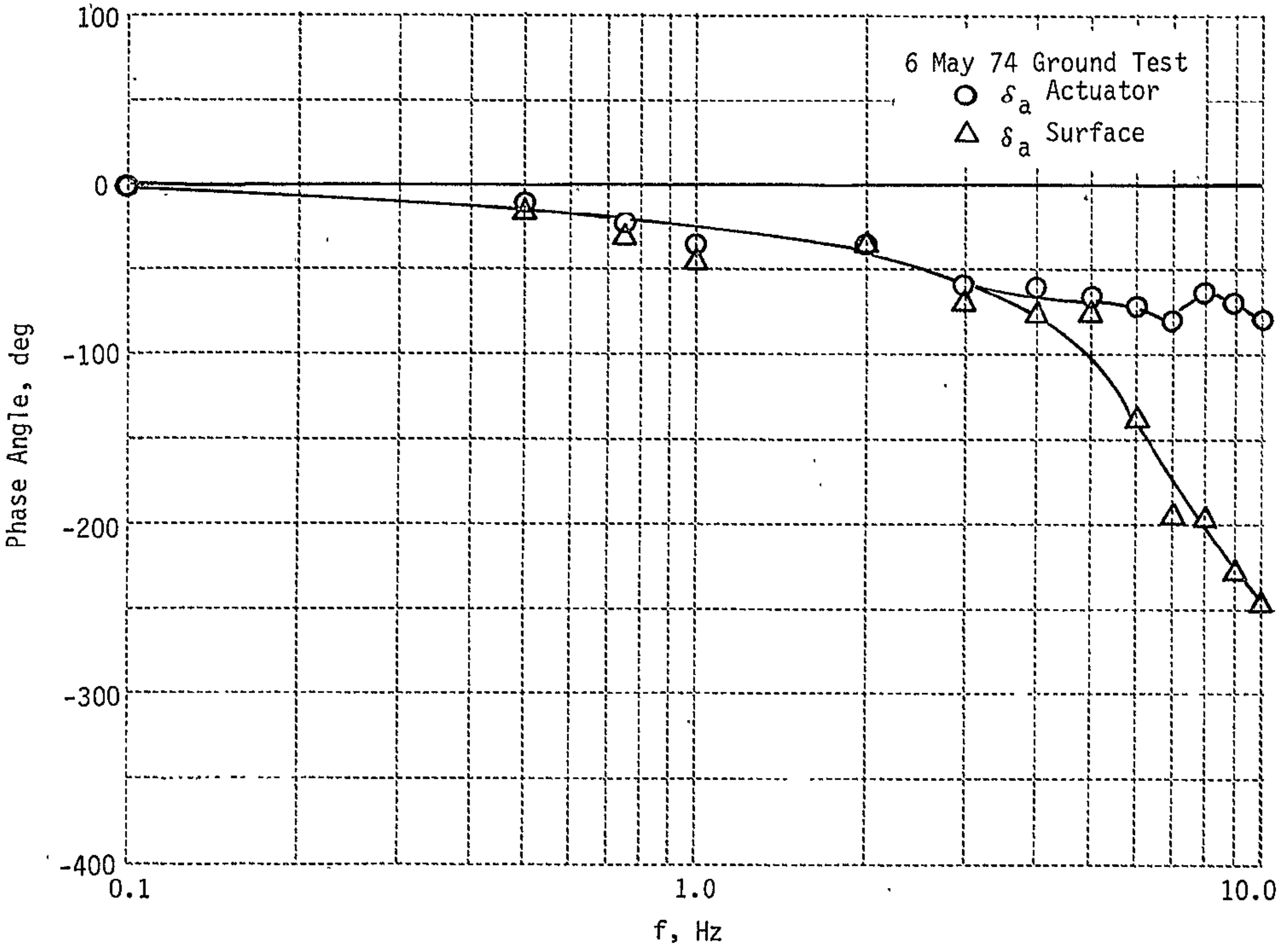

Figure 46 TIFS AILERON FREQUENCY RESPONSE

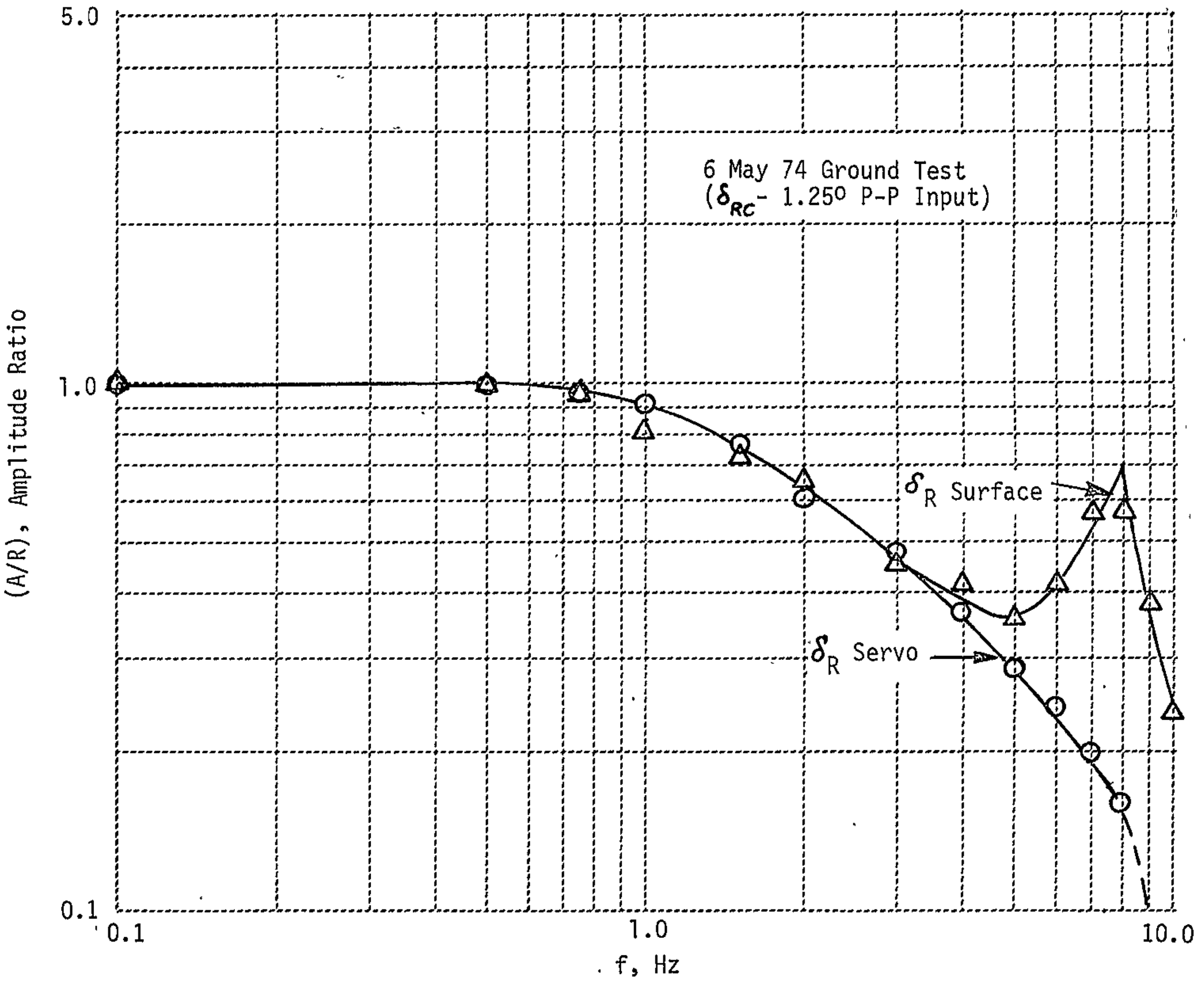

Figure 47 TIFS RUDDER FREQUENCY RESPONSE

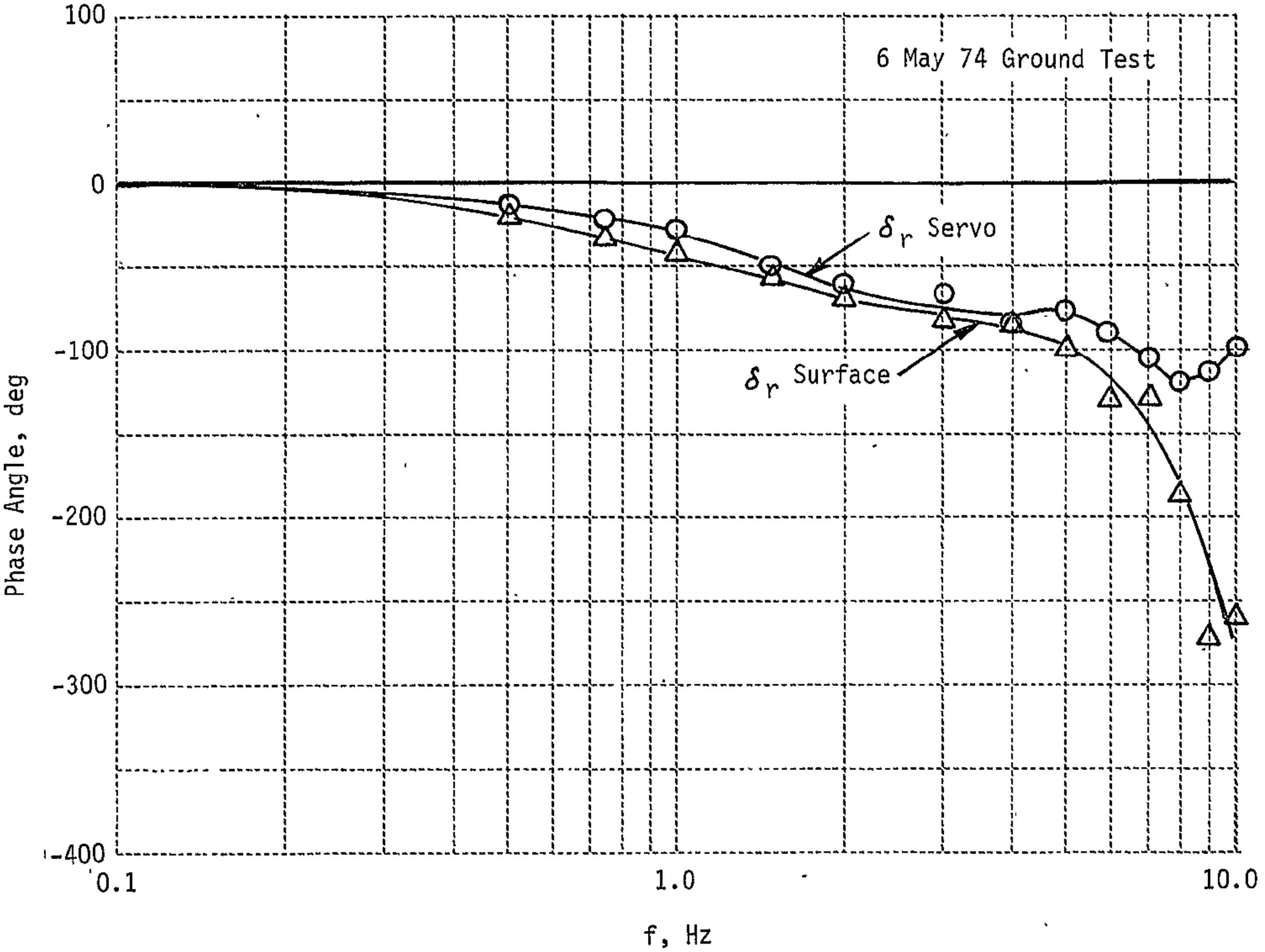

Figure 48 TIFS RUDDER FREQUENCY RESPONSE

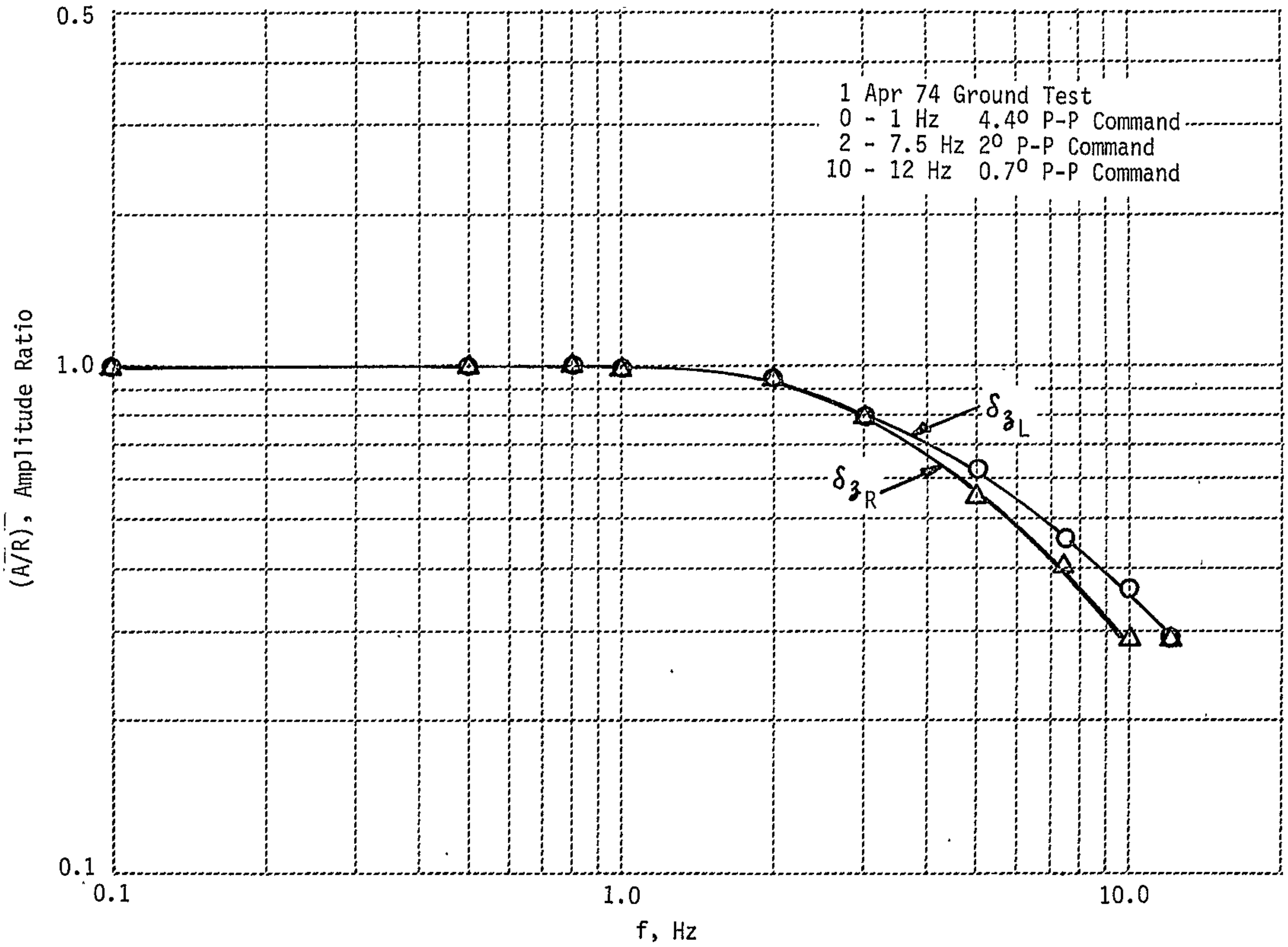

Figure 49 TIFS DLF FREQUENCY RESPONSE

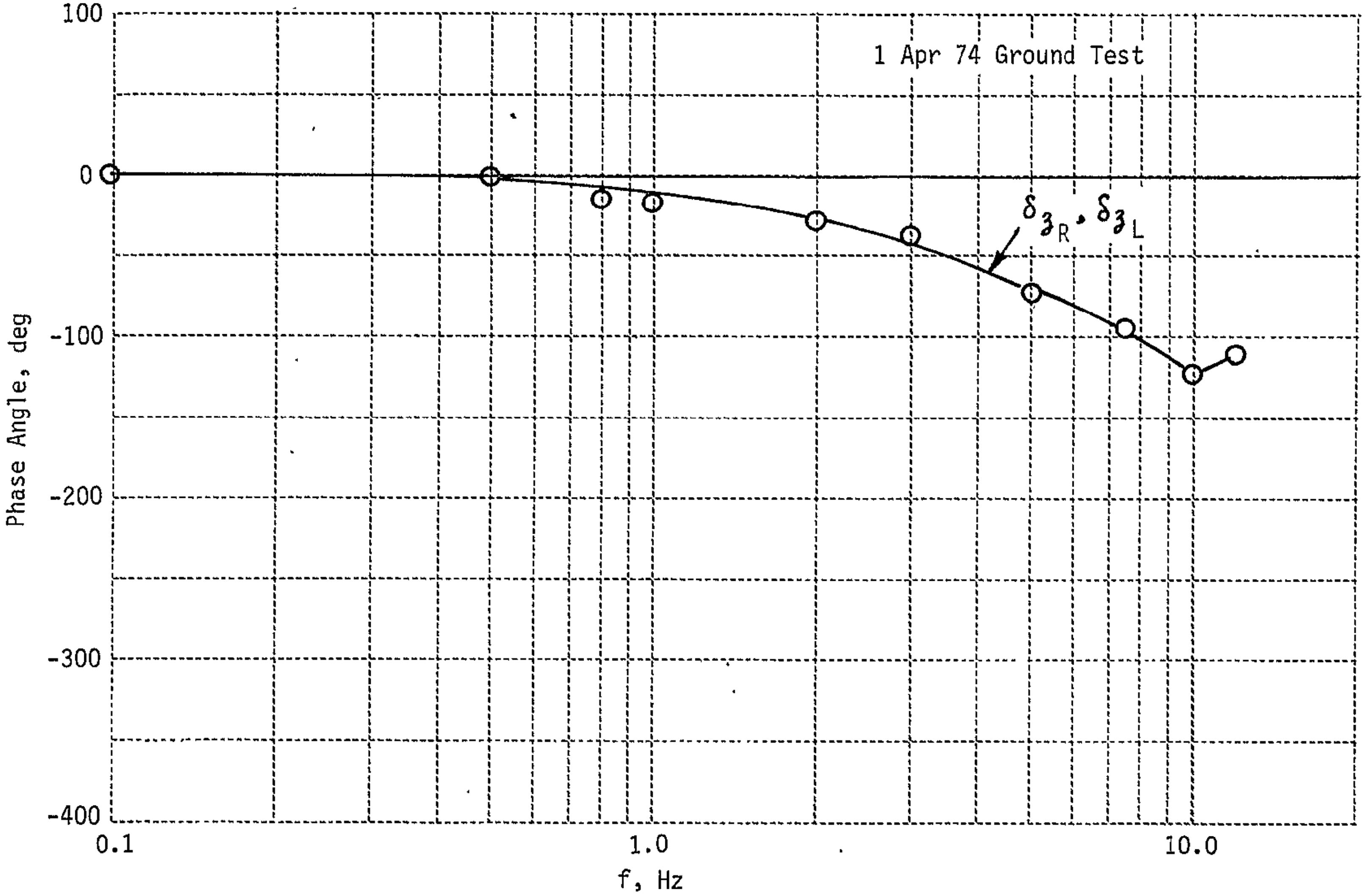

Figure 50 TIFS DLF FREQUENCY RESPONSE

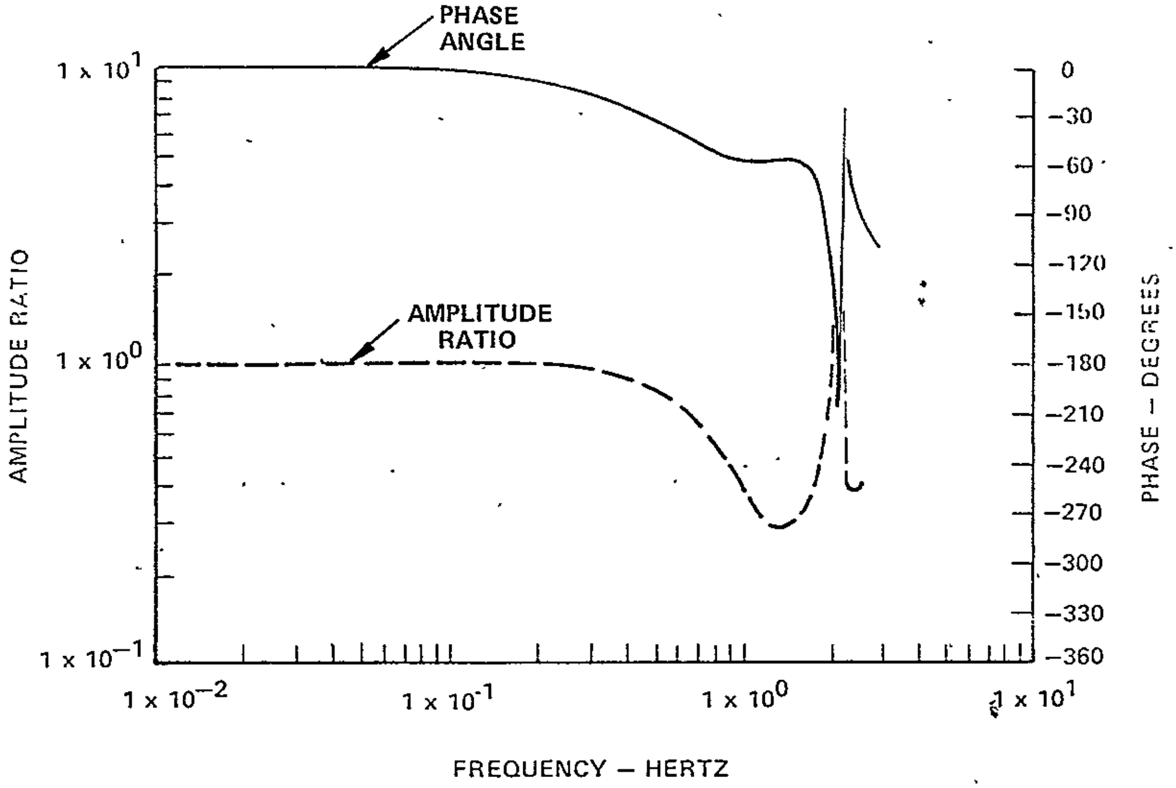

Figure 51 ELEVATOR ANGLE RESPONSE TO SERVO ELECTRICAL COMMAND

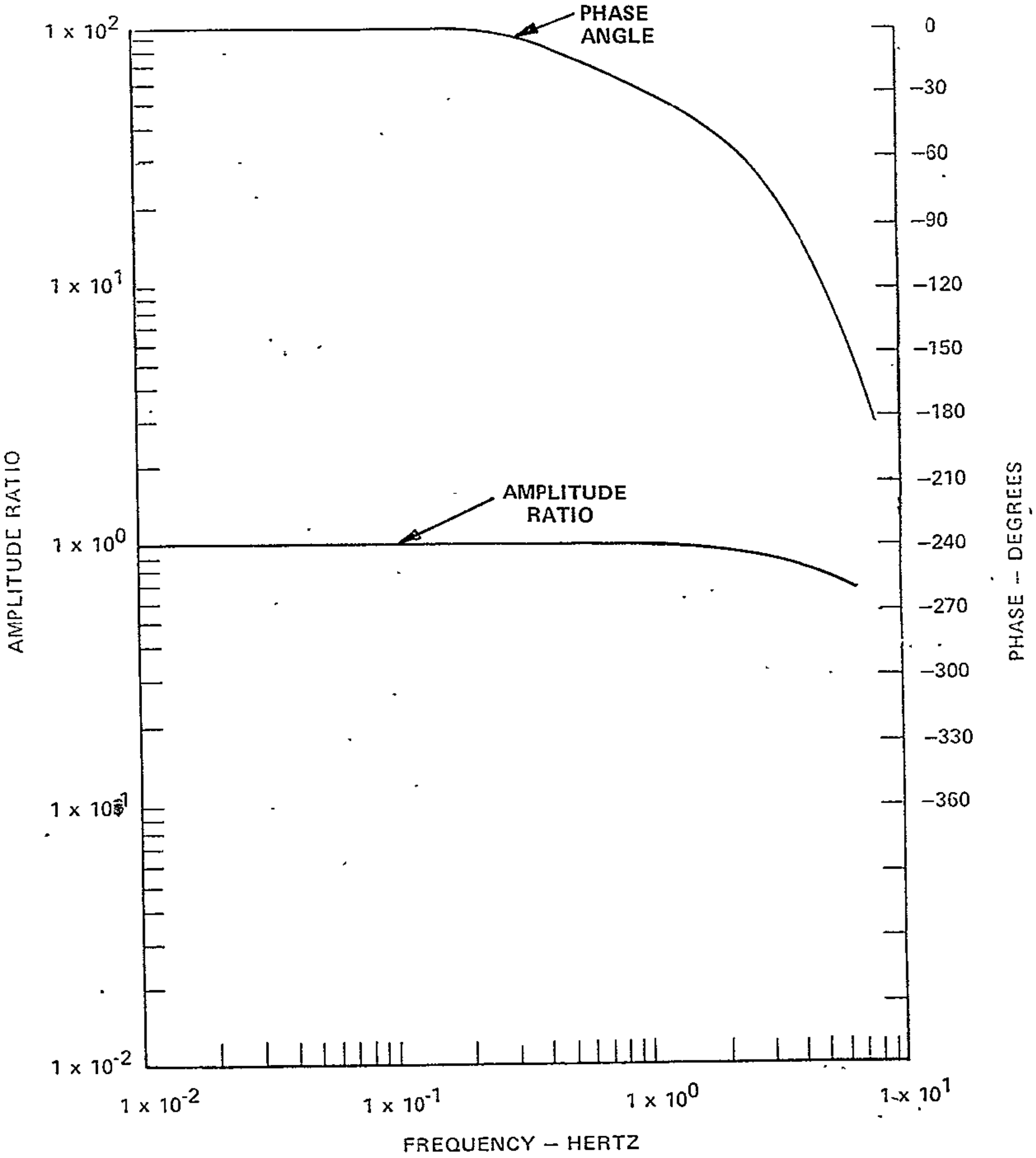

Figure 52 AILERON ANGLE RESPONSE TO SERVO ELECTRICAL COMMAND

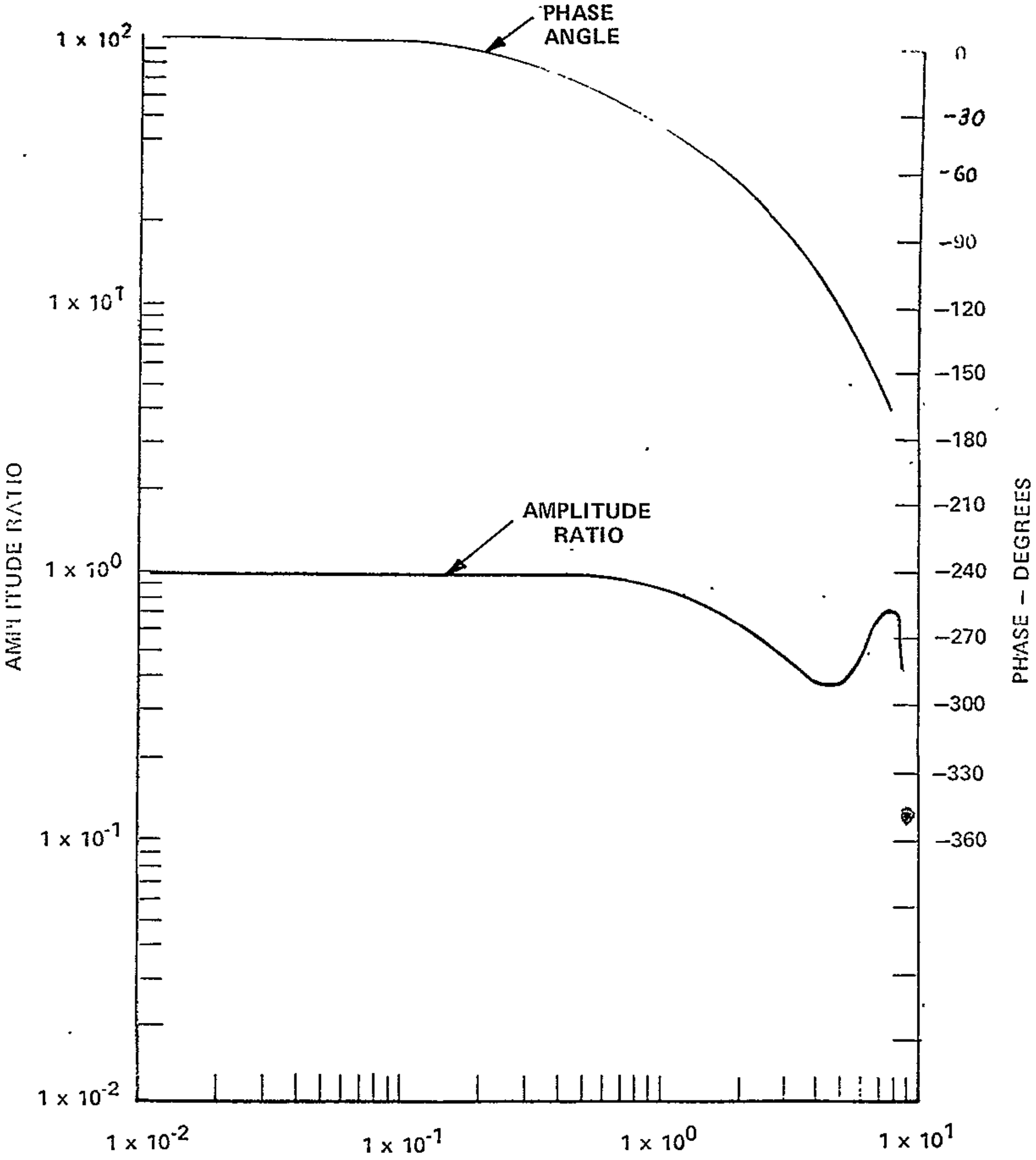

Figure 53 RUDDER ANGLE RESPONSE TO SERVO ELECTRICAL COMMAND

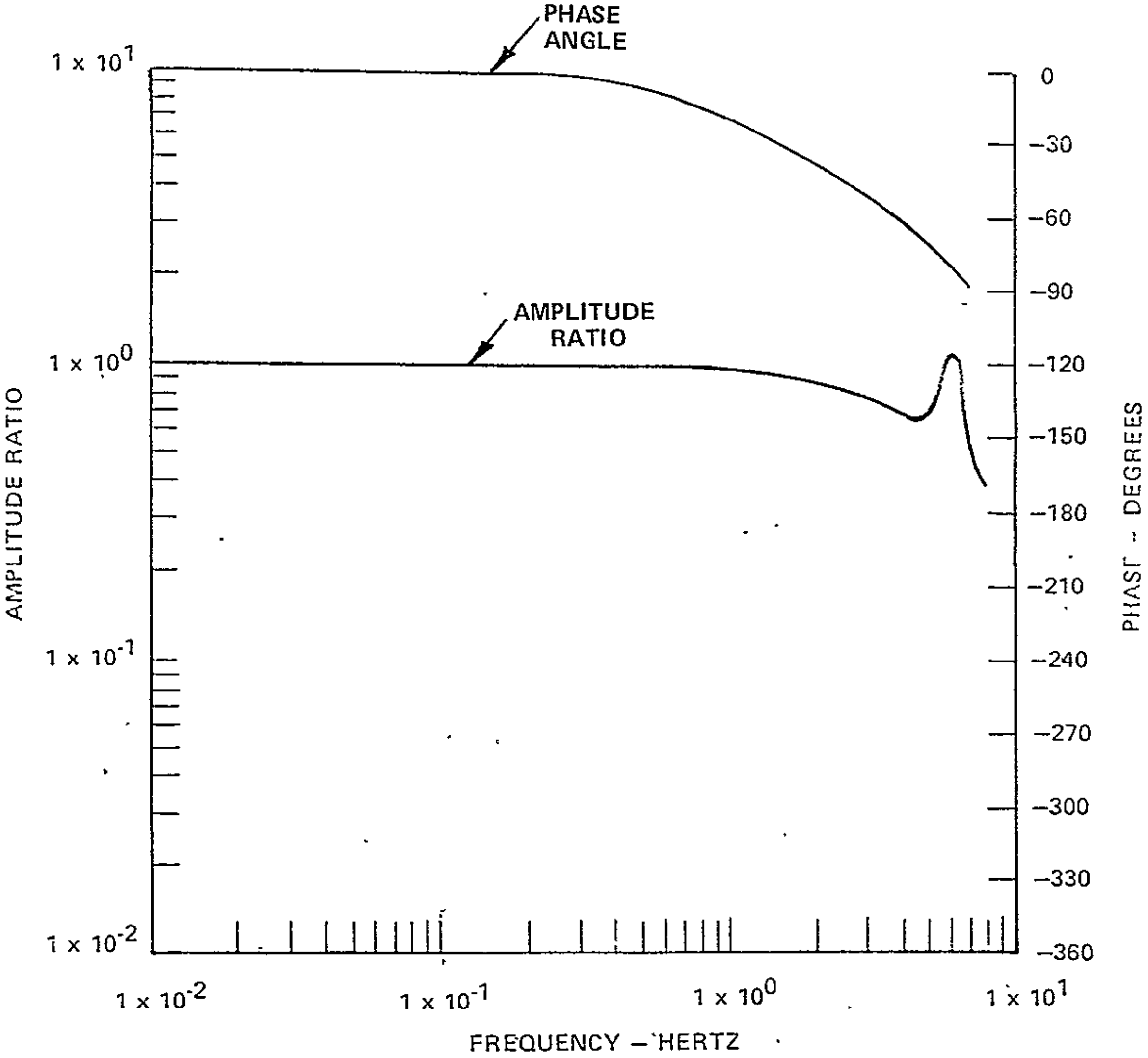

Figure 54 SIDE FORCE SURFACE ANGLE RESPONSE TO SERVO ELECTRICAL COMMAND

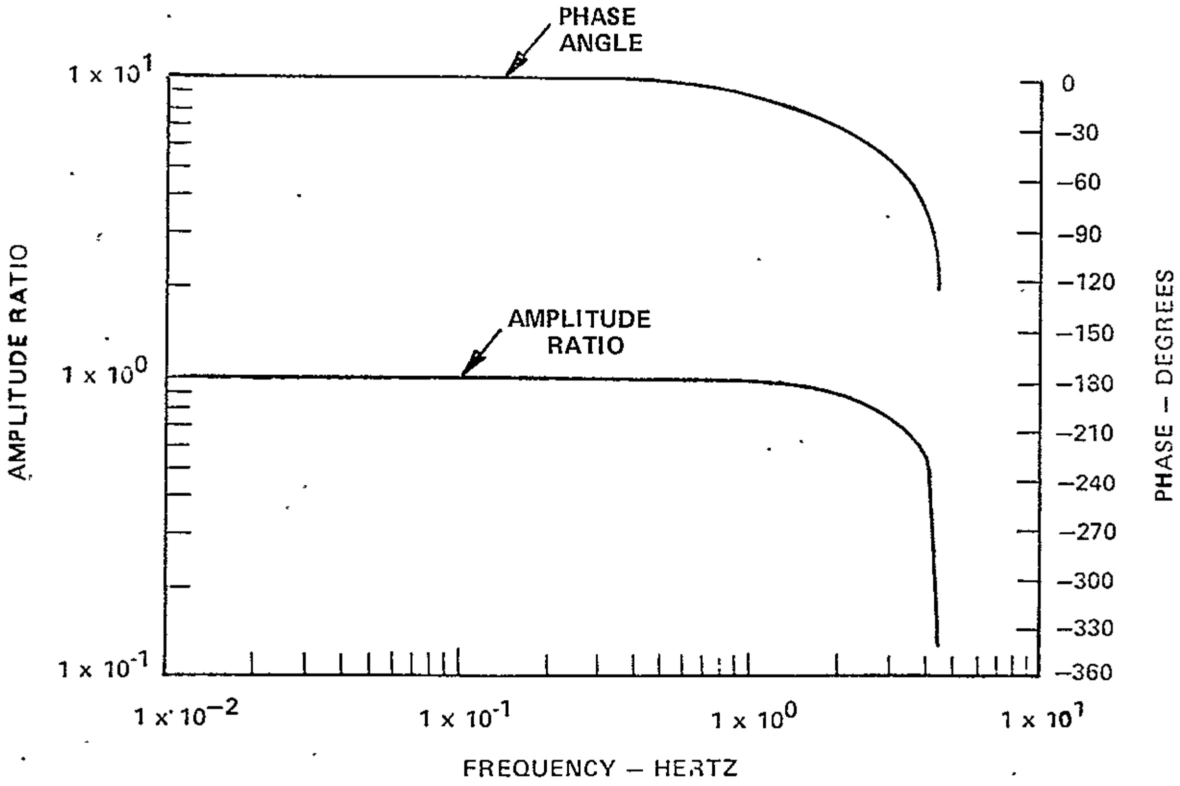

Figure 55 DIRECT LIFT FLAP ANGLE RESPONSE TO SERVO ELECTRICAL COMMAND

3.4 SENSORS AND AIR DATA SYSTEM

This section presents pertinent details of the sensors, sensor signal conditioning and computed signals which are available in the TIFS aircraft.

Scaled DC signals are trunked to the computer patch panel for use in the TIFS flight control system and for recording. These signals are arranged into three groups. Group one consists of directly measured parameters such as gyro and accelerometer signals. The signals are conditioned-demodulated if necessary, filtered, and scaled. Group two consists of air data type signals. These signals are derived from air data sensors and the inertial measurements. In group three are the computed signals for inertial angle of attack, sideslip, rate of change of angle of attack, sideslip and gust. The features and capability of the onboard digital tape recording system are described. The physical locations of the basic sensors in the TIFS are identified in Figure 56. Distances of the C.G. and sensor locations from fixed aircraft reference points may be obtained from Table 17.

3.4.1 Group One. Directly Measured Parameters

Attitude and Heading Channels

The pitch, roll, and heading angle information is provided by synchro outputs from the C.G. located attitude and heading reference system (AHRS). The specifications for the AHRS are presented in Table 18. The AHRS signals are converted to sine and cosine terms of pitch, roll and heading angle by control transformers. The signals are scaled, amplified and then converted to DC by phase sensitive demodulators. The demodulated signals are filtered to remove the 800 Hz carrier frequency. The outputs of these channels are sine and cosine of pitch, roll, and heading angles, pitch angle change from perturbation engage and roll angle.

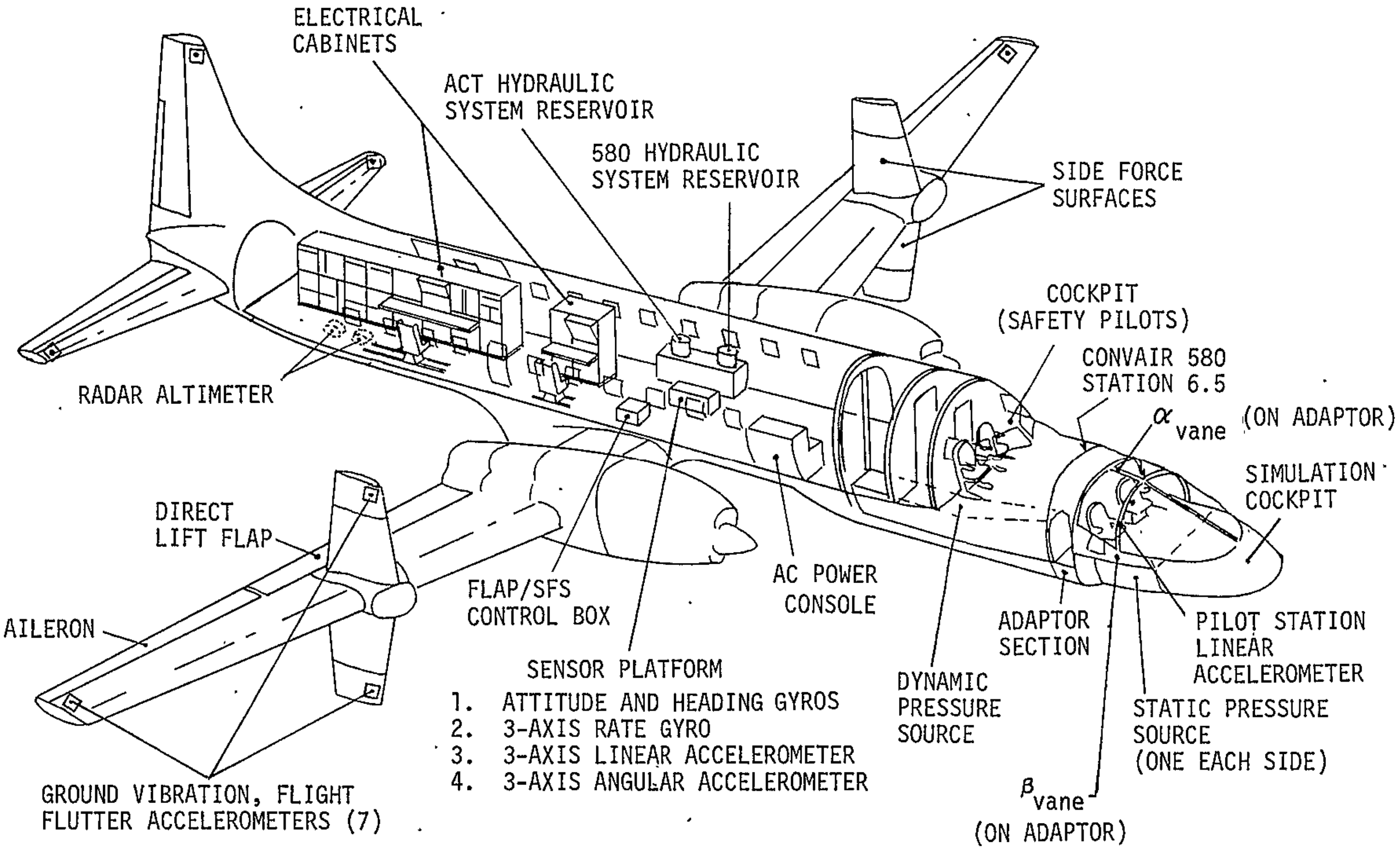

Figure 56 USAF/CALSPAN TIFS AIRPLANE

TABLE 17

TIFS SENSOR LOCATIONS

Sensor	Vertical Location (In. From Waterline) (1)	Longitudinal Location (in.) (2)	Lateral Location (In. From Butt Line) (3)
Radar altimeter antennas	0.0	654 (ave)	0.0
Attitude & Hdg. Gyro	+35.5	351	4 LBL
Angular Rate Gyro	+44.5	370	3 LBL
Angular Accelerometer	+37	369	4 RBL
Linear Accelerometer (cg)	+37	369	1 LBL
Linear Accel. (Sim. Cockpit)	+ 3	- 36	0
α Vane	+19	- 16	46 LBL
β Vane	-11	- 16	0
Static Pressure Source	+10	- 47	43 LBL
Dynamic Pressure Probe	+65	+ 78	45 LBL
TIFS c.g. Range	≈ +36	370-379	0

(1) Waterline — Horizontal plane tangent to lower fuselage skin. Measurement above waterline is positive.

(2) Fuselage Ref. — Extreme forward point of original aircraft nose. Distances aft of point are positive.

(3) Buttock Line — Vertical plane disecting aircraft fore-to-aft. Distances are measured to left (LBL) or right (RBL) of buttock line.

All distances measured in inches.

TABLE 18

ATTITUDE AND HEADING REFERENCE SYSTEM

Lear Siegler, Inc.
AN/ASN-50
Model 5010R

Bench Vertical Error	± .25 deg max
Dynamic Vertical Error	± 1 deg max
Free Vertical Drift	± 10 deg/hr max
Erection Rate	1.3 ± .5 deg/min
Erection Gradient	2.6 ± 1.0 deg/min/deg
Roll Follow-up Rate	360°/sec
Magnetic Heading (static)	± 0.3 deg
Heading Follow-up Rate	180 deg/sec
Heading Slew Rate	50 deg/sec
Heading Drift (corrected for Earth's Rate and Gyro Bias)	± .3 deg/hr RMS
Magnetic Slaving Rate	$1.0 \begin{smallmatrix} + .5 \\ - .3 \end{smallmatrix}$ deg/min
Magnetic Slaving Gradient	1.5 ± .3 deg/min/deg

Features

Two-Gyro Platform with Servoed Outer Roll Gimbal.
All-Attitude-No Gimbal Lock.
Vertically Stabilized Directional Gyro.
    No Roll and Pitch Coupling.

Functions

Provides Gyro Roll and Pitch Data.
Provides Three Modes of Heading
    Gyro Stabilized Compass.
    Free Gyro.
    Compass (no gyro).

For additional information, reference:

NAVAIR 05-35-LAA-1
Handbook, Operation and Maintenance
Attitude and Heading Reference System AN/ASN-50

Three Axis Angular Rates

The pitch, roll and yaw rate gyros sense body axis angular rates and are mounted mutually orthogonal in a single package located at the TIFS c.g. The performance specifications for the rate gyro package are given in Table 19. The AC outputs of the package are amplified, scaled and demodulated. The signals are then filtered to remove the 800 Hz carrier frequency. Additional first order filters are installed in each rate gyro channel. A notch filter is also provided in the roll rate channel. The outputs of these channels are pitch, roll and yaw rates.

TABLE 19

3-AXIS RATE GYRO

United States Time Corp.
Part #400750

p Rated sensor output ± 125 deg/sec = 4V DC
Threshold .005 deg/sec
Resolution $<$ .01 deg/sec
Ave. Hysteresis .07 deg/sec
Linearity .5%
$\omega_n = 49$ Hz
$\zeta = .6$

q Rated sensor output ± 40 deg/sec = 4V DC
Threshold .005 deg/sec
Resolution $<$ .01 deg/sec
Ave. Hysteresis .080 deg/sec
Linearity .5%
$\omega_n = 28$ Hz
$\zeta = .7$

r Rated sensor output ± 40 deg/sec = 4V DC
Threshold .006 deg/sec
Resolution $<$ .01 deg/sec
Ave. Hysteresis .104 deg/sec
Linearity .5%
$\omega_n = 29$ Hz
$\zeta = .7$

Three-Axis Linear Accelerations

The three axis linear accelerometer package is mounted directly to the airframe at the TIFS C.G.. These sensors measure acceleration in the aircraft x, y and z axes. The DC output signals are scaled prior to low pass and notch filtering to remove high frequency noise. The performance specifications for the linear accelerometer sensors are presented in Table 20. The channel outputs are n_x, n_y, n_z , and $(n_z -1)$ at the TIFS c.g..

TABLE 20

3-AXIS LINEAR ACCELEROMETER
C.G. Location

Unico Controls, Inc.
Model MCA-5-6X3

n_x	$\pm .5g = \pm 5V$ DC Linearity .1% Hysteresis < .2% Output Noise 1 mv $\omega_n = 40$ Hz $\zeta = .8$	Threshold 10^{-4} g
n_y	$\pm 1g = \pm 5V$ DC Linearity = .1% Hysteresis < .002V $\omega_n = 38$ Hz $\zeta = .8$	Threshold 10^{-4} g
n_z	$\pm 2.5g = \pm 5V$ DC Linearity .1% Hysteresis < .003V Output Noise --- $\omega_n = 45$ Hz $\zeta = .8$	Threshold 10^{-4} g

These acceleration units mounted mutually orthogonal on a common base.

Axis alignment to base ± 1°.

Three Axis Angular Accelerations

The pitch, roll and yaw angular accelerometers are mounted mutually orthogonal in a package located at the TIFS C.G. These body axis angular acceleration signals are both low passed and notch filtered. These acceleration signals are available for recording but the hysteresis has increased to a level that negates their use for stability and control applications. The original performance characteristics of the angular accelerometers are presented in Table 21. The outputs of these channels are pitch, roll, and yaw angular acceleration.

TABLE 21

3-AXIS ANGULAR ACCELEROMETER

Unico Controls, Inc.
Model MCA-6-8G

$\dot{p}$ Full Scale Output ± 500 deg/sec^2 = ± 8.28V DC

Threshold .01 deg/sec^2
Dynamic Linearity .1%
Hysteresis < 1%
ω_n = 19.4 Hz
ζ = .7

$\dot{q}$ Full Scale Output ± 200 deg/sec^2 = ± 3.48V DC
Threshold .01 deg/sec^2
Dynamic Linearity .1%
Hysteresis < 1%
ω_n = 18.3 Hz
ζ = .7

$\dot{r}$ Full Scale Output ± 200 deg/sec^2 = 2.9V DC
Threshold .01 deg/sec^2
Dynamic Linearity .1%
Hysteresis < 1%
ω_n = 17 Hz
ζ = .7

These angular accelerometers have been found to be unacceptable for stability and control feedback usage.

Two-Axis Linear Acceleration Package

This two-axis package is mounted between the pilot and copilot seats in the simulation cockpit. These body axis acceleration signals are scaled and low pass filtered. Performance characteristics of these sensors are presented in Table 22. The outputs of these channels are simulation pilot location n_{y_p}, n_{z_p}, and $(n_{z_p} - 1)$.

TABLE 22

2-AXIS LINEAR ACCELEROMETER
(Simulation Pilot Station)

Unico Controls, Inc.
Model MCA-5-6X2

n_{y_p} ± 1g = ± 5V DC
Threshold 10^{-4} g
Linearity ± .1%
Hysteresis @ zero g = .003V
ω_n = 35 Hz
ζ = .7

n_{z_p} ± 2.5g = ± 5V DC
Linearity ± .1%
Hysteresis @ 1g = .002V
ω_n = 35 Hz
ζ = .7

Both sensors mounted on common base. Axis alignment to base ± 1°.

Radar Altitude

The radar altimeter DC output measures distance from the TIFS to the closest object within an angular cone from the antennas. The transmitting and receiving antennas are flush mounted units located in a horizontal plane on the bottom of the TIFS fuselage just aft of the cargo door. The output signal is scaled and differentiated to obtain instantaneous vertical speed information. The performance specifications for the radar altimeter are presented in Table 23. The channel outputs are radar altitude and rate of change of radar altitude.

TABLE 23

RADAR ALTIMETER

Honeywell Aerospace Division
AN/APN-171 (V)
HG 9000 Series

Range 0 to 1000 feet   0 to -40V DC
RF Frequency 4.3 GHz, 100 Watts peak power
Pulse repetition frequency 10 KHz
Pulse Width 35 nanoseconds low altitude
125 nanoseconds high altitude

System transient response: First order with .1 second time constant

Altitude Accuracy — Standard Conditions

Assume present altitude = x (feet)
and rate of change of altitude = $\dot{x}$ feet/sec
Accuracy = $\pm \left[1.5 + .01\,(x) + .05\,(\dot{x}) \right]$ feet

Altitude Accuracy — Service Conditions

(worst case with component value drift not compensated for)

Accuracy = $\pm \left[5 + .03\,(x) + .05\,(\dot{x}) \right]$ feet

This statement applies to dynamic range subject to the limitations of a first-order system with a transient response time constant of .1 seconds.

Vibration and Flutter Accelerometers

These accelerometers are mounted on the wing tips, horizontal and vertical stabilizers and the right side force surface. Low noise coaxial wire is used to trunk the signals to high gain amplifiers and low pass filters. The accelerometer characteristics are given in Table 24.

TABLE 24

GROUND VIBRATION AND FLIGHT FLUTTER TEST ACCELEROMETERS

Metrix Instrument Company
Model 502

Voltage Sensitivity	25 mv/g*
Charge Sensitivity	150 PCMB/g*
Capacitance	6000 pf*
Cross Axis Sensitivity	3%
First Resonance	3000 Hz
Linearity	± 1%

---

*Nominal values.

Angle of Attack and Sideslip Channels

The vanes are Calspan Corporation designed and built units. Each vane consists of a symmetrical airfoil surface with a mean aerodynamic chord located 2.0 inches aft of the vane axis for stability. The distance from the inboard edge of the vane airfoil to the aircraft skin is 7 inches. A balance weight is installed to eliminate error due to acceleration terms acting upon the vane mass. The synchro output of vane angle is AC amplified, scaled and demodulated. The 800 Hz ripple is removed in the third order filter. Correction terms are added to the DC vane signals to compensate for location of the vane from the TIFS C.G.. These terms are $q\ell_1/V$ and $p\ell_2/V$ for the angle of attack vane and $r\ell_3/V$ and $p\ell_4/V$ for the angle of sideslip vane.

ℓ_1 = longitudinal distance from C.G. to angle of attack vane.

ℓ_2 = lateral distance from C.G. to angle of attack vane.

ℓ_3 = longitudinal distance from C.G. to sideslip vane.

ℓ_4 = vertical distance from C.G. to sideslip vane.

Each vane signal is corrected for position error due to the air flow distribution at their location on the fuselage. The vane deflections are larger than the actual aircraft angle of attack and sideslip changes. The angle of attack vane rotates 1.45 degrees for a one degree change in true angle of attack. The sideslip vane position calibration factor is 1.25 degrees. The corrected vane signals are notch filtered. The vane outputs are adjusted to obtain zero volts when the angle of attack vane is parallel to the fuselage reference line and the sideslip vane is parallel with the aircraft buttock line

Sensor Signal Conditioning

The basic sensor signals contain conditioning networks which consist of AC to DC conversion, filtering and scaling. The format of the sensor channels (sensor dynamics and electronic signal conditioning) except for angle of attack and sideslip is as outlined in Figure 57. The angle of attack and sideslip channels are outlined in Figure 58. Sensors with AC outputs require a carrier amplifier and phase sensitive demodulator. The AC to DC conversion is followed by a low pass filter to remove the 800 Hz ripple frequency. Notch filters or additional low pass filters are installed where needed. Table 25 is a compilation of the dynamic transfer functions for each sensor channel except for angle of attack and sideslip. The transfer functions for the angle of attack and sideslip channels are given in Table 26. In these tables, second order transfer functions have the form:

$$E_0/E_{IN} = \frac{1}{\frac{s^2}{\omega_n^2} + \frac{2(\zeta)s}{\omega_n} + 1}$$

where ω_n = undamped natural frequency in radians/second
and ζ = damping ratio.

First order transfer functions have the form:

$$E_0/E_{IN} = \frac{1}{\frac{s}{\omega} + 1}$$

where ω = corner frequency (radians/sec).

No attempt is made to indicate the gains of each step of the signal conditioning process. During calibration, the gain of each sensor channel is adjusted to produce the desired scale factor at the final output.

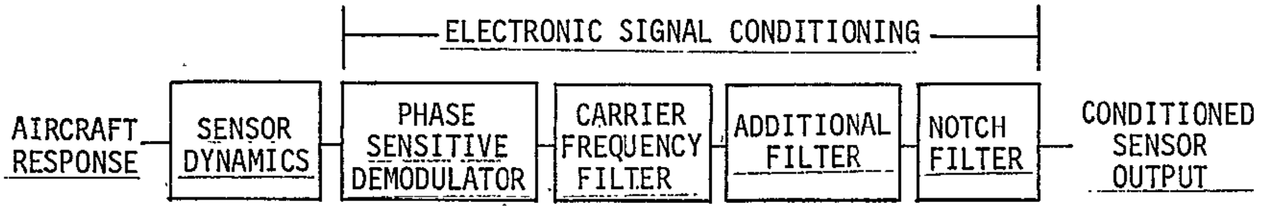

Figure 57 SENSOR CHANNEL FORMAT

Scale factor information is added to the signal identification symbols. As an example, the symbol 0.5q identifies the rate of change of pitch angle signal with a scaling of 0.5 volts per degree per second of pitch rate. Since the TIFS electronics is based on a 10 volt signal level, the maximum usable pitch rate is 20 degrees per second. For trigonometric functions, similar scaling is used. The symbol 20 sin θ identifies a pitch angle signal which can have a maximum value of 30° [20 (sin 30°) = 20 (0.5) = 10 volts].

TABLE 25

SENSOR CHANNEL CHARACTERISTICS

The AC amplifier and phase sensitive demodulator response lag is negligible and is not included in the table.

Aircraft Parameter	Sensor Dynamics	800 Hz Carrier Freq. Filter (1)	Additional Filter	Notch Filter (2)	Output Scale Factor	Output Sensitivity
Pitch Angle	>25 Hz	Yes	No	No	$20 \sin \theta$	$10V = \sin 30^{o}$
		Yes	No	No	$20 \cos \theta$	$10V = \cos 0^{o}$
					$0.5 \Delta\theta$ (3)	.5V/deg
Roll Angle	>25 Hz	Yes	No	No	$10 \sin \phi$	$10V = \sin 90^{o}$
		Yes	No	No	$10 \cos \phi$	$10V = \cos 0^{o}$
					0.1ϕ (4)	0.1 volt/deg
Heading	>25 Hz	Yes	No	No	$10 \sin \psi$	$10V = \sin 90^{o}$
		Yes	No	No	$10 \cos \psi$	$10V = \cos 0^{o}$
Pitch Rate	$\frac{1}{\frac{s^2}{(176)^2} + \frac{2(.6)s}{176} + 1}$	Yes	$\frac{1}{\frac{s}{213} + 1}$	No	0.5q	.5V/deg/sec
Roll Rate	$\frac{1}{\frac{s^2}{(308)^2} + \frac{2(.7)s}{308} + 1}$	Yes	$\frac{1}{\frac{s}{213} + 1}$	No	0.2p	.2V/deg/sec
Yaw Rate	$\frac{1}{\frac{s^2}{(182)^2} + \frac{2(.7)s}{182} + 1}$	Yes	$\frac{1}{\frac{s}{213} + 1}$	No	0.5r	.5V/deg/sec

TABLE 25 (CONT'D)

Aircraft Parameter	Sensor Dynamics	800 Hz Carrier Freq. Filter (1)	Additional Filter	Notch Filter	Output Scale Factor	Output Sensitivity
Pitch Acceleration	$\frac{1}{\frac{s^2}{(115)^2}+\frac{2(.7)s}{115}+1}$	No	$\frac{1}{\frac{s^2}{(85)^2}+\frac{2(.9)s}{85}+1}$	Yes	$0.1\dot{q}$	$.1V/deg/sec^2$
Roll Acceleration	$\frac{1}{\frac{s^2}{(122)^2}+\frac{2(.7)s}{122}+1}$	No	$\frac{1}{\frac{s^2}{(85)^2}+\frac{2(.9)s}{85}+1}$	Yes	$0.2\dot{p}$	$.2V/deg/sec^2$
Yaw Acceleration	$\frac{1}{\frac{s^2}{(107)^2}+\frac{2(.7)s}{107}+1}$	No	$\frac{1}{\frac{s^2}{(85)^2}+\frac{2(.9)s}{85}+1}$	Yes	$0.1\dot{r}$	$.1V/deg/sec^2$
Longitudinal Acceleration @ C.G.	$\frac{1}{\frac{s^2}{(251)^2}+\frac{2(.8)s}{251}+1}$	No	$\frac{1}{\frac{s^2}{(85)^2}+\frac{2(.9)s}{85}+1}$	Yes	$20\ n_x$	2V/0.1g
Lateral Acceleration @ C.G.	$\frac{1}{\frac{s^2}{(238)^2}+\frac{2(.8)s}{238}+1}$	No	$\frac{1}{\frac{s^2}{(85)^2}+\frac{2(.9)s}{85}+1}$	Yes	$10\ n_y$	1V/0.1g
Vertical Acceleration @ C.G.	$\frac{1}{\frac{s^2}{(238)^2}+\frac{2(.8)s}{238}+1}$	No	$\frac{1}{\frac{s^2}{(85)^2}+\frac{2(.9)s}{85}+1}$	Yes	$4\ n_z$ $4\Delta n_z$ (5)	4V/g 4V/g
Lateral Acceleration (simulation pilot station)	$\frac{1}{\frac{s^2}{(220)^2}+\frac{2(.7)s}{220}+1}$	No	$\frac{1}{\frac{s^2}{(85)^2}+\frac{2(.9)s}{85}+1}$	No	$10\ n_{y_p}$	1V/.1g
Vertical Acceleration (simulation pilot station)	$\frac{1}{\frac{s^2}{(220)^2}+\frac{2(.7)s}{220}+1}$	No	$\frac{1}{\frac{s^2}{(85)^2}+\frac{2(.9)s}{85}+1}$	No	$4\ n_{z_p}$ $4\Delta n_{z_p}$ (6)	4V/g 4V/g

TABLE 25 (CONT'D)

Aircraft Parameter	Sensor Dynamics	800 Hz Carrier Freq. Filter (1)	Additional Filter	Notch Filter	Output Scale Factor	Output Sensitivity
Radar Altimeter	$\frac{1}{\frac{s}{10}+1}$	No	No $\frac{20s}{\left(\frac{s}{4.5}+1\right)\left(\frac{s}{25}+1\right)}$	No No	$0.01\ h_r$ $0.2\ \dot{h}_r$ (7)	0.01V/ft .2V/ft/sec
Right Wing Tip Accelerometer	>1000 Hz Bandpass	No	$\frac{10}{1s+1}$	No		2.56 V/g
Left Wing Tip Accelerometer	>1000 Hz Bandpass	No	$\frac{1}{\frac{s^2}{(62.8)^2}+\frac{2(.7)s}{62.8}+1}$	No		1.73 V/g
Right Horiz. Stab. Accel.	>1000 Hz Bandpass	No	$\frac{10}{1s+1}$	No		2.45 V/g
Left Horiz. Stab. Accel.	>1000 Hz Bandpass	No	$\frac{1}{\frac{s^2}{(126)^2}+\frac{2(.7)s}{126}+1}$	No		2.60 V/g
Vertical Stab. Tip	>1000 Hz Bandpass	No	$\frac{10}{1s+1}$	No		2.78 V/g
Right Side Force Surface Top	>1000 Hz Bandpass	No	$\frac{10}{1s+1}$	No		2.23 V/g
Right Side Force Surface Bottom	>1000 Hz Bandpass	No	$\frac{10}{1s+1}$	No		2.52 V/g

TABLE 25 (CONT'D)

NOTE:

(1) 800 Hz carrier frequency filter has transfer function $\frac{E_o}{E_{IN}} = \frac{1}{\left(\frac{s}{1000}+1\right)\left(\frac{s^2}{(380)^2}+\frac{2(.8)s}{380}+1\right)}$

(2) The notch filter has a transfer function of $\frac{E_o}{E_{in}} = \frac{\frac{s^2}{(108)^2}+1}{\frac{s^2}{(108)^2}+\frac{2(.7)s}{108}+1}$

(3) $0.5\Delta\theta$ is a small angle linear approximation of the conditioned 20 sin θ signal. The 'Δ' identifies this signal as change of pitch angle after system engagement.

(4) 0.1 ϕ is the output of a nonlinear function generator. The function generator input is the conditioned 10 sin ϕ signal.

(5) $4\,\Delta\,n_z$ is the same signal as $4\,n_z$ with the 1g gravity term removed.

(6) $4\,\Delta\,n_{zp}$ is the same signal as $4\,n_{zp}$ with the 1g gravity term removed.

(7) The 0.2 $\dot{h}_r$ is an electronically differentiated 0.01 h_r signal.

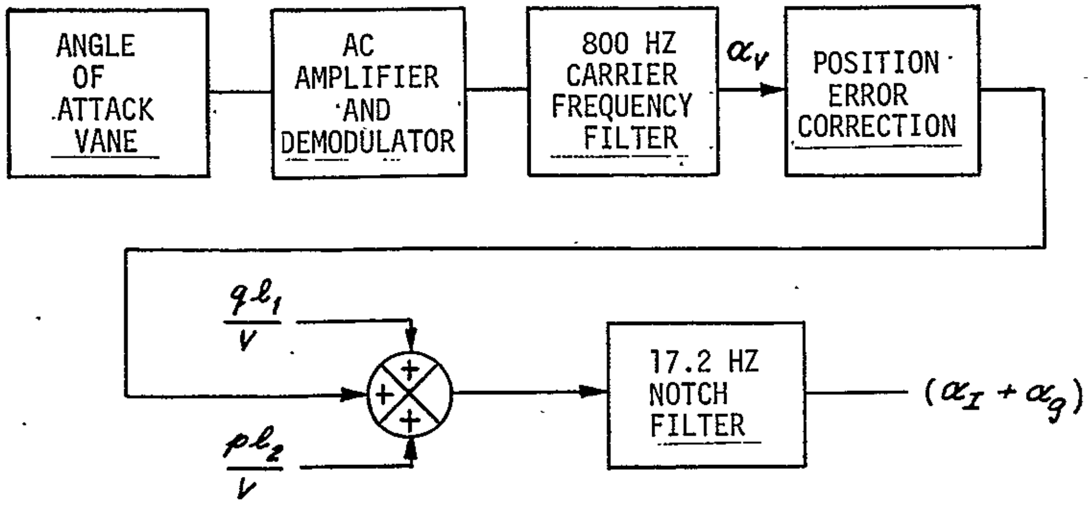

p,q = filtered rate gyro signals
V = true airspeed
(Eq ___)
ℓ_1 = 31.8 ft.
ℓ_2 = 3.8 ft.

$$(\alpha_I + \alpha_g) = \alpha_V \times \text{Position Error Correction} + \frac{q\ell_1}{V} + \frac{p\ell_2}{V} \quad \text{(Equation 1)}$$

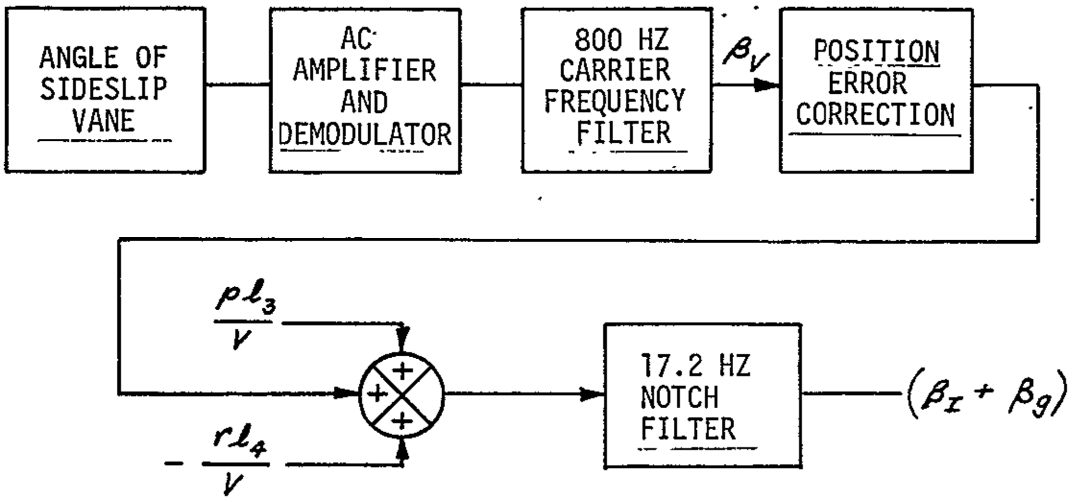

p,r = filtered rate gyro signals
V = true airspeed
ℓ_3 = 3.0 ft.
ℓ_4 = 31.8 ft.

$$(\beta_I + \beta_g) = \beta_V \times \text{Position Error Correction} + \frac{p\ell_3}{V} + \frac{r\ell_4}{V} \quad \text{(Equation 2)}$$

Figure 58 ANGLE OF ATTACK AND SIDESLIP VANE CHANNELS

TABLE 26

α AND β VANE CHANNEL CHARACTERISTICS

Aircraft Parameter	Vane Characteristics or Additional Filters	800 Hz Carrier Filter (1)	Position Error Correction	Shift to TIFS C.G. (2)	Notch Filter (3)	Sensor Signal	Scale Factor
Angle of Attack		Yes	0.690	$\frac{q\ell_1}{V}+\frac{p\ell_2}{V}$	Yes	$.5(\alpha_I+\alpha_g)$	.5V/deg
Angle of Attack Rate	$\frac{.2s}{\frac{s^2}{(67)^2}+\frac{2s}{67}+1}$					$.1(\dot{\alpha}_I+\dot{\alpha}_g)$	.1V/deg/sec
Angle of Sideslip		Yes	0.800	$\frac{p\ell_3}{V}-\frac{r\ell_4}{V}$	Yes	$.5(\beta_I+\beta_g)$	.5V/deg
Angle of Sideslip Rate	$\frac{.2s}{\frac{s^2}{(67)^2}+\frac{2s}{67}+1}$					$.1(\dot{\beta}_I+\dot{\beta}_g)$	.1V/deg/sec

(1) 800 Hz carrier Frequency Filter = $\frac{1}{\left(\frac{s}{1000}+1\right)\left(\frac{s^2}{(380)^2}+\frac{2(.8)s}{380}+1\right)}$

(2) p, q and r terms are filtered gyro signals from Table 9.

ℓ_1 = 31.8 ft $\qquad$ ℓ_3 = 3.0 ft

ℓ_2 = 3.8 ft $\qquad$ ℓ_4 = 31.8 ft

V = true airspeed from Equation 13.

(3) Notch filter transfer function is $\frac{\frac{s^2}{(108)^2}+1}{\frac{s^2}{(108)^2}+\frac{2(.7)s}{108}+1}$

The following plots are presented for the function generator and amplitude and phase responses of the sensor filters.

Figure 59	Sin ϕ to ϕ function generator.
Figure 60	800 Hz carrier freq. filter amplitude vs. frequency.
Figure 61	800 Hz carrier freq. filter phase vs. frequency.
Figure 62	Notch filter amplitude vs. frequency.
Figure 63	Notch filter phase vs. frequency.
Figure 64	Second order low pass vilter, ω_n = 85 rad/sec amplitude vs. frequency.
Figure 65	Second order low pass filter, ω_n = 85 rad/sec phase vs. frequency.
Figure 66	Radar altitude differentiator amplitude vs. frequency.
Figure 67	Radar altimeter differentiator phase vs. frequency.
Figure 68	Low pass filter ω_n = 62.8 rad/sec amplitude vs. frequency.
Figure 69	Low pass filter ω_n = 62.8 rad/sec phase vs. frequency.
Figure 70	Low pass filter ω_n = 126 rad/sec amplitude vs. frequency.
Figure 71	Low pass filter ω_n = 126 rad/sec phase vs. frequency.
Figure 72	Vane differentiator amplitude vs. frequency.
Figure 73	Vane differentiator phase vs. frequency.

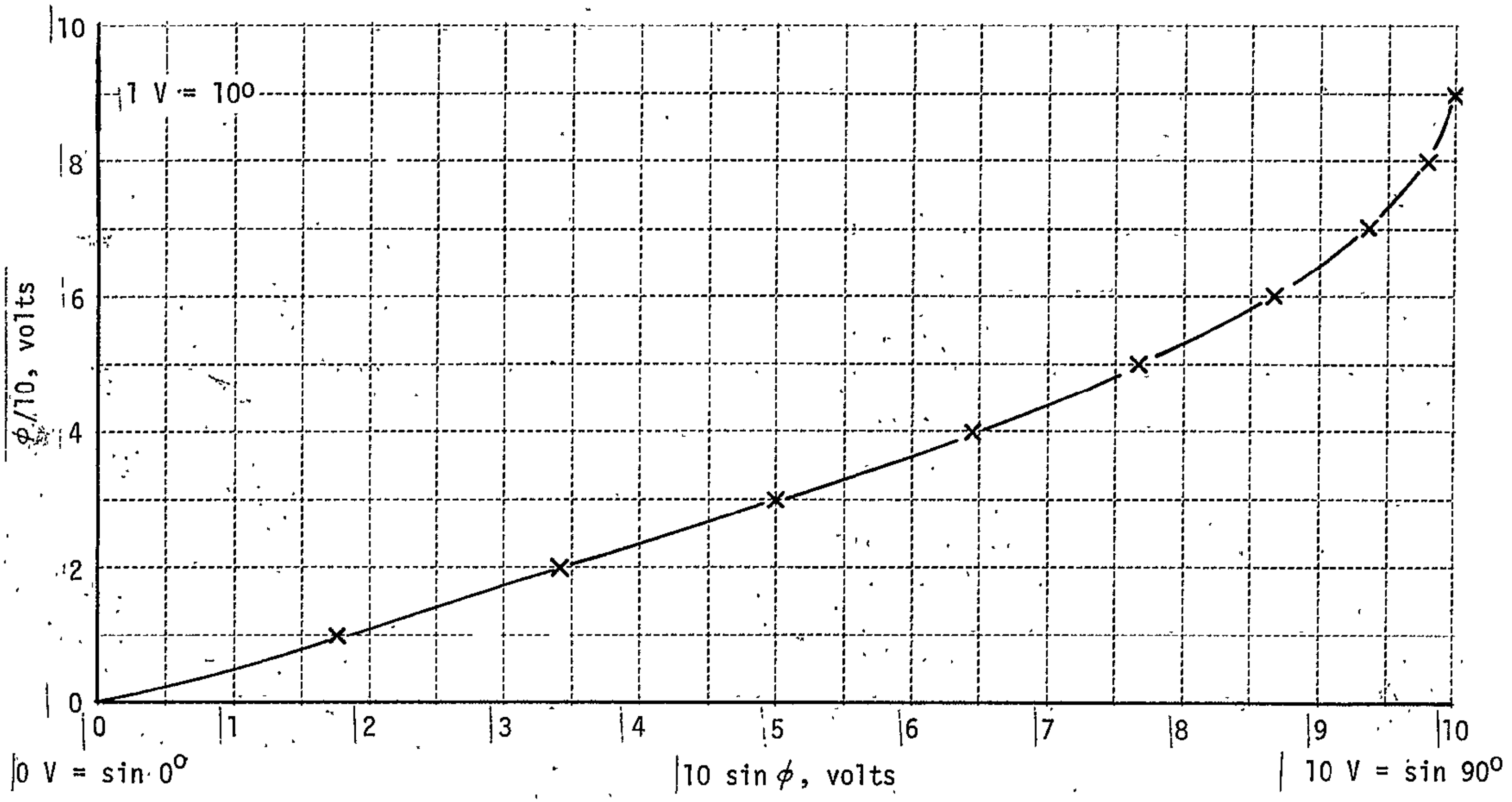

Figure 59 SIN ϕ to ϕ FUNCTION GENERATOR

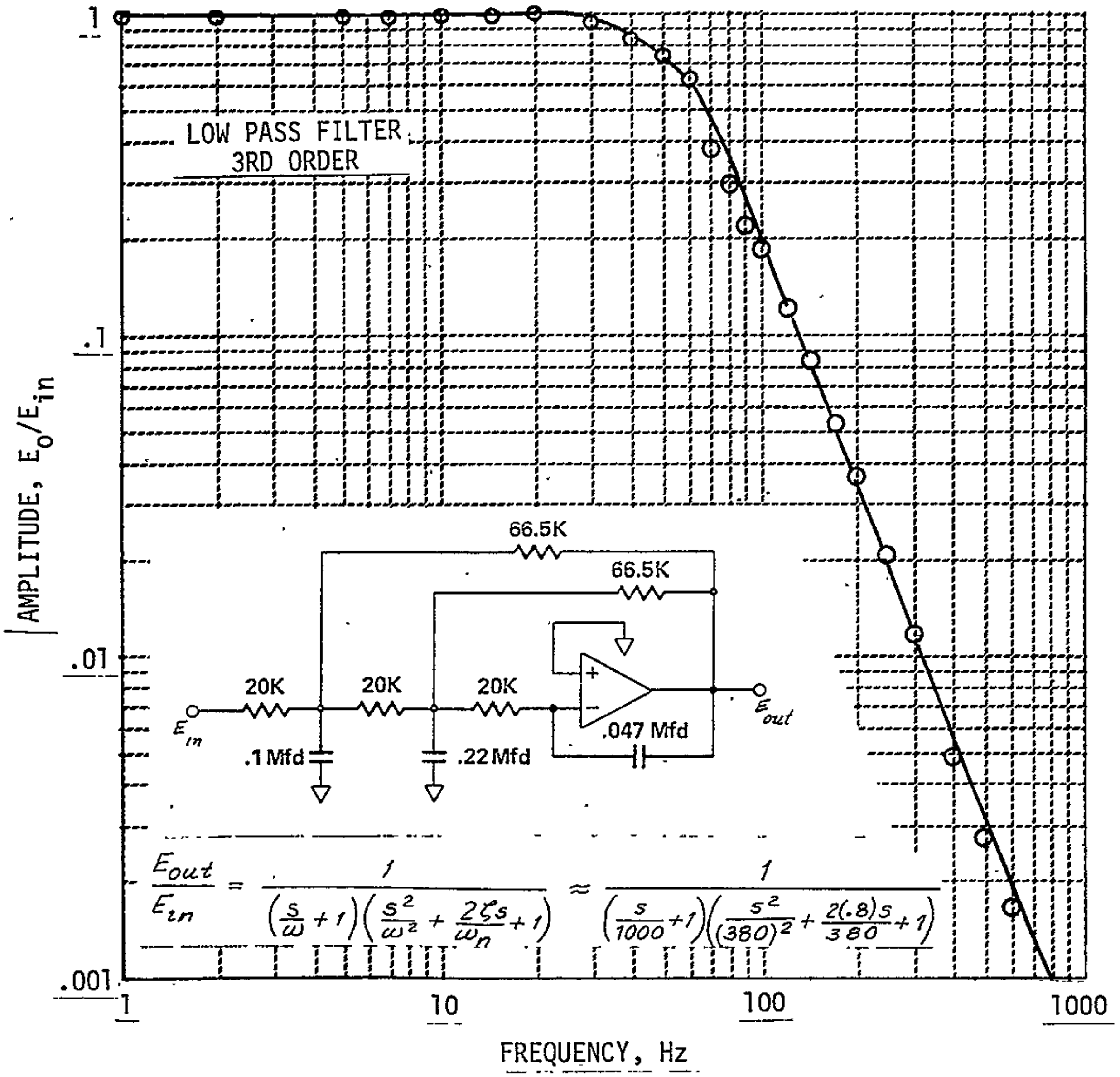

Figure 60 AMPLITUDE VS FREQUENCY, 800 Hz CARRIER FREQUENCY FILTER

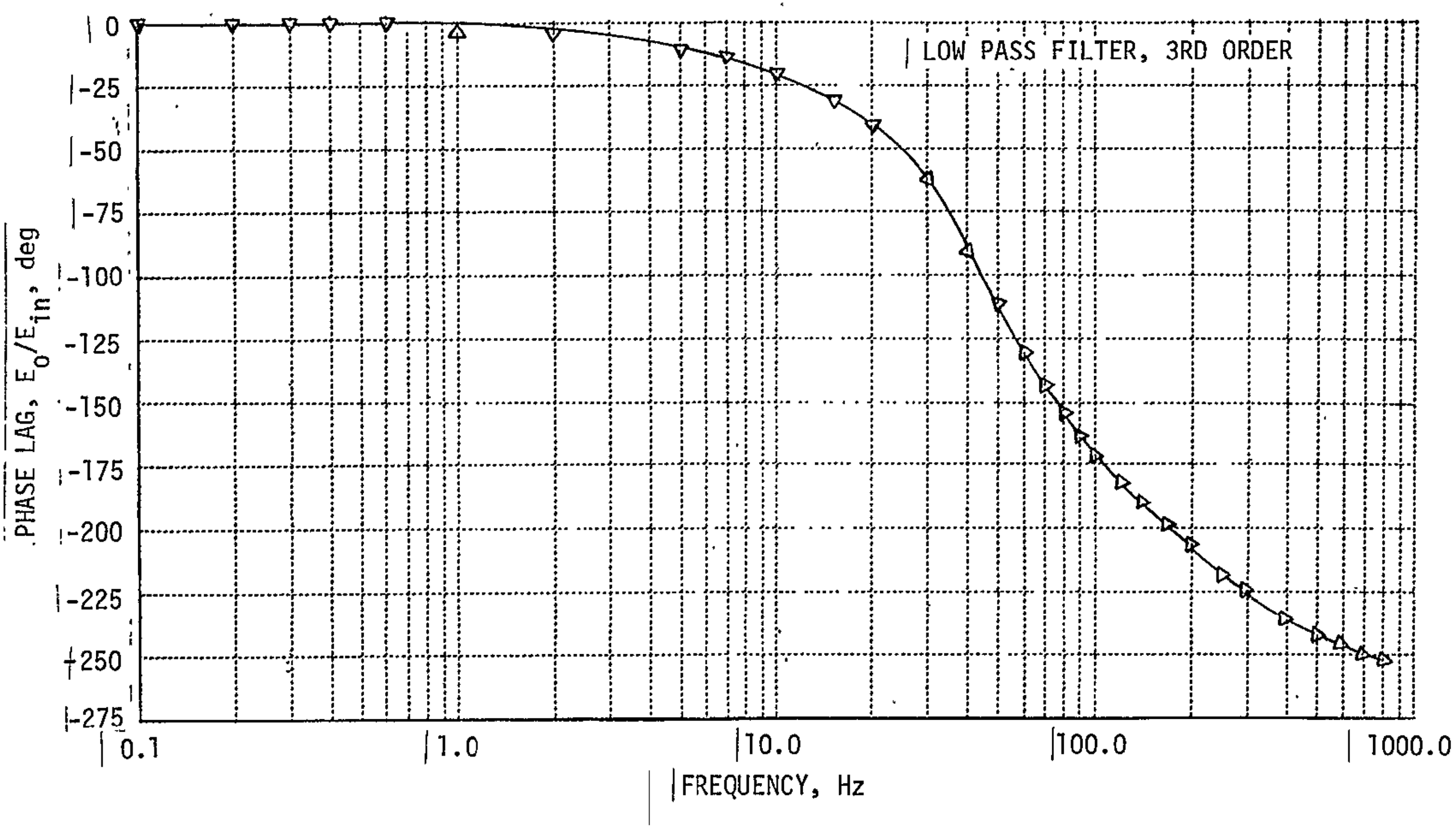

Figure 61 PHASE SHIFT VS FREQUENCY, 800 Hz CARRIER FREQUENCY FILTER

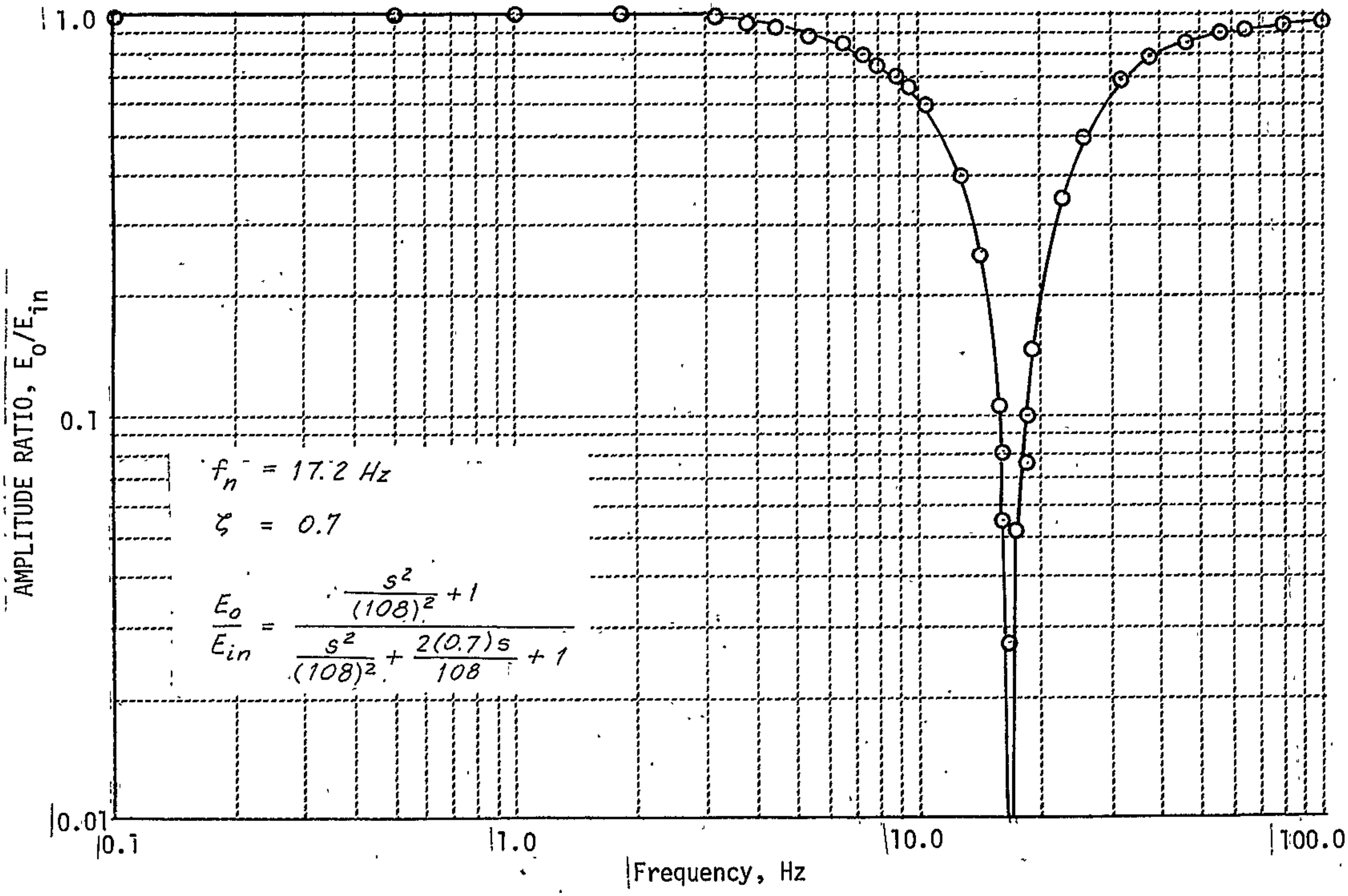

Figure 62 NOTCH FILTER AMPLITUDE VS FREQUENCY

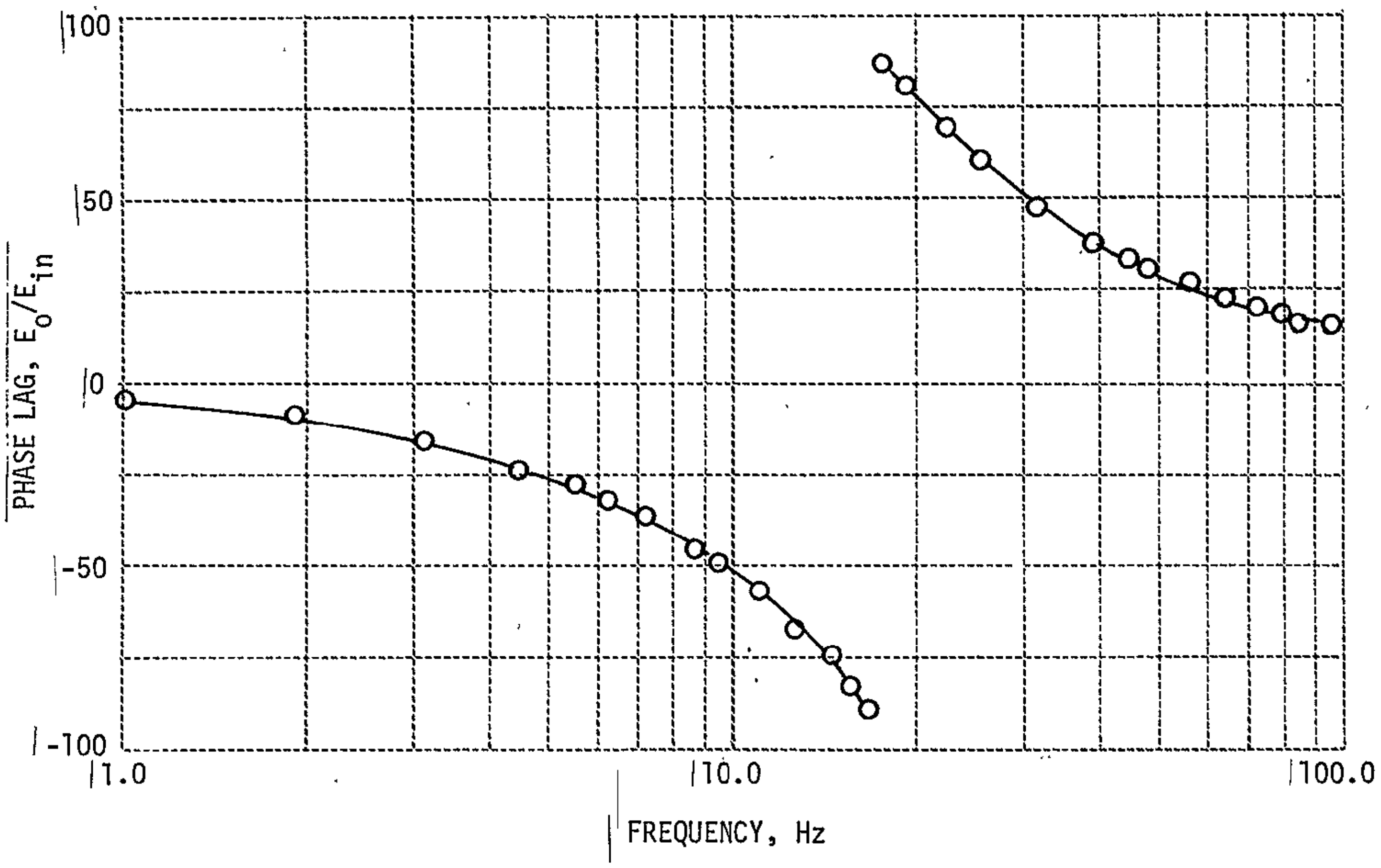

Figure 63 PHASE VS FREQUENCY, NOTCH FILTER

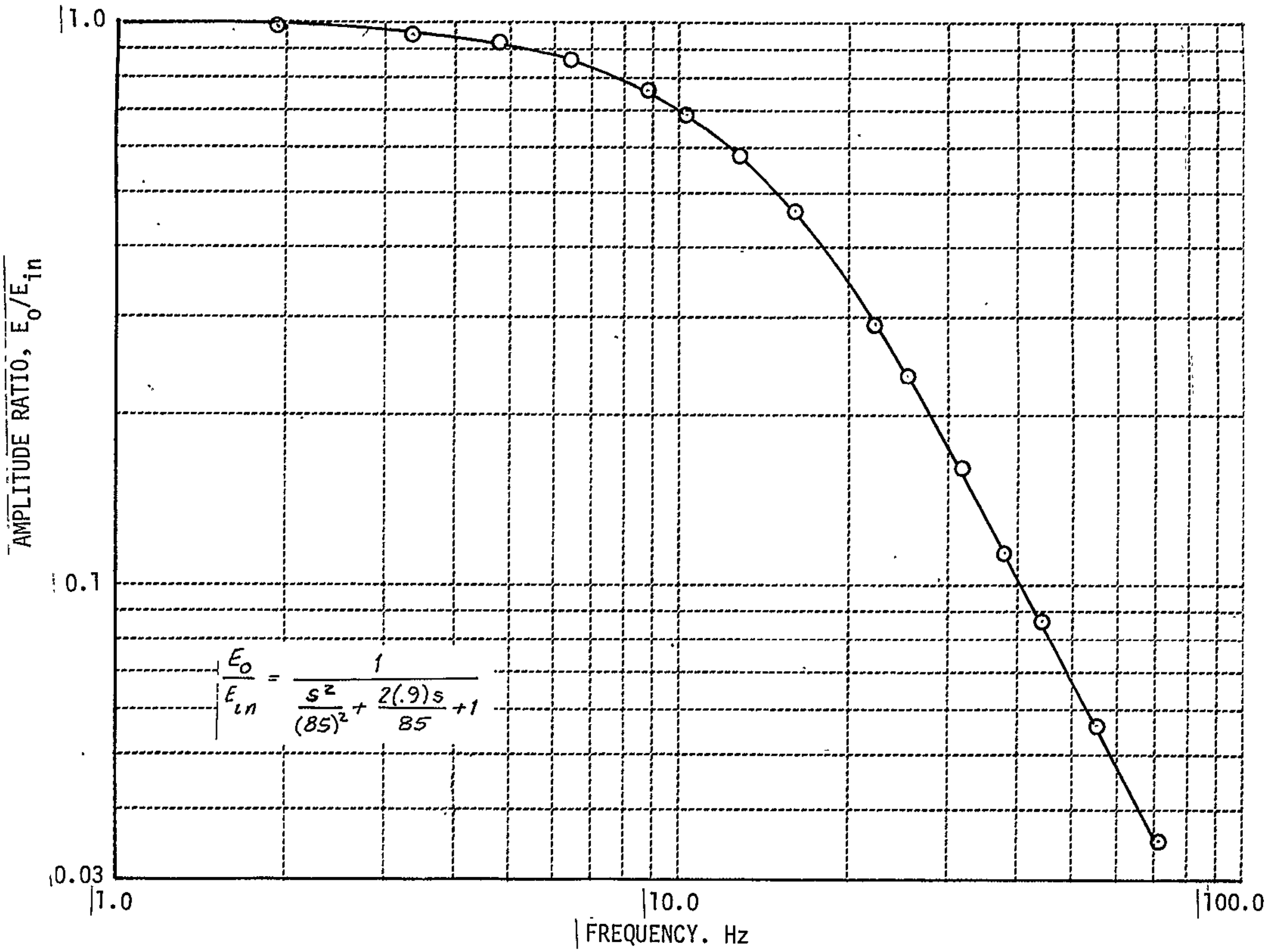

$$\frac{E_o}{E_{in}} = \frac{1}{\frac{s^2}{(85)^2} + \frac{2(.9)s}{85} + 1}$$

Figure 64 AMPLITUDE VS FREQUENCY, 2nd ORDER LOW PASS, 85 rad/sec

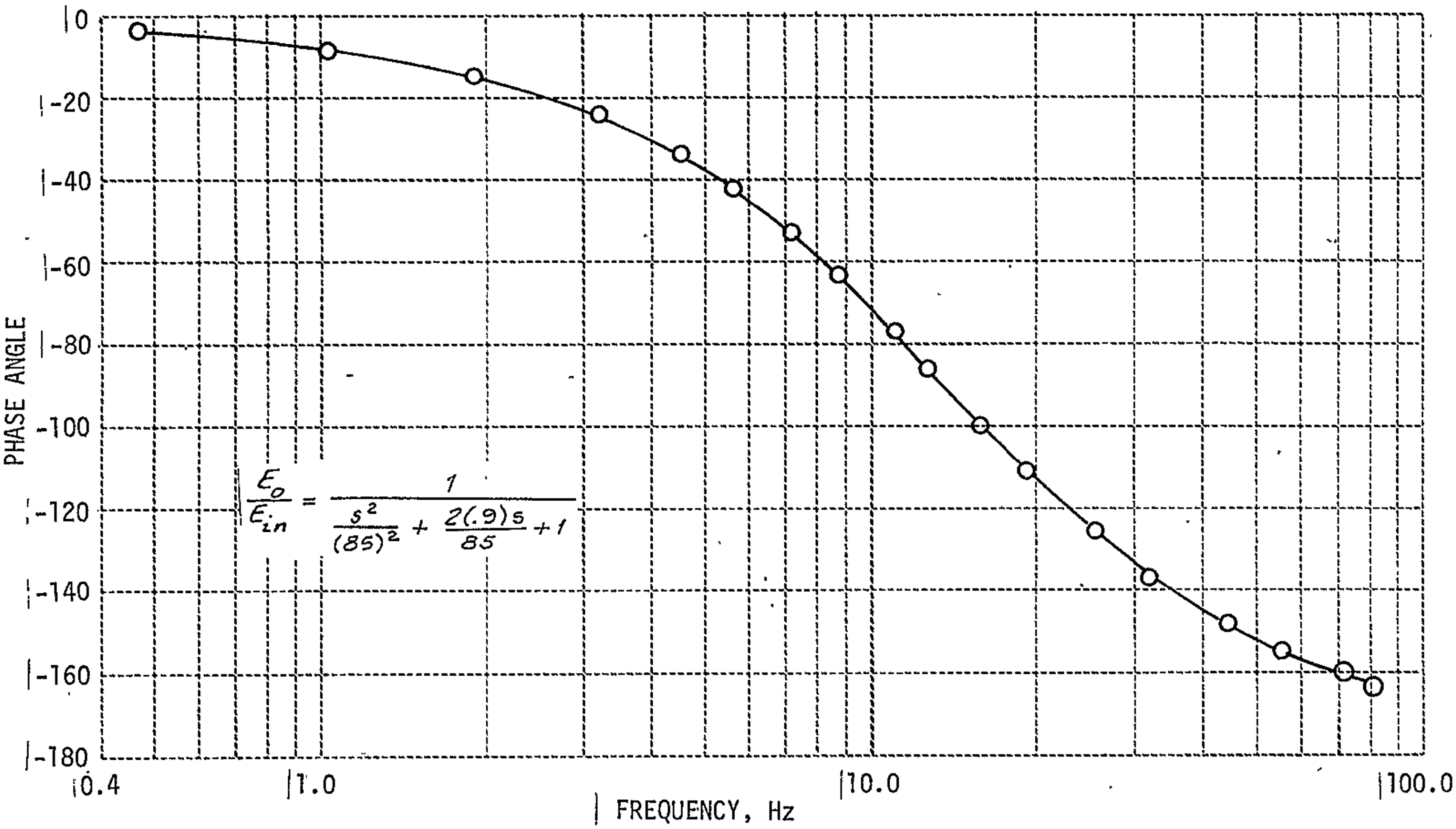

Figure 65 PHASE VS FREQUENCY, 2nd ORDER LOW PASS, 85 rad/sec

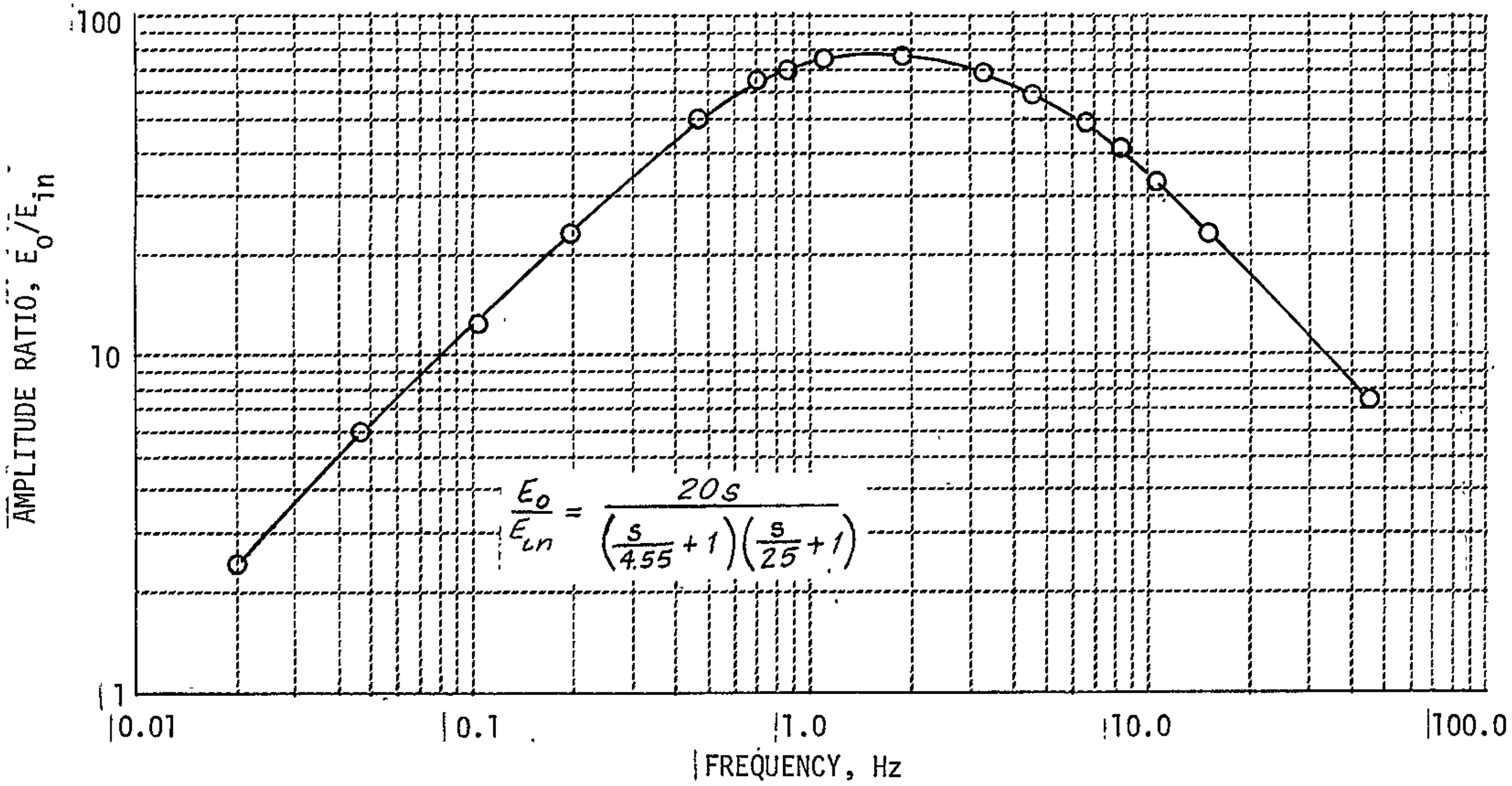

Figure 66 AMPLITUDE VS FREQUENCY, RADAR ALTITUDE DIFFERENTIATOR

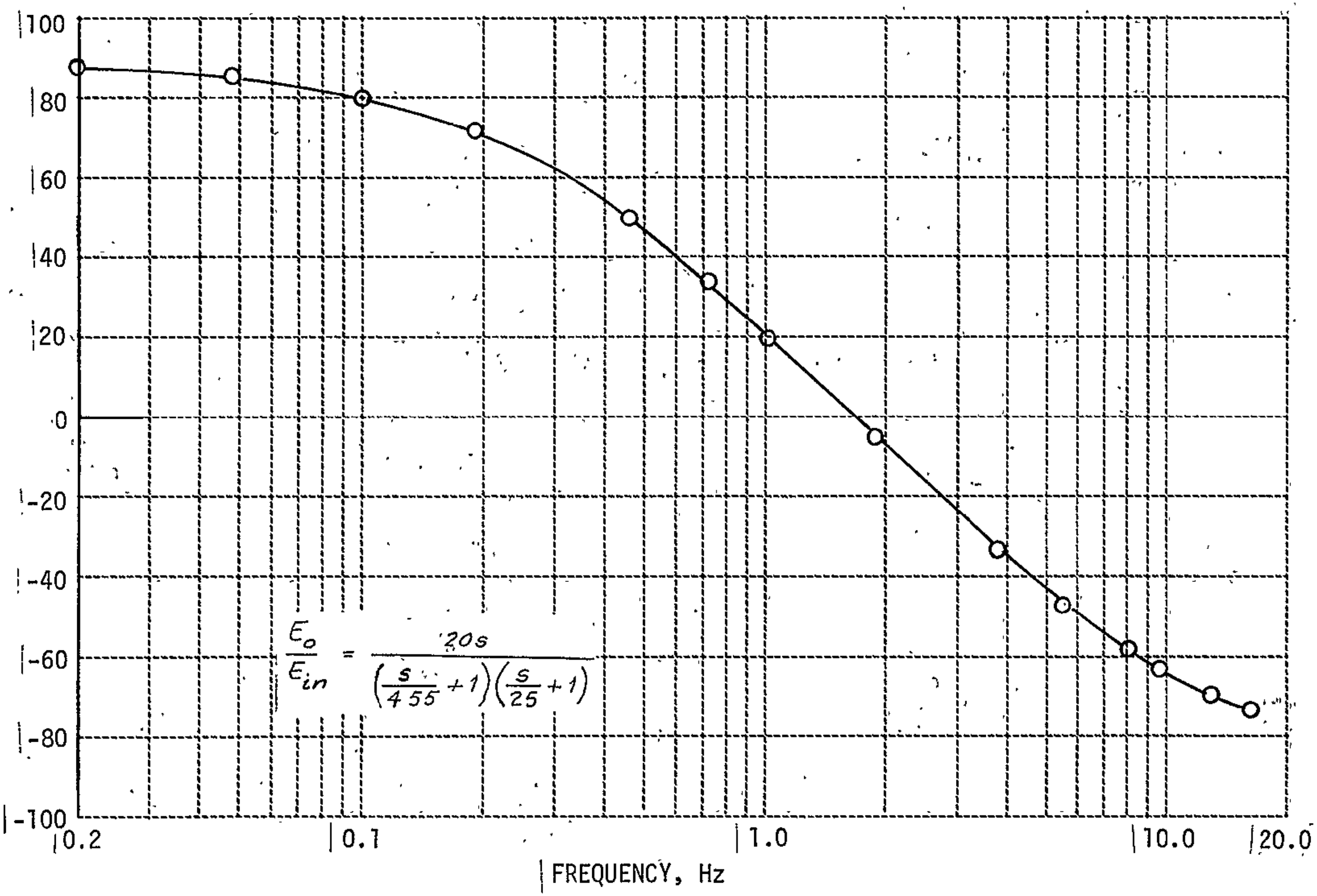

Figure 67 PHASE VS FREQUENCY, RADAR ALTITUDE DIFFERENTIATOR

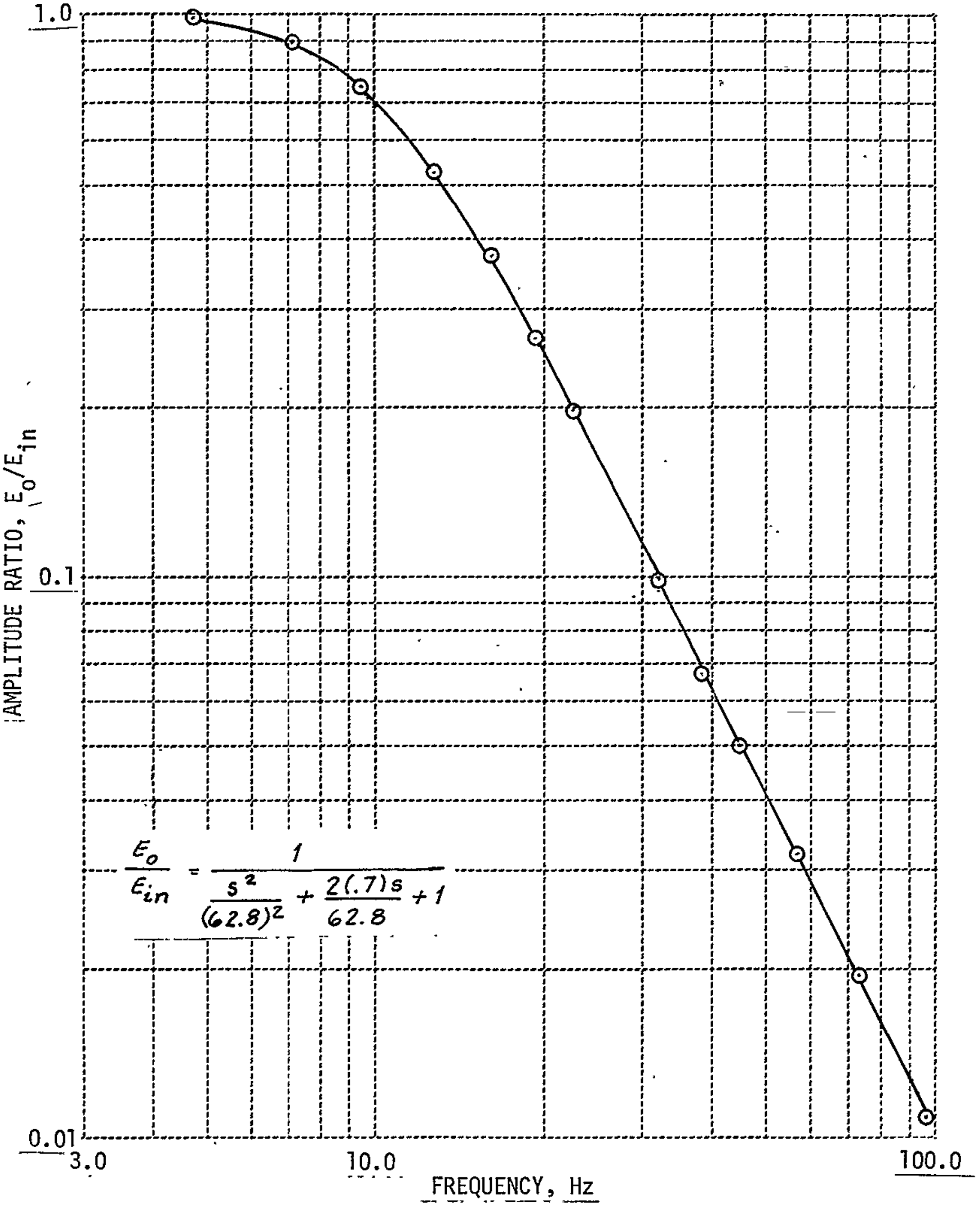

Figure 68 AMPLITUDE VS FREQUENCY, LOW PASS FILTER, 62.8 rad/sec

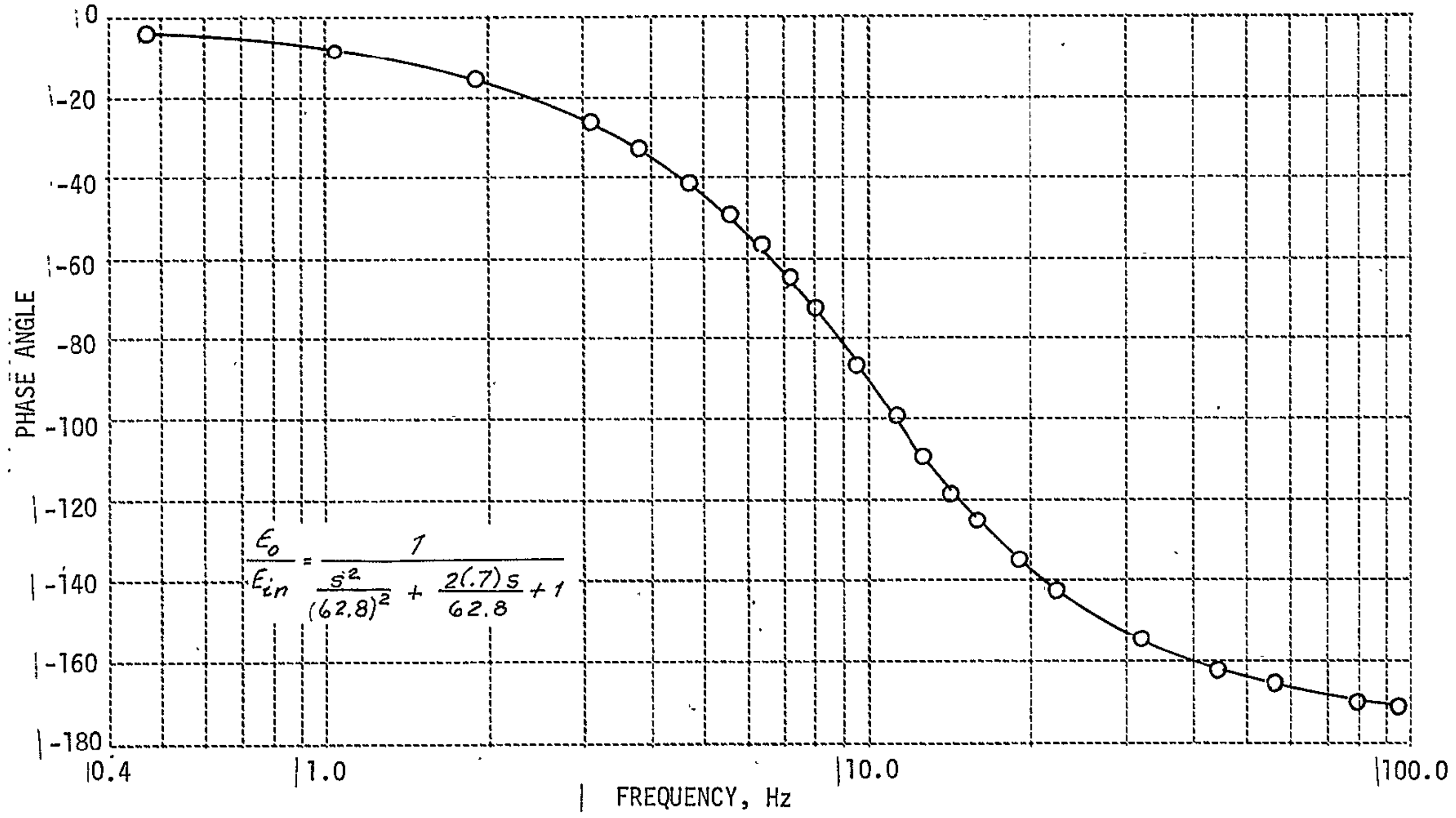

Figure 69 PHASE VS FREQUENCY, LOW PASS FILTER, 62.8 rad/sec

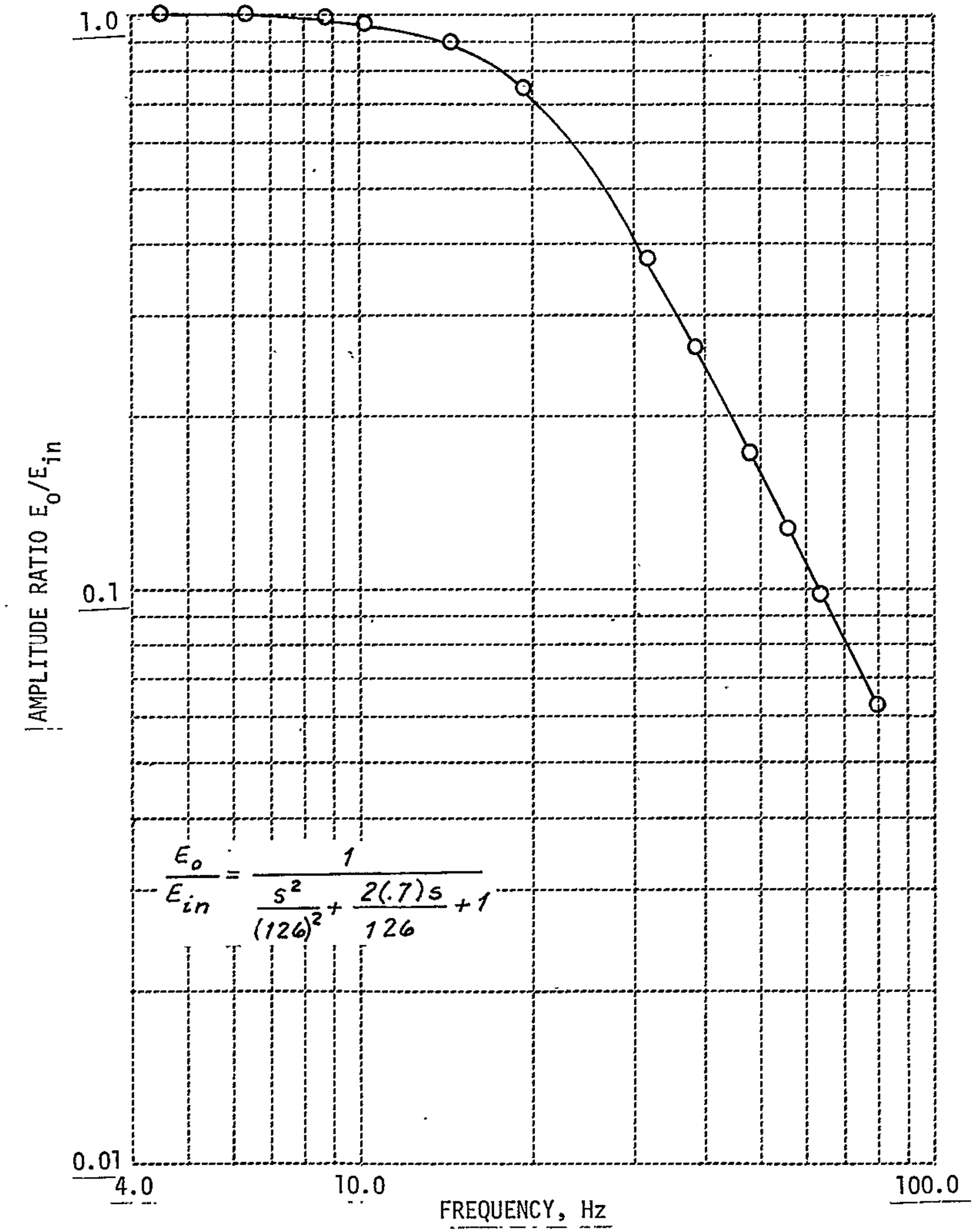

Figure 70 AMPLITUDE VS FREQUENCY, LOW PASS FILTER, 126 rad/sec

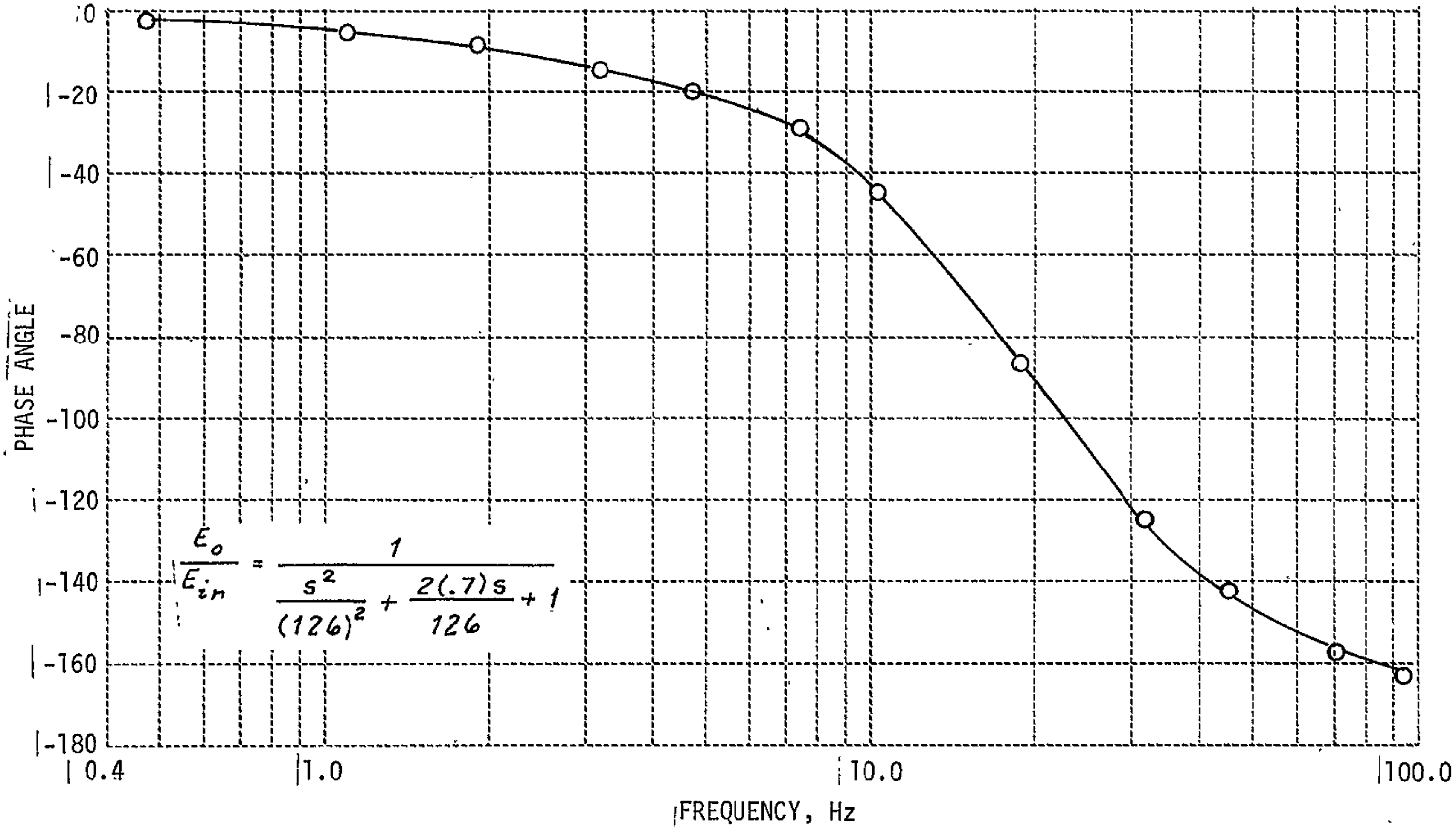

Figure 71 PHASE VS FREQUENCY, LOW PASS FILTER, 126 rad/sec

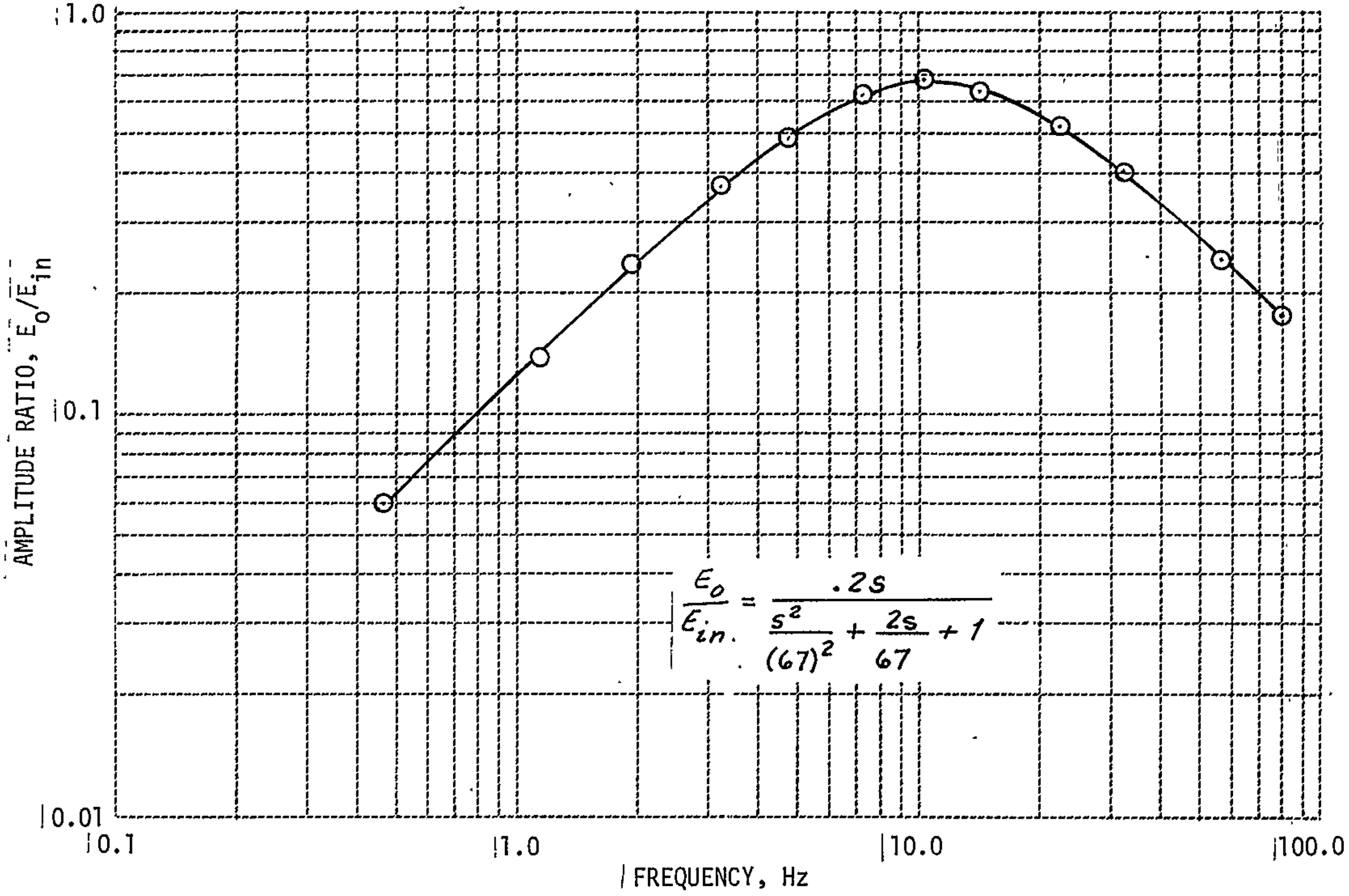

Figure 72 AMPLITUDE VS FREQUENCY, VANE DIFFERENTIATOR

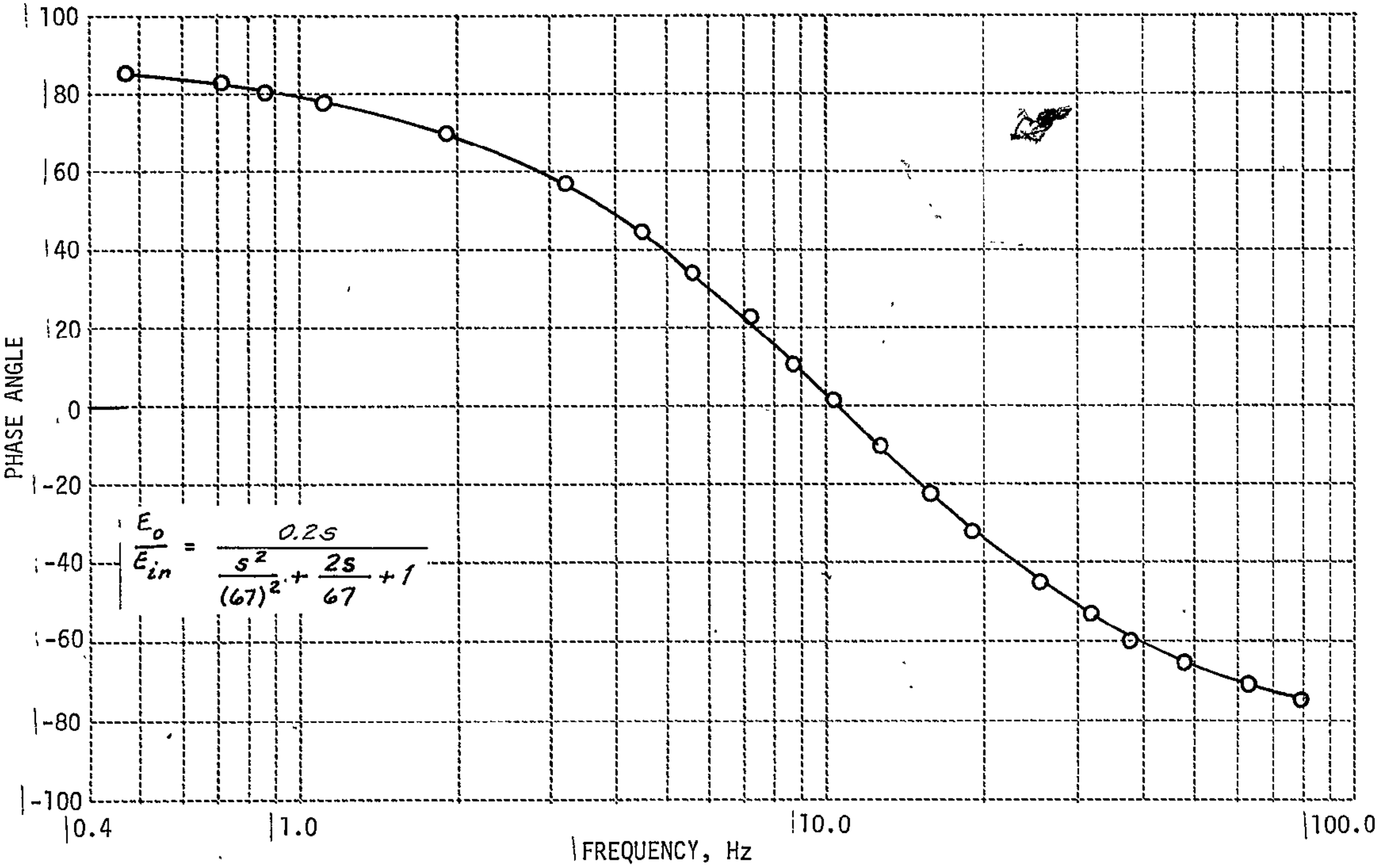

$$\frac{E_o}{E_{in}} = \frac{0.2s}{\frac{s^2}{(67)^2} + \frac{2s}{67} + 1}$$

Figure 73 PHASE VS FREQUENCY, VANE DIFFERENTIATOR

3.4.2 Group Two. Air Data Signals

The Air Data System, shown in Figure 74 provides output signals of altitude, altitude rate, indicated airspeed, true airspeed, true airspeed rate and Mach number. A block diagram of the signal flow through the Air Data Computer is illustrated in Figure 75. Diode function generators, mechanization of inertial equations and complementary filters used to generate these signals are compiled in Table 27. Additional sensors in combination with the group one signals are required. These air data sensors are:

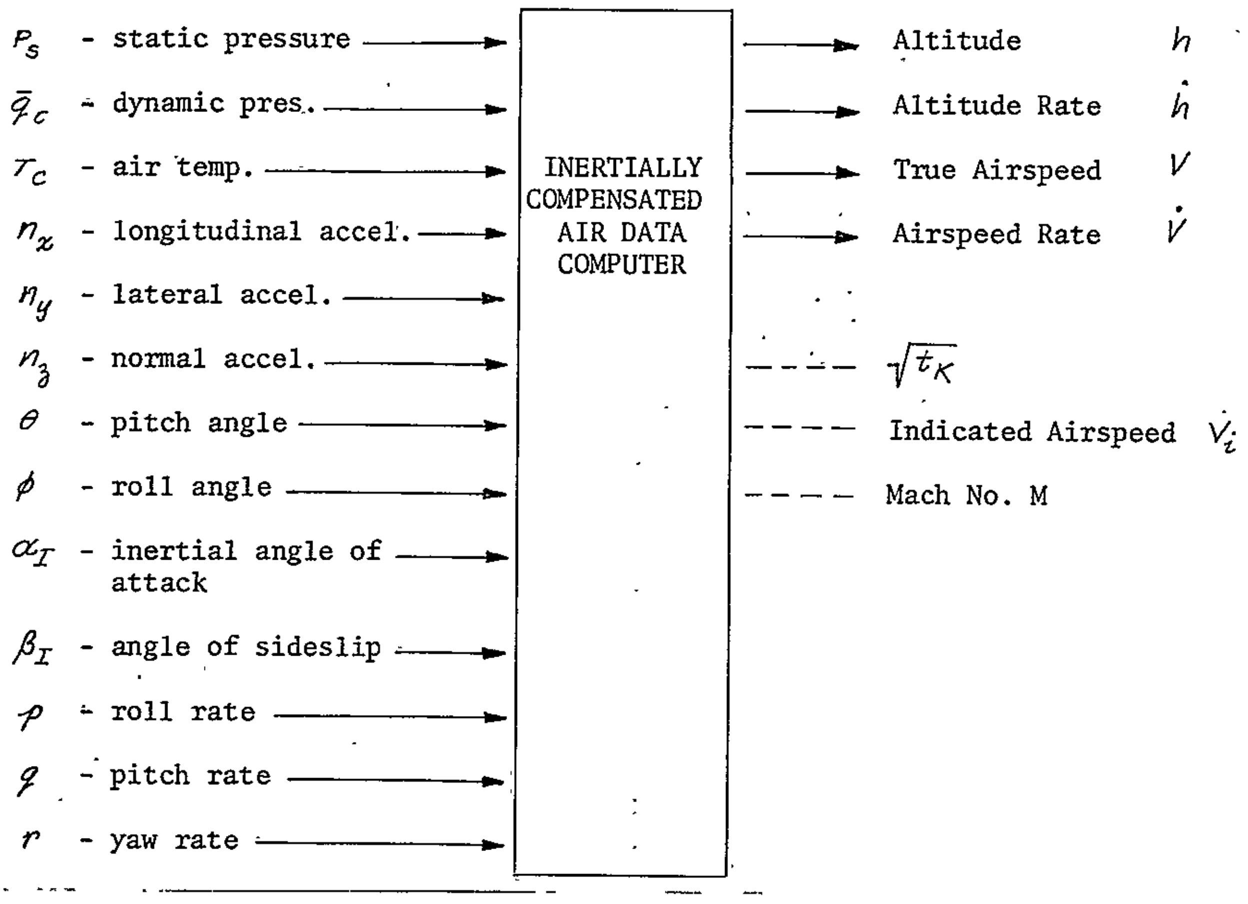

Figure 74 AIR DATA SYSTEM INPUT-OUTPUT SIGNALS

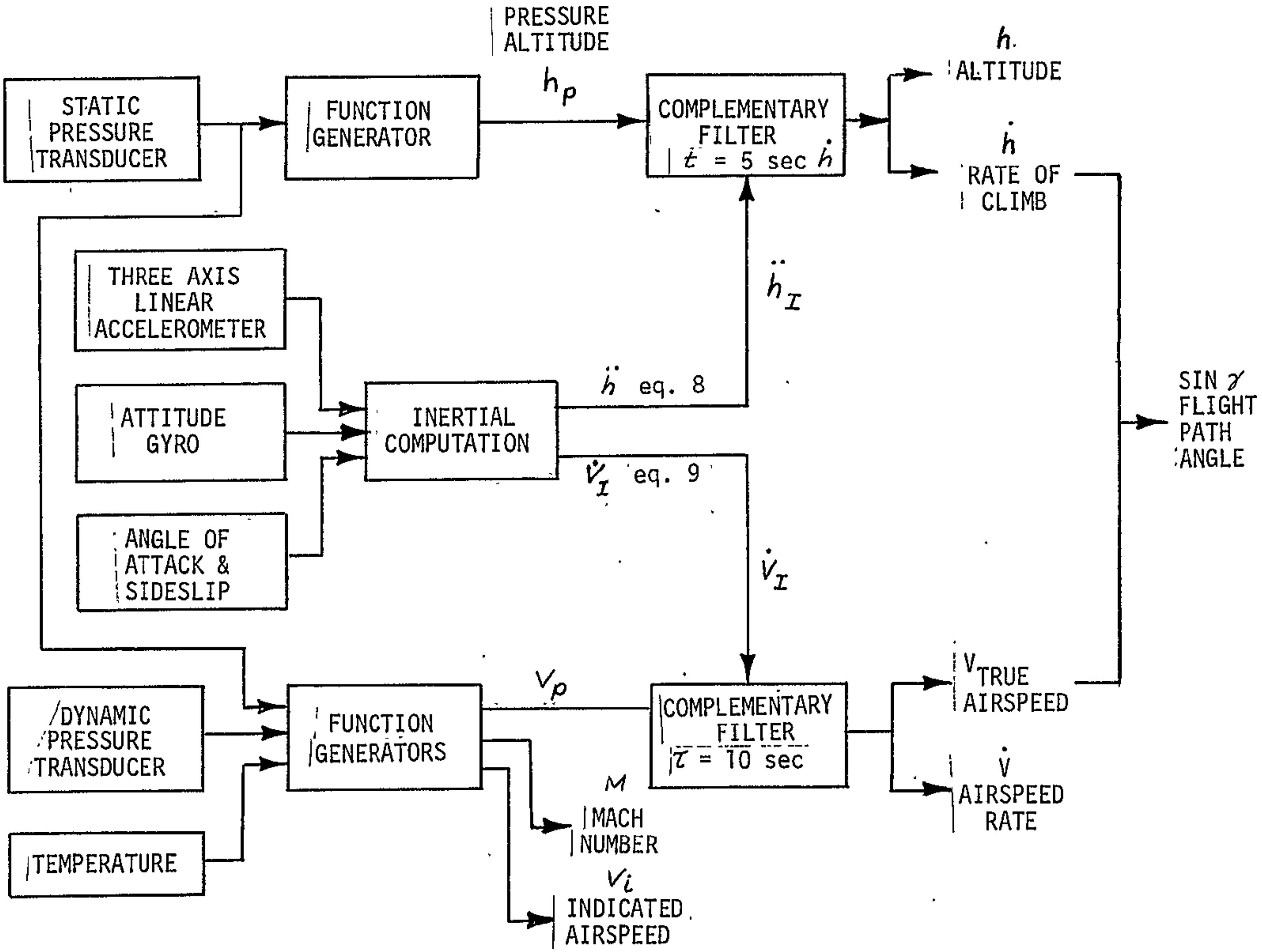

Figure 75 INERTIALLY COMPENSATED AIR-DATA BLOCK DIAGRAM

TABLE 27

AIR DATA EQUATIONS

AIR DATA FUNCTION GENERATORS

$h_p = f_1(p_s)$ Figure 76, Table 30 (Eq. 3)

$M = f_2(\bar{q}_c / p_s)$ Figure 77, Table 31 (Eq. 4)

$\sqrt{t_K} = f_3(t_c)$ Figure 78, Table 32 (Eq. 5)

$V_i = f_4(\bar{q}_c)$ Figure 79, Table 33 (Eq. 6)

AIR DATA EQUATION

$$V_p = 65.77\, M \sqrt{t_K} \qquad \text{(Eq. 7)}$$

M from Eq. 4, $\sqrt{t_K}$ from Eq. 5

INERTIAL EQUATIONS

$$\ddot{h}_I \cong g \left[n_x \sin\theta - n_y \sin\phi - n_z \cos\phi \right] \qquad \text{(Eq. 8)}$$

All variables are filtered sensor signals from GROUP ONE.

$$\dot{V}_I \cong g \left[n_x + n_y \beta_I + n_z \alpha_I - \sin\gamma \right] \qquad \text{(Eq. 9)}$$

α_I is obtained from Eq. 17
β_I is obtained from Eq. 18
$\sin\gamma$ is obtained from Eq. 14

Acceleration terms are obtained from GROUP ONE

COMPLEMENTARY FILTER EQUATIONS

$$\dot{h} = h_p \frac{s}{(\tau_1 s + 1)^2} + \ddot{h}_I \frac{2\tau_1 \left(\frac{\tau_1 s}{2} + 1 \right)}{(\tau_1 s + 1)^2} \qquad \tau_1 = 5 \text{sec.} \qquad \text{(Eq. 10)}$$

h_p from DFG Eq. 3 $\ddot{h}_I$ from Eq. 8

TABLE 27 (CONT'D)

$$h = h_p \frac{1}{\tau_2 s + 1} + \dot{h} \frac{\tau_2}{\tau_2 s + 1} \qquad \tau_2 = 1\,sec \quad \text{(Eq. 11)}$$

h_p from DFG Eq. 3 $\quad \dot{h}$ from Eq. 10

$$\dot{V} = V_p \frac{s}{(\tau_3 s + 1)^2} + \dot{V}_I \frac{2\tau_3 s\left(\frac{\tau_3 s}{2} + 1\right)}{(\tau_3 s + 1)^2} \qquad \tau_3 = 10\,sec \quad \text{(Eq. 12)}$$

V_p from Eq. 7 $\quad \dot{V}_I$ from Eq. 9

$$V = V_p \frac{1}{\tau_4 s + 1} + \dot{V} \frac{\tau_4}{\tau_4 s + 1} \qquad \tau_4 = 10\,sec \quad \text{(Eq. 13)}$$

V_p from Eq. 7 $\quad \dot{V}$ from Eq. 12

AUXILIARY EQUATION

$$\sin \gamma = \frac{\dot{h}}{V} \qquad \text{(Eq. 14)}$$

$\dot{h}$ from Eq. 10

V from Eq. 13

Static Air Pressure

This absolute pressure transducer is pneumatically connected to the basic aircraft copilot static source. The sensor output is DC and properly scaled for direct use in the system. The characteristics of this sensor are listed in Table 28.

TABLE 28

STATIC AIR PRESSURE

Rosemount Engineering Company
Model 830BC

31" Hg = 10V DC
10" Hg = 0V DC
Linearity ± .07% of full scale
Repeatability < ± .02% of full scale
Hysteresis ± .015% of full scale
Resolution < ± .02% of full scale

For step input change, $\tau < .015$ to reach 63% of final value.

Dynamic Air Pressure

This differential pressure transducer is connected to the copilot pitot and static pressure sources. The DC output of this sensor is used directly in the system. The applicable characteristics of this sensor are listed in Table 29.

TABLE 29

DYNAMIC AIR PRESSURE

Rosemount Engineering Company
Model 831BC

$\bar{q}_c$ 0" Hg = 0V DC
5" Hg = 10V DC
Linearity ± .07% of full scale
Repeatability < ± .02% of full scale
Hysteresis ± .015% of full scale
Resolution < ± .02% of full scale

For step input change, $\tau < .015$ to reach 63% of final value.

Outside Air Temperature

A standard aircraft type EDISON temperature bulb is used for this measurement. A temperature change causes a proportional change in bulb resistance. The output of the temperature bulb circuit is scaled to produce the required temperature signal.

Air Data Function Generators

Diode function generators are used where nonlinear transfer functions are required. In the air data computer, function generators are used to obtain:

a) Pressure altitude from static pressure, f_1, Figure 76, Table 30.

b) Mach number from a ratio of dynamic and static pressures, f_2, Figure 77, Table 31.

c) Square root of temperature (Kelvin) from temperature (Centigrade), f_3, Figure 78, Table 32.

d) Indicated airspeed from dynamic pressure, f_4, Figure 79, Table 33.

Actual function generator measurements are presented in the tables. A more complete description of the function generators can be obtained from TIFS Memo No. 53 of 21 March 1967 entitled "Diode Function Generators".

Air Data Computations

The air data signals required for the TIFS operation must have high bandwidth properties, high resolution and accuracy, yet be insensitive to air turbulence. To accomplish this, a complementary filter technique is used to blend air derived signals that are accurate at low frequencies with inertially computed signals which are free of turbulence at higher frequencies. For example, altitude derived from static pressure measurement is accurate at very low frequencies and inaccurate at high frequencies due to air turbulence contamination. Altitude derived from the double integration of vertical acceleration is accurate at high frequencies, however, d.c. offsets in the vertical acceleration measurement result in large errors in the computed altitude signal due to the double integration process. The resultant composite signals are accurate in amplitude and phase throughout a wide bandwidth.

The inertially computed signals $\ddot{h}_I$ and $\dot{V}_I$ are formed from the solutions of equations 8 and 9 in Table 27. The blended signals h, h, $\dot{V}$ and V are computed from equations 10 through 13. A procedure for determining the breakpoint frequency for the complementary filters is detailed in Appendix A. Flight path angle ($\sin \gamma$) is computed in equation 14.

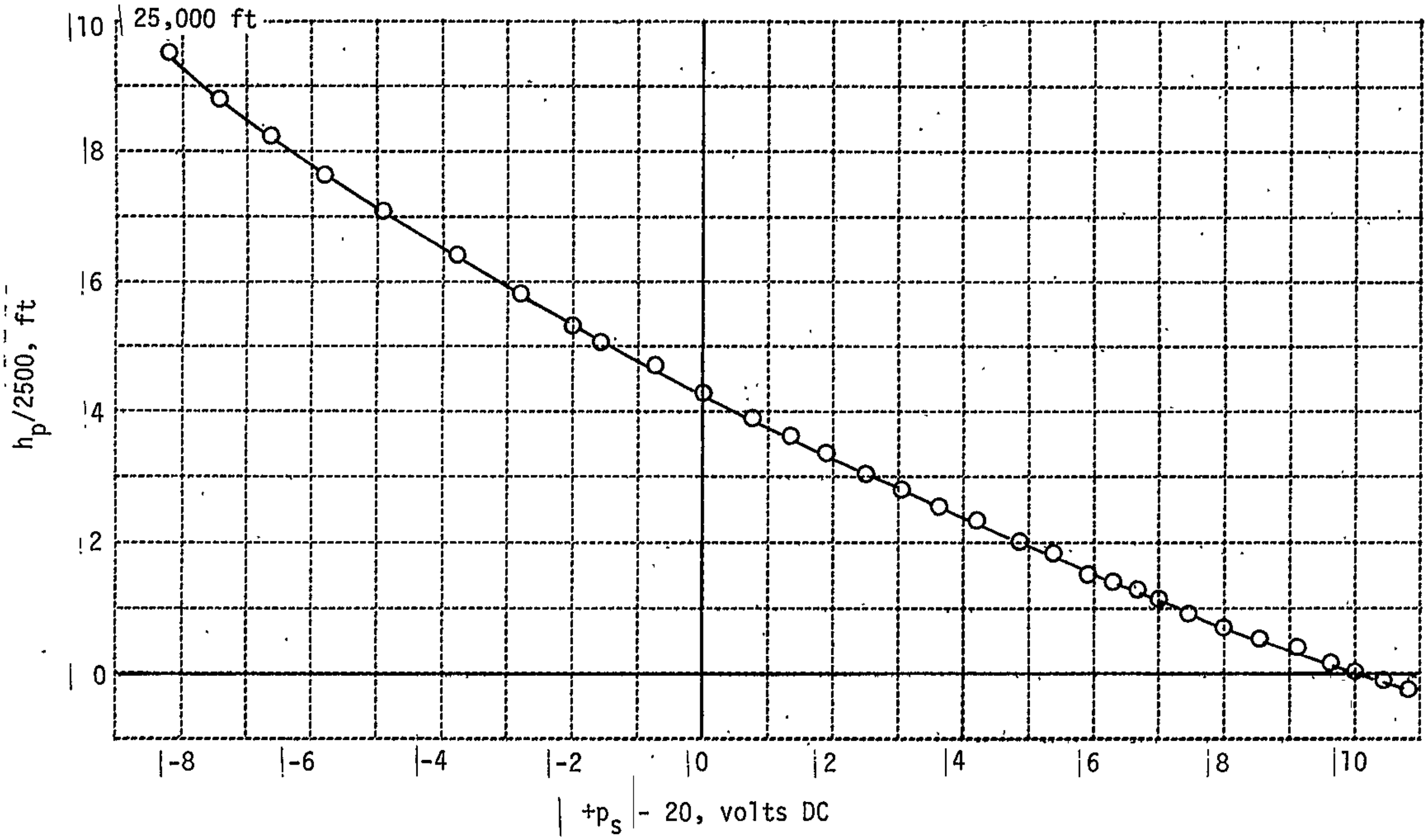

Figure 76 STATIC PRESSURE TO PRESSURE ALTITUDE FUNCTION GENERATOR

TABLE 30

p_s TO ALTITUDE FUNCTION GENERATOR

p_s In. Hg	$p_s/3$ V. DC	INPUT + p_s - 20 V.DC	DESIRED OUTPUT + hp/2500 V.DC	DESIRED + hp/2500 Feet	ACTUAL OUTPUT + hp/2500 V.DC
31.354	-10.451	11.354	-0.5200	-1300.00	-0.5160
30.00	-10.000	10.00	-0.00289	-72.36	-0.0020
29.00	-9.667	9.00	+0.3451	862.84	+0.3461
28.00	-9.333	8.00	+0.7300	1824.90	+0.7293
27.00	-9.000	7.00	+1.1261	2815.29	1.1255
26.00	-8.667	6.00	+1.5343	3835.75	1.5329
25.00	-8.333	5.00	1.9554	4888.46	1.9537
24.00	-8.000	4.00	2.3904	5975.91	2.3888
23.00	-7.667	3.00	2.8403	7100.69	2.8381
22.00	-7.333	2.00	3.3063	8265.84	3.3030
21.00	-7.000	1.00	3.7909	9477.16	3.7877
20.00	-6.667	0.00	4.2924	10730.9	4.2904
19.00	-6.333	-1.00	4.8157	12039.3	4.8121
18.00	-6.000	-2.00	5.3618	13404.5	5.3601
17.00	-5.667	-3.00	5.9331	14832.7	5.9299
16.00	-5.333	-4.00	6.5322	16330.6	6.5306
15.00	-5.000	-5.00	7.1625	17906.2	7.1624
14.00	-4.667	-6.00	7.8278	19569.4	7.8277
13.00	-4.333	-7.00	8.5327	21331.8	8.5353
12.00	-4.000	-8.00	9.2830	23207.6	9.2858
11.00	-3.667	-9.00	10.0858	25214.6	10.089
10.00	-3.333	-10.00	10.9500	27375.1	10.952

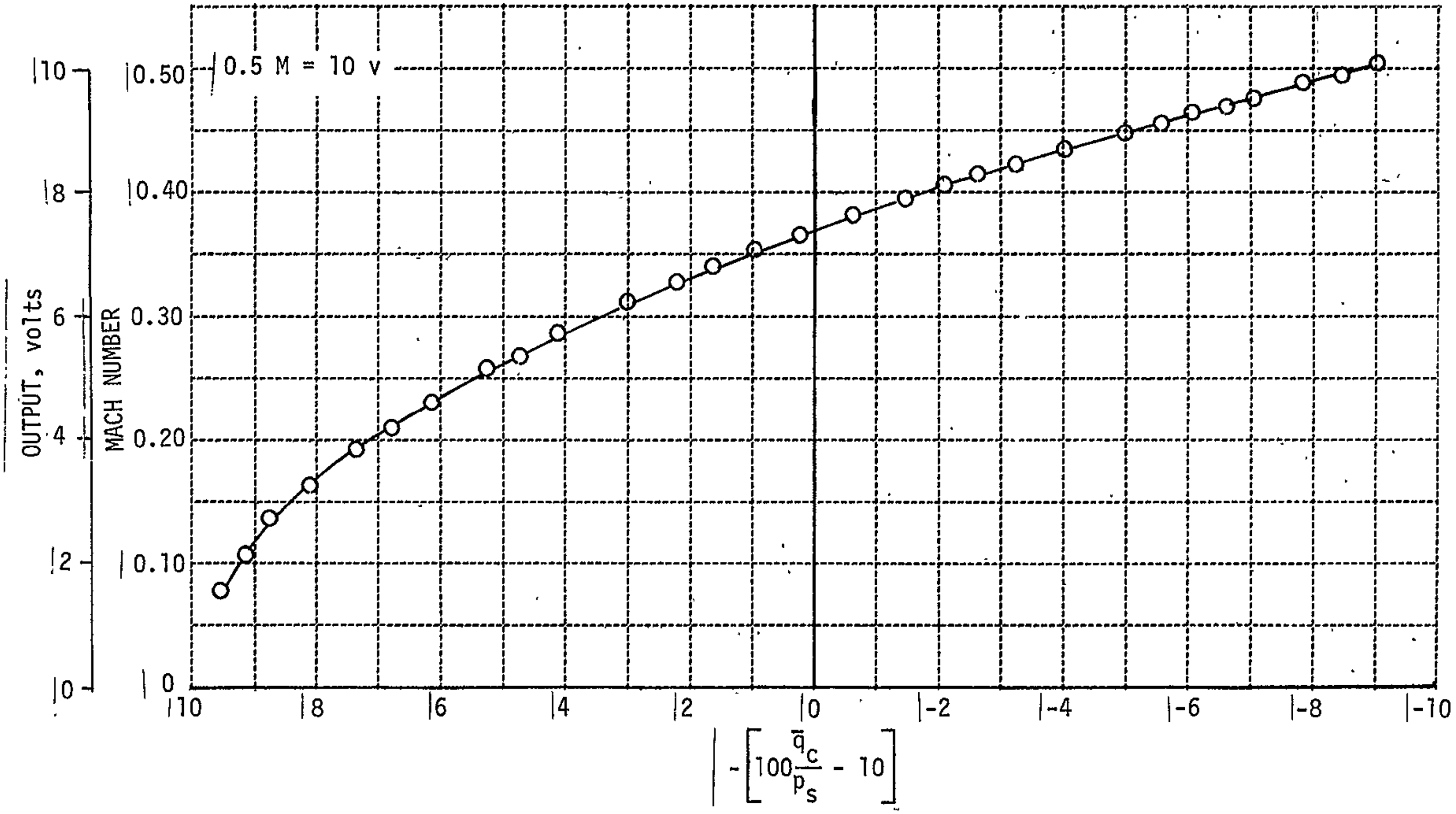

Figure 77 $\bar{q}_c/p_s$ TO M FUNCTION GENERATOR

TABLE 31

$\bar{q}_c / p_s$ TO MACH NO. FUNCTION GENERATOR

$\frac{\bar{q}_c}{p_s}$	INPUT $-\frac{100\,\bar{q}_c}{p_s}+10$	DESIRED OUTPUT V. DC	ACTUAL OUTPUT V. DC	M MACH NO.
0.00	+10.00	0.914	0.910	0.0457
0.01	+9.00	2.388	2.382	0.1194
0.02	+8.00	3.368	3.363	0.1684
0.03	+7.00	4.118	4.114	0.2059
0.04	+6.00	4.748	4.752	0.2374
0.05	+5.00	5.298	5.302	0.2649
0.06	+4.00	5.794	5.793	0.2897
0.07	+3.00	6.248	6.246	0.3124
0.08	+2.00	6.668	6.667	0.3334
0.09	+1.00	7.060	7.060	0.3530
0.10	0.00	7.430	7.430	0.3715
0.11	-1.00	7.780	7.775	0.3890
0.12	-2.00	8.112	8.110	0.4056
0.13	-3.00	8.430	8.426	0.4215
0.14	-4.00	8.734	8.734	0.4367
0.15	-5.00	9.026	9.024	0.4513
0.16	-6.00	9.308	9.308	0.4654
0.17	-7.00	9.580	9.577	0.4790
0.18	-8.00	9.842	9.842	0.4921
0.19	-9.00	10.096	10.091	0.5048
0.20	-10.00	10.342	10.341	0.5171

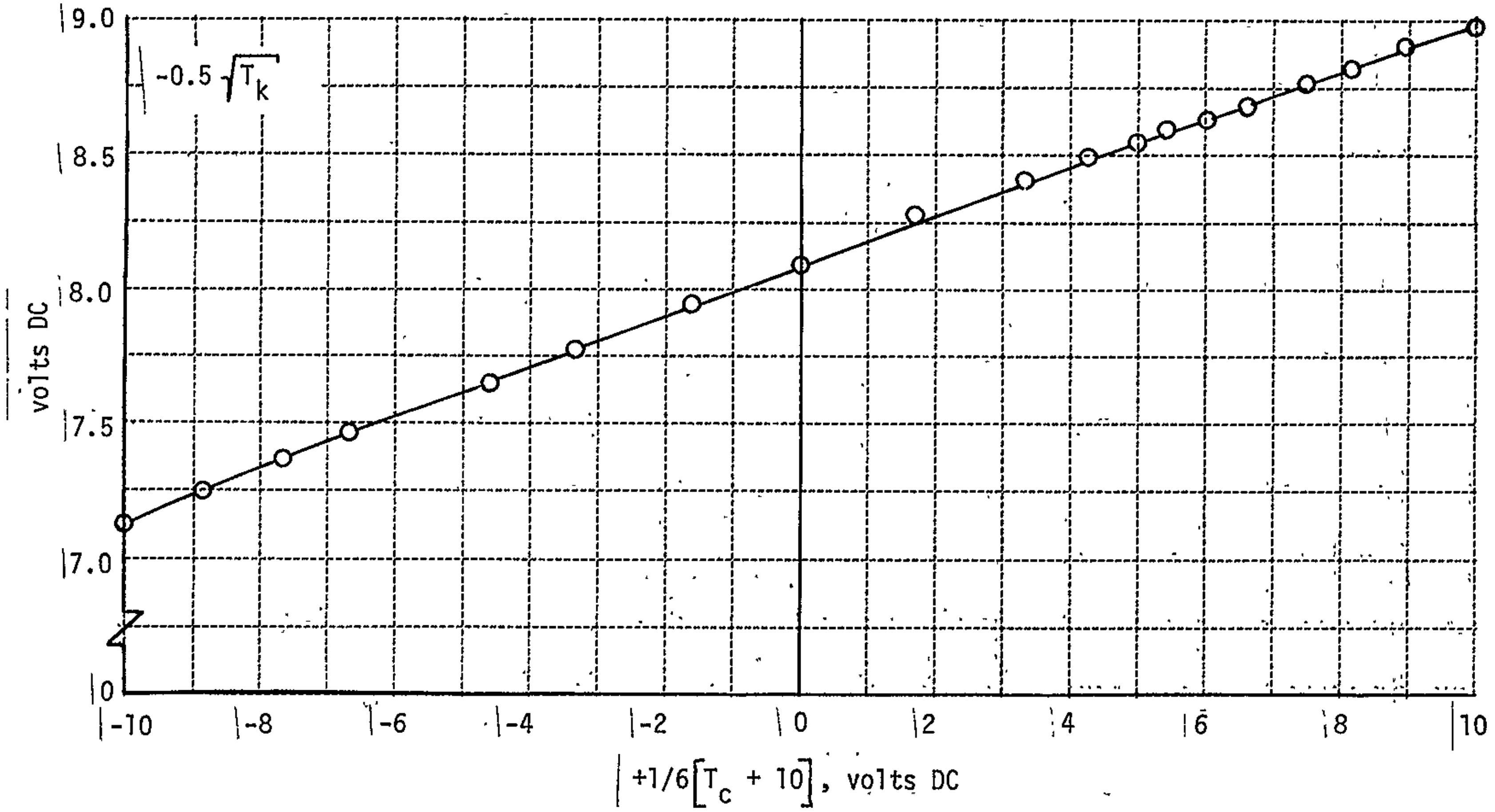

Figure 78 T_c TO $\sqrt{T_k}$ FUNCTION

TABLE 32

t_c TO $\sqrt{t_K}$ FUNCTION GENERATOR

t Deg. K	t Deg. C	INPUT $+ 1/6\, t_c + 10$ V. DC	DESIRED OUTPUT $\sqrt{t_K}$ (Deg. K)$^{\frac{1}{2}}$	DESIRED OUTPUT $-.5\sqrt{t_K}$ V. DC	ACTUAL OUTPUT $-.5\sqrt{t_K}$ V. DC
203	-70	-10.0000	14.248	7.124	7.1238
213	-60	- 8.3334	14.595	7.296	7.2964
223	-50	- 6.6667	14.933	7.467	7.4666
233	-40	- 5.0000	15.264	7.632	7.6328
243	-30	- 3.3334	15.589	7.795	7.7956
253	-20	- 1.6667	15.906	7.953	7.9529
263	-10	0	16.216	8.109	8.1084
273	0	+ 1.6667	16.523	8.262	8.2628
283	10	+ 3.3334	16.823	8.412	8.4123
293	20	+ 5.0000	17.117	8.559	8.5589
303	30	+ 6.6667	17.407	8.704	8.7049
313	40	+ 8.3334	17.692	8.846	8.8461
323	50	+10.0000	17.972	8.986	8.9861

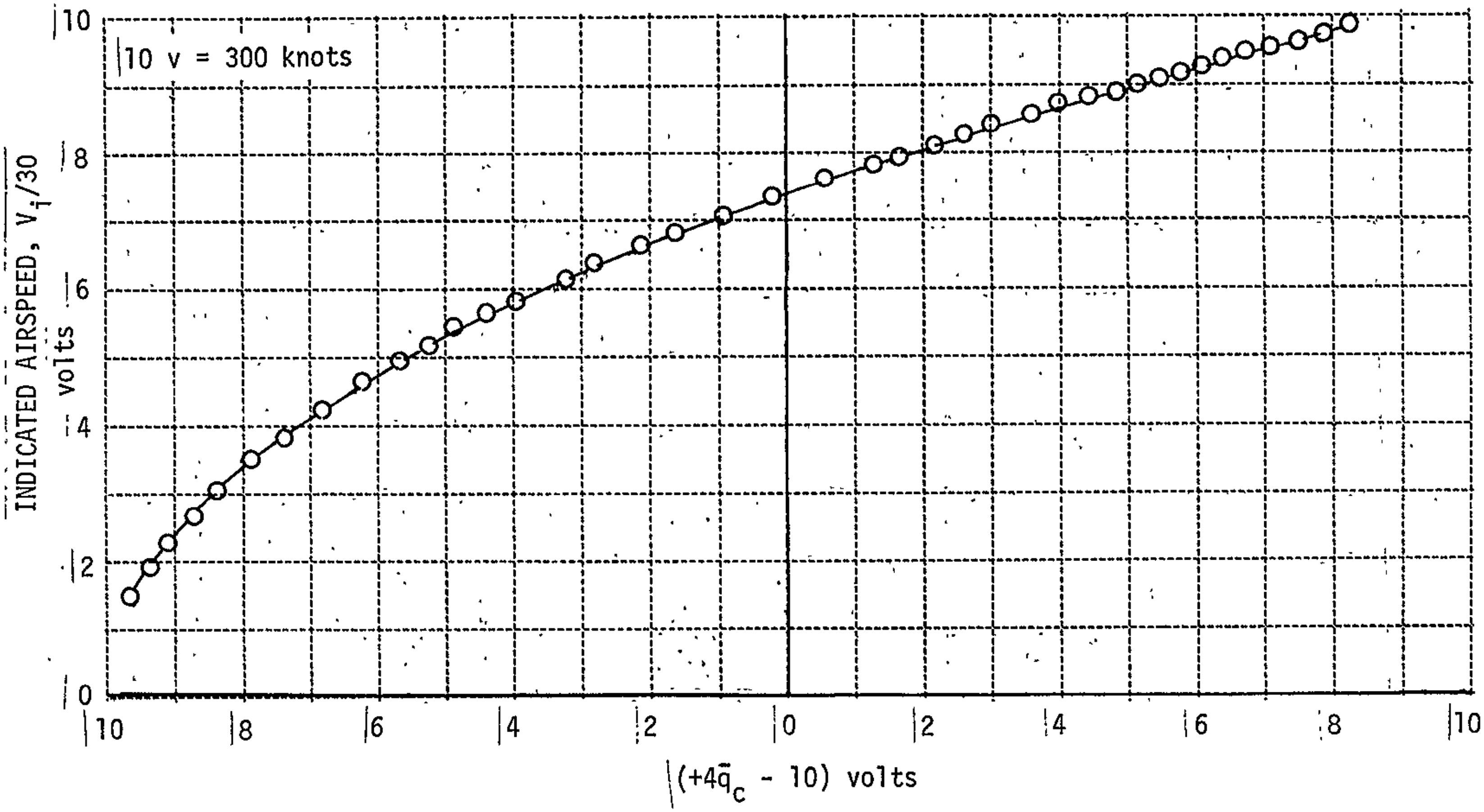

Figure 79 DYNAMIC PRESSURE TO INDICATED AIRSPEED FUNCTION

TABLE 33

$\bar{q}_c$ TO INDICATED AIRSPEED FUNCTION GENERATOR

$\bar{q}_c$ In. HG	$\bar{q}_c$ lb/ft^2	$-2\bar{q}_c$ V. DC	INPUT $-4\bar{q}_c + 10$ V. DC	DESIRED OUTPUT $V_i/30$ V. DC	ACTUAL OUTPUT $V_i/30$ V. DC	V_i Knots
0.00	0.000	0.000	-10.00	1.000	1.0000	30.00
0.25	17.6825	0.500	-9.00	2.4035	2.4033	72.10
0.50	35.365	1.000	-8.00	3.3936	3.3929	101.81
0.75	53.0475	1.500	-7.00	4.1501	4.1517	124.50
1.00	70.73	2.000	-6.00	4.7852	4.7834	143.55
1.25	88.4125	2.500	-5.00	5.3423	5.3423	160.27
1.50	106.095	3.000	-4.00	5.8443	5.8469	175.33
1.75	123.7775	3.500	-3.00	6.3042	6.3036	189.13
2.00	141.46	4.000	-2.00	6.7300	6.7300	201.90
2.25	159.1425	4.500	-1.00	7.1276	7.1282	213.83
2.50	176.825	5.000	0.00	7.5025	7.5023	225.07
2.75	194.5075	5.500	1.00	7.8570	7.8562	235.71
3.00	212.190	6.000	2.00	8.1959	8.1959	245.88
3.25	229.8725	6.500	3.00	8.5188	8.5132	255.56
3.50	247.555	7.000	4.00	8.8259	8.8253	264.78
3.75	265.2375	7.500	5.00	9.1244	9.1206	273.73
4.00	282.92	8.000	6.00	9.4114	9.4106	282.34
4.25	300.6025	8.500	7.00	9.6879	9.6847	290.64
4.50	318.2850	9.000	8.00	9.9549	9.9539	298.65
4.75	335.9675	9.500	9.00	10.2140	10.2098	306.42
5.00	353.65	10.000	10.00	10.4646	10.4658	313.94
5.25	371.3325	10.500		10.7102		321.30

3.4.3 Group Three. Angle of Attack, Sideslip and Gust Computations

High feedback gains of angle of attack, sideslip and their rates are desirable for the TIFS control system, To achieve these feedback gains, inertial signals must be used. The vane signals contain gust information which make them unusable for feedback.

Inertial signals are computed for angle of attack α_I, angle of sideslip β_I , angle of attack rate $\dot{\alpha}_I$ and angle of sideslip rate $\dot{\beta}_I$. Gust signals are computed from the difference between the vane signals and these inertial computations. The equations for these computations are listed in Table 34.

The inertial computations are the following:

- Inertial angle of attack rate is computed from the following equation mechanized in the TIFS sensor electronics.

generated from z force equation

$$\dot{\alpha}_I = \frac{57.3g}{V}\left[n_z + \cos\phi\right] + q - \frac{p\beta_I}{57.3} \qquad \text{(Eq. 15)}$$

where: n_z , p, q, cos ϕ are conditioned basic sensor signals from Table 9.

V is obtained from equation 13.

β_I is obtained from equation 18.

- Inertial angle of sideslip rate is computed from:

generated from y force equation

$$\dot{\beta}_I = \frac{57.3g}{V}\left[n_y + \sin\phi\right] - r + \frac{p\alpha_I}{57.3} \qquad \text{(Eq. 16)}$$

where: n_y , p, r, sin ϕ are conditioned basic sensor signals.

V is obtained from equation 13.

α_I is obtained from equation 17.

- The inertial angle of attack is computed from the following equation.

$$\alpha_I = 57.3\left[\frac{-\sin\gamma + \sin\theta - \frac{\beta_I}{57.3}\sin\phi}{\cos\phi}\right] \qquad \text{(Eq. 17)}$$

where: sin γ is obtained from equation 14.

sin θ, sin ϕ, cos ϕ are conditioned basic sensor signals from Table 9.

β_I is obtained from equation 18.

Inertial angle of sideslip cannot be obtained in the same manner as inertial angle of attack. In TIFS, a complementary filter is used to generate inertial sideslip angle. In this filter, low frequency information from the corrected angle of sideslip vane is blended with the inertial angle of sideslip rate term. The complementary filter equation mechanized is:

$$\beta_I \cong \overbrace{(\beta_I + \beta_g)}^{VANE} \frac{1}{(\tau s + 1)^2} + \overbrace{\dot{\beta}_I}^{INERTIAL} \frac{2\tau\left(\frac{\tau s}{2} + 1\right)}{(\tau s + 1)^2}, \quad where\ \tau = 1\,sec \qquad \text{(Eq. 18)}$$

$(\beta_I + \beta_g)$ is the angle of sideslip vane signal corrected for position error and for location from the CG (Table 26).

$\dot{\beta}_I$ is obtained from Equation 16.

Angle of attack and sideslip gust terms are computed from the difference between corrected vane and inertially computed terms. The gust equations mechanized in the TIFS sensor system are:

$$\alpha_{gust} = (\alpha_I + \alpha_g) - \alpha_I \qquad \text{(Eq. 19)}$$

where: $(\alpha_I + \alpha_g)$ is corrected angle of attack vane from Table 26.

α_I is computed from Equation 17.

A small DC term may be present on the α_{gust} signal because of improper vane alignment in the local airstream at all airspeeds. A DC washout (high pass) filter with higher frequency rolloff characteristics is available on the computer patch panel to eliminate this DC term. The filter transfer function is $E_0/E_{IN} = 5s/\left(\left(\frac{s}{10}+1\right)\left(\frac{s}{.2}+1\right)\right)$.

$$\beta_{\text{gust}} = (\beta_I + \beta_g) - \beta_I \qquad \text{(Eq. 20)}$$

where: $(\beta_I + \beta_g)$ is corrected angle of attack vane from Table 26.

β_I is computed from Equation 18.

$$\dot{\alpha}_{\text{gust}} = (\dot{\alpha}_I + \dot{\alpha}_g) - \dot{\alpha}_I \qquad \text{(Eq. 21)}$$

where: $(\dot{\alpha}_I + \dot{\alpha}_g)$ is the derivative of the corrected angle of attack vane signal from Table 26.

$\dot{\alpha}_I$ is computed from Equation 15.

$$\dot{\beta}_{\text{gust}} = (\dot{\beta}_I + \dot{\beta}_g) - \dot{\beta}_I \qquad \text{(Eq. 22)}$$

where: $(\dot{\beta}_I + \dot{\beta}_g)$ is the derivative of the corrected sideslip vane signal from Table 26.

and $\dot{\beta}_I$ is computed from Equation 16.

TABLE 34

ANGLE OF ATTACK AND SIDESLIP EQUATIONS

ANGLE OF ATTACK COMPUTATIONS

$$\alpha_I = 57.3\left[\frac{-\sin\gamma + \sin\theta - \beta_I/57.3\sin\phi}{\cos\phi}\right] \qquad \text{(Eq. 17)}$$

$$\dot{\alpha}_I \cong \frac{(57.3)(32.2)}{V}\left[n_z + \cos\phi\right] + q - \frac{p\beta_I}{57.3} \qquad \text{(Eq. 15)}$$

ANGLE OF SIDESLIP COMPUTATIONS

$$\dot{\beta}_I \cong \frac{(57.3)(32.2)}{V}\left[n_y + \sin\phi\right] + \frac{\alpha_I p}{57.3} - r \qquad \text{(Eq. 16)}$$

$$\beta_I \cong \frac{\overbrace{\beta_I + \beta_g}^{VANE}}{(\tau s + 1)^2} + \frac{\overbrace{\dot{\beta}_I}^{INERTIAL}\, 2\tau\left(\frac{\tau s}{2} + 1\right)}{(\tau s + 1)^2} \qquad \tau = 1\ sec \qquad \text{(Eq. 18)}$$

GUST EQUATIONS

$$\overbrace{}^{\text{Corrected Vane Signals}} \qquad \overbrace{}^{\text{Inertial}}$$

$$\alpha_{\text{gust}} = (\alpha_I + \alpha_g) - \alpha_I \qquad \text{(Eq. 19)}$$

$$\beta_{\text{gust}} = (\beta_I + \beta_g) - \beta_I \qquad \text{(Eq. 20)}$$

$$\dot{\alpha}_{\text{gust}} = (\dot{\alpha}_I + \dot{\alpha}_g) - \dot{\alpha}_I \qquad \text{(Eq. 21)}$$

$$\dot{\beta}_{\text{gust}} = (\dot{\beta} + \dot{\beta}_g) - \dot{\beta}_I \qquad \text{(Eq. 22)}$$

Excellent correlation of vane and inertially computed angle of attack and rate terms for an elevator doublet can be seen in the flight record, Figure 80. The inertial angle of attack and inertial angle of attack rate signals at the TIFS C.G. are derived from independent computations (Equations 17 and 15). These signals can be directly compared with the vane angle of attack signal and its rate term corrected for position error and location from the C.G. The angle of sideslip vane rate signal and the inertially computed sideslip rate signal for a rudder doublet can be directly compared in Figure 81. The sideslip vane is corrected for position error and for location from the C.G. This corrected vane signal can be directly compared with the output of the sideslip complementary filter (β_I). Mechanization of the $\dot{\alpha}_I$ and $\dot{\beta}_I$ computations were included to provide noise free signals that can be used in high gain feedback loops. A comparison of the noise content between the differentiated vane signals and the computed signals can be made from Figures 80 and 81. In addition, the inertial computations allow the generation of gust terms (Figures 86 and 87) which are the difference between the corrected vane signals and the inertial computations.

If the vane and inertially computed angle of attack signals are compared for lateral aircraft motions, a difference between the vane and inertial signals is apparent (Figure 82). The independent computations of α_I (Equation 17) and $\dot{\alpha}_I$ (Equation 15) maintain correlation during these lateral maneuvers. Therefore, it is suspected that the angle of attack vane is affected by aircraft sideslip. To check this effect, a percentage of the corrected angle of sideslip vane signal was subtracted from the corrected angle of attack vane signal. The equation used was the following:

$$\alpha_{COMPENSATED} = +0.5\,(\alpha_I + \alpha_g) - K\,0.5\,(\beta_I + \beta_g).$$

a dramatic improvement in correlation between the compensated angle of attack vane and the inertially computed signals was obtained for an aileron doublet (Figure 83) and a rudder doublet (Figure 84) with a compensation factor of K = 0.125.

To check the correlation of angle of attack vane deflection with sideslip, records should be obtained at various airspeeds and angles of attack for lateral-directional inputs.

The angle of sideslip vane response for an elevator doublet input is presented in Figure 85. No difference between angle of sideslip vane and computed sideslip is apparent from this record. The above record was taken at a zero sideslip angle. To determine if crosscoupling exists from angle of attack to sideslip at steady state sideslip angles, additional flight checks should be made.

The aircraft configuration for the records in Figures 80 to 85 was 165 knots indicated airspeed, 10,000 feet MSL, gear up, flaps at zero, and the angle of attack and sideslip vanes mounted on the nose faring. For the records of light to moderate turbulence, the airspeed was 150 knots indicated, 1800 feet MSL, gear up, and flaps at zero. The α and $\dot{\alpha}$ gust records are presented in Figure 86 and the β and $\dot{\beta}$ gust signals are presented in Figure 87. From these figures, it is evident that the inertially computed signals remain clean in the presence of light to moderate turbulence.

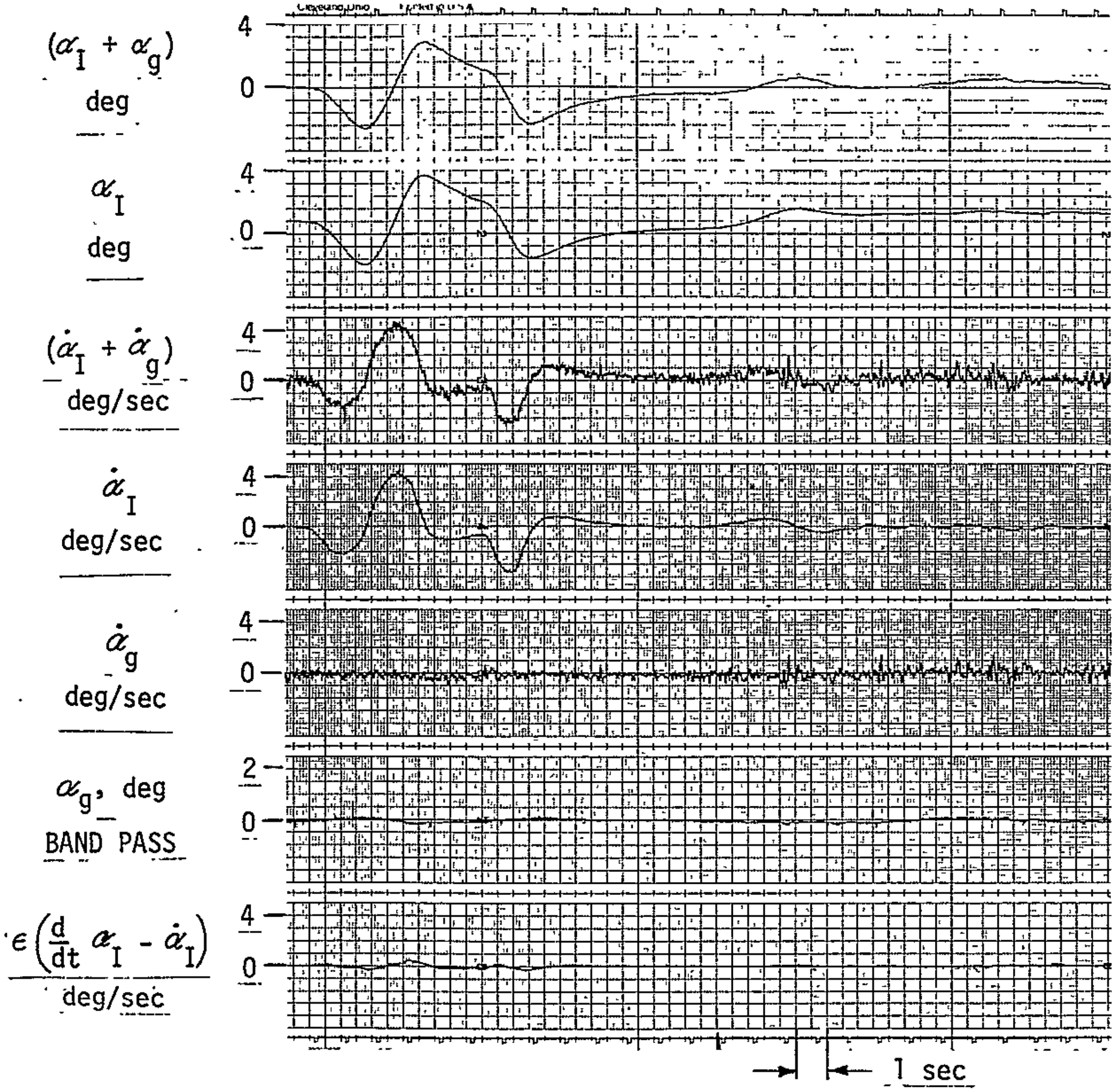

Figure 80 ANGLE OF ATTACK RESPONSE TO ELEVATOR DOUBLET AT 165 kt IAS

ORIGINAL PAGE IS
OF POOR QUALITY

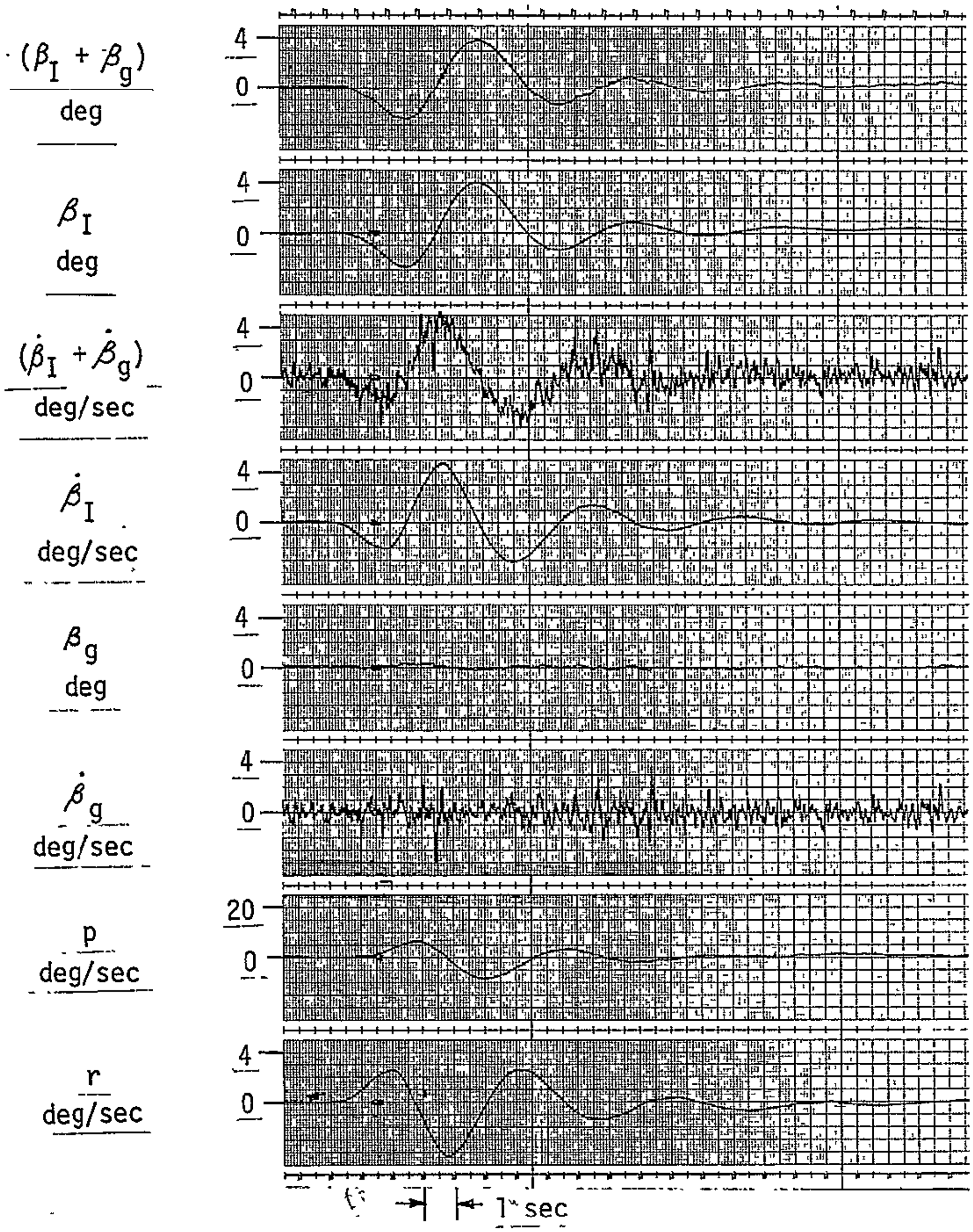

Figure 81 AIRCRAFT SIDESLIP RESPONSE TO A RUDDER DOUBLET AT 165 kt IAS

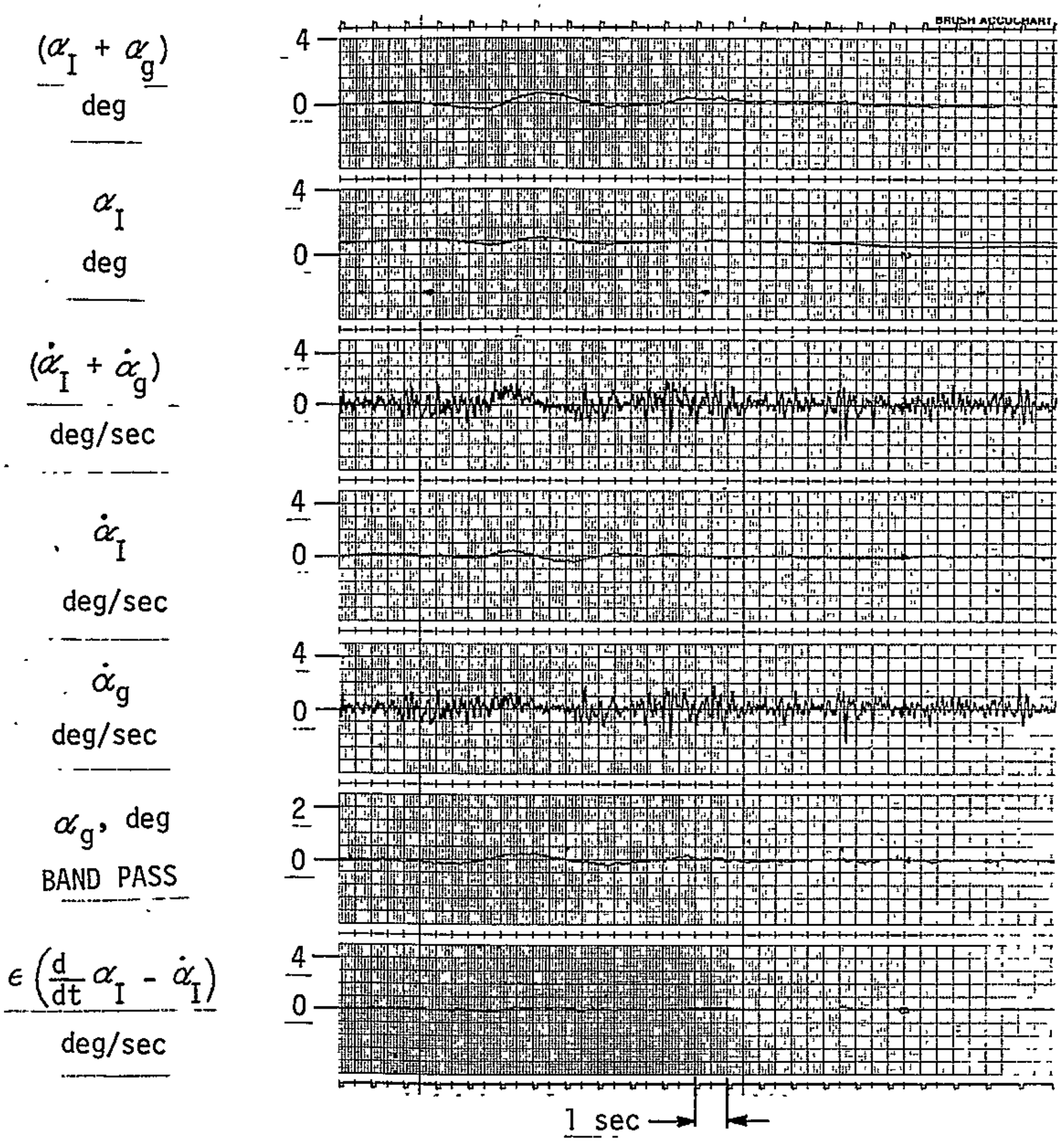

Figure 82 ANGLE OF ATTACK RESPONSE TO A RUDDER DOUBLET AT 165 kt IAS

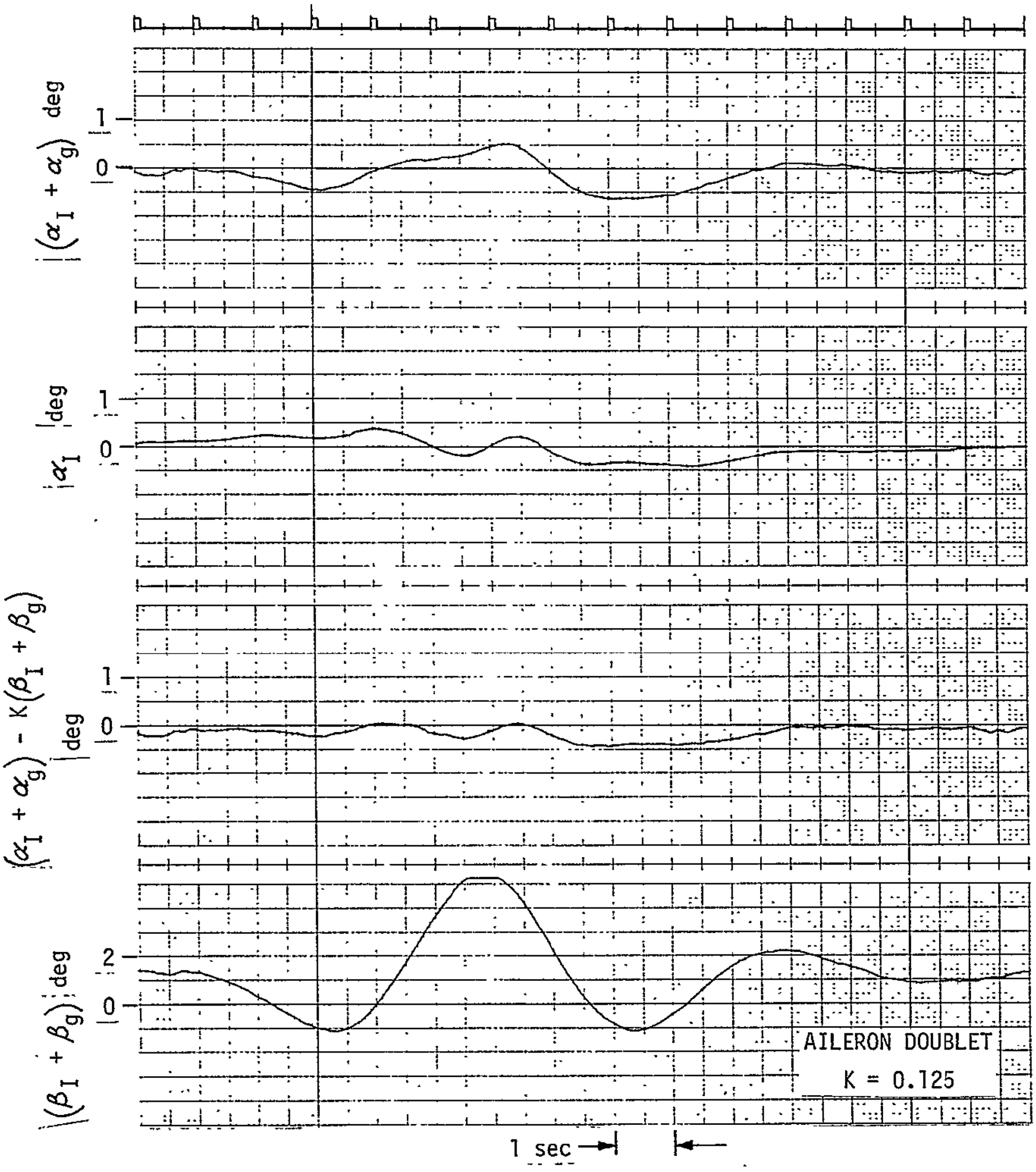

Figure 83 ANGLE OF ATTACK RESPONSE WITH SIDESLIP CORRECTION FOR AN AILERON INPUT

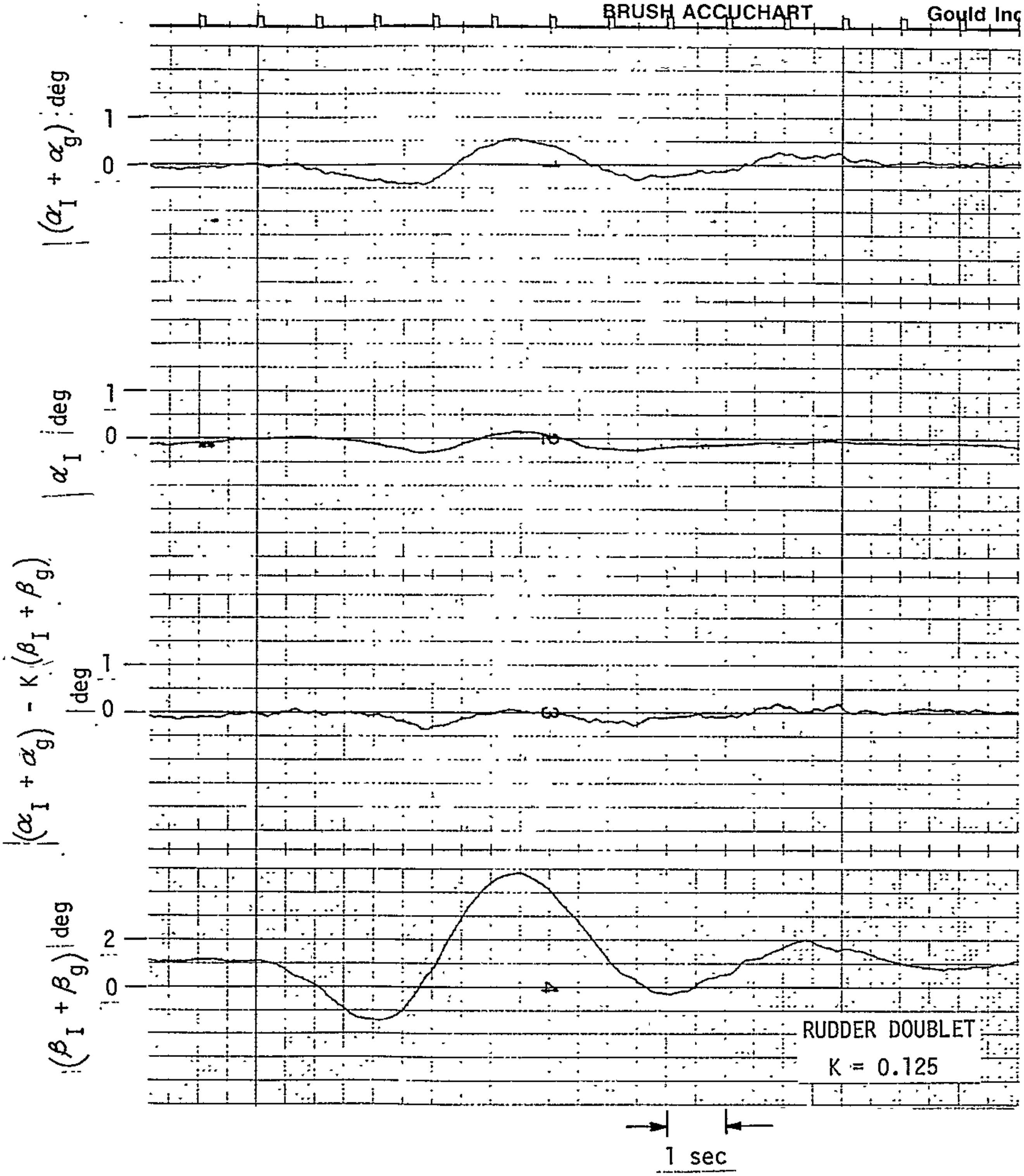

Figure 84 ANGLE OF ATTACK RESPONSE WITH SIDESLIP CORRECTION FOR A RUDDER INPUT

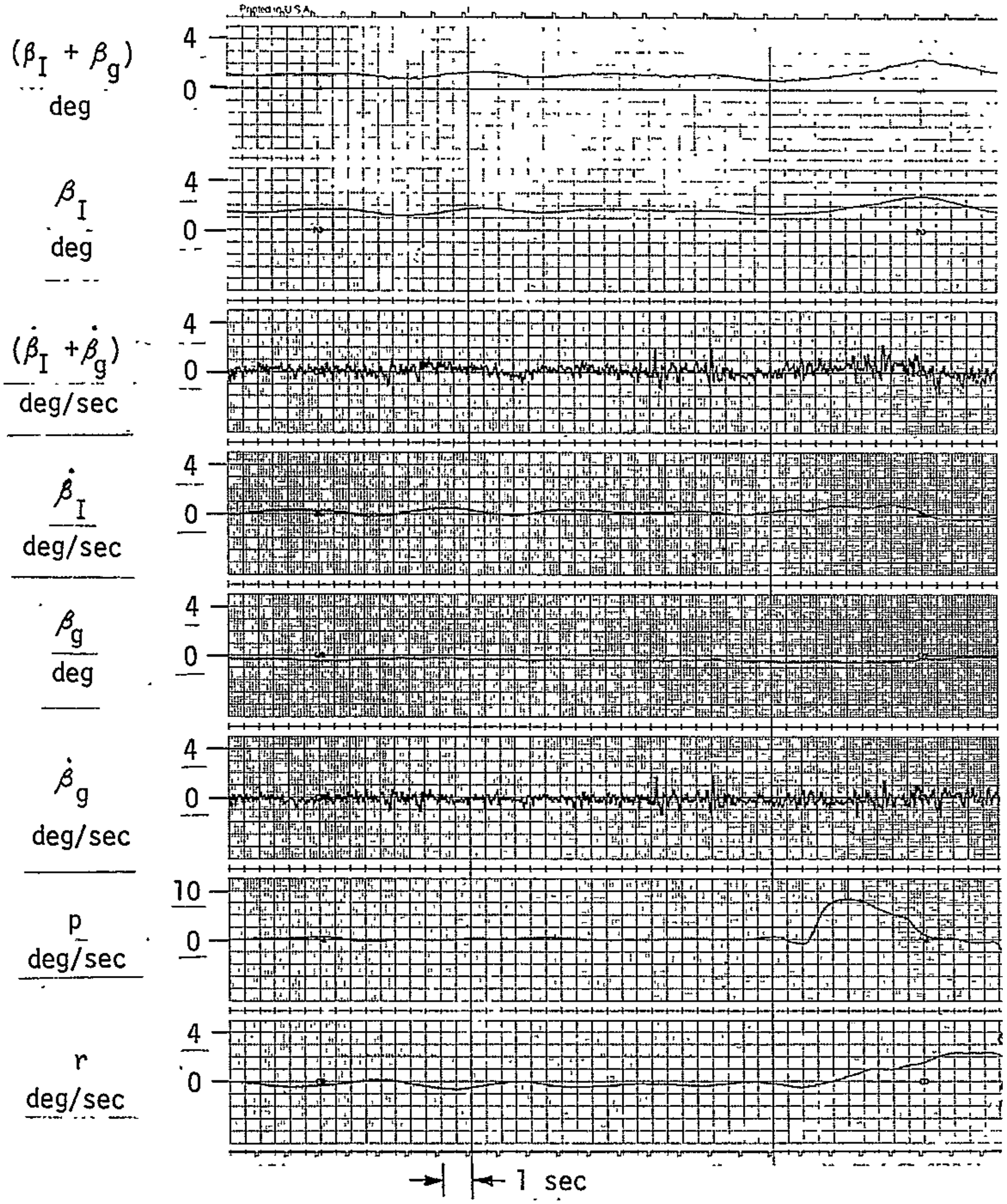

Figure 85 ANGLE OF SIDESLIP RESPONSE TO AN ELEVATOR INPUT AT 165 kt IAS

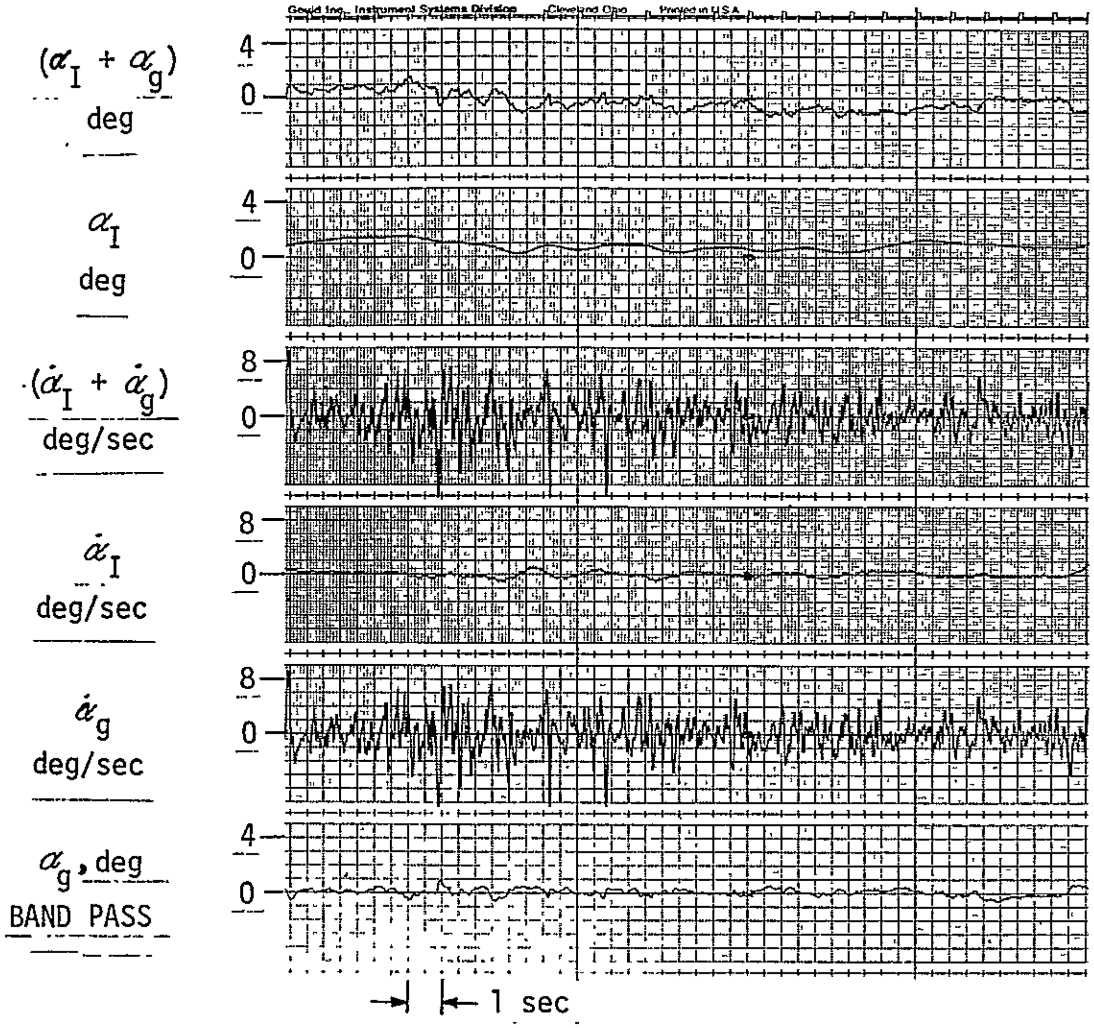

Figure 86 ANGLE OF ATTACK RESPONSE IN LIGHT TO MODERATE TURBULENCE AT 150 kt IAS

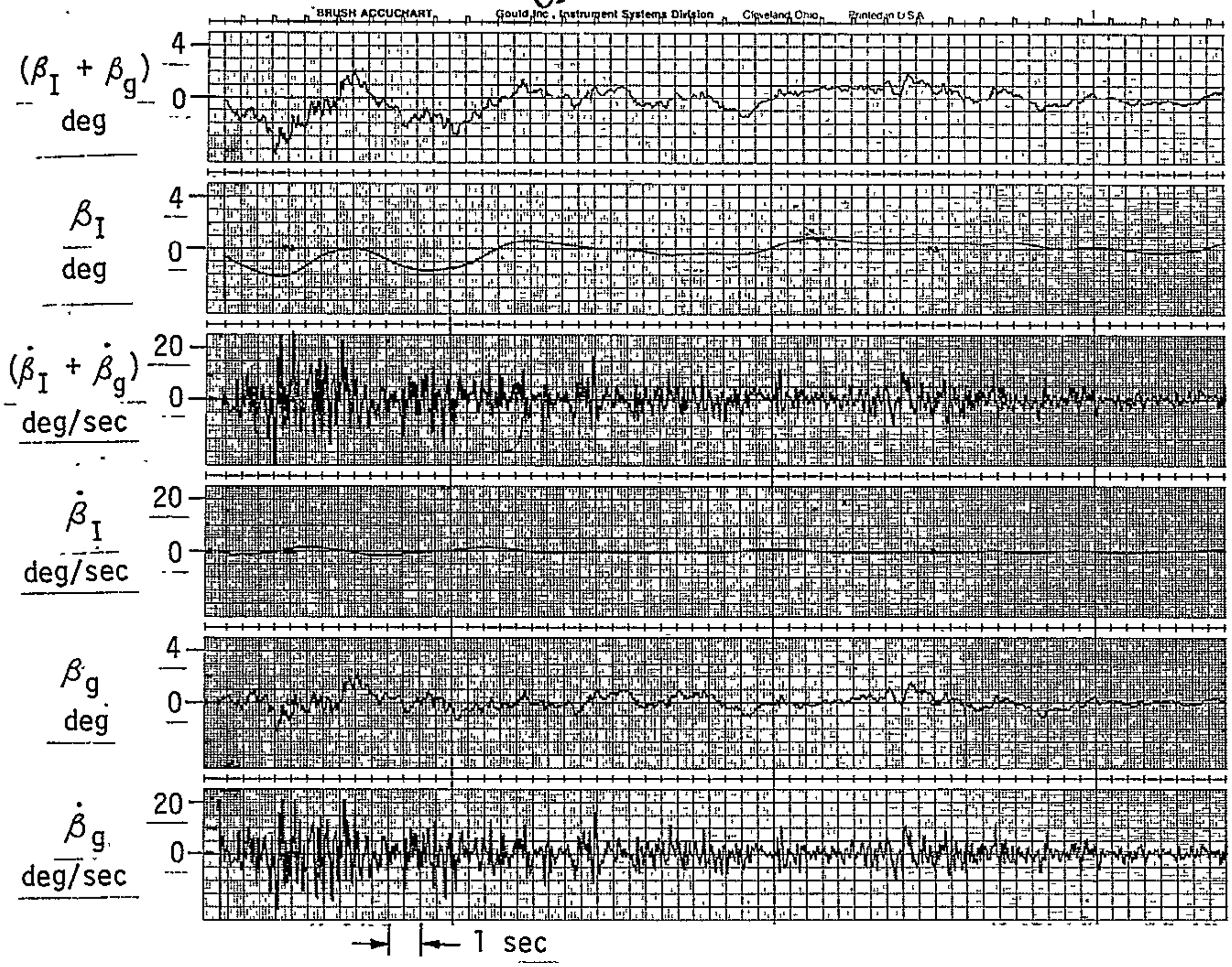

Figure 87 ANGLE OF SIDESLIP RESPONSE IN LIGHT TO MODERATE TURBULENCE AT 150 kt IAS

Complementary Filter Fidelity

To verify the overall fidelity of the TIFS complementary filters, flight records of the input and output signals of the V, $\dot{V}$, $\dot{h}$ and β_I complementary filters were evaluated. The derivative input terms $\dot{V}_I$, $\ddot{h}_I$ and $\dot{\beta}_I$ were integrated electronically during ground playback to allow direct comparison with the filter output signals. If close correlation is maintained between signals and their derivatives on both a short term and a long term basis, proper operation of the complementary filter is verified.

During the flight record ground playback, the inertially computed $\dot{V}_I$ input signal was integrated electronically for approximately 20 seconds. The $\dot{V}$ complementary filter output can be verified by direct comparison to the $\dot{V}_I$ input in Figure 88.

For the V complementary filter, a similar comparison of the $\dot{V}$ and V_p input signals can be made by integration of the $\dot{V}$ input signal. Proper V complementary filter operation is indicated by comparison of the V output signal with both the integrated $\dot{V}$ and the V_p input signals in Figure 88.

In the $\dot{h}$ complementary filter, accurate correlation of the inertial input signal with the filter output can be seen from Figure 89. The $\ddot{h}_I$ input signal was electronically integrated during playback of the flight record and can be directly compared with the $\dot{h}$ output signal. The $\sin\gamma$ computed signal waveform can be directly compared with the $\dot{h}$ signal in Figure 89. A magnitude comparison can also be made, with proper scaling, since the record was taken at a relatively constant indicated airspeed of 155 knots.

The input signals $\dot{\beta}_I$ and $(\beta_I + \beta_g)$ to the β_I complementary filter can be compared by integration of the $\dot{\beta}_I$ signal during ground playback. The integrated $\dot{\beta}_I$ signal and the $(\beta_I + \beta_g)$ signal have excellent correlation (Figure 90) with the β_I complementary filter output. Also shown in Figure 90 is the differentiated sideslip vane signal $(\dot{\beta}_I + \dot{\beta}_g)$ which can be directly compared with the inertially computed $\dot{\beta}_I$ signal.

C-3

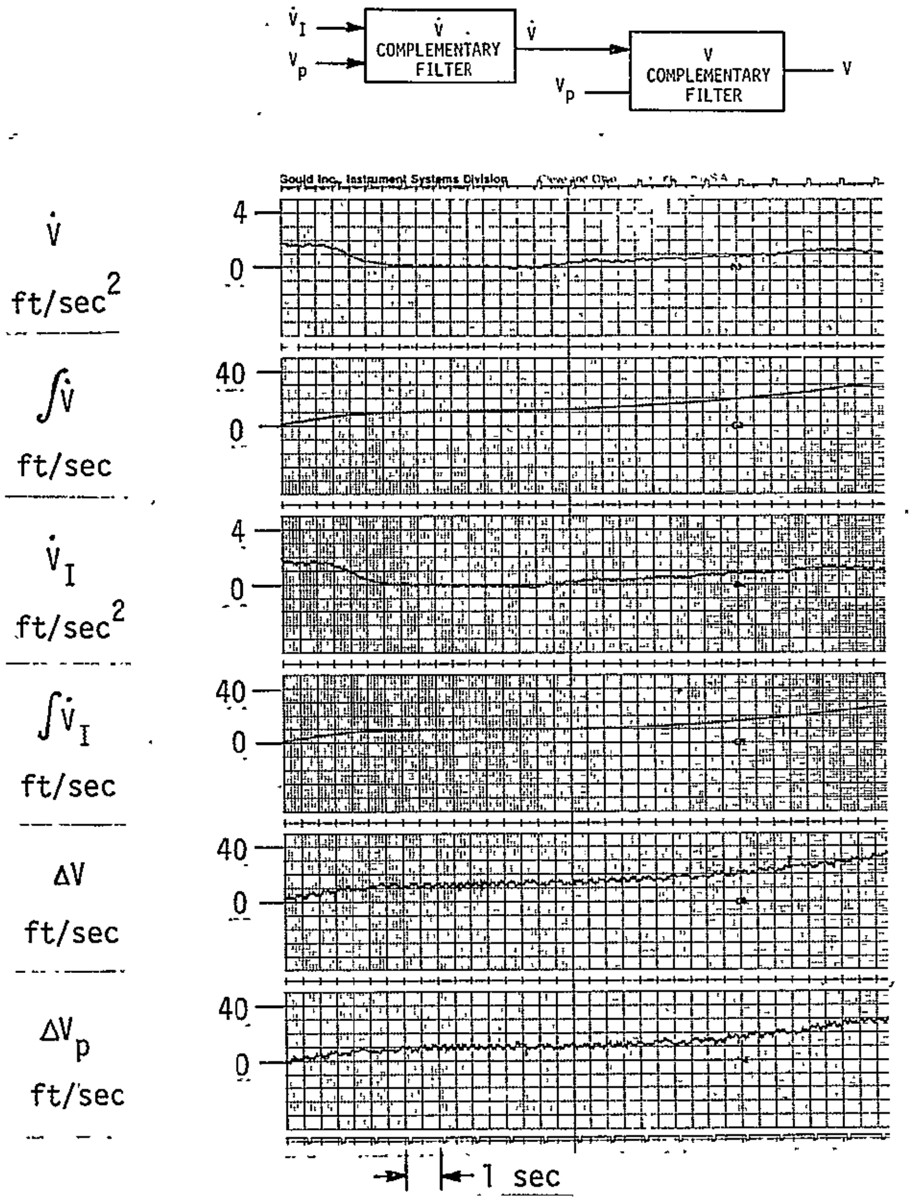

Figure 88 V AND $\dot{V}$ COMPLEMENTARY FILTER RESPONSE

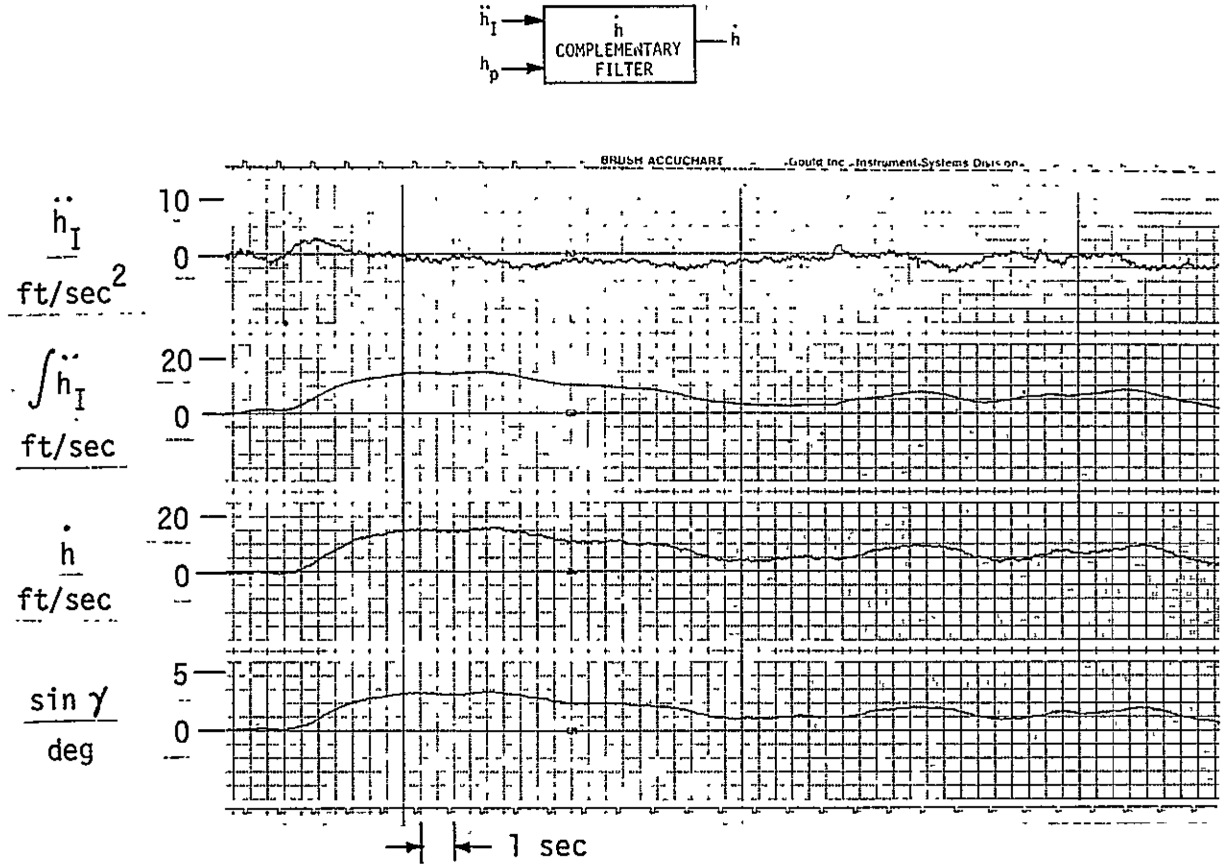

Figure 89 $\dot{h}$ COMPLEMENTARY FILTER RESPONSE

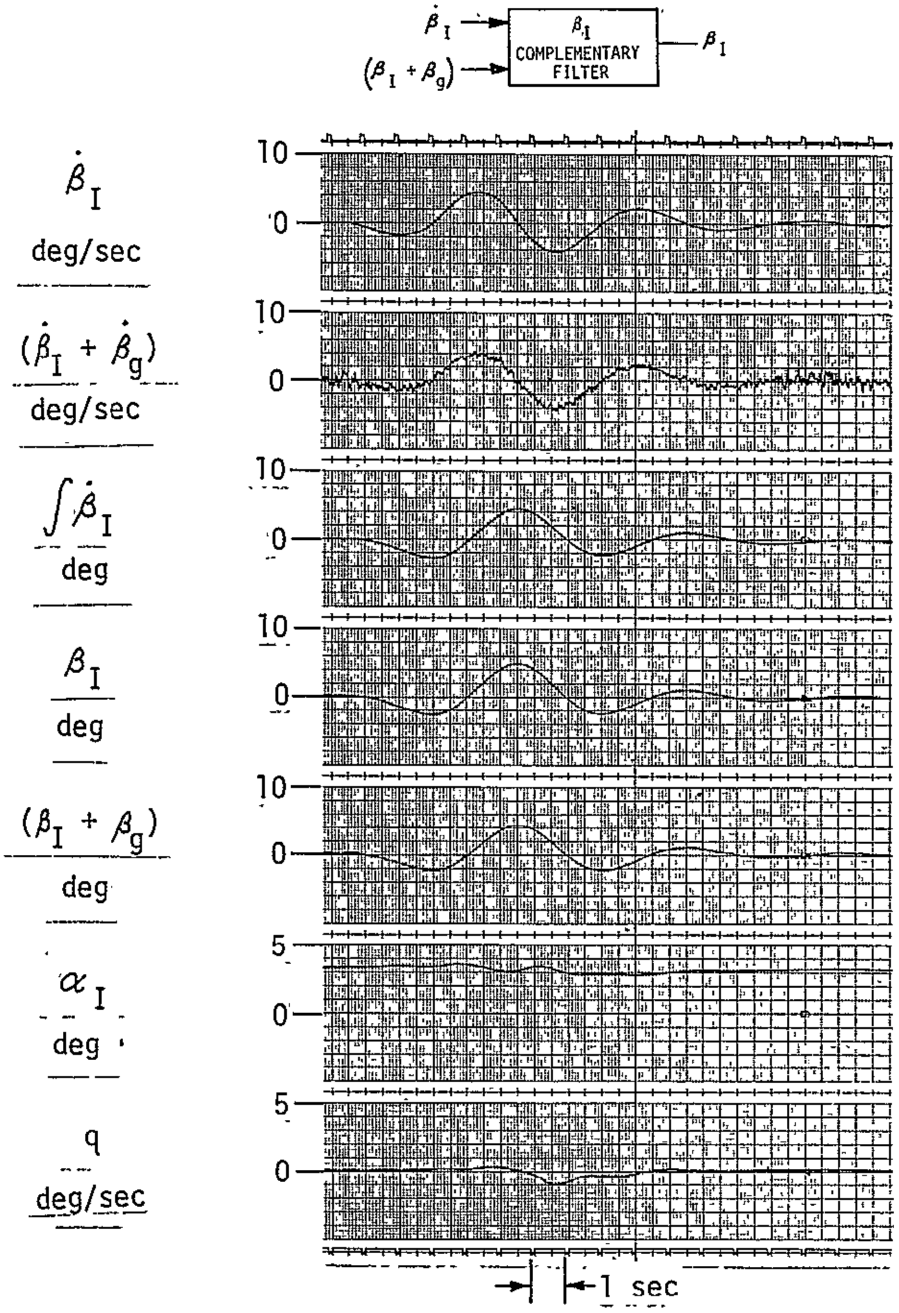

Figure 90 β_I COMPLEMENTARY FILTER RESPONSE

DIGITAL TAPE RECORDING SYSTEM

The primary flight data recording device on TIFS is a system built around an Ampex 9-track, 800-byte-per-inch digital recorder. Any preselected 58 analog data signals available in the TIFS electronics can be readily patched to the recording system. Each signal is sampled, converted to a digital word, bookkeeping digits added, formed into an IBM 370/195 compatible format, parity bits added for error detection and bit location specified. This is accomplished in an interface/control unit built by Interland Electronics to Calspan Corporation specifications. The input data channels can be sampled at selectable rates of 50 or 100 updates of each channel per second. The 10V maximum analog signals are converted to a 10 bit-plus-sign digital word which results in discrete bit steps of 10 MV. Each analog input channel is filtered with a second order low pass filter prior to sampling to avoid aliasing errors. The cutoff frequency is automatically selected to 7.5 Hz and damping of .8 for 50 sample-per-second rate and 18 Hz with damping of .8 for the 100 sample-per-second rate.

A complete ground playback system is available for quick-look purposes. Any 8 of the 58 channels can be selected and played back on an 8-channel strip chart recorder in analog form.

Accuracy:

Total system accuracy from input signal level to digital codes is ± 0.2% of full scale for steady state signals. This includes multiplexing, digitizing linearity, comparator and reference drift, and quantizing errors. No aperture or aliasing errors are included in this figure since these values depend upon signal rate of change and frequency content.

Recorder:

Input Level:	0 VDC ± 1V for "0", 4 VDC ± 1V for "1".
Input Impedance:	10K ohm minimum.
Input Format:	NRZ (nonreturn to zero) mark (NRZ-IBM).
Bit Packing:	800 bytes per inch.
Interchannel Timing:	6 microseconds max at 60 in/sec.
Dropout Rate:	Approximately one bit in 10^6 bits.
Temperature:	0^oC to 60^oC.
Vibration:	5 g random per procedure XIII of MIL-E-5272C.
Shock:	25 g for 11 milliseconds.
Altitude:	12,000 feet.
Tape Speed:	15 in/sec (100 samples/sec/channel) 7.5 in/sec (50 samples/sec/channel)

Performance Specification

The digital tape recording system operates to the following specifications over the entire system environment specified.

Input:

Signal Capacity:	58 channels of analog information and up to 6 true-false inputs (0 and +28 VDC).
Frame Size:	60 channels normal, or 30 channels when one multiplexer is not installed.
Frame Rate:	100 frames per second and 50 frames per second for 60 channels.
Clock Stability:	System timing shall derive from a crystal oscillator stable within ± .05%.
Impedance:	1 megohm minimum shunted by less than 100 picofarads.
Level:	0 to 5 volts bipolar.

Encoding:

Code:	Each sample is encoded into a 10 bit-plus-sign code of sign-plus-absolute-value configuration.
Linearity:	Conversion linearity will be within ± .05% ± 1/2 LSB (least significant bit).
Aperture:	Encoding time is approximately 12 microseconds permitting data frequencies up to 10 Hz without increase in error.

LIST OF REFERENCES

1. NASA Symposium on Advanced Control and Its Potential for Future Transport Aircraft, NASA TM X-3409, August 1976.

2. Hood, R. V.: "A Summary of the Application of Active Controls Technology in the ATT System Studies." NASA Symposium on Advanced Control Technology and Its Potential for Future Transport Aircraft. NASA TM X-3409, Aug. 1976

3. Rynaski, E. G. and Weingarten, N. C.: "Flight Control Principles for Control Configured Vehicles." Air Force Flight Dynamics Laboratory Report AFFDL-TR-71-154, January 1972.

4. Stockdale, C. R. and Poyncer, R. D.: "Control Configured Vehicle Ride Control System (CCVRCS)," Air Force Flight Dynamics Laboratory Report AFFDL-TR-73-83, July 1973.

5. Reynolds, P. A., Wasserman, R., Fabian, G. J., and Motyka, P. R.: "Capability of the Total In-Flight Simulator (TIFS). Air Force Flight Dynamics Laboratory AFFDC TR X-72-39, July 1972.

6. Chen, R. T. N. et al: "A Study for Active Control Research and Validation Using the Total In-Flight Simulator (TIFS) Aircraft," NASA CR-1322614, April 1975.

7. "A Method for Predicting the Stability Characteristics of Control Configured Vehicles." Air Force Flight Dynamics Laboratory Report AFFDL-TR-74-91, Nov. 1974. Vol. I, "FLEXSTAB 2.01.00 Theoretical Description," Dusto, A. R. et al. Vol. II, "FLEXSTAB 2.01.00 Users Manual," Hink, G. R., Bells, G. R., and Dornfield, G. M. Vol. III, "FLEXSTAB 2.01.00 Programmer's Manual," Hink, G. R., Bells, G. R., and Munjce, S. A. Fol. IV, "FLEXSTAB 2.01.00 B-52E LAMS Demonstration Curve and Results," Dornfield, G. M.

8. Johnson, N. S., and Krueger, N. A.: "Wing Stress Analysis -- Model 340." Report ZS-340-006, Part I, Consolidated Vultee Aircraft Corp., 31 October 1951. NASA CR-158891.

9. Pancu, C. D., and Hiroshige, K.: "Model 340 Main Fixed and Movable Control Surface Flutter Analysis," Report ZU-340-003, Consolidated Vultee Aircraft Corp., 28 August 1951. NASA CR-158893.

10. Krueger, J. A., and Johnson, N. S.: "Wing Stress Analysis -- Model 340," Report ZS-340-006, Part II, Consolidated Vultee Aircraft Corp., 18 February 1952. NASA CR-158892.

11. Rodriguez, M. B.: "Commercial Total In-Flight Simulator Empennage Flutter Analysis," General Dynamics Convair Division Report GDE-DDE-69-001, 13 March 1969. NASA CR-158892.

12. Balcerak, J. C. and White, Jr., R. P.: "Ground Vibration Tests, AF/TIFS Convair 580 Airplane," TIFS Memo No. 569 (RASA Report 71-06), May 1971. NASA CR-158895.

13. Riedler, A. D., et al: "Aerodynamic Data Flight Criteria and Unit Load Distribution for Structural Design of the Model 340 Airplane Turboprop Configuration," Consolidated Vultee Aircraft Corp. Report ZU-340-001, August 1951. NASA CR-158890.

14. Flight Research Staff: "Development, Design and Fabrication of the Total In-Flight Simulator (TIFS). Air Force Flight Dynamics Laboratory Report AFFDL-TR-71-77, August 1971.

APPENDIX A

INPUTS TO ISIC PROGRAM OF FLEXSTAB

INTRODUCTION

This appendix contains a reproduction of the inputs to the Internal Structural Influence Coefficient Program which generated the parameters used in obtaining the normal mode results presented in this report. The structural model made provision for representing vertical and lateral translation of the engine on its mounts and rocking, bending, and torsional degrees of freedom of the side force surfaces. These motions were essentially eliminated in the case considered in this appendix by assuming very high stiffnesses for the beams used to represent these motions.

Figure A-1 is a reproduction of the FLEXSTAB elastic axis plot and shows the locations of the concentrated masses used to model the inertia properties of TIFS .

The FLEXSTAB thin body representation was used for the wing, horizontal tail, vertical tail, and side force surfaces while the FLEXSTAB slender body representation was used for the fuselage and nacelle. It had originally been intended to use an additional slender body at Y = 9.182 m because the side force surface (SFS) elastic axis intersects the wing forward of the wing elastic axis. A strategem introduced to avoid this involved assuming that the SFS elastic axis intersected the wing elastic axis and then was swept abruptly forward to its true position. The swept portion of the SFS elastic axis was made very stiff so that it would have no effect on the computed vibration modes.

FLEXSTAB does not allow concentrated masses to be located at junction points. Consequently, the masses which were to have been located in a slender body at Y = 9.187 m were divided and placed slightly inboard and outboard of this station.

A few details should be mentioned which cannot be seen on Figure A-1. FLEXSTAB requires the wing elastic axis to be perpendicular to the X axis at the junctions with the fuselage, nacelle and SFS elastic axis. This was accomplished with short jogs in the wing elastic axis.

A discussion of the cards used in the ISIC input is given in Reference 7.

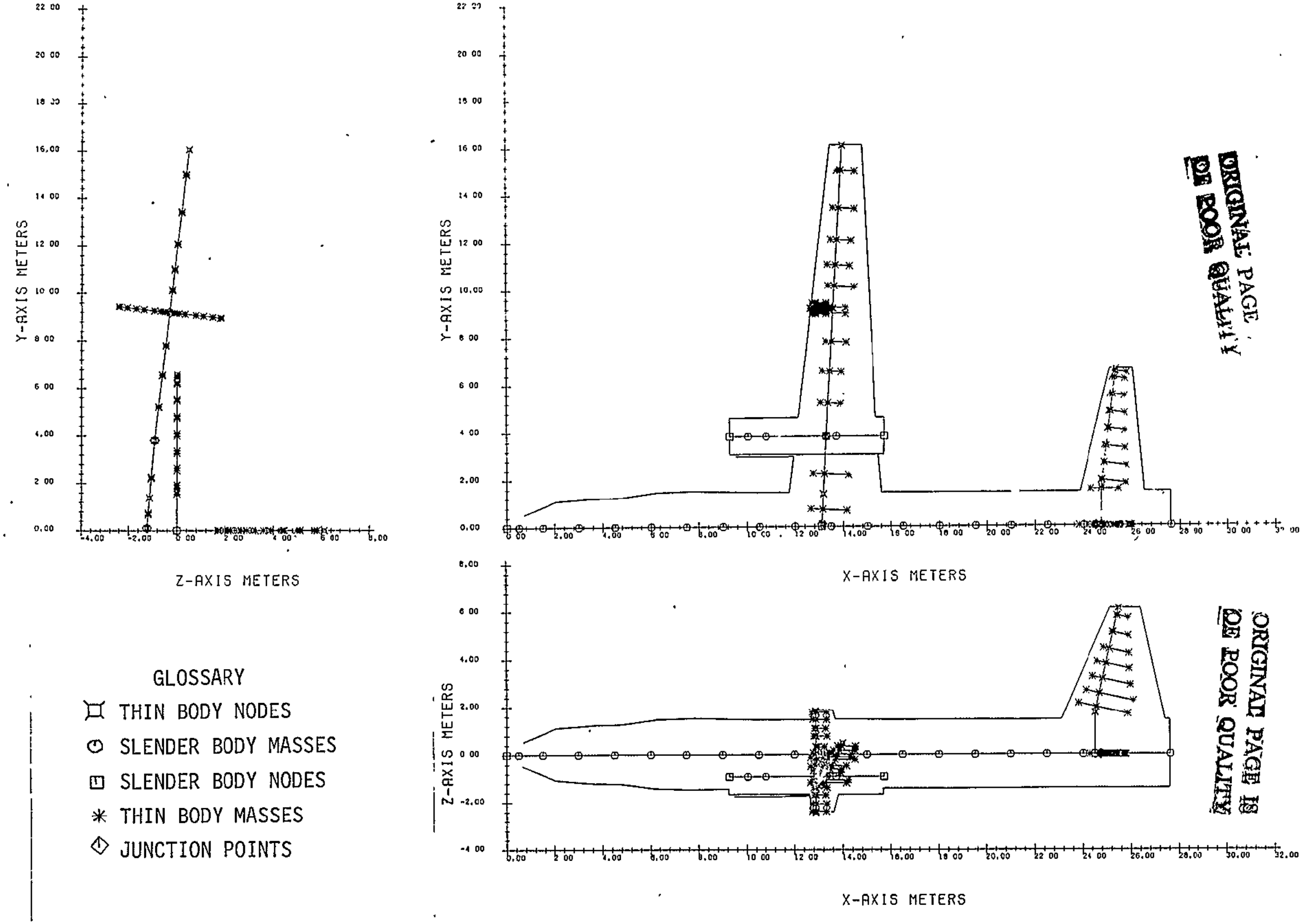

Figure A-1 FLEXSTAB ELASTIC AXIS PLOT

```
TIFS CASE 1, CRUISE , REVISED, NACE + SFS STIFF

                            ****************************
                            *                          *
                            * LIST OF INPUT DATA CARDS *
                            *                          *
                            ****************************

         NO.    CARD IMAGES

          1     $CASE FOR INTERNAL STRUCTURAL INFLUENCE COEFFICIENT PROGRAM             1
          2     TIFS CASE 1, CRUISE , REVISED, NACE + SFS STIFF
          3     D.ANDRISANI, H.DAUGHADAY                                                3
          4     $GEOMETRY TAPE DATA                                                     4
          5     1.                                                                      5
          6     $OPTION FOR ELASTIC FORMULATION                                         6
          7     RESIDUAL ELASTIC                                                        7
          8     $STRUCTURAL DATA                                                        8
          9     $SENSOR MATRICES                                                        9
         10     $JUNCTION POINT DATA                                                    10
         11     6.0                                                                     11
         12      0.0      1.0                                                           12-1
         13     13.1171   1.0                                                           12-2
         14     24.508    1.0                                                           12-3
         15     24.740    1.0                                                           12-4
         16     13.2948   0.0                                                           12-5
         17     13.5999   0.0                                                           12-7
         18     4.0                                                                     13
         19     3.0                                                                     14-1
         20     1.0       2.0       3.0                                                 15-1
         21     4.0                                                                     14-2
         22     1.0       2.0       3.0       4.0                                       15-2
         23     3.0                                                                     14-3
         24     1.0       2.0       5.0                                                 15-3
         25     4.0                                                                     14-4
         26     1.0       2.0       5.0       6.0                                       15-4
         27     $SLENDER BODY ONE FUSELAGE                                              16A
         28     $PART 1                                                                 17A1
         29     10.0      1.0       2.0                                                 18A1
         30     $COORDINATES OF SEGMENTS                                                19A1
         31     0.50      1.5       3.0       4.5       6.0       7.5                   20A1-1
         32     9.0       10.5      12.0                                                20A1-2
         33     $STIFFNESS DATA                                                         21A1
         34     0.0       2.95  E 082.92  E 082.80  E 08                                22A1-1
         35     0.0       2.95  E 082.92  E 082.80  E 08                                22A1-2
         36     0.0       3.25  E 083.98  E 083.63  E 08                                22A1-3
         37     0.0       3.62  E 084.88  E 083.64  E 08                                22A1-4
         38     0.0       4.31  E 085.27  E 083.64  E 08                                22A1-5
         39     0.0       6.27  E 085.67  E 083.66  E 08                                22A1-6
         40     0.0       7.35  E 086.03  E 083.72  E 08                                22A1-7
```

```
TIFS CASE 1, CRUISE , REVISED, NACE + SFS STIFF

         NO.      CARD IMAGES

         41      0.0          5.97   E 085.54  E 084.05  E 08                                            22A1-8
         42      0.0          6.51   E 084.82  E 085.45  E 08                                            22A1-9
         43      0.0          7.35   E 084.76  E 087.16  E 08                                            22A1-10
         44      $LUMPED MASSES                                                                          23A1
         45      9.0                                                                                     24A1
         46      98.0         137.0        387.6       423.2       662.7       413.8                     25A1-1
         47      300.3        253.3        322.6                                                         25A1-2
         48      $PART 2                                                                                 17A2
         49      9.0          2.0          3.0                                                           18A2
         50      $COORDINATES OF SEGMENTS                                                                19A2
         51      13.5         15.0         16.5        18.0        19.5        21.0                      20A2-1
         52      22.5         24.0                                                                       20A2-2
         53      $STIFFNESS DATA                                                                         21A2
         54      0.0          7.35   E 084.76  E 087.16  E 08                                            22A2-1
         55      0.0          7.44   E 085.48  E 087.28  E 08                                            22A2-2
         56      0.0          6.63   E 085.45  E 085.54  E 08                                            22A2-3
         57      0.0          5.64   E 085.24  E 084.53  E 08                                            22A2-4
         58      0.0          5.12   E 085.00  E 084.21  E 08                                            22A2-5
         59      0.0          4.82   E 084.76  E 082.45  E 08                                            22A2-6
         60      0.0          4.55   E 084.52  E 081.24  E 08                                            22A2-7
         61      0.0          4.37   E 084.37  E 088.39  E 07                                            22A2-8
         62      0.0          4.25   E 084.25  E 085.26  E 07                                            22A2-9
         63      $LUMPED MASSES                                                                          23A2
         64      8.0                                                                                     24A2
         65      290.0        458.6        271.6       395.7       414.2       367.4                     25A2-1
         66      333.3        257.7                                                                      25A2-2
         67      $PART 3                                                                                 17A3
         68      1.0          3.0          4.0                                                           18A3
         69      $STIFFNESS DATA                                                                         21A3
         70      0.0          4.25   E 084.25  E 085.26  E 07                                            22A3
         71      $PART 4                                                                                 17A4
         72      2.0          4.0          0.0                                                           18A4
         73      $COORDINATES OF SEGMENTS                                                                19A4
         74      25.5         27.623                                                                     20A4
         75      $STIFFNESS DATA                                                                         21A4
         76      0.0          4.25   E 084.25  E 085.26  E 07                                            22A4-1
         77      0.0          4.19   E 084.19  E 083.92  E 07                                            22A4-2
         78      $LUMPED MASSES                                                                          23A4
         79      2.0                                                                                     24A4
         80      225.5        33.3                                                                       25A4
```

ORIGINAL PAGE IS
OF POOR QUALITY

IGINAL PAGE IS
OF POOR QUALITY

```
TIPS CASE 1. CRUISE . REVISED. NACE + SFS STIFF

      NO.    CARD IMAGES

      81     $SLENDER BODY TWO NACELLE                                                  16B
      82     $PART 1                                                                    17B1
      83     3.0          5.0         0.0                                               18B1
      84     $COORDINATES OF SEGMENTS                                                   19B1
      85     9.279        10.041      10.798                                            20B1
      86     $STIFFNESS DATA                                                            21B1
      87     0.0                    1.E10       1.E10       1.E10
      88     0.0                    1.E10       1.E10       1.E10
      89     0.0                    1.E10       1.E10       1.E10
      90     $LUMPED MASSES                                                             23B1
      91     3.0                                                                        24B1
      92     0.0          1416.1      814.0                                             25B1
      93     $PART 2                                                                    17B2
      94     2.0          5.0         0.0                                               18B2
      95     $COORDINATES OF SEGMENTS                                                   19B2
      96     13.721       15.729                                                        20B2
      97     $STIFFNESS DATA                                                            21B2
      98     0.0                    1.E10       1.E10       1.E10
      99     0.0                    1.E10       1.E10       1.E10
     100     $LUMPED MASSES                                                             23B2
     101     2.0                                                                        24B2
     102     814.0        0.0                                                           25B2
     103     $THIN BODY ONE     VER TAIL                                                28G
     104     3.0          0.0                                                           29G
     105     $PART 1                                                                    30G
     106     9.0                                                                        31G
     107     $COORDINATES OF SEGMENTS                                                   32G
     108     0.0          1.732       0.053       1.971       0.182       2.548         33G1
     109     0.319        3.164       0.462       3.804       0.597       4.410         33G2
     110     0.752        5.104       0.908       5.806       0.977       6.115         33G3
     111     $STIFFNESS DATA                                                            34G
     112     0.0          7.08   E 084.70   E 08                                        35G1
     113     0.0          7.08   E 064.70   E 06                                        35G2
     114     0.0          5.60   E 063.95   E 06                                        35G3
     115     0.0          3.47   E 062.98   E 06                                        35G4
     116     0.0          1.78   E 062.07   E 06                                        35G5
     117     0.0          1.03   E 061.30   E 06                                        35G6
     118     0.0          6.0    E 057.2    E 05                                        35G7
     119     0.0          3.0    E 053.60   E 05                                        35G8
     120     0.0          1.8    E 052.2    E 05                                        35G9
```

```
TIFS CASE 1, CRUISE , REVISED, NACE + SFS STIFF

         NO.     CARD IMAGES

         121     $LUMPED MASSES                                                                   36G
         122     9.0                                                                              37G
         123     0.0                                                                              38G1
         124     2.0                                                                              38G2
         125     13.61       1.327       13.61       -0.771                                       39G2
         126     2.0                                                                              38G3
         127     11.07       1.429       11.07       -0.571                                       39G3
         128     2.0                                                                              38G4
         129     9.12        1.172       9.12        -0.428                                       39G4
         130     2.0                                                                              38G5
         131     7.42        0.973       7.42        -0.374                                       39G5
         132     2.0                                                                              38G6
         133     6.24        0.824       6.24        -0.237                                       39G6
         134     2.0                                                                              38G7
         135     7.23        0.629       7.23        -0.036                                       39G7
         136     2.0                                                                              38G8
         137     5.24        0.465       5.24        0.025                                        39G8
         138     0.0                                                                              38G9
         139     $THIN BODY TWO    IN-WING                                                        28A
         140     2.0         5.0                                                                  29A
         141     $PART 1                                                                          30A
         142     7.0                                                                              31A
         143     $COORDINATES OF SEGMENTS                                                         32A
         144     0.0         0.100       0.0261      0.6163      0.0576      1.2416               33A1
         145     0.0628      1.3432      0.1030      2.1403      0.1777      3.6190               33A2
         146     $STIFFNESS DATA                                                                  34A
         147     0.0         1.0    E 101.000 E 10                                                35A1
         148     0.0         1.0    E 101.000 E 10                                                35A2
         149     0.0         1.0    E 101.000 E 10                                                35A3
         150     0.0         1.408 E 071.936 E 08                                                 35A4
         151     0.0         1.611 E 086.945 E 07                                                 35A5
         152     0.0         1.271 E 085.745 E 07                                                 35A6
         153     0.0         1.271 E 085.745 E 07                                                 35A7
         154     $LUMPED MASSES                                                                   36A
         155     3.0                                                                              37A
         156     0.0                                                                              38A1
         157     2.0                                                                              38A2
         158     113.8       0.998       113.8       -0.488                                       39A2
         159     2.0                                                                              38A3
         160     [illegible]                                                                      38A4
```

```
TIFS CASE 1, CRUISE , REVISED, NACE + SFS STIFF

      NO.    CARD IMAGES

      161    2.0                                                                      38A5
      162    128.4      1.000       128.4       -0.467                                39A5
      163    0.0                                                                      38A6
      164    $THIN BODY THREE MID-WING                                                28B
      165    5.0        6.0                                                           29B
      166    $PART 1                                                                  30B
      167    7.0                                                                      31B
      168    $COORDINATES OF SEGMENTS                                                 32B
      169    0.0        0.10        0.0295      0.484       0.0819      1.4025        33B1
      170    0.1599     2.7685      0.2310      4.0131      0.3051      5.3116        33B2
      171    $STIFFNESS DATA                                                          34B
      172    0.0        9.0170E 073.8680E 07                                          35B1
      173    0.0        9.0170E 073.8680E 07                                          35B2
      174    0.0        9.0170E 073.8680E 07                                          35B3
      175    0.0        6.2820E 072.7400E 07                                          35B4
      176    0.0        4.2870E 071.9670E 07                                          35B5
      177    0.0        2.7190E 071.3800E 07                                          35B6
      178    0.0        2.719 E 071.380 E 07                                          35B7
      179    $LUMPED MASSES                                                           36B
      180    6.0                                                                      37B
      181    0.0                                                                      38B1
      182    0.0                                                                      38B2
      183    2.0                                                                      38B3
      184    421.6      0.523       421.6       -0.309                                39B3
      185    2.0                                                                      38B4
      186    305.3      0.478       305.3       -0.311                                39B4
      187    2.0                                                                      38B5
      188    187.3      0.619       187.3       -0.214                                39B5
      189    2.0                                                                      38B6
      190    73.8       0.548       73.8        -0.640                                39B6
      191    $THIN BODY  FOUR TIP-WING                                                28C
      192    6.0        0.0                                                           29C
      193    $PART 1                                                                  30C
      194    8.0                                                                      31C
      195    $COORDINATES OF SEGMENTS                                                 32C
      196    0.0        0.10        0.040       0.6         0.0603      0.9566        33C1
      197    0.1107     1.8392      0.1717      2.9078      0.2487      4.2563        33C2
      198    0.3404     5.8618      0.4003      6.910                                 33C3
      199    $STIFFNESS DATA                                                          34C
      200    0.0        1.833 E 079.714 E 06                                          35C1
```

```
TIFS CASE 1, CRUISE , REVISED, NACE + SFS STIFF

        NO.    CARD IMAGES

        201    0.0        1.833 E 079.714 E 06                                                 35C2
        202    0.0        1.833 E 079.714 E 06                                                 35C3
        203    0.0        1.389 E 077.18  E 06                                                 35C4
        204    0.0        1.005 E 075.415 E 06                                                 35C5
        205    0.0        7.390 E 063.757 E 06                                                 35C6
        206    0.0        5.17  E 062.21  E 06                                                 35C7
        207    0.0        4.1   E 061.35  E 06                                                 35C8
        208    $LUMPED MASSES                                                                  36C
        209    8.0                                                                             37C
        210    2.0                                                                             38C1
        211    73.8       0.548      73.8       -0.640                                         39C1
        212    0.0                                                                             38C2
        213    2.0                                                                             38C3
        214    29.3       0.838      29.3       -0.259                                         39C3
        215    2.0                                                                             38C4
        216    22.5       0.589      22.5       -0.338                                         39C4
        217    2.0                                                                             38C5
        218    29.7       0.596      29.7       -0.257                                         39C5
        219    2.0                                                                             38C6
        220    21.3       0.653      21.3       -0.234                                         39C6
        221    2.0                                                                             38C7
        222    20.6       0.578      20.6       -0.157                                         39C7
        223    0.0                                                                             38C8
        224    $THIN BODY FIVE  TOP-SFS                                                        28D
        225    6.0        0.0                                                                  29D
        226    $PART 1                                                                         30D
        227    10.0                                                                            31D
        228    $COORDINATES OF SEGMENTS                                                        32D
        229    0.0        0.050      -0.719     0.147      -0.719     0.197                    33D1
        230    -0.719     0.381      -0.719     0.635      -.719      1.080                    33D2
        231    -0.719     1.397      -0.719     1.778      -0.719     2.096                    33D3
        232    -0.719     2.159                                                                33D4
        233    $STIFFNESS DATA                                                                 34D
        234    0.0              1.E8       1.E8
        235    0.0              1.E8       1.E8
        236    0.0              1.E8       1.E8
        237    0.0              1.E8       1.E8
        238    0.0              1.E8       1.E8
        239    0.0              1.E8       1.E8
        240    0.0              1.E8       1.E8
```

```
TIFS CASE 1, CRUISE , REVISED, NACE + SFS STIFF

    NO.    CARD IMAGES

    241    0.0                1.E8       1.E8
    242    0.0                1.E8       1.E8
    243    0.0                1.E8       1.E8
    244    $LUMPED MASSES                                                             360
    245    10.0                                                                       370
    246    0.0                                                                        3801
    247    0.0                                                                        3802
    248    2.0                                                                        3801
    249    5.989     0.332     5.989     -0.209                                       3901
    250    2.0                                                                        3802
    251    3.568     0.554     3.568     -0.106                                       3902
    252    2.0                                                                        3803
    253    7.838     0.353     7.838      0.075                                       3903
    254    2.0                                                                        3804
    255    2.443     0.458     2.443     -0.074                                       3904
    256    2.0                                                                        3805
    257    2.674     0.402     2.674     -0.049                                       3905
    258    2.0                                                                        3806
    259    1.420     0.442     1.420     -0.122                                       3906
    260    2.0                                                                        3807
    261    0.254     0.431     0.254     -0.146                                       3907
    262    0.0                                                                        3808
    263    $THIN BODY SIX  BOT-SFS                                                    28E
    264    6.0       0.0                                                              29E
    265    $PART 1                                                                    30E
    266    10.0                                                                       31E
    267    $COORDINATES OF SEGMENTS                                                   32E
    268    0.0       0.050     -0.719    0.147     -0.719    0.197                    33E1
    269    -0.719    0.381     -0.719    0.635     -.719     1.080                    33E2
    270    -0.719    1.397     -0.719    1.778     -0.719    2.096                    33E3
    271    -0.719    2.159                                                            33E4
    272    $STIFFNESS DATA                                                            34E
    273    0.0                1.E8       1.E8
    274    0.0                1.E8       1.E8
    275    0.0                1.E8       1.E8
    276    0.0                1.E8       1.E8
    277    0.0                1.E8       1.E8
    278    0.0                1.E8       1.E8
    279    0.0                1.E8       1.E8
    280    0.0                1.E8       1.E8
```

```
TIFS CASE 1, CRUISE , REVISED, NACE + SFS STIFF

        NO.    CARD IMAGES

        281    0.0                1.E8       1.E8
        282    0.0                1.E8       1.E8
        283    $LUMPED MASSES                                                     36E
        284    10.0                                                               37E
        285    0.0                                                                38E1
        286    0.0                                                                38E2
        287    2.0                                                                38E1
        288    5.989      0.332      5.989      -0.209                            39E1
        289    2.0                                                                38E2
        290    3.568      0.554      3.568      -0.106                            39E2
        291    2.0                                                                38E3
        292    7.838      0.353      7.838       0.075                            39E3
        293    2.0                                                                38E4
        294    2.443      0.458      2.443      -0.074                            39E4
        295    2.0                                                                38E5
        296    2.674      0.402      2.674      -0.049                            39E5
        297    2.0                                                                38E6
        298    1.420      0.442      1.420      -0.122                            39E6
        299    2.0                                                                38E7
        300    0.254      0.431      0.254      -0.146                            39E7
        301    0.0                                                                38E8
        302    $THIN BODY SEVEN HOR TAIL                                          28F
        303    4.0        0.0                                                     29F
        304    $PART 1                                                            30F
        305    11.0                                                               31F
        306    $COORDINATES OF SEGMENTS                                           32F
        307    0.0        1.551      0.0        1.641      0.035      1.924       33F1
        308    0.124      2.643      0.213      3.361      0.302      4.078       33F2
        309    0.391      4.797      0.480      5.513      0.569      6.232       33F3
        310    0.603      6.503      0.613      6.589                             33F4
        311    $STIFFNESS DATA                                                    35F
        312    0.0        3.65    E082.10    E08                                  35F1
        313    0.0        3.65   E 062.10   E 06                                  35F2
        314    0.0        3.28   E 061.85   E 06                                  35F3
        315    0.0        2.41   E 061.43   E 06                                  35F4
        316    0.0        1.42   E 061.01   E 06                                  35F5
        317    0.0        7.23   E 056.80   E 05                                  35F6
        318    0.0        3.62   E 054.0    E 05                                  [illegible]
        319    0.0        1.52   E 052.0    E 05
        320    0.0        6.3    E 041.1    E 05
```

APPENDIX B

FLEXIBLE AIRCRAFT EQUATIONS OF MOTION

The flexible equations of motion of the TIFS aircraft have been computed at two flight conditons, climb and cruise, for symmetric motion only. Time prohibited computation at the third flight condition.

The form of the equations of motion are as follows:

$$Ax + B\dot{x} + C\ddot{x} = 0$$

where

$$x' = [u, w, q, \theta, \eta_1, \eta_2, \eta_3, \eta_4, \eta_5, \eta_6, \eta_7]$$

A, B, C are square matrices of dimension 11 x 11

u = component of inertial velocity in X direction, m/sec

w = component of inertial velocity in Z direction, m/sec

q = pitch rate, rad/sec

θ = pitch attitude, rad

η_i are structural mode deflections of the aircraft

The seven structural modes are those modes discussed in Section 2.3 of this report in order of increasing vibration frequency. Sensor equations have not yet been formulated. The equations of motion were computed using the Residual Elastic formulation in which the differential equations are corrected for the static effects of higher order structural modes above the seventh mode. The corrected equations are included in Case 2, Climb and Case 3, Cruise.

The set of stability and control derivatives of the rigid body degrees of freedom corresponding to the above equations of motion are labeled as Revised Modes, Cases 1, 2 and 3. The column labeled "elastic increment" represents the static elastic correction for the structural modes not modeled dynamically in the equations of motion.

TIFS CASE 2, CLIMB

```
                    ***** PPINT CUT OF THE SYSTEM MATRIX *****
                       NOTF - CENOMINATORS HAVE PEEN CLEARFD
                         NUMBEP OF POWS IN SYSTEM=  11
                      NUMBEF OF COLUMNS (TOTAL) =  11
                     THERE APE  11 VARIAPLES IN THE SYSTEM
                       OF WHICH  11 AFE OUTPUT VAPIABLES
                     AND    0 ARE INPUT VARIABLES
          THE ORDERING OF THE VARIABLES WITHIN THE SYSTEM IS AS FOLLOWS
                       * * * * *  OUTPUT VARIAPLES  * * * * *
 POSITION  NAME      TYPE              POSITION  NAME      TYPE              POSITION  NAME      TYPE
     1     U      AIRPLANE MOTION          2     W      AIRPLANE MOTION          3     Q      AIRPLANE MOTION
     4     THETA  AIRPLANE MOTION          5     UE1    AIRPLANE MOTION          6     UE2    AIRPLANE MOTION
     7     UE3    AIRPLANE MOTION          8     UE4    AIRPLANE MOTION          9     UE5    AIRPLANE MOTION
    10     UE6    AIRPLANE MOTION         11     UE7    AIRPLANE MOTION
```

TIFS CASE 2, CLIMB

A =

```
MATRIX TITLE -- COEFFICIENT MATRIX FOR S ** 00TERM
STORAGE ------- IN CORE
MATRIX SIZE --- 11 X 11
PART ---------- 1 OF 2

          1           2           3           4           5           6           7           8           9          10          11
 1   .1283E+03  -.1524E+04   .1632E+06   .2414E+06  -.7604E+02  -.3960E+03  -.7354E+03   .4347E+03  -.3226E+03   .1195E+04  -.4674E+04
 2   .5906E+04   .2257E+05  -.1949E+07   .1960E+05   .3839E+03   .5492E+04   .4887E+04  -.7142E+04   .2308E+04  -.1681E+05   .4415E+05
 3   .5283E+03   .2146E+05   .6574E+06  0.          -.4685E+04   .1624E+05  -.3985E+05  -.2984E+05  -.7841E+04  -.7562E+05   .2264E+05
 4  0.          0.          -.1000E+01  0.          0.          0.          0.          0.          0.          0.          0.
 5   .9607E+02   .3033E+03   .9329E+01  0.           .7456E+03   .7990E+02   .2023E+03  -.6429E+02   .1104E+03  -.2373E+03   .1178E+04
 6   .2659E+02   .1267E+03   .9156E+03  0.           .1307E+01   .1753E+04  -.1779E+02  -.7747E+02   .3552E+02  -.2113E+03   .4383E+03
 7  -.7970E+01  -.1206E+03  -.1533E+04  0.           .8993E+01  -.5418E+02   .3038E+04   .1372E+03  -.1108E+02   .2289E+03  -.2159E+03
 8  -.3899E+01  -.8347E+02  -.1928E+04  0.           .2045E+02  -.3867E+02   .1996E+03   .3930E+04   .3618E+02   .1385E+03   .2119E+03
 9   .1981E+02   .7118E+02   .2238E+03  0.           .6745E+01   .2638E+02   .1864E+02  -.2524E+02   .6457E+04  -.9204E+02   .3917E+03
10   .1620E+01   .2338E+02  -.2163E+03  0.           .2724E+01   .4502E+01   .1425E+02  -.1934E+02   .1225E+02   .1798E+05   .1131E+03
11  -.2807E+02  -.1716E+03  -.1743E+03  0.          -.9004E+01  -.4732E+02  -.8647E+02   .4691E+02  -.4059E+02   .1371E+03   .2202E+05
```

TIFS CASE 2, CLIMB

B =

```
MATRIX TITLE -- COEFFICIENT MATRIX FOR S ** 01TERM
STORAGE ------- IN CORE
MATRIX SIZE --- 11 X 11
PART ---------- 1 OF 2

          1           2           3           4           5           6           7           8           9          10          11
 1   .2470E+05  -.4672E+01  -.2331E+02  0.          -.3694E+02  -.1794E+02   .1481E+01   .1037E+00  -.6137E+01   .4543E+01  -.2897E+02
 2  0.           .2450E+05  -.1779E+04  0.           .2963E+03   .1248E+03  -.2385E+03  -.2934E+02  -.3464E+02   .4113E+03  -.1230E+04
 3  0.           .2817E+04   .7523E+06  0.          -.1941E+03   .1425E+04  -.1377E+04  -.1741E+04  -.4026E+03   .7068E+03  -.2079E+04
 4  0.          0.          0.           .1000E+01  0.          0.          0.          0.          0.          0.          0.
 5  0.          -.1231E+02  -.2303E+02  0.           .1281E+02   .2677E+01  -.2797E+01   .5399E+01   .4663E+01   .3715E+01  -.9631E+01
 6  0.           .2021E+01  -.7105E+01  0.           .3622E+01   .6986E+01  -.3795E+01  -.2299E+01   .2968E+01   .7605E+00  -.3486E+01
 7  0.          -.3683E+01   .8292E+01  0.          -.1212E+01  -.4918E+01   .1054E+02   .9014E+01  -.2242E+01  -.1832E+01   .6400E+01
 8  0.          -.6681E+01   .9330E+01  0.           .3624E+01  -.3936E+01   .5715E+01   .2051E+02   .6948E+00  -.1658E+01   .7902E+00
 9  0.          -.1109E+01  -.4637E+01  0.           .4957E+01   .2988E+01  -.2881E+01   .1106E+01   .1312E+02   .5633E+00  -.8767E+00
10  0.          -.1693E+01  -.2554E+01  0.           .8014E+00   .2742E+00  -.9316E+00  -.8421E+00  -.2488E+00   .1111E+02  -.1704E+01
11  0.           .7261E+01   .1531E+02  0.          -.4363E+01   .1315E+00   .4086E+01  -.2769E+01   .7613E+00  -.6287E+01   .3219E+02
```

TIFS CASE 2, CLIMB

C =

```
MATRIX TITLE -- COEFFICIENT MATRIX FOR S ** 02TERM
STORAGE ------- IN CORE
MATRIX SIZE --- 11 X 11
PART ---------- 1 OF 2

          1           2           3           4           5           6           7           8           9          10          11
 1  0.          0.          0.          0.          -.1075E+00  -.8190E-01   .1197E-01   .4375E-01  -.3863E-02   .3603E-01  -.1576E+00
 2  0.          0.          0.          0.          -.1343E+02  -.8637E+01   .4139E+01   .3155E+01  -.2656E+00   .4656E+01  -.1521E+02
 3  0.          0.          0.          0.          -.2695E+02  -.3259E+02   .5319E+02  -.2942E+01   .5368E+01   .1686E+02  -.1158E+02
 4  0.          0.          0.          0.          0.          0.          0.          0.          0.          0.          0.
 5  0.          0.          0.          0.           .1871E+01  -.7444E-01  -.6052E-01   .5325E-01  -.3081E-01   .3822E-01  -.2233E+00
 6  0.          0.          0.          0.          -.6357E-01   .1950E+01   .6413E-01  -.1275E-02  -.1327E-01   .2800E-01  -.5156E-01
 7  0.          0.          0.          0.           .5862E-01   .6872E-01   .1893E+01   .3937E-01   .4605E-01  -.2125E-01  -.9702E-02
 8  0.          0.          0.          0.           .1022E-01   .5807E-01  -.1336E+00   .2083E+01   .8183E-01  -.1164E-01  -.1067E+00
 9  0.          0.          0.          0.          -.2033E-01  -.1315E-01   .1131E-02   .1147E-02   .2014E+01   .5483E-02  -.2433E-01
10  0.          0.          0.          0.          -.4029E-02  -.2599E-02  -.5905E-02  -.5185E-02  -.2368E-01   .2018E+01   .2761E-02
11  0.          0.          0.          0.           .1459E+00   .8017E-01   .9343E-02  -.2473E-01   .2242E-01  -.2374E-01   .2157E+01
```

TIFS CASE 3, CRUISE

```
                         ***** PRINT OUT OF THE SYSTEM MATRIX *****
                         NOTE - DENOMINATORS HAVE BEEN CLEARED
                              NUMBER OF ROWS IN SYSTEM=  11
                            NUMBER OF COLUMNS (TOTAL) =  11
                          THERE ARE  11 VARIABLES IN THE SYSTEM
                          OF WHICH   11 ARE OUTPUT VARIABLES
                                AND      0 ARE INPUT VARIABLES
                THE ORDERING OF THE VARIABLES WITHIN THE SYSTEM IS AS FOLLOWS
                          * * * * *  OUTPUT VARIABLES  * * * * *
POSITION   NAME          TYPE          POSITION   NAME          TYPE          POSITION   NAME          TYPE
    1    U       AIRPLANE MOTION           2     W        AIRPLANE MOTION          3     Q        AIRPLANE MOTION
    4    THETA   AIRPLANE MOTION           5     UE1      AIRPLANE MOTION          6     UE2      AIRPLANE MOTION
    7    UE3     AIRPLANE MOTION           8     UE4      AIRPLANE MOTION          9     UE5      AIRPLANE MOTION
   10    UE6     AIRPLANE MOTION          11     UE7      AIRPLANE MOTION
```

TIFS CASE 3, CRUISE

A =

```
 MATRIX TITLE -- COEFFICIENT MATRIX FOR S ** 00TERM
 STORAGE ------- IN CORE
 MATRIX SIZE ---  11 X  11
 PART ----------   1 OF  2

            1           2           3          4          5          6          7          8          9         10         11
  1    .1074E+03  -.2362E+03  -.3212E+05  .2422E+06  -.4900E+02 -.1248E+03 -.4456E+03  .7505E+02 -.1744E+03  .3807E+03  -.2038E+04
  2    .3086E+04   .3570E+05  -.3549E+07 -.2193E+04   .1090E+04  .1708E+05  .1372E+05 -.2276E+05  .7193E+04 -.5295E+05   .1358E+06
  3   -.1132E+04   .1063E+05   .1165E+07  0.         -.1534E+05  .5283E+05 -.1356E+06 -.1024E+06 -.2517E+05 -.2464E+06   .6833E+05
  4   0.          0.          -.1000E+01  0.         0.         0.         0.         0.         0.         0.          0.
  5    .5539E+02   .5148E+03  -.5556E+02  0.          .7981E+03  .2439E+03  .6343E+03 -.1894E+03  .3447E+03 -.7216E+03   .3638E+04
  6    .9620E+01  -.2229E+03   .1683E+04  0.          .2086E+01  .1859E+04 -.7395E+02 -.2562E+03  .1086E+03 -.6789E+03   .1359E+04
  7    .1435E+02  -.2227E+03  -.2886E+04  0.          .3184E+02 -.1823E+03  .3314E+04  .4583E+03 -.3022E+02  .7730E+03  -.6945E+03
  8    .5538E+01  -.1542E+03  -.3642E+04  0.          .6948E+02 -.1346E+03  .6777E+03  .4315E+04  .1219E+03  .5076E+03   .6722E+03
  9    .7590E+01   .1298E+03   .4004E+03  0.          .2117E+02  .8585E+02  .6222E+02 -.8459E+02  .6588E+04 -.3025E+03   .1230E+04
 10   -.8422E+01   .3590E+02  -.3384E+03  0.          .7517E+01  .1273E+02  .3769E+02 -.5631E+02  .3459E+02  .1794E+05   .3081E+03
 11    .9546E+01  -.2925E+03  -.2794E+03  0.         -.2820E+02 -.1459E+03 -.2671E+03  .1450E+03 -.1282E+03  .4257E+03   .2173E+05
```

TIFS CASE 3, CRUISE

B =

```
 MATRIX TITLE -- COEFFICIENT MATRIX FOR S ** 01TERM
 STORAGE ------- IN CORE
 MATRIX SIZE ---  11 X  11
 PART ----------   1 OF  2

            1           2           3          4          5          6          7          8          9         10         11
  1    .2470E+05  -.5438E+01  -.2629E+02  0.         -.1055E+02 -.3984E+01 -.1758E+01 -.3756E+01 -.1351E+01  .5160E+01  -.1249E+02
  2   0.           .2442E+05  -.2132E+04  0.          .5016E+03  .1805E+03 -.4659E+03 -.1843E+02 -.5677E+02  .8776E+03  -.2520E+04
  3   0.           .2906E+04   .7500E+06  0.         -.3455E+03  .2539E+04 -.2129E+04 -.3303E+04 -.5429E+03  .1771E+04  -.3319E+04
  4   0.          0.          0.          .1000E+01 0.         0.         0.         0.         0.         0.          0.
  5   0.          -.1348E+02  -.2503E+02  0.          .2040E+02  .3661E+01 -.6318E+01  .1048E+02  .7559E+01  .8288E+01  -.2562E+02
  6   0.           .1845E+01  -.9876E+01  0.          .6478E+01  .9859E+01 -.6558E+01 -.4141E+01  .5078E+01  .2888E+01  -.8330E+01
  7   0.          -.3954E+01   .1315E+02  0.         -.2092E+01 -.8732E+01  .1511E+02  .1597E+02 -.4008E+01 -.5345E+01   .1260E+02
  8   0.          -.7520E+01   .1505E+02  0.          .6297E+01 -.7367E+01  .9024E+01  .3336E+02  .8136E+00 -.4839E+01   .4411E+00
  9   0.          -.1496E+01  -.6054E+01  0.          .8500E+01  .4911E+01 -.5177E+01  .2091E+01  .1792E+02  .1869E+01  -.4320E+01
 10   0.          -.1755E+01  -.3230E+01  0.          .1216E+01  .3010E+00 -.1651E+01 -.1228E+01 -.4379E+00  .1253E+02  -.4103E+01
 11   0.           .8063E+01   .1727E+02  0.         -.7440E+01  .6877E+00  .7936E+01 -.5386E+01  .1392E+01 -.1219E+02  -.5293E+02
```

TIFS CASE 3, CRUISE

C =

```
 MATRIX TITLE -- COEFFICIENT MATRIX FOR S ** 02TERM
 STORAGE ------- IN CORE
 MATRIX SIZE ---  11 X  11
 PART ----------   1 OF  2

            1           2           3          4          5          6          7          8          9         10         11
  1   0.          0.          0.          0.         -.1151E+00 -.8754E-01  .1060E-01  .4920E-01 -.5031E-02  .3788E-01  -.1702E+00
  2   0.          0.          0.          0.         -.1412E+02 -.9655E+01  .4752E+01  .3868E+01 -.7307E+00  .5048E+01  -.1620E+02
  3   0.          0.          0.          0.         -.2372E+02 -.3572E+02  .6233E+02  .1163E+01  .2901E+01  .1932E+02  -.7309E+01
  4   0.          0.          0.          0.         0.         0.         0.         0.         0.         0.          0.
  5   0.          0.          0.          0.          .1841E+01 -.8637E-01 -.6815E-01  .5337E-01 -.3657E-01  .4159E-01  -.2551E+00
  6   0.          0.          0.          0.         -.6862E-01  .1930E+01  .7971E-01  .5787E-02 -.1941E-01  .3479E-01  -.5533E-01
  7   0.          0.          0.          0.          .6150E-01  .8578E-01  .1861E+01  .2268E-01  .5026E-01 -.3136E-01  -.9007E-02
  8   0.          0.          0.          0.          .4483E-02  .7516E-01 -.1759E+00  .2059E+01  .7986E-01 -.2210E-01  -.1123E+00
  9   0.          0.          0.          0.         -.3115E-01 -.2111E-01  .5237E-02  .3080E-02  .2007E+01  .8249E-02  -.3437E-01
 10   0.          0.          0.          0.         -.7863E-02 -.5845E-02 -.3753E-02 -.3112E-02 -.2206E-01  .2017E+01   .6442E-03
 11   0.          0.          0.          0.          .1611E+00  .8841E-01  .1077E-01 -.2733E-01  .2601E-01 -.3157E-01   .2183E+01
```

TIFS CASE 1, ~~LANDING CONFIGURATION, REVISED MODES~~

```
                              *******************************
                              *                             *
                              * STATIC STABILITY DERIVATIVES *
                              *                             *
                              *******************************

                                  RIGID        ELASTIC         TOTAL        UNITS
                                              INCREMENT

          CL(0)                  .326523      -.007895        .318629
          CD(0)                  .005236      -.000113        .005124
          CM(0)                  .069187      -.008027        .061160

          CL(U)                 1.990973      -.008623       1.982350     (1/RAD)
          CD(U)                  .283675      -.001305        .282370     (1/RAD)
          CM(U)                 -.058454      -.040236       -.098690     (1/RAD)

          CL(ALPHA)              .100586       .000229        .100815     (1/DEG)
          CD(ALPHA)              .020882       .000227        .021109     (1/DEG)
          CM(ALPHA)             -.031751      -.000485       -.032236     (1/DEG)

          CL(Q)                15.387735      -.185018      15.202717     (1/RAD)
          CD(Q)                 1.351531      -.022846       1.328685     (1/RAD)
          CM(Q)               -39.524090       .718435     -38.805656     (1/RAD)

          CL(DE)                 .014856      -.000805        .014051     (1/DEG)
          CD(DE)                 .001550      -.000098        .001452     (1/DEG)
          CM(DE)                -.057258       .003716       -.053541     (1/DEG)

          CL(THRUST)             .000001      -.000000        .000001     (1/NEWTON)
          CD(THRUST)            -.000004      -.000000       -.000004     (1/NEWTON)
          CM(THRUST)             .000001       .000000        .000001     (1/NEWTON)
```

TIFS CASE I, LANDING CONFIGURATION, REVISED MODES

```
                                 **********************************
                                 *                                *
                                 * DYNAMIC STABILITY DERIVATIVES *
                                 *                                *
                                 **********************************

                      RIGID            RIGID           ELASTIC            TOTAL       UNITS
                     COMPUTED          OUTPUT          INCREMENT

CL(U)                1.990973         1.990973          .009897          2.000870    (1/RAD)
CD(U)                 .283675          .283675          .001240           .284916    (1/RAD)
CM(U)                -.058454         -.058454         -.021495          -.079949    (1/RAD)

CL(ALPHA)             .100586          .100586          .000884           .101470    (1/DEG)
CD(ALPHA)             .020082          .020082          .000112           .020194    (1/DEG)
CM(ALPHA)            -.031751         -.031751         -.001832          -.033582    (1/DEG)

CL(Q)               15.387735        15.387735          .322058         15.709793    (1/RAD)
CD(Q)                1.351531         1.351531          .039898          1.391429    (1/RAD)
CM(Q)              -39.524090       -39.524090        -1.250171        -40.774261    (1/RAD)

CY(BETA)              .000000          .000000          .000000           .000000    (1/DEG)
C1(BETA)              .000000          .000000          .000000           .000000    (1/DEG)
CN(BETA)              .000000          .000000          .000000           .000000    (1/DEG)

CY(P)                 .000000          .000000          .000000           .000000    (1/RAD)
C1(P)                 .000000          .000000          .000000           .000000    (1/RAD)
CN(P)                 .000000          .000000          .000000           .000000    (1/RAD)

CY(R)                 .000000          .000000          .000000           .000000    (1/RAD)
C1(R)                 .000000          .000000          .000000           .000000    (1/RAD)
CN(R)                 .000000          .000000          .000000           .000000    (1/RAD)

CL(A-DOT)           -2.734893        -2.734893          .012566         -2.722327    (1/RAD)
CD(A-DOT)            -.404529         -.404529          .001206          -.403322    (1/RAD)
CM(A-DOT)          -14.040751       -14.040751         -.261637        -14.302387    (1/RAD)

CL(Q-DOT)          -17.115211       -17.115211         -.387189        -17.502400    (1/RAD)
CD(Q-DOT)           -2.342168        -2.342168         -.048562         -2.390730    (1/RAD)
CM(Q-DOT)          -21.069772       -21.069772         1.203445        -19.866327    (1/RAD)

CY(B-DOT)             .000000          .000000          .000000           .000000    (1/RAD)
C1(B-DOT)             .000000          .000000          .000000           .000000    (1/RAD)
CN(B-DOT)             .000000          .000000          .000000           .000000    (1/RAD)

CY(P-DOT)             .000000          .000000          .000000           .000000    (1/RAD)
C1(P-DOT)             .000000          .000000          .000000           .000000    (1/RAD)
CN(P-DOT)             .000000          .000000          .000000           .000000    (1/RAD)

CY(R-DOT)             .000000          .000000          .000000           .000000    (1/RAD)
C1(R-DOT)             .000000          .000000          .000000           .000000    (1/RAD)
CN(R-DOT)             .000000          .000000          .000000           .000000    (1/RAD)
```

TIFS CASE 1, LANDING CONFIGURATION, REVISED MODES

```
                                     ******************************
                                     *                            *
                                     * ACTIVE CONTROL DERIVATIVES *
                                     *                            *
                                     ******************************

                                  * SYMMETRICALLY DEFLECTED CONTROLS *

 NAME                    RIGID            RIGID            ELASTIC              TOTAL        UNITS
                        COMPUTED          OUTPUT          INCREMENT

                                        CONTROL  1 - AILS
 CL(DS)                  .012626          .012626          -.000069            .012557      (1/DEG)
 CD(DS)                  .000759          .000759          -.000009            .000750      (1/DEG)
 CM(DS)                 -.005329         -.005329          -.000036           -.005365      (1/DEG)
 CL(DS-DOT)            -1.669583        -1.669583          -.022295          -1.691878      (1/RAD)
 CD(DS-DOT)             -.221478         -.221478          -.002820           -.224298      (1/RAD)
 CM(DS-DOT)             1.304015         1.304015           .045911           1.349927      (1/RAD)

                                        CONTROL  2 - DLE
 CL(DS)                  .023603          .023603          -.000197            .023407      (1/DEG)
 CD(DS)                  .001782          .001782          -.000026            .001757      (1/DEG)
 CM(DS)                 -.003323         -.003323           .000376           -.002947      (1/DEG)
 CL(DS-DOT)            -2.771666        -2.771666           .029255          -2.742410      (1/RAD)
 CD(DS-DOT)             -.380244         -.380244           .003571           -.376673      (1/RAD)
 CM(DS-DOT)             -.919782         -.919782          -.156628          -1.076410      (1/RAD)

                                        CONTROL  3 - ELVT
 CL(DS)                  .014856          .014856          -.000144            .014712      (1/DEG)
 CD(DS)                  .001550          .001550          -.000018            .001532      (1/DEG)
 CM(DS)                 -.057258         -.057258           .000580           -.056678      (1/DEG)
 CL(DS-DOT)            -1.137629        -1.137629          -.034431          -1.172060      (1/RAD)
 CD(DS-DOT)             -.150547         -.150547          -.004290           -.154837      (1/RAD)
 CM(DS-DOT)             2.078389         2.078389           .124176           2.202565      (1/RAD)

                                        CONTROL  4 - HT
 CL(DS)                  .020792          .020792           .000716            .021508      (1/DEG)
 CD(DS)                  .002109          .002109           .000089            .002198      (1/DEG)
 CM(DS)                 -.077093         -.077093          -.002720           -.079813      (1/DEG)
 CL(DS-DOT)            -1.260639        -1.260639          -.048898          -1.309537      (1/RAD)
 CD(DS-DOT)             -.169831         -.169831          -.006093           -.175924      (1/RAD)
 CM(DS-DOT)             1.549343         1.549343           .177078           1.726421      (1/RAD)
```

TIES CASE 2 CLIMB. REVISED MODES

```
                    ********************************
                    *                              *
                    * STATIC STABILITY DERIVATIVES *
                    *                              *
                    ********************************

                        RIGID          ELASTIC          TOTAL        UNITS
                                      INCREMENT

     CL(0)             .329428        -.010397         .319031
     CD(0)             .015333        -.000148         .005185
     CM(0)             .070229        -.010360         .059869

     CL(U)            1.554462        -.015283        1.539179     (1/RAD)
     CD(U)             .158253        -.001549         .156705     (1/RAD)
     CM(U)            -.032734        -.038390        -.071124     (1/RAD)

     CL(ALPHA)         .102325         .000304         .102630     (1/DEG)
     CD(ALPHA)         .014888         .000024         .014912     (1/DEG)
     CM(ALPHA)        -.031854        -.000647        -.032501     (1/DEG)

     CL(Q)           15.524966        -.241726       15.283240     (1/RAD)
     CD(Q)             .938506        -.019707         .918799     (1/RAD)
     CM(Q)           -39.797429         .929954      -38.867475     (1/RAD)

     CL(DE)            .015004        -.001051         .013953     (1/DEG)
     CD(DE)            .001058        -.000084         .000975     (1/DEG)
     CM(DE)           -.057701         .004823        -.052878     (1/DEG)

     CL(THRUST)        .000000        -.000000         .000000     (1/NEWTON)
     CD(THRUST)       -.000003        -.000000        -.000003     (1/NEWTON)
     CM(THRUST)        .000001         .000000         .000001     (1/NEWTON)
```

ORIGINAL PAGE IS OF POOR QUALITY

TIFS CASE 2, CLIMB, REVISED MODES

```
                          ********************************
                          *                              *
                          * DYNAMIC STABILITY DERIVATIVES *
                          *                              *
                          ********************************

                 RIGID           RIGID          ELASTIC          TOTAL       UNITS
               COMPUTED          OUTPUT         INCREMENT

CL(U)          1.554462         1.554462         .007026        1.561488    (1/RAD)
CD(U)           .158253          .158253         .000579         .158832    (1/RAD)
CM(U)          -.032734         -.032734        -.015076        -.047810    (1/RAD)

CL(ALPHA)       .102325          .102325         .001173         .103499    (1/DEG)
CD(ALPHA)       .014888          .014888         .000099         .014988    (1/DEG)
CM(ALPHA)      -.031854         -.031854        -.002426        -.034280    (1/DEG)

CL(Q)         15.524966        15.524966         .429217       15.954183    (1/RAD)
CD(Q)           .938506          .938506         .035137         .973643    (1/RAD)
CM(Q)        -39.797429       -39.797429       -1.659416      -41.456845    (1/RAD)

CY(BETA)        .000000          .000000         .000000         .000000    (1/DEG)
C1(BETA)        .000000          .000000         .000000         .000000    (1/DEG)
CN(BETA)        .000000          .000000         .000000         .000000    (1/DEG)

CY(P)           .000000          .000000         .000000         .000000    (1/RAD)
C1(P)           .000000          .000000         .000000         .000000    (1/RAD)
CN(P)           .000000          .000000         .000000         .000000    (1/RAD)

CY(R)           .000000          .000000         .000000         .000000    (1/RAD)
C1(R)           .000000          .000000         .000000         .000000    (1/RAD)
CN(R)           .000000          .000000         .000000         .000000    (1/RAD)

CL(A-DOT)     -2.982224        -2.982224         .016536       -2.965688    (1/RAD)
CD(A-DOT)      -.312355         -.312355         .000884        -.311472    (1/RAD)
CM(A-DOT)    -14.290997       -14.290997        -.350494      -14.641491    (1/RAD)

CL(Q-DOT)    -17.890330       -17.890330        -.525633      -18.415964    (1/RAD)
CD(Q-DOT)     -1.694267        -1.694267        -.043827       -1.738095    (1/RAD)
CM(Q-DOT)    -20.940744       -20.940744        1.629167      -19.311577    (1/RAD)

CY(B-DOT)       .000000          .000000         .000000         .000000    (1/RAD)
C1(B-DOT)       .000000          .000000         .000000         .000000    (1/RAD)
CN(B-DOT)       .000000          .000000         .000000         .000000    (1/RAD)

CY(P-DOT)       .000000          .000000         .000000         .000000    (1/RAD)
C1(P-DOT)       .000000          .000000         .000000         .000000    (1/RAD)
CN(P-DOT)       .000000          .000000         .000000         .000000    (1/RAD)

CY(R-DOT)       .000000          .000000         .000000         .000000    (1/RAD)
C1(R-DOT)       .000000          .000000         .000000         .000000    (1/RAD)
CN(R-DOT)       .000000          .000000         .000000         .000000    (1/RAD)
```

TIFS CASE 2, CLIMB, REVISED MODES

```
                         ******************************
                         *                            *
                         * ACTIVE CONTROL DERIVATIVES *
                         *                            *
                         ******************************

                       * SYMMETRICALLY DEFLECTED CONTROLS *

 NAME              RIGID           RIGID          ELASTIC            TOTAL       UNITS
                  COMPUTED         OUTPUT         INCREMENT

                                 CONTROL  1 - AILS
CL(DS)              .012740         .012740        -.000092          .012649     (1/DEG)
CD(DS)              .000565         .000565        -.000008          .000557     (1/DEG)
CM(DS)             -.005358        -.005358        -.000049         -.005408     (1/DEG)
CL(DS-DOT)        -1.725481       -1.725481        -.030091        -1.755571     (1/RAD)
CD(DS-DOT)         -.156273        -.156273        -.002541         -.158815     (1/RAD)
CM(DS-DOT)         1.322656        1.322656         .061488         1.384144     (1/RAD)

                                 CONTROL  2 - DLF
CL(DS)              .023831         .023831        -.000261          .023570     (1/DEG)
CD(DS)              .001322         .001322        -.000023          .001299     (1/DEG)
CM(DS)             -.003354        -.003354         .000500         -.002854     (1/DEG)
CL(DS-DOT)        -2.870501       -2.870501         .039240        -2.831261     (1/RAD)
CD(DS-DOT)         -.272916        -.272916         .003140         -.269777     (1/RAD)
CM(DS-DOT)         -.967404        -.967404        -.209804        -1.177209     (1/RAD)

                                 CONTROL  3 - ELVT
CL(DS)              .015004         .015004        -.000192          .014812     (1/DEG)
CD(DS)              .001058         .001058        -.000016          .001043     (1/DEG)
CM(DS)             -.057701        -.057701         .000773         -.056928     (1/DEG)
CL(DS-DOT)        -1.183489       -1.183489        -.046871        -1.230360     (1/RAD)
CD(DS-DOT)         -.106788        -.106788        -.003870         -.110658     (1/RAD)
CM(DS-DOT)         2.153215        2.153215         .168493         2.321708     (1/RAD)

                                 CONTROL  4 - HT
CL(DS)              .020983         .020983         .000954          .021937     (1/DEG)
CD(DS)              .001464         .001464         .000078          .001543     (1/DEG)
CM(DS)             -.077642        -.077642        -.003611         -.081253     (1/DEG)
CL(DS-DOT)        -1.314917       -1.314917        -.066445        -1.381362     (1/RAD)
CD(DS-DOT)         -.121715        -.121715        -.005486         -.127202     (1/RAD)
CM(DS-DOT)         1.618584        1.618584         .239812         1.858396     (1/RAD)
```

TIFS CASE 3, ~~CRUISE,ENGINE IN , REVISED MODES~~

```
                    ********************************
                    *                              *
                    * STATIC STABILITY DERIVATIVES *
                    *                              *
                    ********************************

                      RIGID      ELASTIC         TOTAL       UNITS
                                INCREMENT

CL(0)               .353030     -.034849        .318181
CD(0)               .005981     -.000474        .005507
CM(0)               .078810     -.029248        .049563

CL(U)               .558380     -.081902        .476478     (1/RAD)
CD(U)               .013762     -.000181        .013580     (1/RAD)
CM(U)              -.002974     -.006716       -.009689     (1/RAD)

CL(ALPHA)           .110243      .001063        .111306     (1/DEG)
CD(ALPHA)           .003238     -.000012        .003226     (1/DEG)
CM(ALPHA)          -.032883     -.002350       -.035233     (1/DEG)

CL(Q)             16.450161     -.738504      15.711656     (1/RAD)
CD(Q)               .021674      .006080        .027754     (1/RAD)
CM(Q)            -42.026824     2.710491     -39.316334     (1/RAD)

CL(DE)              .015891     -.003193        .012697     (1/DEG)
CD(DE)             -.000046      .000032       -.000013     (1/DEG)
CM(DE)             -.061319      .014343       -.046976     (1/DEG)

CL(THRUST)         -.000000     -.000000       -.000000     (1/NEWTON)
CD(THRUST)         -.000001      .000000       -.000001     (1/NEWTON)
CM(THRUST)          .000000      .000000        .000000     (1/NEWTON)
```

TIFS CASE 3, ~~CRUISE,ENGINE IN , REVISED MODES~~

```
                                   **********************************
                                   *                                *
                                   * DYNAMIC STABILITY DERIVATIVES  *
                                   *                                *
                                   **********************************

                    RIGID              RIGID            ELASTIC              TOTAL        UNITS
                   COMPUTED            OUTPUT           INCREMENT

CL(U)               .558380            .558300          -.025468            .532832      (1/RAD)
~~CD(U)               .013762            .013600           .000108            .013708      (1/RAD)~~
CM(U)              -.002974            .008767           .058520            .067287      (1/RAD)

CL(ALPHA)           .110243            .103323           .004106            .107429      (1/DEG)
~~CD(ALPHA)           .003238            .003211          -.000024            .003187      (1/DEG)~~
CM(ALPHA)          -.032883           -.002379          -.008656           -.011035      (1/DEG)

CL(Q)             16.450161          16.450707          1.562276          18.012983      (1/RAD)
~~CD(Q)               .021674            .015748          -.013132            .002616      (1/RAD)~~
CM(Q)            -42.026824         -41.683927         -6.031389         -47.715317      (1/RAD)

CY(BETA)            .000000            .000000           .000000            .000000      (1/DEG)
~~C1(BETA)            .000000            .000000           .000000            .000000      (1/DEG)~~
CN(BETA)            .000000            .000000           .000000            .000000      (1/DEG)

CY(P)               .000000            .000000           .000000            .000000      (1/RAD)
~~C1(P)               .000000            .000000           .000000            .000000      (1/RAD)~~
CN(P)               .000000            .000000           .000000            .000000      (1/RAD)

CY(R)               .000000            .000000           .000000            .000000      (1/RAD)
~~C1(R)               .000000            .000000           .000000            .000000      (1/RAD)~~
CN(R)               .000000            .000000           .000000            .000000      (1/RAD)

CL(A-DOT)         -5.070920          -5.070920           .060618          -5.010301      (1/RAD)
~~CD(A-DOT)          -.049114           -.049114          -.002404           -.051518      (1/RAD)~~
CM(A-DOT)        -16.460042         -16.460042         -1.378287         -17.838329      (1/RAD)

CL(Q-DOT)        -23.981482         -23.981482         -2.193535         -26.175017      (1/RAD)
~~CD(Q-DOT)          -.101083           -.101083           .015327           -.085756      (1/RAD)~~
CM(Q-DOT)        -19.811921         -19.811921          6.870396         -12.941525      (1/RAD)

CY(B-DOT)           .000000            .000000           .000000            .000000      (1/RAD)
~~C1(B-DOT)           .000000            .000000           .000000            .000000      (1/RAD)~~
CN(B-DOT)           .000000            .000000           .000000            .000000      (1/RAD)

CY(P-DOT)           .000000            .000000           .000000            .000000      (1/RAD)
~~C1(P-DOT)           .000000            .000000           .000000            .000000      (1/RAD)~~
CN(P-DOT)           .000000            .000000           .000000            .000000      (1/RAD)

CY(R-DOT)           .000000            .000000           .000000            .000000      (1/RAD)
~~C1(R-DOT)           .000000            .000000           .000000            .000000      (1/RAD)~~
CN(R-DOT)           .000000            .000000           .000000            .000000      (1/RAD)
```

```
TIFS CASE 3, CRUISE,ENGINE IN , REVISED MODES

                              ******************************
                              *                            *
                              * ACTIVE CONTROL DERIVATIVES *
                              *                            *
                              ******************************

                         * SYMMETRICALLY DEFLECTED CONTROLS *

NAME                RIGID          RIGID          ELASTIC          TOTAL       UNITS
                  COMPUTED        OUTPUT         INCREMENT

                              CONTROL  1 - AILS
CL(DS)             .013731        .013731        -.000318         .013413     (1/DEG)
CD(DS)             .000163        .000163        -.000000         .000163     (1/DEG)
CM(DS)            -.005797       -.005797        -.000204        -.006001     (1/DEG)
CL(DS-DOT)       -2.157571      -2.157571        -.119514       -2.277085     (1/RAD)
CD(DS-DOT)        -.000670       -.000670         .000682         .000012     (1/RAD)
CM(DS-DOT)        1.469189       1.469189         .238862        1.708051     (1/RAD)

                              CONTROL  2 - DLF
CL(DS)             .025615        .025615        -.000901         .024713     (1/DEG)
CD(DS)             .000352        .000352         .000002         .000354     (1/DEG)
CM(DS)            -.003513       -.003513         .001844        -.001668     (1/DEG)
CL(DS-DOT)       -3.643225      -3.643225         .152252       -3.490973     (1/RAD)
CD(DS-DOT)        -.017502       -.017502        -.001598        -.019100     (1/RAD)
CM(DS-DOT)       -1.414440      -1.414440        -.824275       -2.238715     (1/RAD)

                              CONTROL  3 - ELVT
CL(DS)             .015891        .015891        -.000720         .015170     (1/DEG)
CD(DS)            -.000046       -.000046         .000006        -.000040     (1/DEG)
CM(DS)            -.061319       -.061319         .002889        -.058430     (1/DEG)
CL(DS-DOT)       -1.536891      -1.536891        -.200245       -1.737135     (1/RAD)
CD(DS-DOT)         .000309        .000309         .001558         .001867     (1/RAD)
CM(DS-DOT)       -2.804017      -2.804017        -.724096       -3.528113     (1/RAD)

                              CONTROL  4 - HT
CL(DS)             .022141        .022141         .003456         .025596     (1/DEG)
CD(DS)             .000015        .000015        -.000028        -.000013     (1/DEG)
CM(DS)            -.082134       -.082134        -.013122        -.095256     (1/DEG)
CL(DS-DOT)       -1.732485      -1.732485        -.280140       -2.012625     (1/RAD)
CD(DS-DOT)        -.003353       -.003353         .002180        -.001173     (1/RAD)
CM(DS-DOT)       -2.215582      -2.215582       -1.015986       -3.231569     (1/RAD)
```

ORIGINAL PAGE IS
OF POOR QUALITY

APPENDIX C

PRESSURE DISTRIBUTION DATA LANDING CONFIGURATION

This appendix contains pressure distribution data computed by FLEXSTAB for the landing configuration. The coordinates given are of the aerodynamic panel centroids in the reference axis system. Panel numbers start on the leading edge and progress rearward on the thin bodies. The pressure coefficient C_p is defined as follows.

$$C_p = \frac{p_{LOWER} - p_{UPPER}}{\bar{q}}$$

where p_{LOWER} and p_{UPPER} are lower surface and upper surface pressures

$\bar{q}$ is dynamic pressure.

TIFS CASE 1, LANDING CONFIGURATION, REVISED MODES

```
                         ************************************
                         *                                  *
                         * STEADY AIC PRESSURE DISTRIBUTION *
                         *                                  *
                         ************************************




                  *  NUMBER OF SLENDER BODIES ------             2

                  *  NUMBER OF THIN BODIES ---------             7

                  *  MACH NUMBER ------------------            .20

                  *  ANGLE OF ATTACK ---------------        7.0227
                                                             (DEG)

                  *  SIDESLIP ANGLE ----------------         .0000
                                                             (DEG)

                  *  DYNAMIC PRESSURE --------------       2819.68
                                                     (NEWTONS/M**2)

                         DATA FOR SLENDER BODY NUMBER  1

                  *  SLENDER BODY NAME--------------- FUSELAGE
                  *  Y-COORDINATE ------------------       .0000 (METERS)
                  *  Z-COORDINATE ------------------       .0000 (METERS)
                  *  ON/OFF PLANE OF SYMMETRY ------      ON
                  *  NUMBER OF DOUBLETS ------------          20

              NO.         X             CP(X)           CP(Y)          CP(Z)
                       (METERS)

               1        .690575        .000000         .000000        .352408
               2       2.071725        .000000         .000000        .150461
               3       3.452875        .000000         .000000        .017441
               4       4.834025        .000000         .000000        .022176
               5       6.215175        .000000         .000000        .012919
               6       7.596325        .000000         .000000        .012294
               7       8.977475        .000123         .000000        .055169
               8      10.358625        .006110         .000000        .302103
               9      11.739775        .000000         .000000        .098100
              10      13.120925        .000000         .000000        .113105

              11      14.502075        .000000         .000000        .116748
              12      15.883225        .000000         .000000        .075395
              13      17.264375        .000000         .000000        .062232
              14      18.645525        .000000         .000000        .051194
              15      20.026675        .000000         .000000        .014893
              16      21.407825        .000000         .000000       -.014801
              17      22.788975        .000000         .000000       -.053082
              18      24.170125        .000000         .000000       -.082996
              19      25.551275        .000000         .000000       -.152734
              20      26.932425        .000000         .000000       -.194066
```

ORIGINAL PAGE IS
OF POOR QUALITY

TIFS CASE 1, LANDING CONFIGURATION, REVISED MODES

```
                       DATA FOR SLENDER BODY NUMBER  2

                 *  SLENDER BODY NAME-------------- NACELLE
                 *  Y-COORDINATE ------------------      3.8104 (METERS)
                 *  Z-COORDINATE ------------------      -.9212 (METERS)
                 *  ON/OFF PLANE OF SYMMETRY ------     OFF
                 *  NUMBER OF DOUBLETS ------------        15

             NO.        X             CP(X)          CP(Y)          CP(Z)
                    (METERS)

              1     9.494000        .008470       -.005354        .454995
              2     9.924000        .000000       -.005486        .288405
              3    10.354000        .000000       -.021039        .250457
              4    10.784000        .000000       -.036605        .235744
              5    11.214000        .000000       -.036618        .077912
              6    11.644000       -.255242       -.055411        .444494
              7    12.074000       -.187520       -.056232        .598250
              8    12.504000       -.187054       -.063615        .555473
              9    12.934000       -.135799       -.072069        .563264
             10    13.364000       -.083633       -.074722        .561508

             11    13.794000       -.043455       -.056098        .294158
             12    14.224000       -.011095       -.067320        .252115
             13    14.654000       -.007296       -.071154        .269764
             14    15.084000       -.007130       -.080021        .213768
             15    15.514000       -.014260       -.239102       1.540847
```

```
TIFS CASE 3, LANDING CONFIGURATION, REVISED MODES

                     DATA FOR THIN BODY NUMBER  1

                *  THIN BODY NAME ---------------- VER TAIL
                *  DIHEDRAL ANGLE ----------------    90.0000 (DEG.)
                *  ON/OFF PLANE OF SYMMETRY ------     ON
                *  NUMBER OF PANELS --------------        6
                *  NUMBER OF Y-STATIONS ----------        3

             PANEL      X           X/C              CP             CP             CP
    NO.       NO.    (METERS)                     SYMMETRIC     RIGHT SIDE      LEFT SIDE

                     Y-STATION  1 (Y =     2.1803 (METERS))

     1         1    23.829982    .096621         .000000        .000000        .000000
     2         2    25.735172    .599597         .000000        .000000        .000000

                     Y-STATION  2 (Y =     3.7276 (METERS))

     1         3    24.430080    .093706         .000000        .000000        .000000
     2         4    25.803215    .599249         .000000        .000000        .000000

                     Y-STATION  3 (Y =     5.2604 (METERS))

     1         5    24.964816    .084403         .000000        .000000        .000000
     2         6    25.870618    .598138         .000000        .000000        .000000
```

```
TIFS CASE 1, LANDING CONFIGURATION, REVISED MODES

                              DATA FOR THIN BODY NUMBER  2

                      *  THIN BODY NAME ---------------- IN-WING
                      *  DIHEDRAL ANGLE ----------------    4.8278 (DEG.)
                      *  ON/OFF PLANE OF SYMMETRY ------    OFF
                      *  NUMBER OF PANELS --------------      18
                      *  NUMBER OF Y-STATIONS ----------      3

              PANEL       X            X/C            CP              CP              CP
      NO.      NO.     (METERS)                    SYMMETRIC      RIGHT SIDE      LEFT SIDE

                              Y-STATION  1 (Y =     1.1290 (METERS))

       1        7    11.939303      .049954       3.470485        3.470485        3.470485
       2        8    12.327974      .149962       1.225009        1.225009        1.225009
       3        9    12.910980      .299974       1.005248        1.005248        1.005248
       4       10    13.688321      .499990        .670036         .670036         .670036
       5       11    14.465662      .700006        .412171         .412171         .412171
       6       12    15.243093      .900123        .287104         .287104         .287104

                              Y-STATION  2 (Y =     1.8646 (METERS))

       1       13    12.022533      .049900       3.812639        3.812639        3.812639
       2       14    12.396591      .149917       1.310160        1.310160        1.310160
       3       15    12.957679      .299944       1.036208        1.036208        1.036208
       4       16    13.705795      .499979        .669765         .669765         .669765
       5       17    14.453911      .700014        .416863         .416863         .416863
       6       18    15.202027      .900049        .309292         .309292         .309292

                              Y-STATION  3 (Y =     2.6670 (METERS))

       1       19    12.113334      .049921       4.191875        4.191875        4.191875
       2       20    12.471450      .149935       1.247277        1.247277        1.247277
       3       21    13.008625      .299955        .988019         .988019         .988019
       4       22    13.724858      .499983        .625773         .625773         .625773
       5       23    14.441090      .700011        .384563         .384563         .384563
       6       24    15.157323      .900039        .306956         .306956         .306956
```

ORIGINAL PAGE IS
OF POOR QUALITY

```
TIFS CASE 1, LANDING CONFIGURATION, REVISED MODES.

                              DATA FOR THIN BODY NUMBER  3

                         *  THIN BODY NAME ---------------- MID-WING
                         *  DIHEDRAL ANGLE ----------------      6.5000 (DEG.)
                         *  ON/OFF PLANE OF SYMMETRY ------    OFF
                         *  NUMBER OF PANELS --------------         32
                         *  NUMBER OF Y-STATIONS ----------          4

           PANEL       X            X/C              CP              CP              CP
   NO.      NO.    (METERS)                      SYMMETRIC       RIGHT SIDE       LEFT SIDE

                           Y-STATION  1 (Y =    4.9075 (METERS))

    1       25    12.349734      .045424         3.876601        3.876601        3.876601
    2       26    12.636784      .136345         1.486227        1.486227        1.486227
    3       27    13.067254      .272692         1.140606        1.140606        1.140606
    4       28    13.641203      .454486          .804061         .804061         .804061
    5       29    14.071751      .590858          .580679         .580679         .580679
    6       30    14.358488      .681679          .516295         .516295         .516295
    7       31    14.717271      .795321          .517191         .517191         .517191
    8       32    15.148276      .931838          .231261         .231261         .231261

                           Y-STATION  2 (Y =    5.9056 (METERS))

    1       33    12.461199      .045878         3.633942        3.633942        3.633942
    2       34    12.737235      .138098         1.582404        1.582404        1.582404
    3       35    13.151149      .276381         1.225154        1.225154        1.225154
    4       36    13.703055      .460765          .884290         .884290         .884290
    5       37    14.117044      .599074          .676378         .676378         .676378
    6       38    14.392774      .691192          .598626         .598626         .598626
    7       39    14.727249      .802935          .593626         .593626         .593626
    8       40    15.121034      .934493          .277121         .277121         .277121

                           Y-STATION  3 (Y =    7.2223 (METERS))

    1       41    12.607731      .046714         3.576674        3.576674        3.576674
    2       42    12.868745      .140658         1.596329        1.596329        1.596329
    3       43    13.260268      .281575         1.255788        1.255788        1.255788
    4       44    13.782279      .469456          .924902         .924902         .924902
    5       45    14.173799      .610371          .712820         .712820         .712820
    6       46    14.434743      .704290          .630955         .630955         .630955
    7       47    14.738016      .813444          .622751         .622751         .622751
    8       48    15.084022      .937978          .298002         .298002         .298002

                           Y-STATION  4 (Y =    8.5201 (METERS))

    1       49    12.751932      .047523         3.629623        3.629623        3.629623
    2       50    12.997456      .143191         1.639137        1.639137        1.639137
    3       51    13.365797      .286715         1.293954        1.293954        1.293954
    4       52    13.856876      .478063          .951542         .951542         .951542
    5       53    14.225154      .621562          .725361         .725361         .725361
    6       54    14.470685      .717233          .638074         .638074         .638074
    7       55    14.744288      .823842          .627961         .627961         .627961
    8       56    15.046208      .941485          .302423         .302423         .302423
```

TIFS CASE 1, LANDING CONFIGURATION, REVISED MODES

```
                          DATA FOR THIN BODY NUMBER  4

                   *  THIN BODY NAME ---------------- TIP-WING
                   *  DIHEDRAL ANGLE ----------------      6.5000 (DEG.)
                   *  ON/OFF PLANE OF SYMMETRY ------    OFF
                   *  NUMBER OF PANELS --------------        40
                   *  NUMBER OF Y-STATIONS ----------         5

          PANEL      X             X/C            CP            CP             CP
   NO.     NO.    (METERS)                     SYMMETRIC     RIGHT SIDE      LEFT SIDE

                          Y-STATION  1 (Y =    9.8687 (METERS))

    1      57    12.901415      .048304       3.326991       3.326991       3.326991
    2      58    13.130640      .145760       1.385255       1.385255       1.385255
    3      59    13.472978      .291944       1.133156       1.133156       1.133156
    4      60    13.930218      .486852        .847347        .847347        .847347
    5      61    14.273148      .633033        .658125        .658125        .658125
    6      62    14.501773      .730489        .584040        .584040        .584040
    7      63    14.745695      .834466        .591697        .591697        .591697
    8      64    15.005198      .945085        .284817        .284817        .284817

                          Y-STATION  2 (Y =   11.2212 (METERS))

    1      65    13.049573      .048523       3.371692       3.371692       3.371692
    2      66    13.258289      .146736       1.414688       1.414688       1.414688
    3      67    13.571310      .294031       1.158699       1.158699       1.158699
    4      68    13.988682      .490429        .860510        .860510        .860510
    5      69    14.301756      .637749        .659383        .659383        .659383
    6      70    14.510416      .735935        .582305        .582305        .582305
    7      71    14.729097      .838838        .588938        .588938        .588938
    8      72    14.957833      .946472        .282833        .282833        .282833

                          Y-STATION  3 (Y =   12.5394 (METERS))

    1      73    13.193857      .048639       3.324212       3.324212       3.324212
    2      74    13.382459      .147399       1.397570       1.397570       1.397570
    3      75    13.665264      .295489       1.147312       1.147312       1.147312
    4      76    14.042410      .492979        .851411        .851411        .851411
    5      77    14.325360      .641144        .649983        .649983        .649983
    6      78    14.513949      .739898        .573595        .573595        .573595
    7      79    14.709035      .842053        .582296        .582296        .582296
    8      80    14.910589      .947596        .278879        .278879        .278879

                          Y-STATION  4 (Y =   13.8572 (METERS))

    1      81    13.338050      .048730       3.176815       3.176815       3.176815
    2      82    13.506280      .148025       1.335660       1.335660       1.335660
    3      83    13.758630      .296970       1.099952       1.099952       1.099952
    4      84    14.095113      .495572        .816035        .816035        .816035
    5      85    14.347582      .644587        .620825        .620825        .620825
    6      86    14.515834      .743894        .548064        .548064        .548064
    7      87    14.687618      .845286        .562789        .562789        .562789
    8      88    14.862895      .948740        .266846        .266846        .266846

                          Y-STATION  5 (Y =   15.2704 (METERS))

    1      89    13.492503      .048301       2.762077       2.762077       2.762077
    2      90    13.638635      .148237       1.154320       1.154320       1.154320
    3      91    13.857824      .298133        .956580        .956580        .956580
    4      92    14.150107      .498017        .712907        .712907        .712907
    5      93    14.363305      .647920        .552433        .552433        .552433
    6      94    14.515425      .747847        .522601        .522601        .522601
    7      95    14.662708      .848569        .451678        .451678        .451678
    8      96    14.811067      .950641        .222237        .222237        .222237
```

```
TIFS CASE 1, LANDING CONFIGURATION, REVISED MODES

                                  DATA FOR THIN BODY NUMBER  5

                         *  THIN BODY NAME ---------------- TOP-SFS
                         *  DIHEDRAL ANGLE ----------------    96.5000  (DEG.)
                         *  ON/OFF PLANE OF SYMMETRY ------    OFF
                         *  NUMBER OF PANELS --------------            4
                         *  NUMBER OF Y-STATIONS ----------            2

            PANEL       X           X/C             CP              CP              CP
    NO.      NO.    (METERS)                    SYMMETRIC       RIGHT SIDE      LEFT SIDE

                                 Y-STATION  1 (Y =     9.1107 (METERS))

     1       97    12.754888     .099159         .168947         .168947         .168947
     2       98    13.448056     .603810         .061212         .061212         .061212

                                 Y-STATION  2 (Y =     8.9854 (METERS))

     1       99    12.786759     .099627         .135594         .135594         .135594
     2      100    13.303664     .601690         .045465         .045465         .045465
```

```
TIFS CASE 1, LANDING CONFIGURATION, REVISED MODES

                                  DATA FOR THIN BODY NUMBER  6

                         *  THIN BODY NAME ---------------- BOT-SFS
                         *  DIHEDRAL ANGLE ----------------   276.5000  (DEG.)
                         *  ON/OFF PLANE OF SYMMETRY ------    OFF
                         *  NUMBER OF PANELS --------------            4
                         *  NUMBER OF Y-STATIONS ----------            2

            PANEL       X           X/C             CP              CP              CP
    NO.      NO.    (METERS)                    SYMMETRIC       RIGHT SIDE      LEFT SIDE

                                 Y-STATION  1 (Y =     9.2646 (METERS))

     1      101    12.754888     .099159         .446161         .446161         .446161
     2      102    13.448056     .603810         .133769         .133769         .133769

                                 Y-STATION  2 (Y =     9.3898 (METERS))

     1      103    12.786759     .099627         .390156         .390156         .390156
     2      104    13.303664     .601690         .106392         .106392         .106392
```

TIFS CASE 1, LANDING CONFIGURATION, REVISED MODES

```
                              DATA FOR THIN BODY NUMBER  7

                        *  THIN BODY NAME ---------------- HOR TAIL
                        *  DIHEDRAL ANGLE ----------------         .0000  (DEG.)
                        *  ON/OFF PLANE OF SYMMETRY ------     OFF
                        *  NUMBER OF PANELS --------------          42
                        *  NUMBER OF Y-STATIONS ----------           7

          PANEL      X           X/C              CP             CP              CP
   NO.     NO.   (METERS)                      SYMMETRIC      RIGHT SIDE      LEFT SIDE

                              Y-STATION  1 (Y =     1.8599 (METERS))

    1     105   24.100630     .049296          .274402        .274402         .274402
    2     106   24.512203     .211464          .081692        .081692         .081692
    3     107   25.208321     .485750          .000754        .000754         .000754
    4     108   25.731680     .691964         -.228268       -.228268        -.228268
    5     109   25.955251     .780056         -.066623       -.066623        -.066623
    6     110   26.290667     .912193         -.036582       -.036582        -.036582

                              Y-STATION  2 (Y =     2.6630 (METERS))

    1     111   24.278597     .049365          .596473        .596473         .596473
    2     112   24.647538     .211517          .191823        .191823         .191823
    3     113   25.271550     .485774          .045508        .045508         .045508
    4     114   25.740697     .691968         -.218478       -.218478        -.218478
    5     115   25.941109     .780050         -.054499       -.054499        -.054499
    6     116   26.241728     .912175         -.028189       -.028189        -.028189

                              Y-STATION  3 (Y =     3.4163 (METERS))

    1     117   24.445508     .049123         1.210552       1.210552        1.210552
    2     118   24.774465     .211333          .358009        .358009         .358009
    3     119   25.330850     .485688          .101203        .101203         .101203
    4     120   25.749153     .691956         -.199463       -.199463        -.199463
    5     121   25.927846     .780070         -.034434       -.034434        -.034434
    6     122   26.195885     .912241         -.014823       -.014823        -.014823

                              Y-STATION  4 (Y =     4.1863 (METERS))

    1     123   24.616144     .048861         1.454053       1.454053        1.454053
    2     124   24.904225     .211134          .434977        .434977         .434977
    3     125   25.391473     .485595          .131876        .131876         .131876
    4     126   25.757798     .691942         -.186354       -.186354        -.186354
    5     127   25.914287     .780090         -.021296       -.021296        -.021296
    6     128   26.149019     .912313         -.005700       -.005700        -.005700

                              Y-STATION  5 (Y =     4.9017 (METERS))

          PANEL      X           X/C              CP             CP              CP
   NO.     NO.   (METERS)                      SYMMETRIC      RIGHT SIDE      LEFT SIDE

    1     129   24.774660     .048898         1.027734       1.027734        1.027734
    2     130   25.024768     .211162          .337450        .337450         .337450
    3     131   25.447790     .485609          .112249        .112249         .112249
    4     132   25.765829     .691944         -.187407       -.187407        -.187407
    5     133   25.901690     .780088         -.024021       -.024021        -.024021
    6     134   26.105482     .912303         -.006762       -.006762        -.006762
```

```
                                  Y-STATION  6 (Y =     5.5586 (METERS))

          1      135     24.920228    .048506        .859076          .859076          .859076
          2      136     25.135465    .210864        .278050          .278050          .278050
          3      137     25.499508    .485469        .086035          .086035          .086035
          4      138     25.773204    .691924       -.197093         -.197093         -.197093
          5      139     25.890123    .780119       -.033794         -.033794         -.033794
          6      140     26.065502    .912410       -.013098         -.013098         -.013098

                                  Y-STATION  7 (Y =     6.2311 (METERS))

          1      141     25.069245    .047624        .783135          .783135          .783135
          2      142     25.248785    .210193        .236154          .236154          .236154
          3      143     25.552450    .485156        .057298          .057298          .057298
          4      144     25.780754    .691880       -.209833         -.209833         -.209833
          5      145     25.878282    .780189       -.045924         -.045924         -.045924
          6      146     26.024573    .912653       -.021131         -.021131         -.021131
```

APPENDIX D

COMPLEMENTARY FILTER CORNER FREQUENCY DETERMINATION

COMPLEMENTARY FILTER CONCEPT

A complementary filter block diagram is presented in Figure D-1.

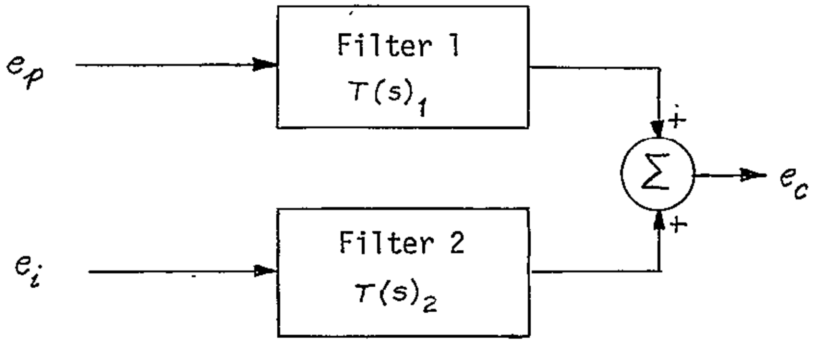

e_p = Signal obtained from air pressure measurements
e_i = Signal obtained from inertial measurements
$T(s)_1$ = Transfer function of filter (1)
$T(s)_2$ = Transfer function of filter (2)
e_c = Composite output signal
(s) = Laplace variable

Figure D-1 BLOCK DIAGRAM FOR ARBITRARY INPUTS e_p AND e_i

The signal flow depicted in block diagram form in Figure D-1 is described by Equation D-1.

$$e_c = e_p T(s)_1 + e_i T(s)_2 \tag{D-1}$$

Also since e_c, e_p and e_i are analogs of the same variable, Equation D-1 can be rewritten as Equation D-2.

$$1 = T(s)_1 + T(s)_2 \tag{D-2}$$

The transfer functions of the complementary filters are forced to yield a solution to Equation 2. That is, one transfer function is assumed and the other is computed from Equation 2. The resultant composite output signal has no "bumps" at or around the frequency that output data transitions from one input signal to another. A simplified example is presented to further illustrate this point. For the block diagram illustrated in Figure D-2, e and the transfer functions of filter (1) and (2) are $T(s)_1$ and $T(s)_2$ respectively.

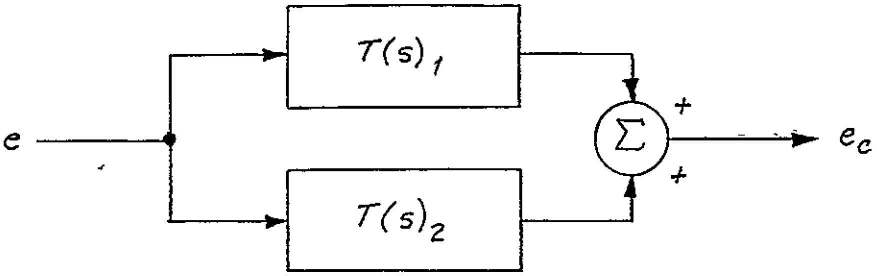

Figure D-2 COMPLEMENTARY FILTER BLOCK DIAGRAM FOR $e_p = e_i$

Assume a transfer function for $T(s)_1$ and compute $T(s)_2$ from Equation D-2.

From Equation

$$e_c = e_p T(s)_1 + e_i T(s)_2$$

also, $e_p = e_i = e$.

Therefore,
$$e_c = e\left[T(s)_1 + T(s)_2\right] \tag{D-3}$$

From Equation D-2.

$$T(s)_2 = 1 - T(s)_1$$

Substitute $T(s)_2$ from Equation D-2 to Equation D-3

$$e_c = e\left[T(s)_1 + 1 - T(s)_1\right] = e\left[1\right]$$

$$\left[e_c = e\right]$$

Thus, it is clear that the composite output signal precisely equals the input signal in amplitude and phase for all frequencies within the bandwidth of the computing electronics.

CORNER FREQUENCY DETERMINATION

The following procedure can be used to determine optimum corner frequencies for the complementary air data filters. Power spectral density functions describe the errors in each input signal and the square of the standard deviation (energy) for each signal is computed from the integral (over all frequencies) of the density function. The density function for the output signal is computed from the product of the input density function and the squared absolute value of the filter transfer function. The integral (over all frequencies) of the output density function results in a relationship between the square of the output error standard deviation and the filter corner frequency. Differentiating this equation and solving for the filter corner frequency for the derivative equal to zero yields an optimum corner frequency. To further clarify this concept, the air data vertical speed complementary filter corner frequency computation is outlined. The system input signals, filter transfer functions and output signal are shown in Figure D-3.

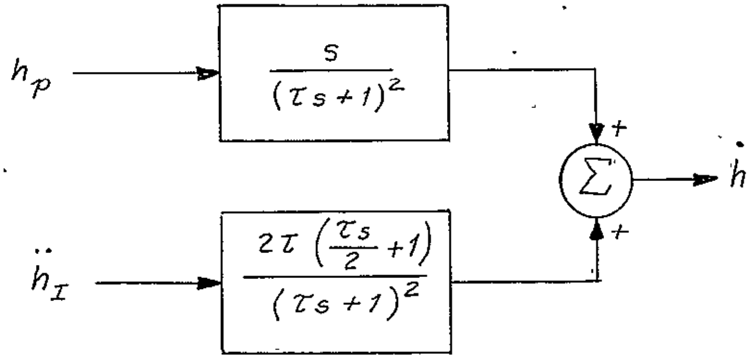

Figure D-3 BLOCK DIAGRAM OF AIR DATA ALTITUDE RATE COMPLEMENTARY FILTER

where

h_p = altitude computed from pressure measurements

$\ddot{h}_I$ = vertical acceleration computed from body axis accelerations and attitude angles

$\dot{h}$ = composite altitude rate signal

$\ddot{h}_I$ results from the body to earth axis transformation of the body axis accelerations n_x , n_y , and n_z and by pitch and roll angle.

In general form:

$$\ddot{h}_I = f(n_x, n_y, n_z, \theta, \phi)$$

An incremental change in $\ddot{h}_I$ is equal to the total differential, that is:

$$\Delta \ddot{h}_I = \frac{\partial f}{\partial n_x}\Delta n_x + \frac{\partial f}{\partial n_y}\Delta n_y + \frac{\partial f}{\partial n_z}\Delta n_z + \frac{\partial f}{\partial \theta}\Delta\theta + \frac{\partial f}{\partial \phi}\Delta\phi \qquad \text{(D-4)}$$

The partial derivatives of Equation D-4
transformation matrix, and the differential variations in each signal represent sensor errors. The significant sensor errors used for this computation are static offsets. The magnitude of the offsets used are:

$\Delta n_x = \pm 5.0 \times 10^{-4}$ g's

$\Delta n_y = \pm 1.0 \times 10^{-3}$ g's

$\Delta n_z = \pm 2.5 \times 10^{-3}$ g's

$\Delta\theta = \pm 1$ deg

$\Delta\phi = \pm 1$ deg

This defines the errors in $\ddot{h}_I$ and results in an impulse when transformed to a power spectral density function.

The errors in h_p result from air turbulence, and power spectral density functions describe the u, v and w velocity components of the turbulence. The assumption was made that the major component of error is introduced by, and subsequent analysis was performed on, the Y axis gust term. The Dryden form of the spectrum for the turbulence velocity is used in this analysis. The velocity spectrum described by the power spectral density function $\Phi(\omega) = \sigma_u \frac{2}{\pi}\frac{L}{V}\left[\frac{1}{1+(\frac{L}{V}\omega)^2}\right]$ is converted to pressure variations at the pitot static system and then into an altitude error spectrum described by:

$$\Phi_{h_p}(\omega) = \sigma_u^2\left(\frac{L}{V}\right)\left(\frac{V_Y}{q}\right)^2\frac{2}{\pi}\left[\frac{1}{1+(\frac{L}{V}\omega)^2}\right]$$

where:

L = 1000 ft altitude

V = 200 ft/sec aircraft velocity

V_Y = 20 ft/sec mean value of wind velocity in Y axis

$\sigma_u \approx \sigma_v \approx 3$ ft/sec standard deviation of wind velocity in Y axis

The altitude rate complementary filter is redrawn in Figure D-4 with input and output power spectral density functions labeled.

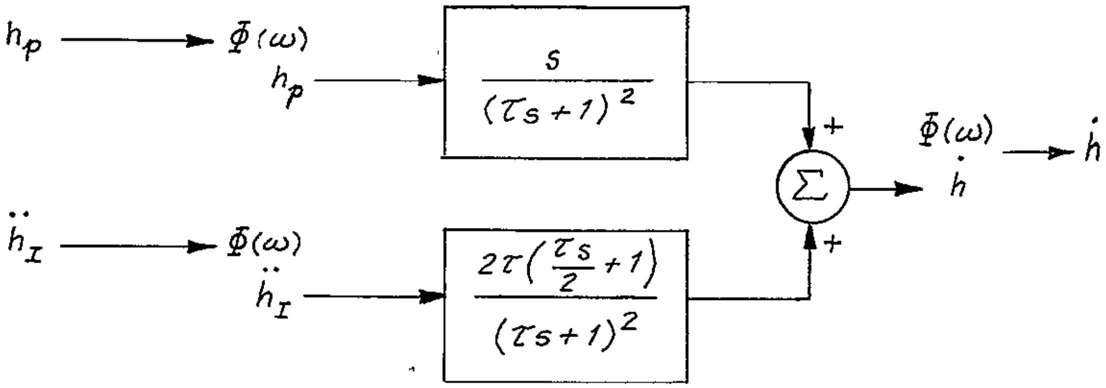

Figure D-4 ALTITUDE RATE COMPLEMENTARY FILTER WITH ERROR DENSITY FUNCTIONS AS INPUTS AND OUTPUTS

$\underset{h_p}{\Phi(\omega)}$ = power spectral density function of the errors in the pressure derived altitude signal

$\underset{\ddot{h}_I}{\Phi(\omega)}$ = power spectral density function of the errors in vertical acceleration

$\underset{\dot{h}}{\Phi(\omega)}$ = power spectral density function of the errors in the composite output signal

The standard deviations of the input and output signals are:

$$\sigma_{h_p}^2 = \int_{-\infty}^{\infty} \underset{h_p}{\Phi(\omega)}\, d\omega \tag{D-5}$$

$$\sigma_{\ddot{h}_I}^2 = \int_{-\infty}^{\infty} \underset{\ddot{h}_I}{\Phi(\omega)}\, d\omega \tag{D-6}$$

$$\sigma_{\dot{h}}^2 = \int_{-\infty}^{\infty} \underset{\dot{h}}{\Phi(\omega)}\, d\omega \tag{D-7}$$

Also, $\underset{\dot{h}}{\Phi(\omega)}$ is related to $\underset{h_p}{\Phi(\omega)}$ and $\underset{\ddot{h}_I}{\Phi(\omega)}$ by:

$$\Phi_{\dot{h}}(\omega) = \Phi_{h_p}(\omega) \left|\left[\frac{s}{(\tau s+1)^2}\right]\right|^2 + \Phi_{\ddot{h}_I}(\omega) \left|\left[\frac{2\tau\left(\frac{\tau s}{2}+1\right)}{(\tau s+1)^2}\right]\right|^2$$

$$\sigma_{\dot{h}}^2 = \frac{20}{\tau(5+\tau)^2} + .2\tau^2$$

Equation D-9 is the standard deviation squared of the error in $\dot{h}$ as obtained from the operations specified by Equations D-7 and D-8.

To obtain an optimum τ for the filter, $\frac{\partial}{\partial\tau}\left(\sigma_{\dot{h}}^2\right)$ is obtained. This expression is set to zero and solved for τ.

$$\frac{\partial}{\partial\tau}\left(\sigma_{\dot{h}}^2\right) = 0$$

$\sigma_{\dot{h}}^2$ is plotted in Figure D-5 to gain additional insight in the shape of the error function and how sensitive the error function is to variations in filter corner frequency. As can be seen, the function has a rather broad minimum and an acceptable result is obtained for filter time constants that range from 0.5 to 5 seconds. A value of 5 seconds is used for the air data altitude rate complementary filter. The development of the altitude, airspeed, and flight path acceleration signal filters is similar to the procedure outlined for the altitude rate system.

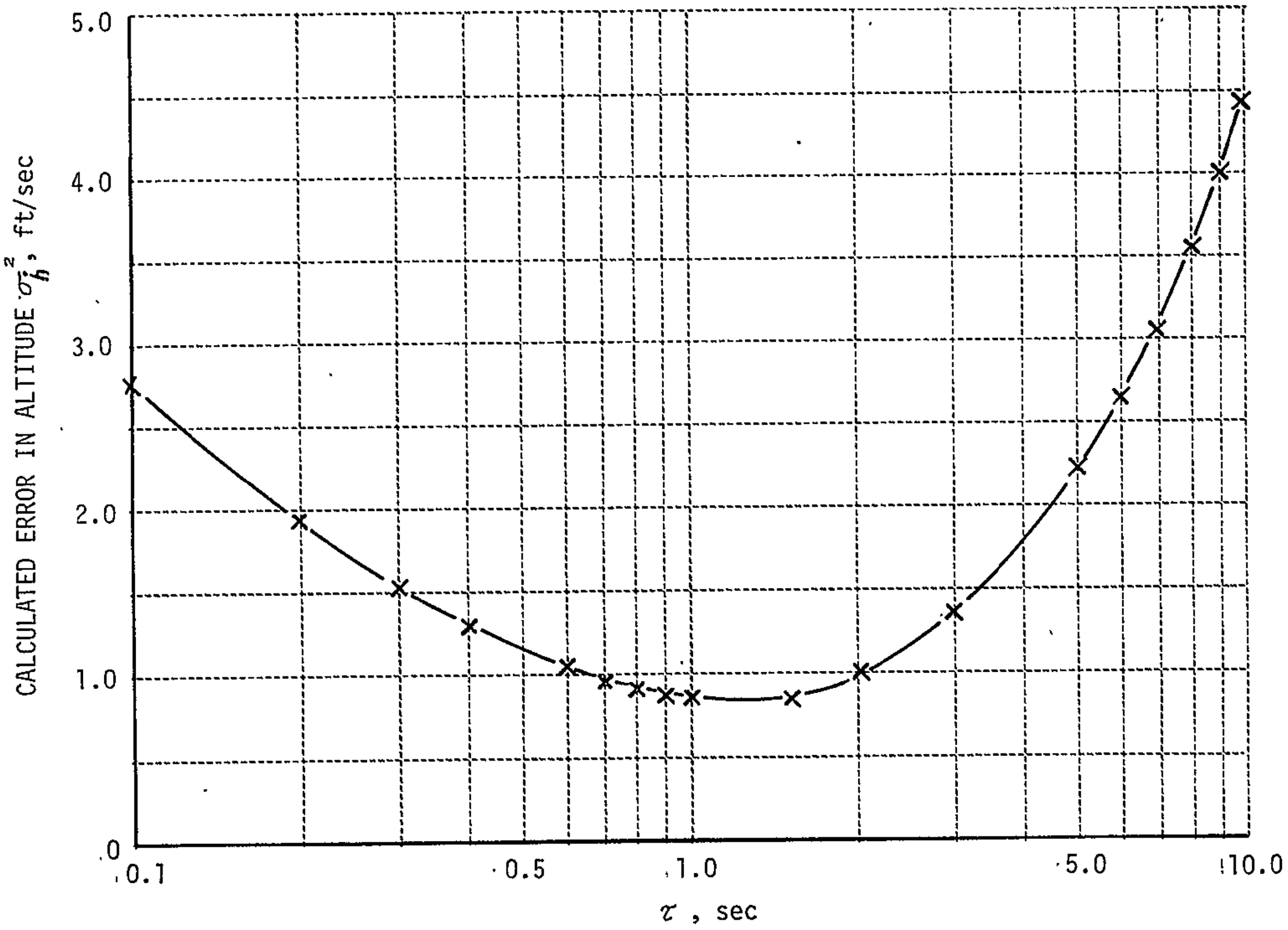
5.0
4.0
3.0
2.0
1.0
0
CALCULATED ERROR IN ALTITUDE $\sigma_{\dot{h}}^2$, ft/sec
0.1
0.5
1.0
5.0
10.0
τ , sec

Figure D-5

APPENDIX E

COLLECTIVE AILERON SYSTEM PRELIMINARY DESIGN

E.1.0 GENERAL

This appendix describes the preliminary design of a servo driven collective aileron system to be used for maneuver load and structural mode control on the AF/TIFS airplane

E.2.0 MECHANICAL DESIGN.

In this section, the existing TIFS aileron control system is described briefly to provide a better understanding of the mechanical arrangement of the proposed Class II modification.

E.2.1 Existing TIFS Aileron Control System

The existing TIFS aileron control system is shown in Figure E-1. In this configuration, a centrally mounted electrohydraulic position servo actuator, when the variable stability system is engaged, moves both ailerons through the standard C-131H cable and drum system. The multiple drum assembly shown in this figure is mounted behind the rear spar at the center of the aircraft (buttock line 0) and is a standard C-131H component. The mechanical system from control wheels to stops at the aileron quadrants was stressed for a condition in which two pilots apply couples at the control wheels in conjunction. Pilot applied wheel loads are given in this reference as two tangential limit forces of 80 lbs each applied in conjunction at the wheel rim. The TIFS position servo has relief valves set at 535 psi differential pressure across the piston which limits servo output forces to 525 lbs. This is equivalent to one pilot applying two tangential forces of 63.28 lbs in conjunction at the wheel rim. The maximum servo output therefore represents 79.1% of the maximum single pilot applied limit force and 39.5% of the maximum two-pilot applied limit force. The control system from the stops

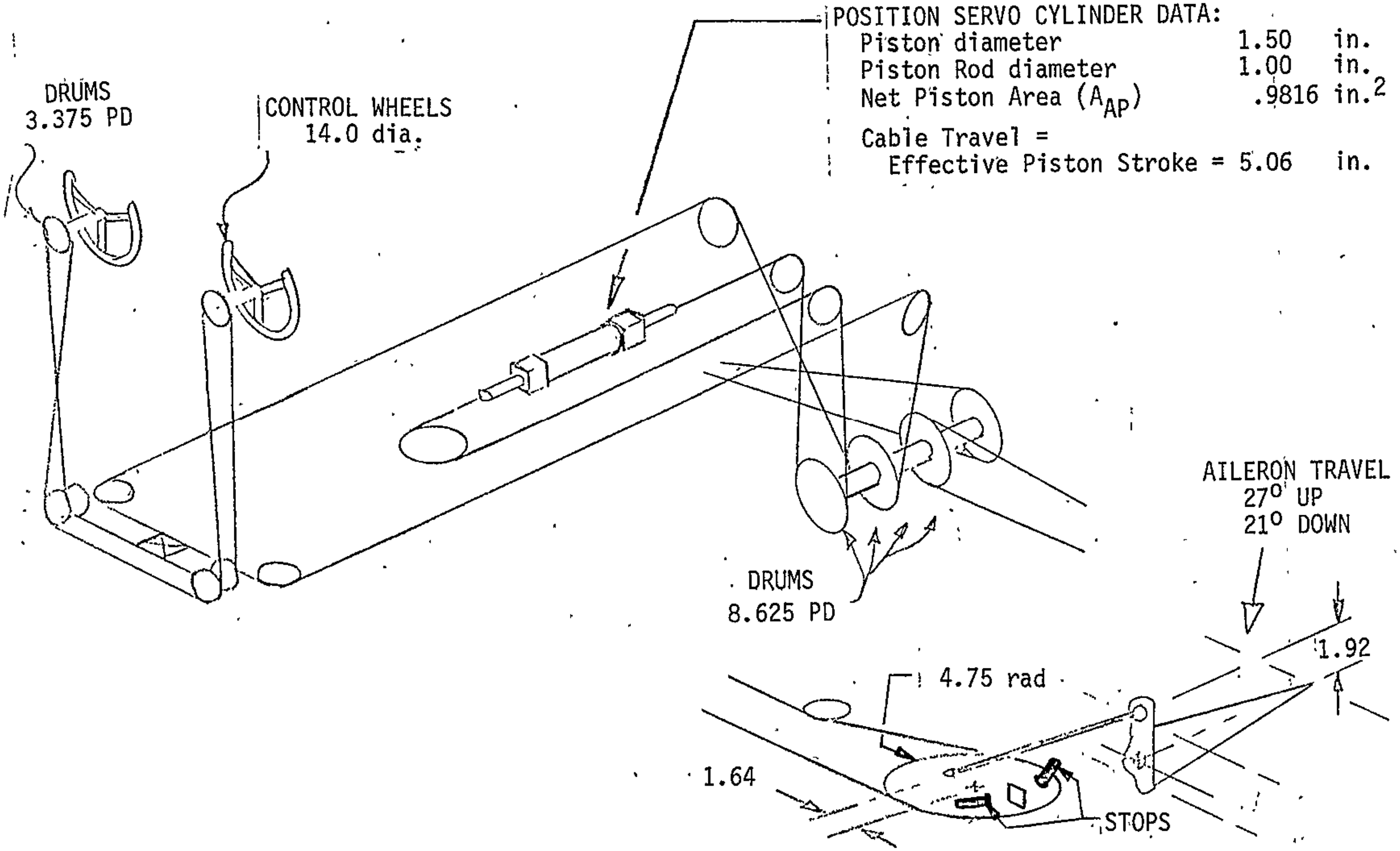

Figure E-1 TIFS AILERON CONTROL SYSTEM

to the aileron is designed for an aileron down limit airload of 410 ft lbs. It should be noted that this same reference assumes that the pilot applied forces at the center drum are distributed unequally 2/3 to one aileron and 1/3 to the other. Using the same assumption, the maximum limit airload which may be applied to one aileron by the position servo with relief valves set at 535 psi is 525 x 2/3 x 475/1.64 x 1.92/12 = 162.19 ft lbs.

There is a geared tab on each aileron. The gearing provides hinge moment relief (i.e. up tab motion for the down moving aileron and vice versa). For each degree of aileron movement, the tab will move approximately the same amount in the opposite direction. The tabs are adjusted for trim purposes by operating a knob on the center pedestal of the pilot's cockpit. Motion is transmitted via gears, pulleys and cables to jackscrews in each wing. Each jackscrew actuates a tab via two push-pull rods and a rocking lever. The maximum aerodynamic hinge moment produced on a tab is 18 ft. lbs. (Reference E-1, page 167) and trim movement on the tab is limited to $\pm 7^{\circ}$.

The TIFS airplane does not have the standard C-131 aileron-rudder interconnect springs. Consequently, manual operation of the TIFS aileron control feel is different from that of a standard C-131. There is no spring resistance in the TIFS system, but there is a higher friction level. This is due partly to the drag of the aileron servo which is in series in the system at all times and partly to the re-routing of the aileron cable controls in the wings through the direct lift flap areas. The effect of the proposed modification on the system friction is analyzed in Section E.2.2.4.

E.2.2 Preliminary General Design of Collective/Differential Aileron System

It is proposed to modify the aileron system as shown in the schematic diagram, Figure E-2. The major changes will be:

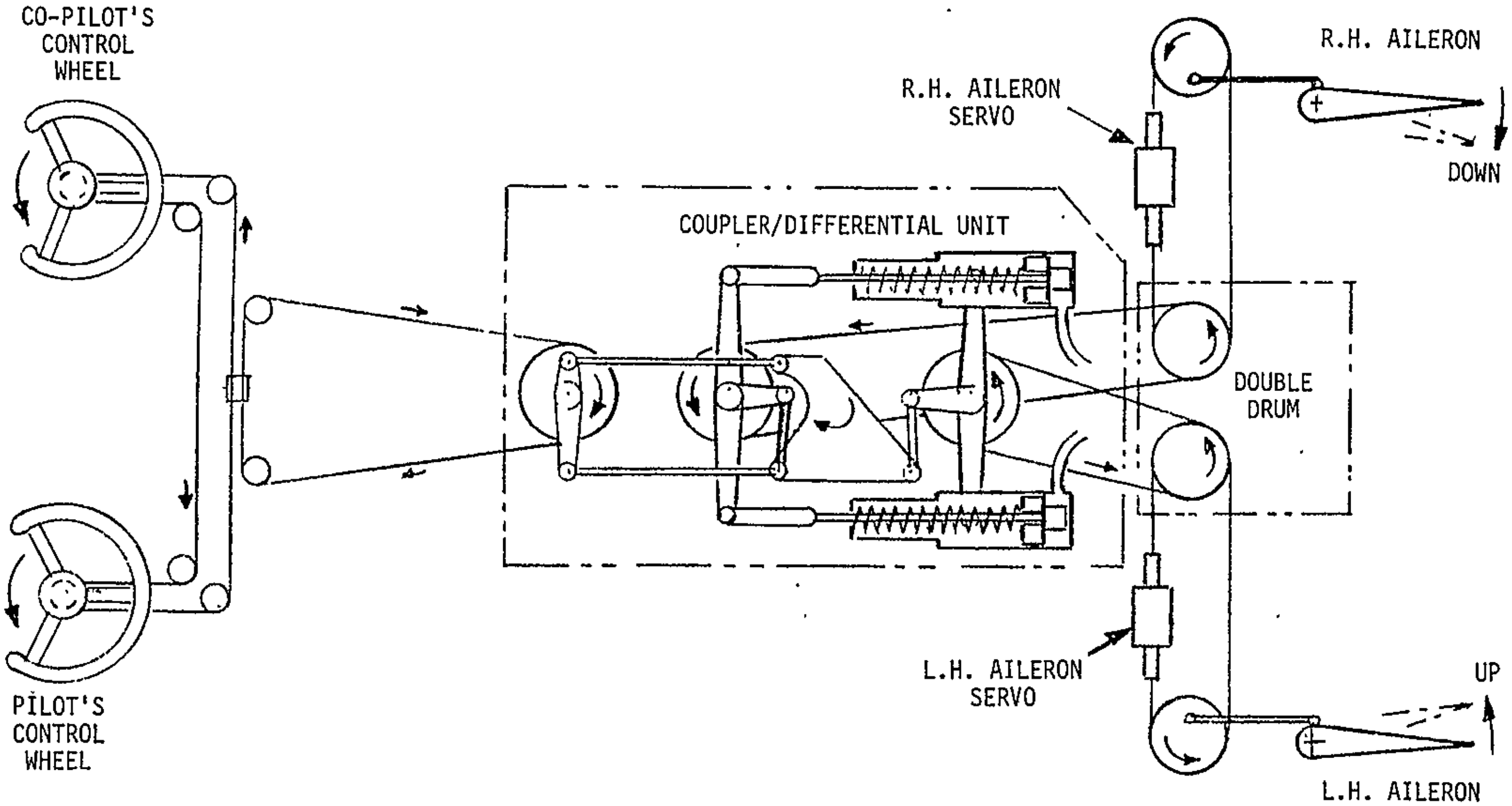

Figure E-2. SCHEMATIC DIAGRAM, ACT AILERON SYSTEM (Shown in Manual Aileron Control Configuration: Left Roll Input)

1. To remove the existing central servo actuator and install a servo actuator in each wing driving each aileron from an adjacent position.

2. To remove the standard C-131H multiple drum assembly at the center of the fuselage and install in its place a new double drum assembly.

3. To install a coupler/differential unit in the fuselage (stations 243 to 281) connected to the cockpit control wheels through the existing cable system and connected by divided cable systems to the new double drum assembly at the center of the fuselage.

4. To install hydraulic connections between the existing position servo subsystem and the new wing servos and coupler/differential unit.

Brief descriptions of the above changes follow:

E.2.2.1 Wing Mounted Aileron Servos

The proposed installation is shown schematically in Figure E-3. The actuator bodies will be mounted on the aft side of the rear spars. A new double quadrant will be mounted inboard of each actuator. Motion of an actuator piston rod will be transmitted to the aileron quadrant via a short run-around cable system. This mechanical arrangement has been selected to give good system dynamics in either direction with a minimum of structural rework in this area. The new double-quadrant support ribs will be braced to the existing quadrant support ribs. The trailing edge structure will be modified to provide clearance for the servo installations inside and to provide large access doors on the underside. The necessary servo control valves, hinge moment limiting valves, maniford blocks, etc. will be installed in the general

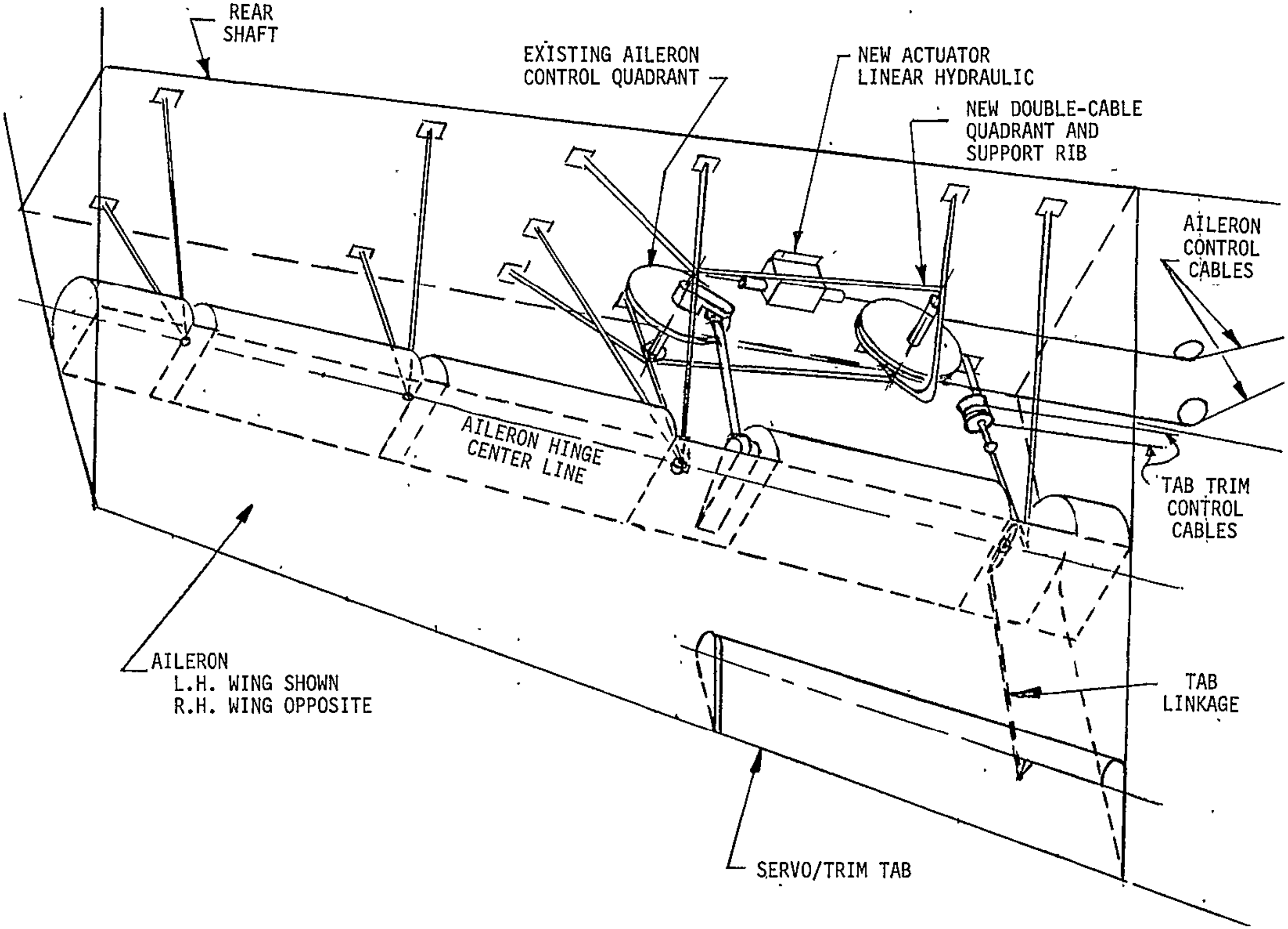

Figure E-3 AILERON SERVO ACTUATOR IN WING area of the actuators. All hydraulic piping will be solid type, no flexible hose being required.

E.2.2.2 Double Drum Assembly, Rear Spar, Buttock Line 0

To provide separate cable drives between the coupler/differential units and the ailerons,it is necessary to replace the existing solid drum assembly by a new double drum assembly. This new assembly will be interchangeable with the existing C-131H assembly, but separates the cable drives to the two wings to permit independent aileron operation. Existing pulley assemblies mounted on the top aft corner of the rear spar will be used for the two cable systems.

E.2.2.3 Coupler/Differential Unit

This assembly, See Figure E-4, has two major functions. When the airplane is being flown manually using the normal aileron system, a rigid mechanical connection is provided between the left and right ailerons. When the airplane is being flown on the ACT system, the left and right ailerons are mechanically disconnected at the coupler/differential unit and are then independently controlled by the wing-mounted actuators. Through the action of the differential linkage, the cockpit control wheel motions will reflect only the rolling deflection of the ailerons. The unit consists basically of three parallel shafts of which the forward one is connected to the pilot control wheels, the center one to the right aileron and the rear one to the left aileron. The coupler units operate on the center and rear shafts only and the differential linkage connects to all three shafts. Before describing the purpose and action of the differential linkage the coupler unit operation must be explained.

E.2.2.3.1 Coupler Units

The internal arrangement of the coupler units is shown in Figure E-5. The coupler bodies are trunnion-mounted on levers attached to the rear shaft. The coupler rods have slotted ends working on rollers between levers mounted

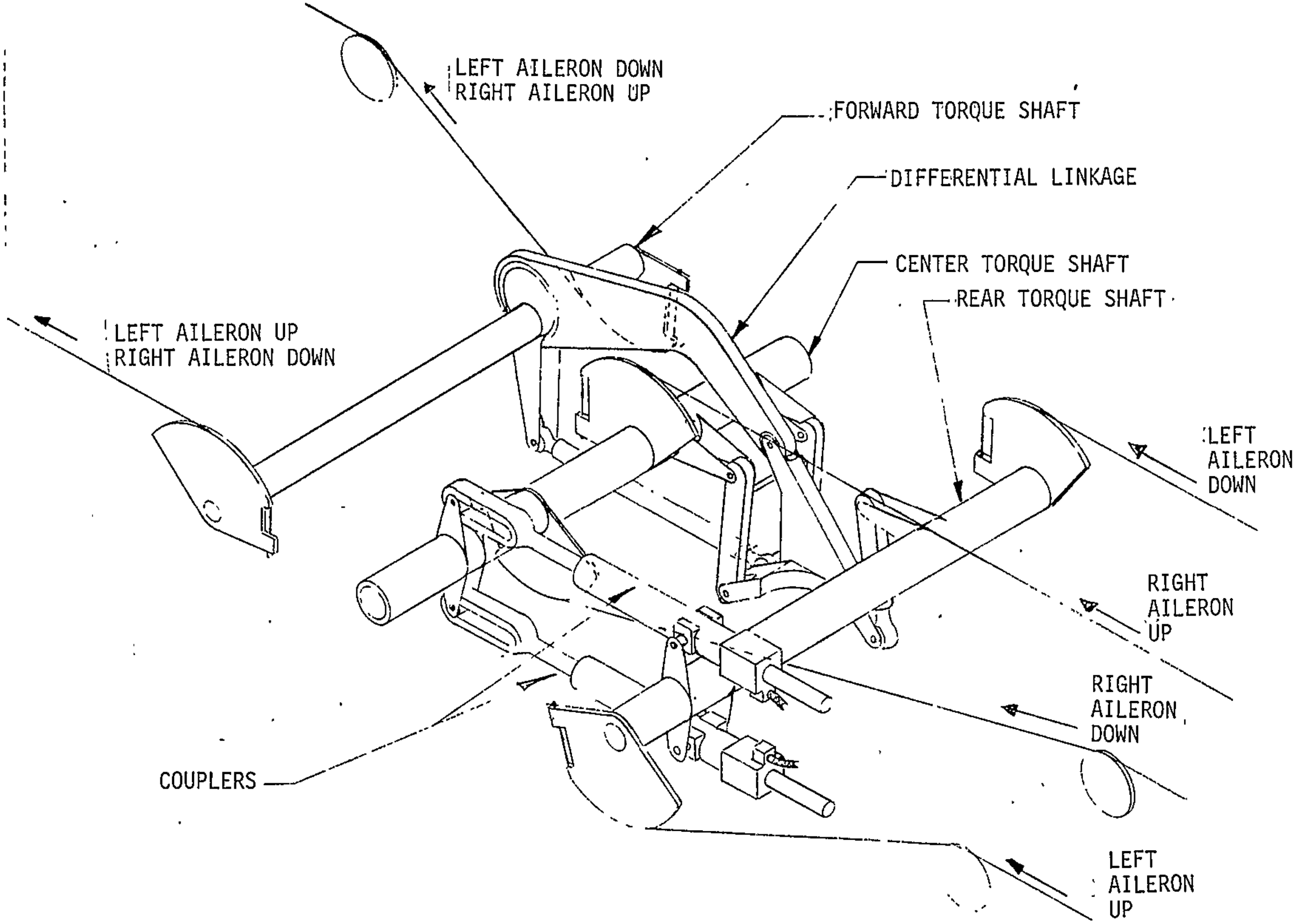

Figure E-4 COUPLER/DIFFERENTIAL UNIT

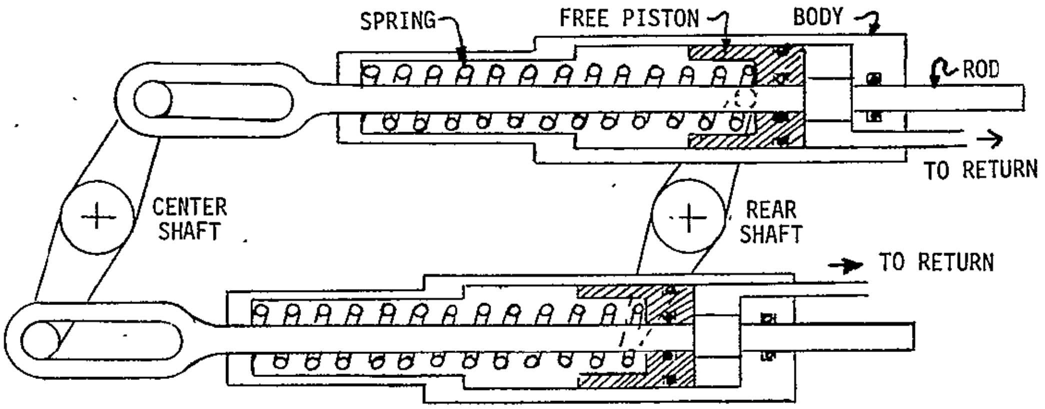

DEPRESSURIZED: MANUAL AILERON CONTROL

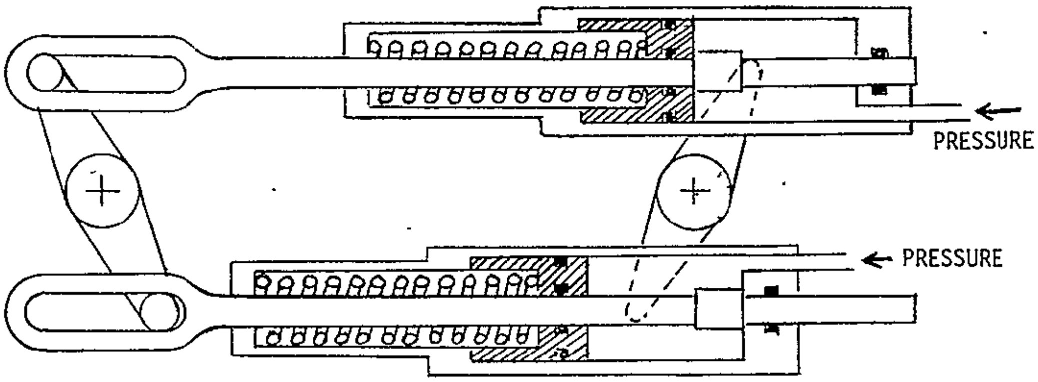

PRESSURIZED: FULL COLLECTIVE AILERON CONTROL

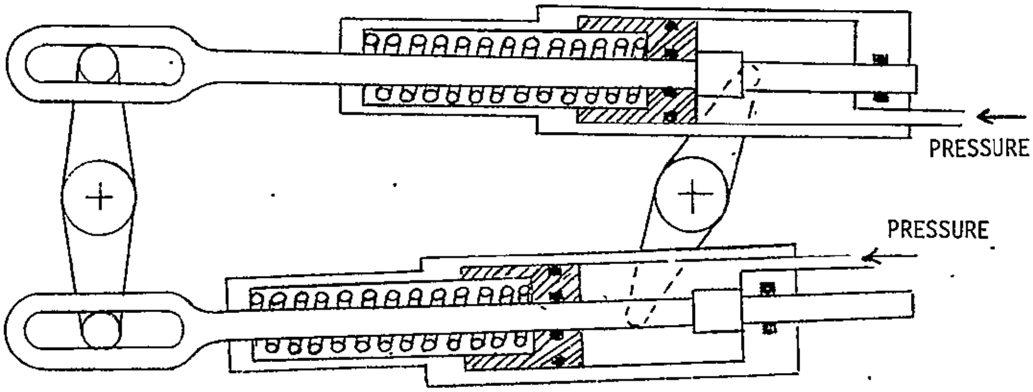

PRESSURIZED: COMBINED COLLECTIVE AND DIFFERENTIAL

Figure E-5. COUPLER UNITS

to the center shaft. Free single-acting hydraulic pistons inside the bodies are spring loaded against the hydraulic action. If the hydraulic chambers are depressurized, the spring forces on the pistons drive them to the "locked" end of their travel, The enlarged diameter portions of the rods are then trapped between piston and body. Linear movement of the rods relative to the coupler bodies is then prevented. Since the rollers on the center shaft are at the forward ends of the coupler rod slotted ends, the center shaft must then rotate in unison with the rear shaft. When hydraulic pressure is applied to the pistons, they are driven to the forward end of their travel compressing the springs more and permitting the coupler rods to slide freely between pistons and ends of bodies. The combination of coupler rod movement and slots then permits the center and rear shafts to rotate independently in the same or opposite directions as required by the movements of the servo actuators mounted in the wings near the ailerons. The springs in the coupler units are preloaded to exert 1289 lbs on each piston in the unpressurized "locked" position. Spring force increases to 2160 lbs when hydraulic pressure moves the piston to the opposite end of its travel. The net piston area is 1.96 in^2 so that a pressure of 2600 psi will produce 5096 lbs of force on the piston. The lowest pressure which will balance the spring in the "unlocked" position is 1102 psi. The supply of hydraulic power to the uncoupling mechanism will be controlled by a solenoid operated three-way valve. Energized, this valve will pressurize the mechanism. De-energized, pressure will be shut off and fluid in the mechanism will be bled through the flow restrictor to the hydraulic return line. See Figure E-14. The rate at which the free pistons can move is controlled by a restrictor. Total piston displacement for the two couplers is 2 x 1.96 x 1.6 = 6.27 in^3. If the time is 0.5 second, then the average flow rate through the restrictor will be 12.54 in^3/sec or 3.25 gpm.

E.2.2.3.2 Differential Linkage

The action of the differential linkage is illustrated in Figure E-6 for the "coupler locked" configuration and in Figure E-7 for the "coupler unlocked" configuration. The design of this linkage is such that in the coupler unlocked condition, when the ailerons are being independently driven by servos,

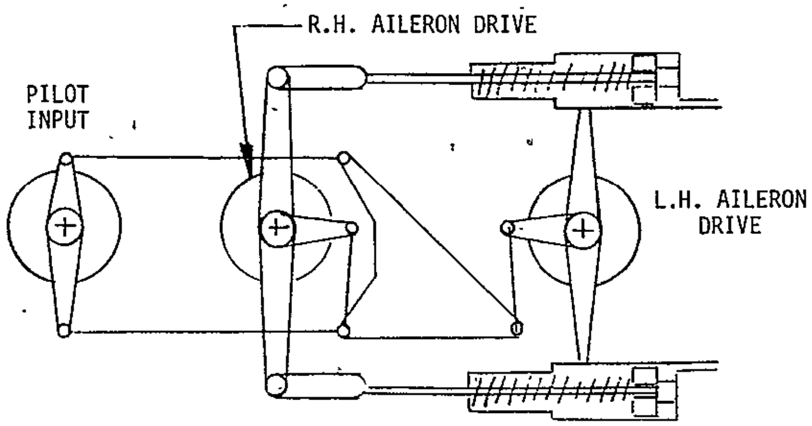

CONTROLS AND AILERONS IN NEUTRAL POSITION

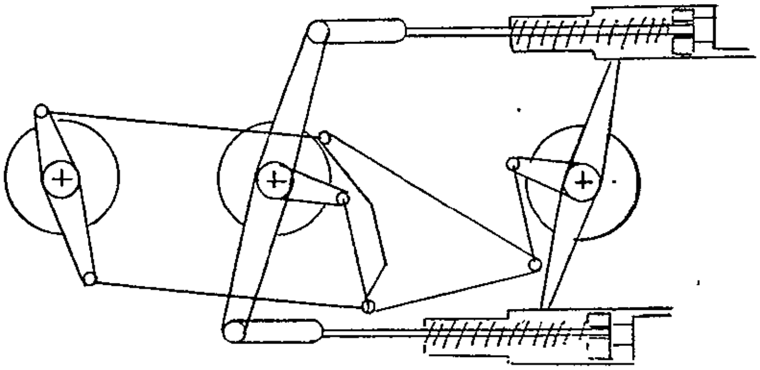

LEFT WING DOWN: LEFT AILERON UP, RIGHT AILERON DOWN

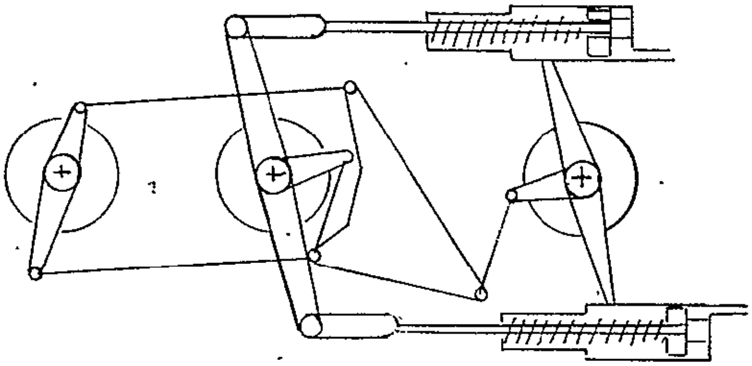

RIGHT WING DOWN: LEFT AILERON DOWN, RIGHT AILERON UP

Figure E-6   NORMAL AILERON OPERATION - COUPLERS UNPRESSURIZED AND LOCKED

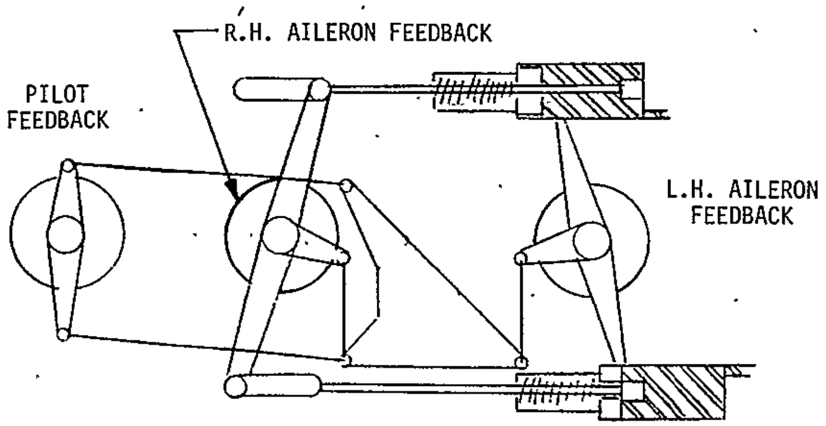

COLLECTIVE OPERATION, AILERONS DOWN
NO PILOT CONTROL FEEDBACK

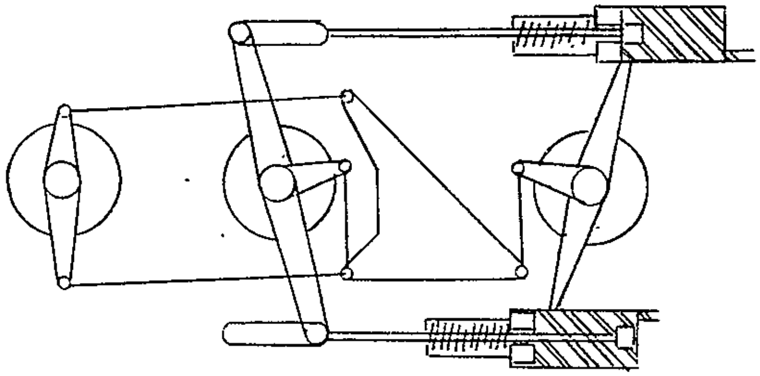

COLLECTIVE OPERATION, AILERONS UP
NO PILOT CONTROL FEEDBACK

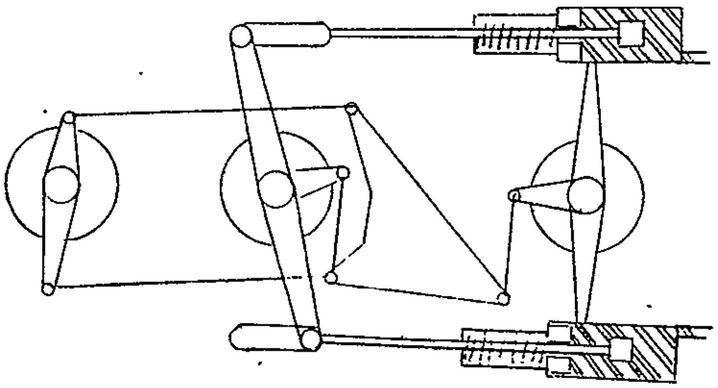

COLLECTIVE AND DIFFERENTIAL OPERATION
PILOT CONTROL FEEDBACK DIFFERENTIAL ONLY

Figure E-7 COLLECTIVE/DIFFERENTIAL AILERON OPERATION
COUPLERS PRESSURIZED AND UNLOCKED

the cockpit control wheels will display only rolling motions of the ailerons to the pilots at all times. The advantage of this is that while the ailerons are being moved by the servos, the normal use of aileron wheel motion as an indicator of roll input will be preserved. Total aileron deflection will be displayed to the pilot by meter movements similar to those used in the TIFS direct lift flap and side force servo systems.

E.2.2.4 Control System Friction

Measurements made during TIFS Flight #486 indicated that the force required at the rim of the control wheel to overcome breakout friction is about 14 lbs. This represents a force in the control cable of about 58 lbs and was measured with the aileron servo actuator in an unpressurized condition. The actuator is a Miller floating seal type modified at Calspan. This type was chosen because of the relatively low friction level which can be achieved with it. Actual bench tests of the aileron servo gave breakout force values of about 8 lbs for the unpressurized condition and 35 lbs pressurized. It may be concluded then that the friction in the aileron system due to cable bending, pulleys, bearings, pressure seals and rubbing strips must be in the order of 50 lbs when the cables are tensioned to standard C-131H requirements. Compared with the existing system, the new collective aileron control system will have increased friction in it, estimated as follows:

existing TIFS aileron system	58 lbs
additional aileron servo	8 lbs
coupling/differential unit (aileron mode)	3 lbs
Total	69 lbs

This represents about 16.5 lbs force at the control wheel rim, an increase of about 18% over the forces presently experienced in flying the TIFS airplane manually.

From the above estimate and discussions with the regular TIFS pilots, it is predicted that the handling qualities rating for ILS tracking or crosswind landing tasks will not be degraded from the current "acceptable but "unsatisfactory" level. In the event that handling qualities are, after preliminary tests, judged "unacceptable", a power boost will be added to the aileron system.

E.3.0 ELECTRICAL AND HYDRAULIC CONTROL DESIGN

The existing TIFS VSS electrical and hydraulic control systems must be understood in order to study the impact of the proposed collective aileron modification.

E.3.1 Normal Engage Sequence

The engagement procedure applies electrical and hydraulic power to the Variable Stability System. Four time-sequential operations are required to engage the VSS. These steps are:

1. Depress Master Power Switch. (SAFETY PILOT)
2. Depress Feel System Engage Switch. (TEST PILOT)
3. Depress Pressurize Switch. (SAFETY PILOT)
4. Depress Engage Switch. (SAFETY PILOT)

These four engage steps are electrically interlocked and the system can only be engaged if the switches are activated in the order shown. Indicator lights display the engagement state in the simulation cockpit, the safety cockpit and at the test engineer's consoles.

The four-step engage sequence is illustrated in Figure E-8 and is described in more detail below.

1. Master Power Switch — applies electrical (AC and DC) power to the variable stability system electronics. Input power is also applied to the VSS sensors. Power is connected to the ready bus

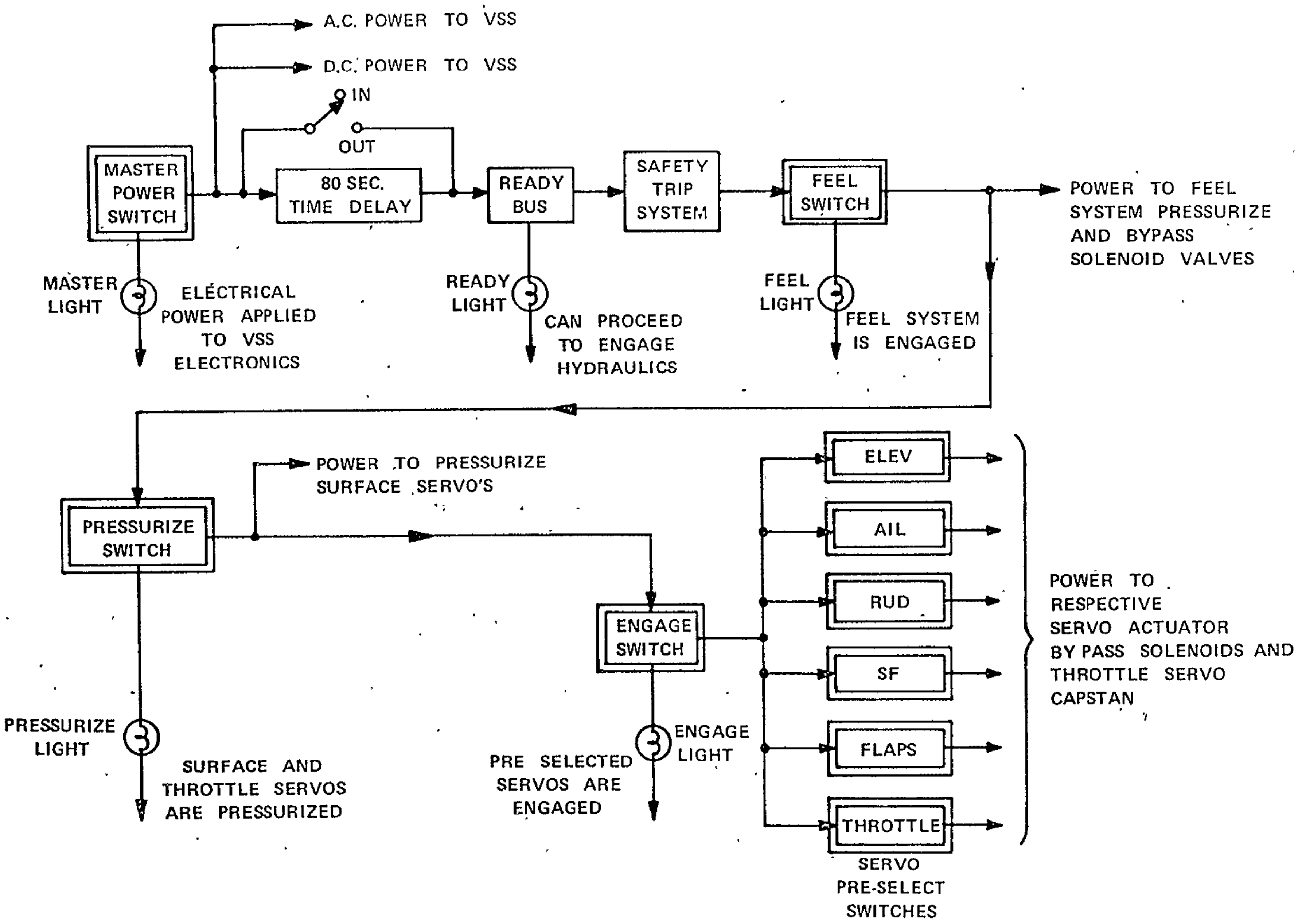

Figure E-8 BLOCK DIAGRAM ENGAGE SEQUENCE through an 80 second time delay. The time delay allows the attitude gyro to erect before the system can be engaged. Power from the ready bus is applied to the feel system activate switch through the safety trip system.

2. Feel System Engage Switch — applies hydraulic power to the feel system, i.e., pressurizes the hydraulic line to the feel system actuators and simultaneously closes the bypass valves across the feel system actuators. In addition, the feel system hydraulic flow control valves are connected to the servo amplifiers. At this point the feel system is engaged. Power is applied to the pressurize switch.

3. Pressurize Switch — applies hydraulic pressure to the surface servo hydraulic lines. However, bypass valves across the servo actuators remain open. (See Section E.3.2). Power is applied to the contacts of the engage switch.

4. Engage Switch — closes the bypass valves across the servo actuators of the servos that have been manually preselected before system engagement or selected after system engagement. Simultaneously, the surface servo hydraulic flow control valves are connected to the respective servo amplifiers.

E.3.2 Existing Hydraulic Servos and Safety Features

The aileron position servo presently installed in the TIFS airplane is powered from a special variable stability system (VSS) hydraulic supply. The three surface servos, elevator, rudder and aileron, form a subsystem controlled by a shutoff valve in the pressure line. This valve, normally closed, energized to open, works in conjunction with a bypass valve which connects the subsystem pressure line to the return line. This bypass valve (Bypass I on Figures E-9, E-10, and E-11) is normally open and energized to close at the same

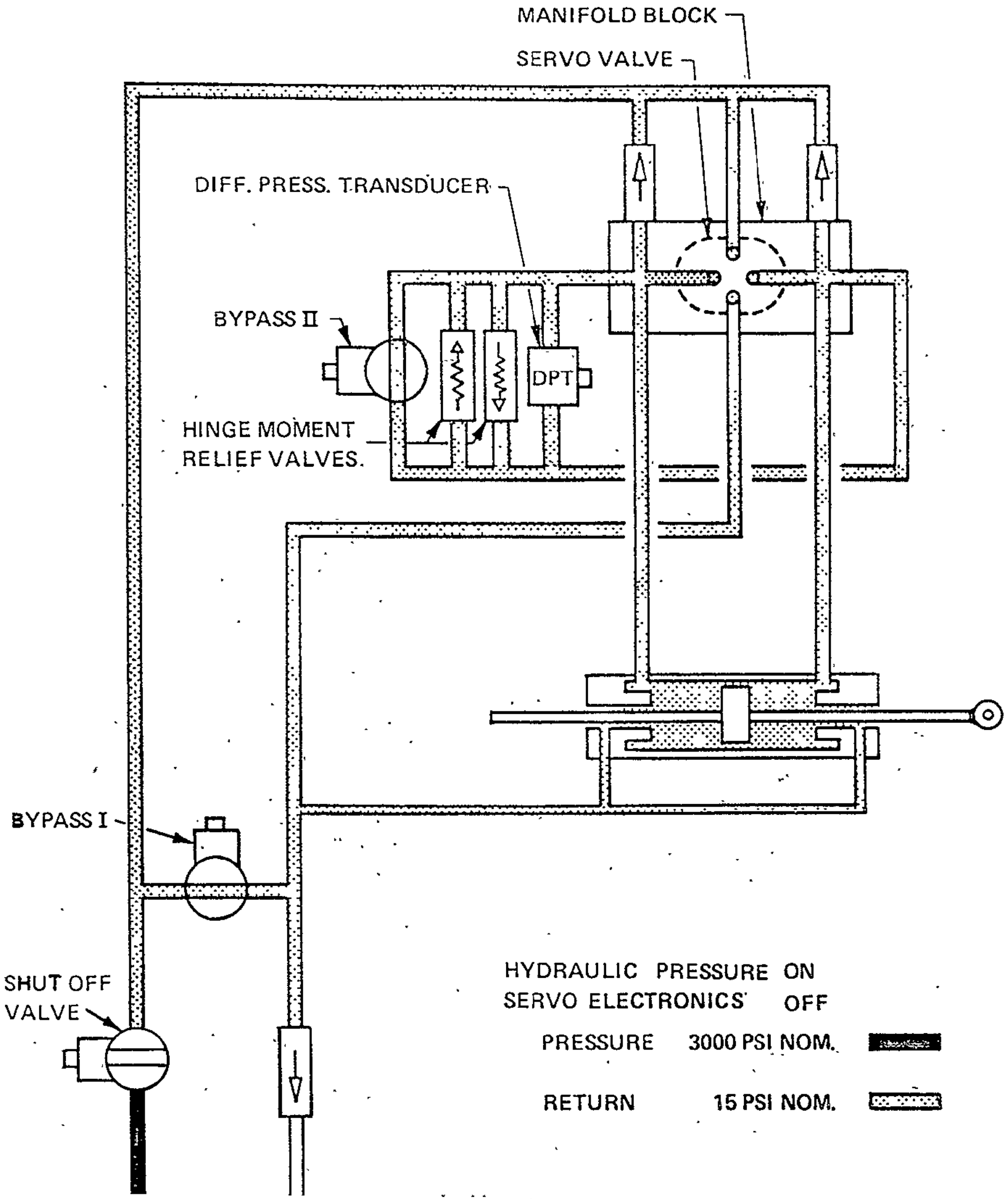

Figure E-9 COMPLETE "OFF" SYSTEM

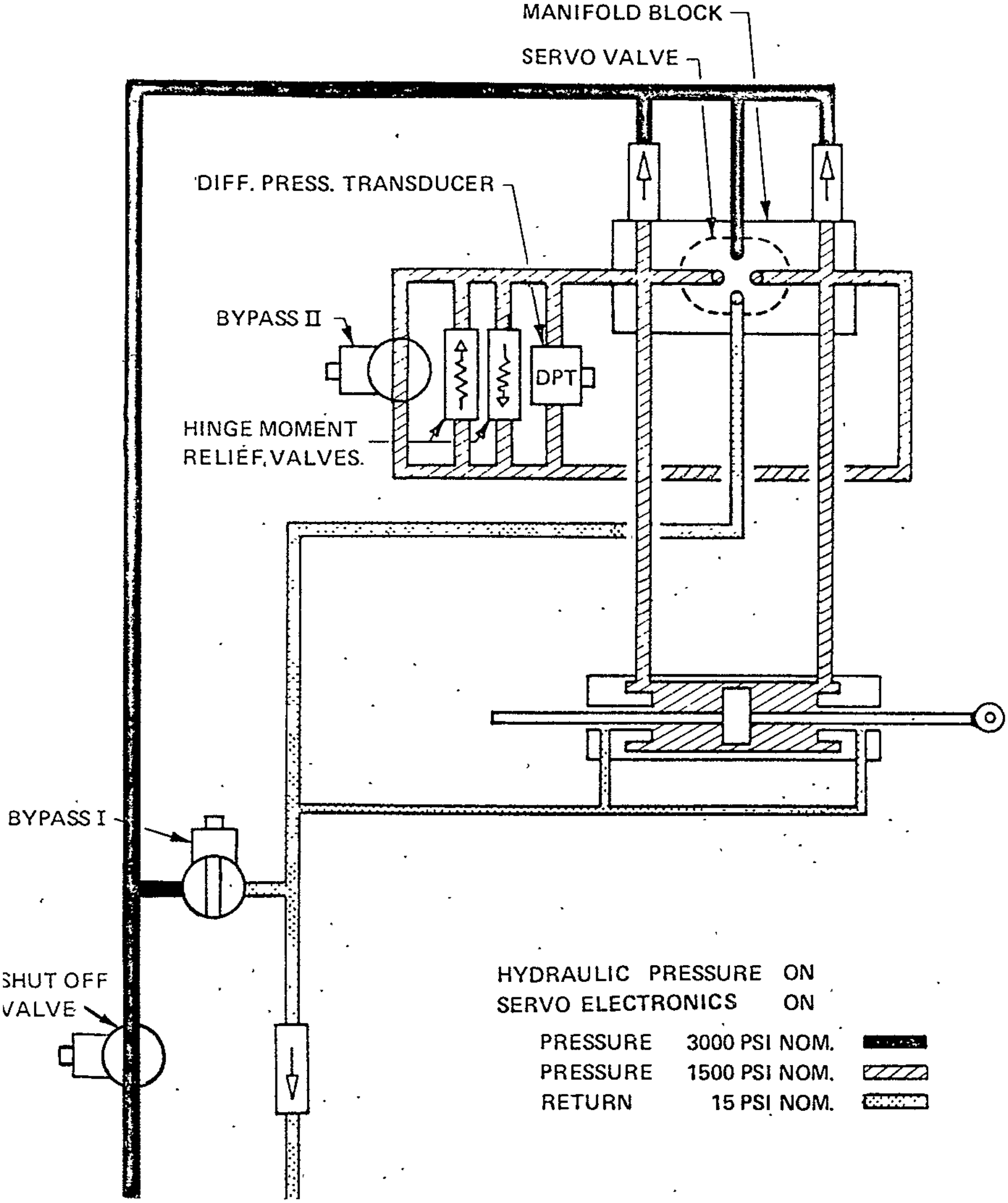

Figure E-10 CYLINDER PRESSURIZED

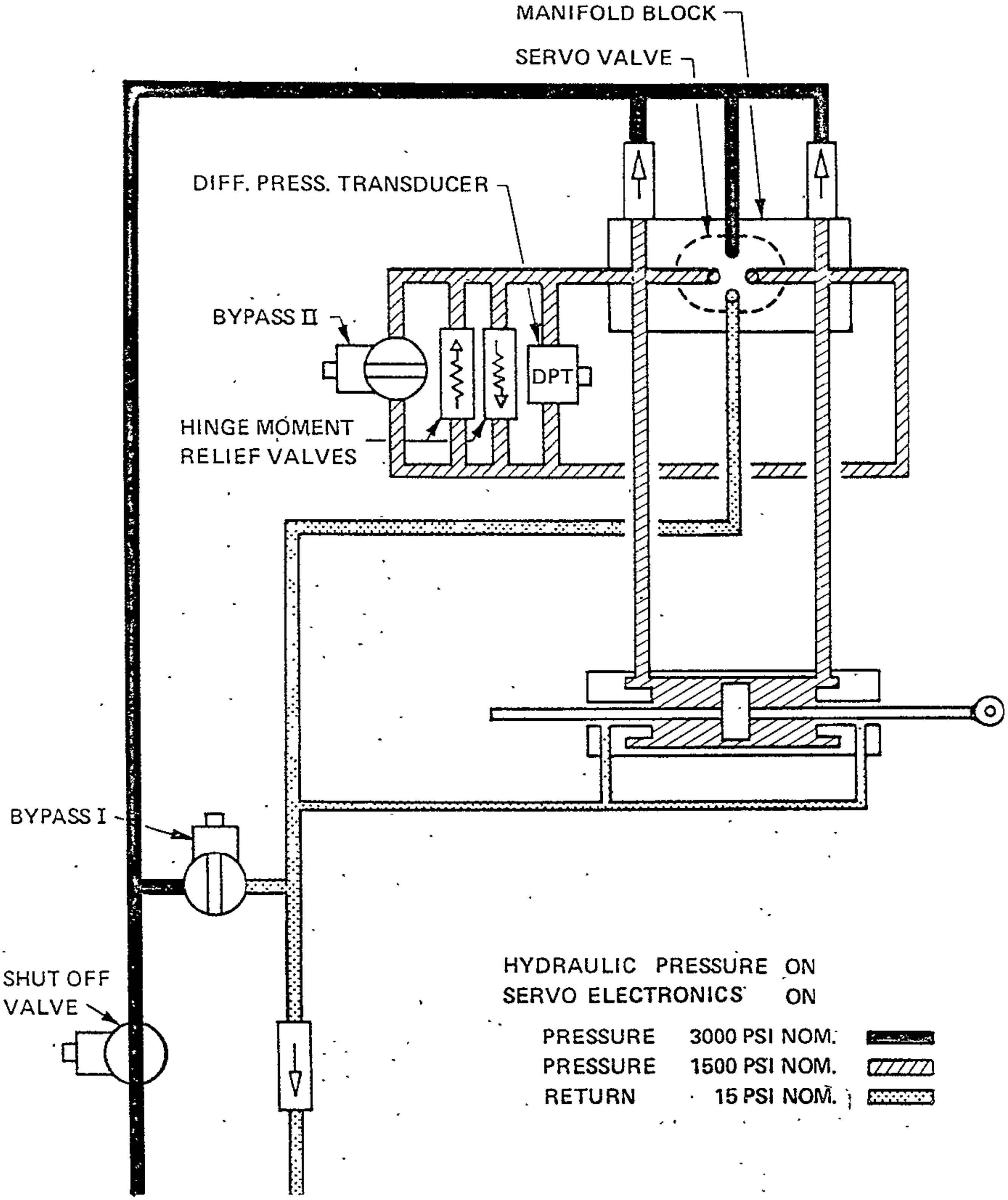

Figure E-11 COMPLETE "ON" SYSTEM

time that the shutoff valve when energized, opens the pressure supply to the surface servos. The following description of the various hydraulic servo states applies, therefore, to all three surface servos. Figure E-9 shows the state of the hydraulic section of the servo when the VSS is OFF. The safety pilot, by moving the control, forces oil from one side of the actuator or the other through the normally open solenoid valve. Upon pressurizing the system, the solenoid valve between the pump and the Moog valve opens and leakage flow through the Moog valve raises the pressure inside the actuator as shown in Figure E-10. However, the solenoid valve across the struts (Bypass II) has remained open. So the safety pilot can still move the controls forcing oil through the open solenoid valve. When the system is engaged, the solenoid valve across the actuator closes (Figure E-11). The computer can now control the actuator position through control of the Moog valve. Disengaging the variable stability system returns the hydraulic section of the servo to the state shown in Figure E-9.

Two groups of safeguards are provided in the existing system to ensure that the flight control surfaces can be easily operated by a safety pilot when the VSS system is "off". The first group consists of the solenoid-operated shutoff valve (Bypass II) fitted as a bypass control in each surface position servo piping system (see Figure E-9). When de-energized, these valves are normally open, and there are neither differential pressures across the servo actuator pistons nor any impediment to the free flow of fluid from one side of each piston to the other side. The second safeguard is provided in case any one of the shutoff valves just mentioned fails to open when de-energized. This consists of a single solenoid-operated shutoff valve (Bypass I) connecting the pressure supply for all surface position servos to the common return line, and a pair of check valves fitted in each position servo manifold block. The Bypass I shutoff valve, also normally open when de-energized, dumps the supply pressure, thus permitting flow through the check valves. Should any servo Bypass II valve fail to operate, fluid can escape freely through one of the check valves when movement of the relevant surface by the safety pilot causes the servo piston to move in the cylinder (see Figure E-12).

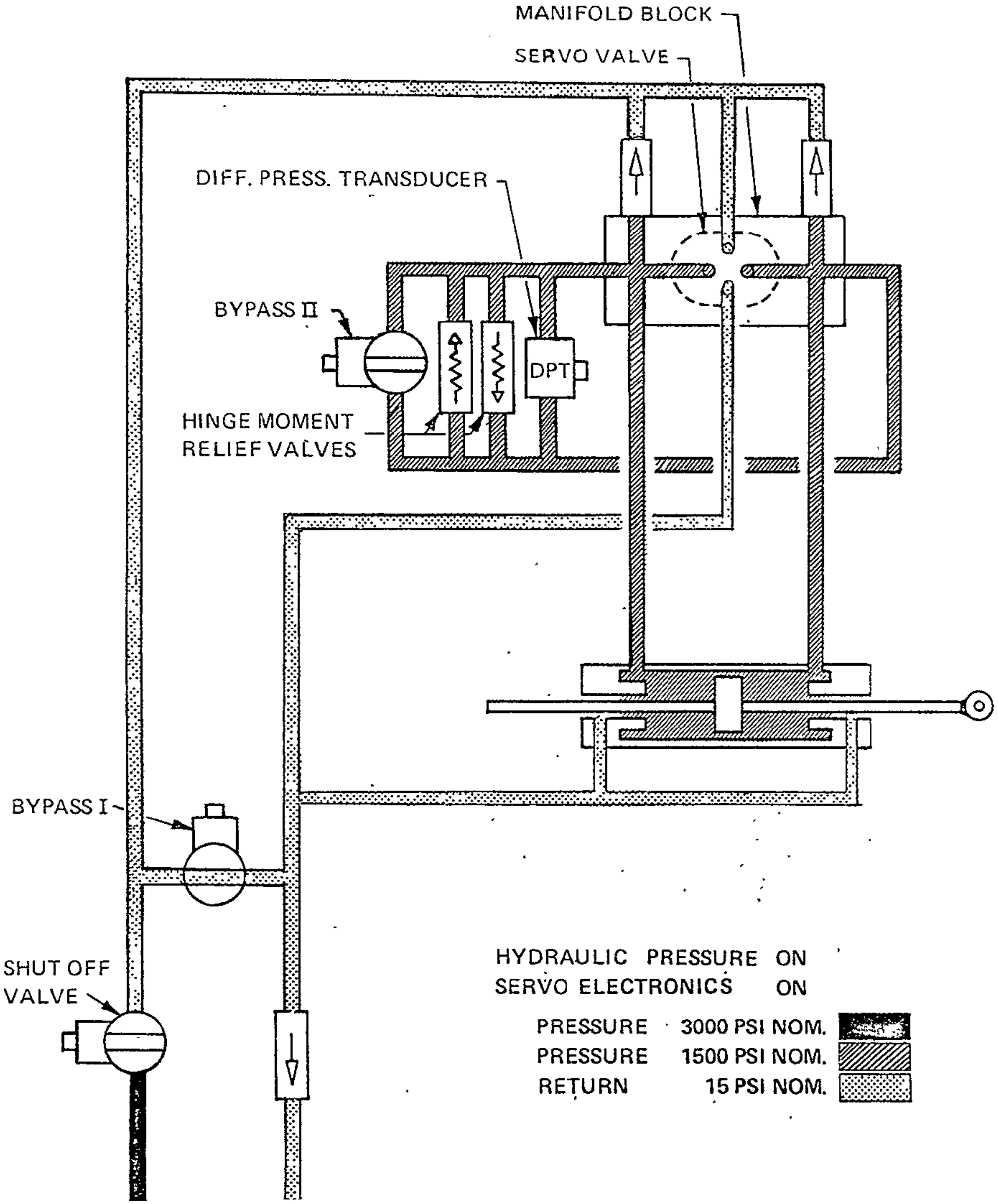

Figure E-12 BYPASS II FAILS TO OPEN

In addition, the safety pilot is able to overpower the servo at any time by exerting forces higher than those determined by the relief valve settings in the existing aileron control system, see Section E.2.1.

E.3.3 Safety System

The safety system consists of both manual (dump buttons) and automatic disengagement capability. The function of the automatic safety system, Figure E-13, is to supplement the action of the safety pilots in situations where rapid transients can occur or where parameters cannot be monitored due to high workload. The safety trip system protects the airplane by disengaging the variable stability system thus restoring normal aircraft control to the safety pilots. A safety trip or system "dump" is indicated by blinking red indicator lamps at all aircraft control stations and a modulated tone in the intercom system. The system dump can be initiated in four ways:

1. By safety pilots:

   The safety pilots can monitor control surface positions and rates of motion; aircraft attitudes, rates and accelerations and the aircraft environment. If either pilot feels and unsafe situation is approaching, he can disengage the system by depressing a dump button located on his control wheel.

2. By simulation pilots:

   The simulation pilots have similar dump buttons which they may depress if they cannot maintain control of the simulation.

3. By test engineers:

   The two test consoles located in the cabin are equipped with panel-mounted dump buttons to be depressed if a computer malfunction is detected by a test engineer.

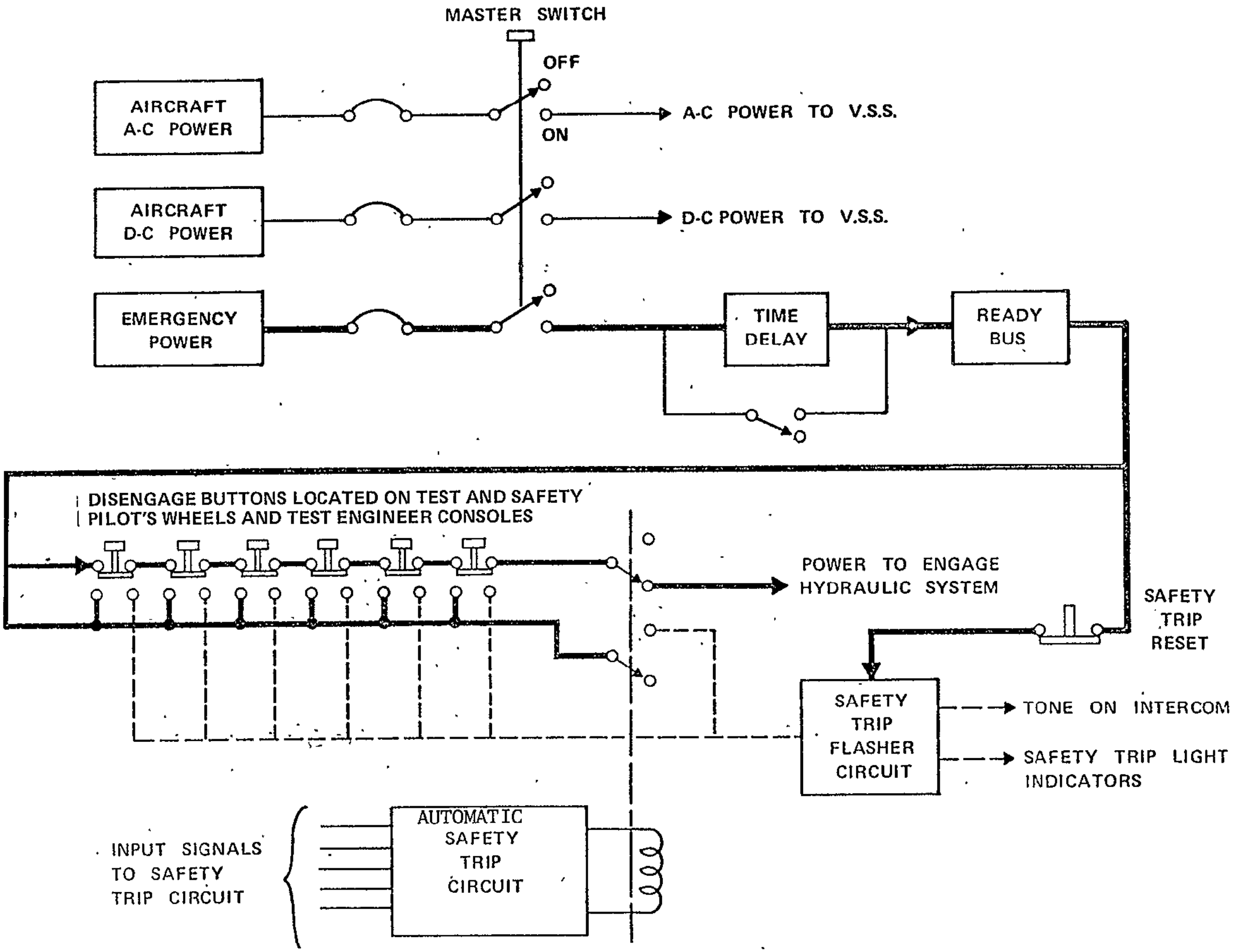

Figure E-13 SAFETY TRIP SYSTEM

4. By automatic safety trip:

The automatic safety trips consist of electronic circuits that continuously monitor selected critical aircraft parameters. If any of these signals exceed a predetermined safe level, a system dump results. Parameters monitored are:

a) control surface hinge moment.
b) control surface rate of motion.
c) aircraft lateral and vertical acceleration.
d) variable feel system controller rate of motion.
e) fuselage, horizontal stabilizer, wing, and vertical fin structural loads.

When any of these monitored variables cause a system dump, the safety trip indicators can be deactivated (reset) by either safety pilot by depressing the safety trip reset button located on the safety cockpit center isle console.

E.3.4 Collective/Differential Aileron Hydraulic System

It is proposed to modify the VSS flight control hydraulic subsystem as shown schematically in Figure E-14 by removing the present centrally mounted aileron actuator, adding two wing-mounted actuators and adding the hydraulically controlled coupler/differential unit. Hydraulic power to the two coupler assemblies in the latter unit is controlled by a solenoid-operated three-way valve so that the unit may either be pressurized to unlock or depressurized to lock. The coupler units will be pressurized only when the aileron servos are selected and the engage button is pressed. It should be noted that the two coupler assemblies provide fail safe action, for, if hydraulic power is shut off, the chambers filled with fluid are then opened to the return line and the pistons being spring loaded will return to the locked positions.

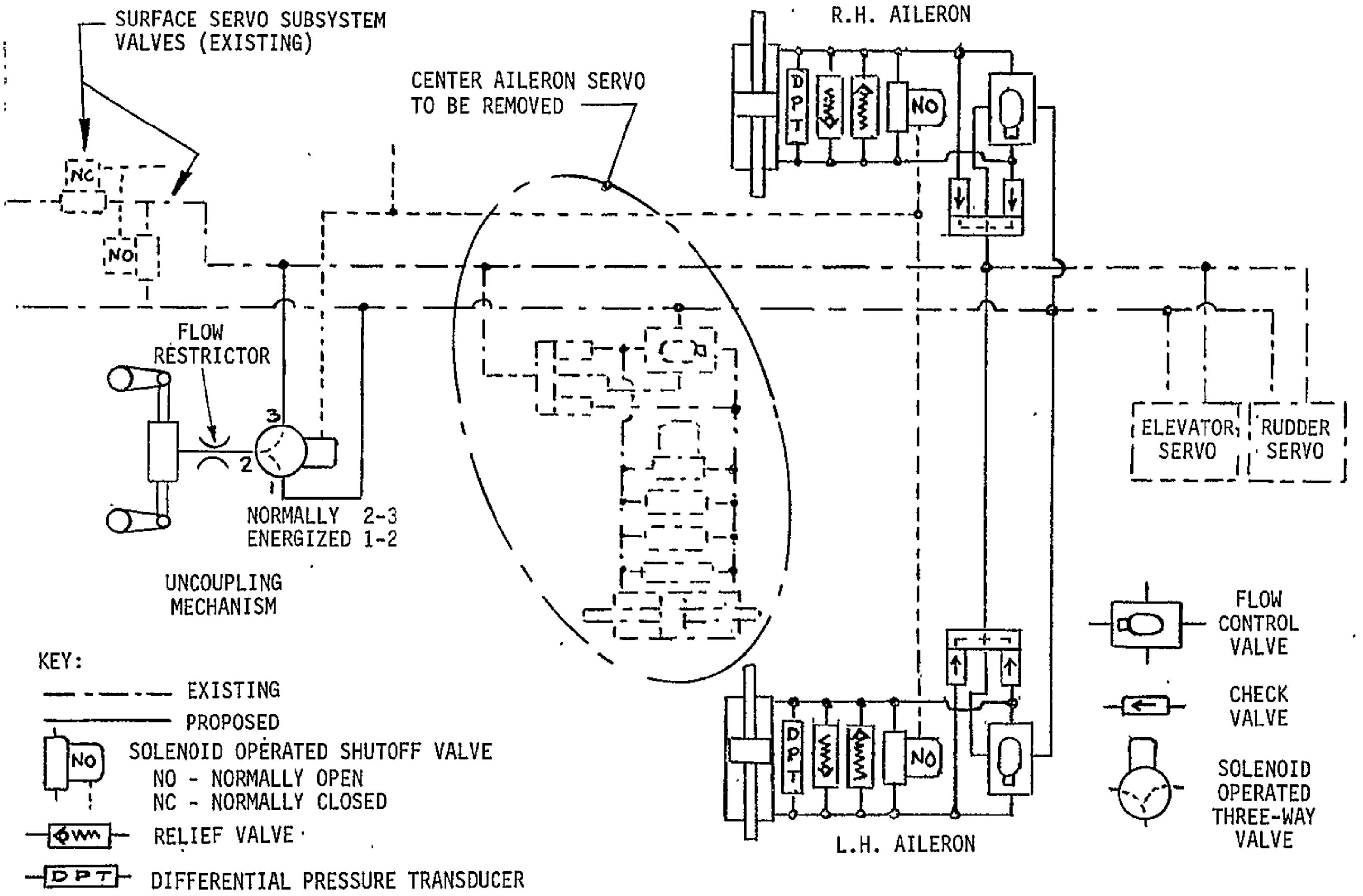

Figure E-14 COLLECTIVE/DIFFERENTIAL AILERON HYDRAULIC SYSTEM

E.3.5 Aileron Electrical Control System

Existing circuitry in the Control Logic Engagement chassis (PNL 11) will be used for the engage and disengage functions of the two aileron servos and for control of the coupler/differential unit. Position servo electronics for both aileron servos will be contained in the existing surface servo card enclosure (Rack 05).

A block diagram of the collective aileron control logic is presented in Figure E-15. The sequence of engagement and the function of each valve will be as outlined in Section E.3.1 with the exception of the coupler three-way valve. This valve is energized only if the system is engaged and the aileron servos are selected. When the three-way valve is activated, the couplers function as described in Section E.2.2.3.1.

The method of applying collective and differential inputs to the modified aileron system is shown in the simplified block diagram, Figure E-16. A more complete block diagram of the mechanization of each aileron position servo is presented in Figure E-17. This mechanization is identical to that used on the direct lift flap and side force surface servo loops presently installed in the TIFS. Position feedback is supplied by an actuator-mounted, infinite resolution potentiometer. Differentiated position feedback and high-pass filtered actuator-differential-pressure signals will be used for servo stabilization. The balance and hold circuit nulls the command signals prior to system engagement, thereby preventing undesirable transients.

Hydraulic components such as servo valves and actuators will be similar to the type used in the present TIFS VSS systems. The electronic components will be similar to the types presently used on TIFS.

E.3.6 Modification of Safety System

The high speed structural limits on direct lift flap deflection as a function of speed and normal acceleration will be recomputed as a function of

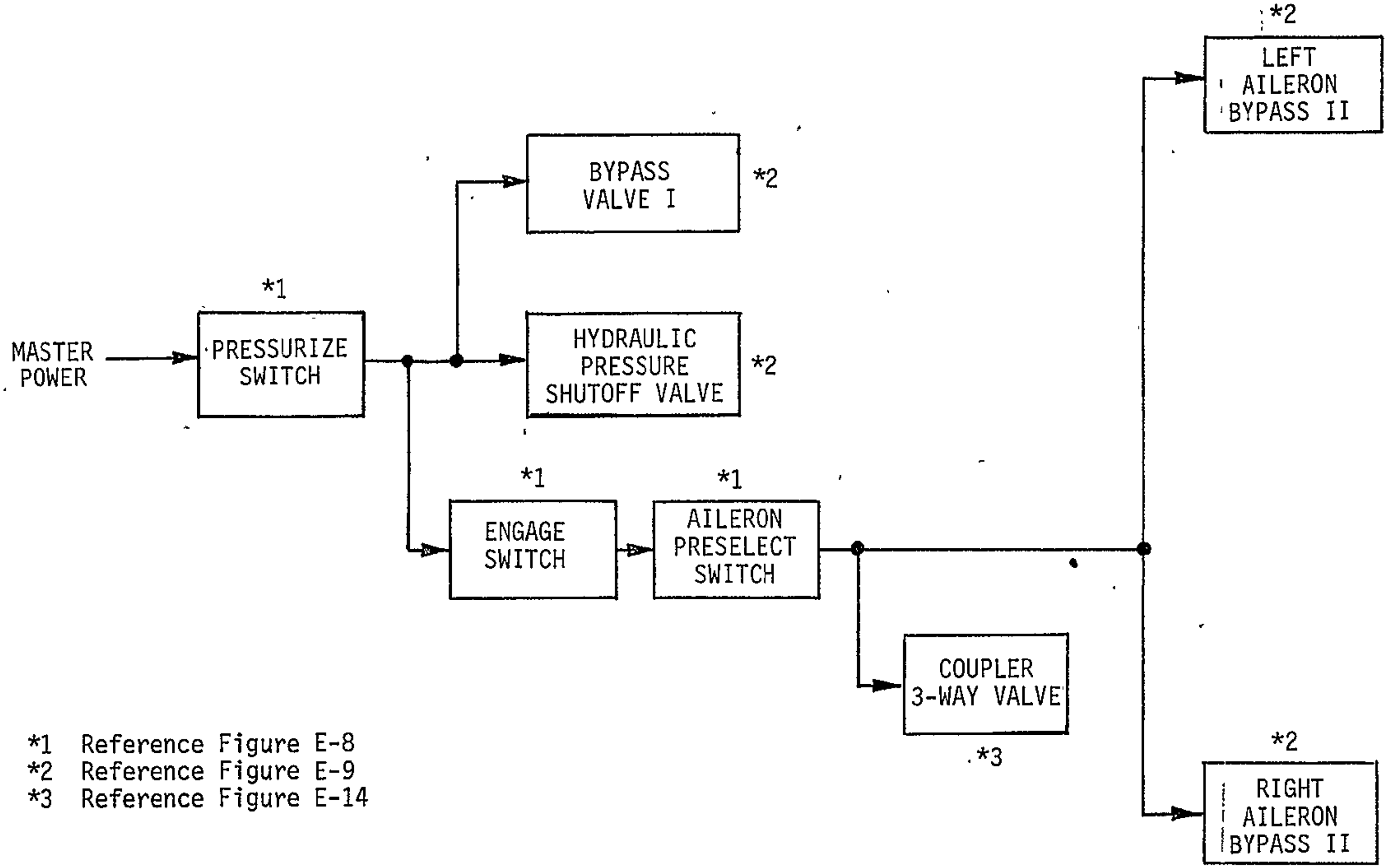

*1 Reference Figure E-8
*2 Reference Figure E-9
*3 Reference Figure E-14

Figure E-15. BLOCK DIAGRAM, COLLECTIVE AILERON CONTROL LOGIC

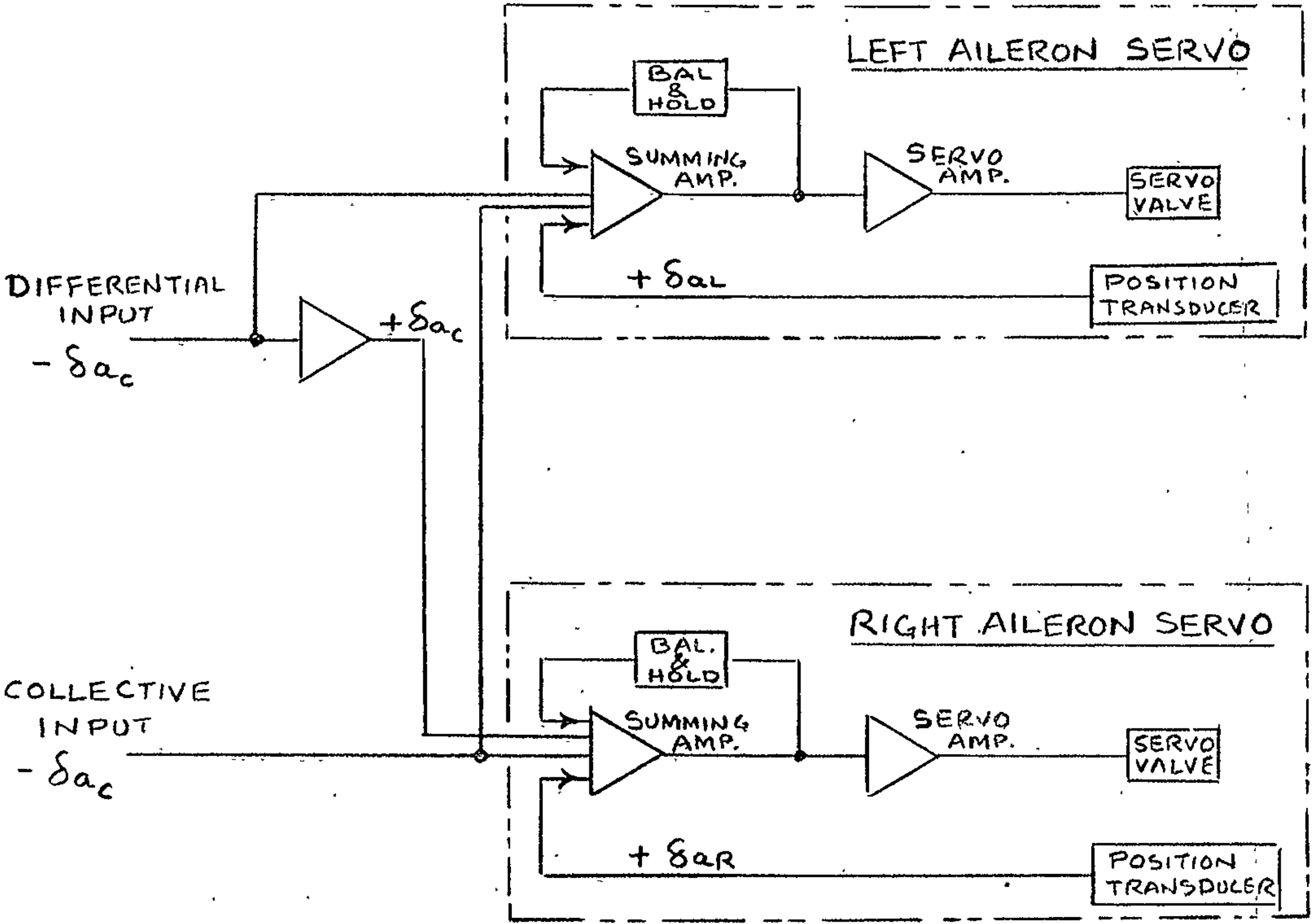

Notes: 1. Positive Surface Position → Aileron Down

2. Pressure Feedback Not Shown

Figure E-16. SIMPLIFIED BLOCK DIAGRAM OF COLLECTIVE AND DIFFERENTIAL CONTROL SYSTEM

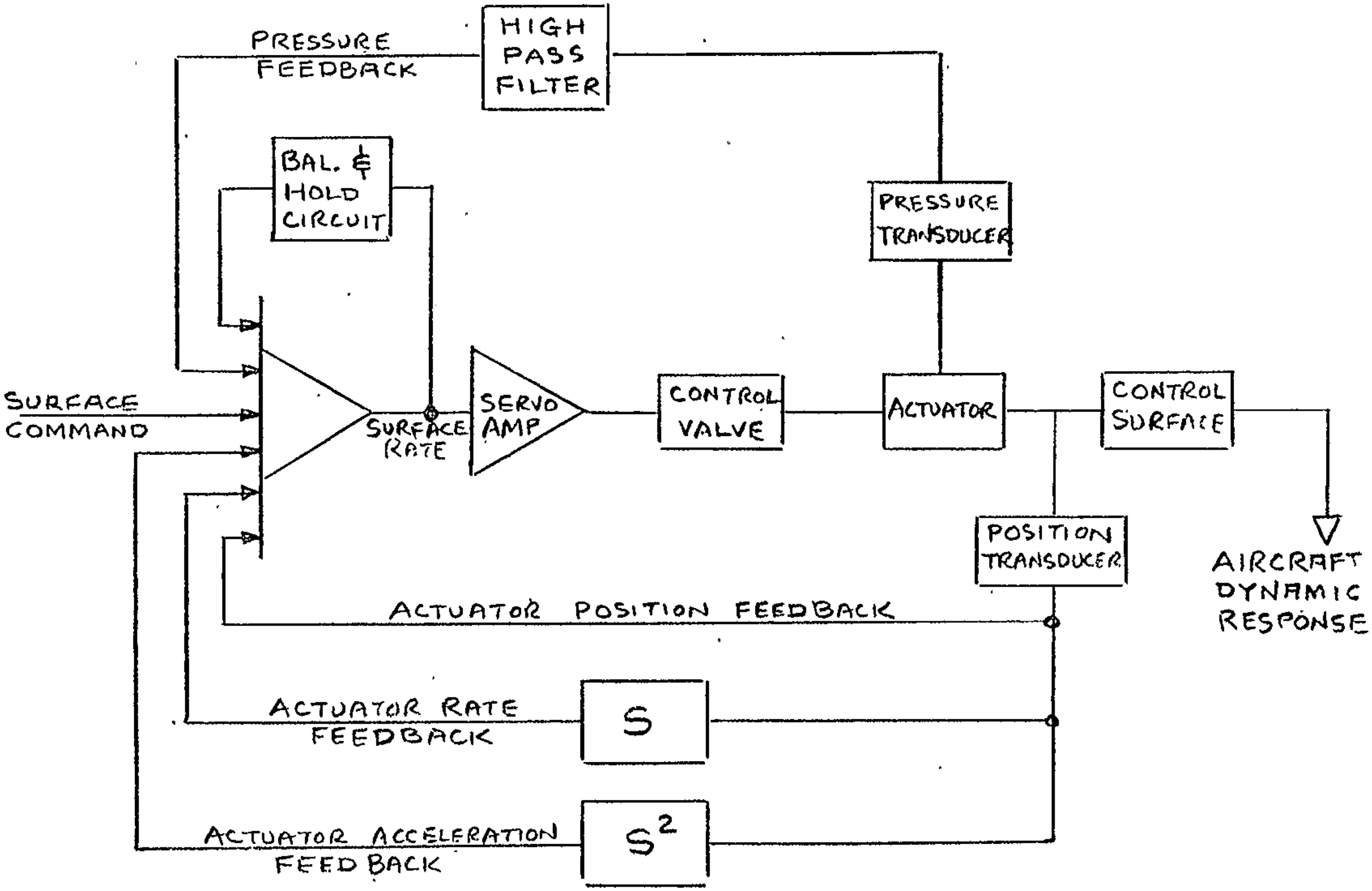

Figure E-17 BLOCK DIAGRAM OF AN AILERON SURFACE POSITION SERVO (Two Required) the collective aileron deflection. These limits will then be implemented, as they are at the present time, by safety trip functions. These functions will be dependent on collective aileron deflection and single aileron deflection as well as the present dependent variables.

In addition, individual aileron servo force output and surface rates will be monitored.

E.4.0 LOAD ANALYSES

Load analyses for the hydraulic system and the electrical systems follow.

E.4.1 Hydraulic

The TIFS VSS hydraulic system is supplied from an engine driven pump which can deliver 42 gpm. There are also two 50 in^3 accumulators, three 100 in^3 accumulators and one 400 in^3 accumulator in the system to supply peak flow demands above the pump capacity.

The collective/differential aileron modification will require hydraulics to actuate the uncouplers and to drive an additional servo. The couplers will require approximately 3.3 gpm for less than 0.5 seconds at each VSS engagement. This demand will occur when minimum flow rate is required for the servo actuators. Thus, the coupler flow rate demand has no impact on system capacity. The additional aileron servo will have a peak no-load requirement of 2.2 gpm. This will change the maximum instantaneous peak demand from 77.1 gpm to 79.3 gpm. This increase of 2.85% should not significantly affect the operation of the VSS hydraulic system.

If a power boost should be installed to augment manual operation of the aileron control, (a possibility indicated in Section 2.2.4) its power requirements will depend on the boost configuration chosen. If one of the servos which will be mounted in the wings for this modification also functions as a boost cylinder, there will be no change in demand. If a separate boost actuator is installed between the pilot control wheels and the forward torque shaft of the coupler/differential unit, it would have a 2.2 gpm instantaneous peak demand but it would only operate as a boost cylinder when the two wing mounted servos were unpowered so that the power required would be less than when the VSS system is operating.

E.4.2 Electrical Load Analysis

The increase in electrical power requirements for the aileron modification is estimated to be less than 5 amperes of MAIN DC BUS power and 0.1 KVA of 115V, 400 Hz power. Should an aileron boost system be installed, an additional 4.0 amperes of MAIN DC BUS will be required. The estimated breakdown of power requirements follows, but in all cases, the increase in loading is well within the TIFS excess capability.

COLLECTIVE AILERON MODIFICATION

System Condition	Power Required
VSS power off	None
VSS power on (not engaged)	2.0 amps MAIN DC BUS 0.1 KVA L.H. Alternator
VSS engaged with aileron servos selected	5.0 amps MAIN DC BUS 0.1 KVA L.H. alternator

POSSIBLE AILERON BOOST SERVO

System Condition	Power Required
VSS power off	4.0 amps MAIN DC BUS
VSS power on (not engaged)	4.0 amps MAIN DC BUS
VSS engaged with aileron servos selected	1.0 amps MAIN DC BUS

The impact of the additional loads to Table III of the current load analysis will be as follows:

1. VSS FLIGHT ELECTRICAL LOADS (ADDITIONAL)

LOAD	L.H. ALT. 40 KVA			DC GEN. 375 AMPS		
	Taxi	Term.Area	Cruise	Taxi	Term.Area	Cruise
Basic	---	---	---	4.0	1.0	1.0
VSS	0.1	0.1	0.1	2.0	5.0	5.0
Former Total Load	11.73	11.73	11.73	333.3	329.6	312.9
Former % of Capacity	29	29	29	89	88	83
New Total Load	11.83	11.83	11.83	339.3	335.6	318.9
New % of Capacity	30	30	30	90	89	85

2. FERRY FLIGHT ELECTRICAL LOADS (ADDITIONAL)

LOAD	DC GEN. 375 AMPS		
	Taxi	Term.Area	Cruise
Basic	4.0	4.0	4.0
Former Total Load	312.1	302.0	270.3
% of Capacity	83	81	72
New Total Load	316.1	306.0	274.3
% of Capacity	84	82	73

3. ELECTRICAL LOADS WITH LEFT ENGINE FAILED

LOAD	TWO 200 AMP TRU'S		
	Taxi	Term.Area	Cruise
Basic	4.0	4.0	4.0
Former Total Load	246.1	239.0	222.3
Former % of Capacity	62	60	56
New Total Load	250.1	243.0	226.3
New % of Capacity	63	61	57

4. ELECTRICAL LOADS WITH MAIN DC BUS DISABLED

No Change

5. ELECTRICAL LOADS WITH MAIN AC BUSES DISABLED

LOADS	DC GEN. 375 AMPS		
	Taxi	Term.Area	Cruise
Basic	4.0	4.0	4.0
Former Total Load	303.4	301.7	270.0
Former % of Capacity	81	80	72
New Total Load	307.4	305.7	274.0
New % of Capacity	82	81	73

E.5.0 STRUCTURAL INTEGRITY

The proposed collective/differential aileron modification will not pose any severe structural problems. The servo actuators will be force limited by relief valves as shown in Figures E-9, E-10, E-11 and E-12. The relief valve settings are yet to be determined. The quadrant assemblies in the wings are designed for two different conditions. The first involves two pilots exerting maximum design force on the control wheels with the aileron quadrants being held against stops. The case has a cable tension force of 996 lbs ultimate. The second case involves a maximum aileron download of 410 ft lbs limit which requires a cable tension force of 1325 lbs ultimate to react. An actuator with dimensions similar to that used on the existing centrally mounted servo would require a differential pressure of 899.5 psi to produce an output force of 883 lbs (1325/1.5 = 883 lbs limit).

The wing servos would be mounted on the aft side of the rear spar. The servo body would be rigidly attached to the spar. Servo output forces would appear therefore as shear forces along the spar web and as a moment in the wing construction plane approximately. The moment would be reacted as forces normal to the spar web and adequate local vertical structure is necessary to transfer these forces into the spar caps and the upper and lower wing skins. However, existing rib structures on the forward side of the rear spar may provide adequate support without reinforcement.

The double drum assembly is interchangeable with the existing drum assembly and loads in this area will not exceed existing structural capacity.

The coupler/differential unit will be mounted along the center of the aircraft between stations 243 and 281, and between the underside of the floor and the topside of the radome box structure. It is not anticipated that detail stress analysis will produce any major problems in transferring local loads into the fuselage structure at this point.

Some new guide pulley brackets will be required fore and aft of the coupler/differential unit. All pulley brackets and other components involved in this modification will be designed in accordance with various pilot load conditions.

When the ailerons will be operating collectively, they will be augmenting the effect of the direct lift flaps. It will be necessary, therefore, to change the safety trip signals on the latter in order to stay within the load factor limitations which result from the combination of wing bending capability, effect of the cargo door cutout on fuselage bending strength, horizontal tail constraints and aerodynamic buffet boundaries. New boundary diagrams for the load factors will have to be prepared.

E.6.0 WEIGHT AND BALANCE

The estimated net additional weight will be about 150 lbs. Removal of the center servo and its valving will reduce weight by about 30 lbs at station 390. The installation of the wing servos and new center drum will add about 95 lbs at station 468. The coupler/differential assembly will add about 85 lbs at station 263. The net effect on the C.G. will therefore be:

		lbs.ins.
center servo removed	30 lbs at 390 =	-11,700
wing servos added	95 lbs at 468 =	+44,460
coupler/diff.unit added	85 lbs at 263 =	+22,355
		+55,115

The added weight represents an increase of about .31% of zero fuel weight and the moment change is about .3%. The effect on the C.G. of the TIFS airplane will be negligible.

E.7.0 STRUCTURAL/AERODYNAMIC TESTS

The aileron control system will be subjected to proof loading tests after the collective/differential control modification is completed. Ground vibration tests of the modified aileron system will also be performed to determine, among other things, the effect on wing bending modes of the added masses of the actuators out at the ailerons.

The collective ailerons at full trailing edge up deflection are predicted to raise the stall speed by about 5 knots. The actual stall speeds will be determined by flight testing. Lateral control at the stall with full up and full down collective aileron deflection will also be investigated in flight.

The wing portion of the ground vibration tests in support of the flutter flight tests which were made in 1971 will be repeated with the new aileron servos engaged to define any change in wing modes. The airplane will also be flutter checked in flight with the servos engaged out to the limit speed of 295 knots.

The aileron hinge moment characteristics predicted for the airplane in Reference 13 will be used for design of new structure. These will be compared with the total aileron hinge moment measured in flight by the differential pressure sensor in the present aileron actuator and later with the individual aileron moments as determined by similar sensors in the new actuators.